CANADIAN THESES ON MICROFICHE

I.S.B.N.

THESES CANADIENNES SUR MICROFICHE

National Library of Canada
Collections Development Branch

Canadian Theses on
Microfiche Service

Ottawa, Canada
K1A 0N4

Bibliothèque nationale du Canada
Direction du développement des collections

Service des thèses canadiennes
sur microfiche

NOTICE

The quality of this microfiche is heavily dependent upon the quality of the original thesis submitted for microfilming. Every effort has been made to ensure the highest quality of reproduction possible.

If pages are missing, contact the university which granted the degree.

Some pages may have indistinct print especially if the original pages were typed with a poor typewriter ribbon or if the university sent us a poor photocopy.

Previously copyrighted materials (journal articles, published tests, etc.) are not filmed.

Reproduction in full or in part of this film is governed by the Canadian Copyright Act, R.S.C. 1970, c. C-30. Please read the authorization forms which accompany this thesis.

THIS DISSERTATION
HAS BEEN MICROFILMED
EXACTLY AS RECEIVED

AVIS

La qualité de cette microfiche dépend grandement de la qualité de la thèse soumise au microfilmage. Nous avons tout fait pour assurer une qualité supérieure de reproduction.

S'il manque des pages, veuillez communiquer avec l'université qui a conféré le grade.

La qualité d'impression de certaines pages peut laisser à désirer, surtout si les pages originales ont été dactylographiées à l'aide d'un ruban usé ou si l'université nous a fait parvenir une photocopie de mauvaise qualité.

Les documents qui font déjà l'objet d'un droit d'auteur (articles de revue, examens publiés, etc.) ne sont pas microfilmés.

La reproduction, même partielle, de ce microfilm est soumise à la Loi canadienne sur le droit d'auteur, SRC 1970, c. C-30. Veuillez prendre connaissance des formules d'autorisation qui accompagnent cette thèse.

LA THÈSE A ÉTÉ
MICROFILMÉE TELLE QUE
NOUS L'AVONS REÇUE

NL-339 (r. 82/08)

Canada

A STUDY OF MOMENTUM TRANSFER PHENOMENA IN COMPOUND CHANNEL FLOWS

by

Panagiotis Prinos, Dip. Civil Eng., M. Hy.

A thesis
presented to the University of Ottawa
in partial fulfillment of the
requirements for the degree of
Doctor of Philosophy
in
CIVIL ENGINEERING DEPARTMENT

OTTAWA, Ontario, 1985

© Panagiotis Prinos, Ottawa, Canada, 1985.

The University of Ottawa requires the signatures of all persons using or photocopying this thesis. Please sign below, and give address and date.

ABSTRACT

A theoretical and experimental study was undertaken to investigate the effects of momentum transfer (MT) phenomena on the hydraulics of compound channel flows. The transfer phenomena (rows of large-scale surface vortices) are generated in the junction regions of compound sections and their effects are significant when the velocity differential, between adjacent deep and shallow zones, is large.

The laboratory investigation was performed in a symmetrical compound channel comprising a deep (main channel) section flanked on either side by wide shallow berms (flood plains). The dimensions of the trapezoidal-shaped main channel were adjusted, during the course of the experiments, to satisfy both "narrow" and "wide" main channel conditions. Another important study variable was the relative boundary roughness between the shallow and deep portions of the model compound section. Three different grades of artificial roughness were employed in the study, giving a maximum value of two for the relative roughness parameter.

The MT mechanism's effect on velocity and boundary shear stress distributions, in the different subsections of the compound flow field, as well as on turbulence characteristics in the mixing regions, were investigated for a wide

range of operating conditions. Empirical relationships were developed to estimate (i) apparent shear stress acting on the imaginary interface planes that separate the deep and shallow regions, and (ii) the effective increase in the main channel resistance to flow produced by the MT effect.

The net effect of MT on system conveyance was also investigated by comparing observed discharge with corresponding values obtained through application of conventional stage-discharge relationships. A modified relationship is introduced to account for the MT effects at small flood stages and this gave superior results for the conditions examined.

A modified version of the K-ε turbulence model was used to generate depth-averaged velocity profiles for the conditions examined. The generated profiles found to compare favorably with those observed in the physical model.

PREFACE

Large differences between estimated and actual discharge can result when conventional stage-discharge predictors, developed for flow in prismatic channels of simple cross-section, are applied directly to compound channel systems.

Recent research on this topic has established that these discrepancies are due, largely to the presence of a strong momentum transfer (MT) mechanism in the "compound" flow field. The MT feature is generated in the junction regions of the cross section (separating adjacent deep and shallow zones) and its influence on system conveyance becomes significant when the velocity differential, between the deep and shallow zones, is large.

The aforementioned deficiency in the conventional discharge prediction methods arises from the fact that the MT mechanism is not properly accounted for when these methods are applied to flow in compound channels.

This theoretical and experimental study investigates the influence of these transfer phenomena on the hydraulic characteristics of both "wide" and "narrow" compound channel flows. The primary objectives of the study were:

1. Development of suitable stage-discharge relationships for compound channel systems (i.e relationships that

account for the MT feature and are sensitive to spatial variation in boundary roughness).

2. Analysis of the related turbulence characteristics in the junction regions of compound sections to better define the transfer mechanism's zone of influence and its effect on system hydraulics under radically different geometric and hydraulic conditions.

3. To improve existing numerical modelling capabilities in regards to predicting the general velocity distribution in compound channel flows.

The first objective was accomplished by studying the MT mechanism in a model compound channel with relative depth, width and boundary roughness being the principal study variables. The channel's cross section comprised a central deep section flanked on either side by wide shallow flood plain zones.

Empirical relationships were developed for the estimation of apparent shear stress acting on the (imaginary) main channel/flood plain vertical interface and also for the increased channel friction factor, which reflect the MT's adverse effect on system conveyance.

This work introduces an alternative procedure for estimating discharge in compound channel systems. The procedure, which is based on momentum balance considerations, gives results that are in close agreement with observed data.

In the experimental program, turbulence characteristics were measured using a cross type hot-film probe. Increased turbulence intensities were observed in the interaction region with the level of increase depending on flood plain depth and roughness. Measured shear stress in the main channel portion of the interaction region was found not to follow the eddy-viscosity concept. Observed apparent shear stresses at the junction interface plane compared favorably with calculated (depth-averaged) values, based on momentum balance considerations.

In the numerical modelling phase of the study, general improvement in the modelling of velocity profiles in compound sections was achieved using a depth-averaged version of the K-ϵ model developed for this purpose.

Comparisons between model generated and observed velocity distributions confirms that the model properly accounts for the MT mechanism when the velocity differential across the junction regions is high.

ACKNOWLEDGEMENTS

The author is deeply grateful to Dr. R. Townsend for the supervision, valuable advice and encouragement throughout this work.

I also wish to thank Dr. S. Tavoularis of the Department of Mechanical Engineering of University of Ottawa for making available the necessary electronic equipment for turbulence measurements and for his valuable advice on the turbulence aspects of the study.

I am grateful to Mr. B. Moore, technical officer of the Hydraulics Laboratory, for constructing the experimental test facility, to C. Siomalas for his assistance with the photographic equipment and to E. Mourelatos for typing this thesis.

Special thanks are due to all my friends and my family for their constant support and encouragement.

LIST OF SYMBOLS

A_t = total cross-sectional area ;

A_c = main channel cross-sectional area ;

A_f = flood plain cross-sectional area ;

A,B = coefficients ;

a = empirical constant;

C = Chezy's roughness coefficient ;

c_f = friction coefficient ;

$c_1, c_2, c_k, c_\varepsilon$ = empirical constants ;

d = external diameter of the Preston tube

E = mean voltage ;

E_1 = wall roughness parameter;

$(e_1+e_2)'$ = rms of the summation of both voltage fluctuations ;

$(e_1-e_2)'$ = rms of the difference of both voltage fluctuations ;

$\overline{e_1^2}, \overline{e_2^2}$ = mean squares of the voltage fluctuations

e_{ik} = the cosine of the angle between the ith axis of the (y,z) coordinate system and the kth axis of the (y',z') coordinate system;

g = acceleration due to gravity ;

h = flow depth;

I = electrical current ;

K = a displacement factor (=1.3)

k = roughness height

K_1 = overheat ratio (Rw/Ra) ;

K_i = correction factor for the ith subsection;

k = von Karman constant ;

n = roughness coefficient for compound channel ;

n_e = composite roughness coefficient ;

n_i = roughness coefficient for the ith subsection;

n_r = relative roughness;

P = mean pressure ;

P_c, P_f = wetted perimeters of main channel and flood plain respectively ;

P_i, R_i = wetted perimeter and hydraulic radius for the ith subsection respectively ;

P_t = wetted perimeter for compound channel;

Q_t = total discharge;

R_t = hydraulic radius of compound channel ;

R_w = electrical resistance of wire at wire temperature ;

R_a = electrical resistance of wire at fluid temperature ;

S = slope of the channel ;

S_1 = slope of calibration curve ;

S_ϕ = volumetric source term ;

$\overline{S}$ = the average value of S_ϕ over the control volume ;

S_c = constant part of S_ϕ;

S_p = coefficient of ϕ.

U_i, U_j = components of mean velocity in x_i, x_j directions respectively ;

$\overline{u_i u_j}$ = turbulent velocity fluctuation (the superscript bar denotes a time average).

U,V,W = components of mean velocity in x,y,z directions respectively ;

$\overline{U}, \overline{W}$ = depth-averaged velocities in x,z directions respectively ;

U_* = the local shear velocity ;

$-\rho\overline{uw}$ = local apparent shear stress ;

u = local mean velocity ;

u_1 = local velocity measured at y_1

u_2 = local velocity measured at y_2

U_s = velocity calculated from "single-channel" method ;

u',v' = rms of the velocity fluctuations in the longitudinal and vertical directions ;

$-\rho\overline{uv}$ = turbulent shear stress;

$\overline{u_i u_j}, \overline{u_k u_l}$ = the components of the tensor in the old (y,z) and the new (y',z') coordinate system respectively;

Umax-Umin = velocity difference across the shear layer;

U_r = resultant velocity ;

y_f = flow depth in the flood plain zone ;

y = vertical distance from the boundary ;

y_r = relative depth;

W_r = relative width;

z^+ = normalised distance from the side wall;

Greek Symbols

Δp = p-po = dynamic pressure

ΔU = differential velocity between the main channel and flood plain;

δ = thickness of the shear layer ;

ν = kinematic viscosity of water ;

ν_t = eddy (turbulent) viscosity ;

$\overline{\nu_t}$ = depth-averaged eddy viscosity ;

ρ = density of water ;

σ_k, σ_ε = empirical constants ;

τ_w = boundary shear stress ;

τ_n, τ_s = the apparent shear stresses acting on the n and s faces respectively ($\tau = \rho \overline{\nu_t} d\overline{U}/dz$) ;

τ_c, τ_f = boundary shear stress for main channel and flood plain respectively ;

τ_a = apparent shear stress acting on the vertical imaginary interface ;

ϕ = dependent variable ($\overline{U}$, $\overline{K}$ or $\overline{\varepsilon}$) ;

CONTENTS

Appendix page

LIST OF FIGURES

LIST OF TABLES

Chapter I

INTRODUCTION

Excessive flow in natural and artificial channels usually results in widespread flooding of those flat land areas (flood plains), adjacent to the main channel. The frequency and extent of flooding are important considerations in all aspects of flood plain management and development. In rural areas, extensive flooding of low lying lands during the spring runoff period can seriously affect agricultural productivity (124). The frequent flooding of highly urbanised areas is equally catastrophic and restricts development in those municipalities unless costly flood prevention measures are introduced (18).

Clearly the adverse effects associated with widespread flooding can amount to millions of dollars annually, in both direct and indirect costs. Therefore, the prevention or mitigation of flooding through improved modelling techniques and appropriate river regulation works are prime objectives in effective flood plain management.

Persistant flooding of rivers is handled in several ways. Storage dams can be constructed to reduce peak flows and flood embankments, (dikes and levees), are frequently built to confine flood flows along the critical reaches of the system. Design of flood-control embankments requires accurate estimation of discharge in the resulting compound sections since errors in discharge prediction can lead to more frequent flooding (89,137). These errors may arise from the use of formulae developed for channels of simple cross section which do not account for the effects of the overbank flow. The 1973 flood of the Mississippi River had stages equivalent to a 200-year return period flood stage, even though the recurrence interval of the flood itself was only 30 years (6). Man-made obstructions were largely responsible for this increased flood stage.

When the flood plain zones of river channels become inundated, high shear zones develop along the junction regions (between adjacent deep and shallow sections) and momentum is transferred across these zones. The MT mechanism is a system of large-scale surface vorticies generated in the mixing region, which move downstream with a velocity equal to the local streamwise velocity in the mixing region. Research has determined that these phenomena produce changes in velocity, boundary shear stress and turbulence characteristics in the junction regions and, under certain conditions, can adversely affect system conveyance (73,93,137). Since the strength of MT is largely dependent on the transverse velocity gradient generated across the junction, one would normally expect its effect on channel conveyance to be greatest when the flood plain zones are just inundated. On the other hand, boundary roughness undoubtedly plays an important role at small flood plain depths. In general the MT's presence in the flow field has the effect of producing additional (apparent) resistance to flow in the system as a whole.

While the first assumption has been validated in earlier studies employing smooth-boundary channels (73,103,137), the effects of variable boundary roughness at small flood stages, as yet, has not been fully investigated. Since flood plain zones are normally much rougher than well-developed river channels (and in any case flood plain flows at small overbank depths are governed largely by bed friction) the present lack of research into this particular aspect of the problem is considered a major limitation.

The three principal objectives of the study were:

1. To develop improved stage-discharge predictors for compound open channel systems. Crucial to this aspect of the study was the assessment of MT effects on velocity and boundary shear stress distributions, based on experiments performed in a specially- designed laboratory channel.
2. To examine the turbulence characteristics of the junction (mixing) regions, among other things, to assist in defining the MT's effective zone of influence in both "wide" and "narrow" compound flow fields.

3. To review existing numerical models of flow in compound channels, with a view to improving simulation - particularly when the velocity differential across the junction regions is large (i.e. when the MT's effect on system conveyance is significant).

The experimental programme was performed in a specially designed symmetrical compound channel comprising a trapezoidal-shaped deep section flanked on either side by wide shallow berms (flood plains). The width of the berms was fixed, however the main channel width and depth were made adjustable so that both "wide" and "narrow" channel conditions could be satisfied in the various experiments.

The net influence of MT on system conveyance was examined by comparing, for any given flood stage, the "compound channel" discharge with the equivalent "separated channels" discharge. In addition to this the MT's effect on velocity distribution, boundary shear stress and turbulence characteristics within the mixing regions (shear zones) were also examined for a wide range of flows and boundary conditions. The aforementioned boundary roughness aspect was studied by introducing in the various experiments four different values of relative roughness (between the main channel and flood plain zones).

In chapter II, the major research contributions of past years are presented in a thematic rather than a chronological order. (This format was considered more appropriate, given the nature of the subject matter).

Theoretical considerations are dealt with in chapter III. The longitudinal depth-averaged momentum equation used in the determination of apparent shear stress merits special consideration. The latter is considered to act on imaginary interface planes separating adjacent deep and shallow zones of compound sections. The discretized form of the momentum equation is also presented in this chapter. Numerical modelling techniques are discussed in a later chapter.

Chapter IV describes the experimental channel and ancillary apparatus together with the instrumentation used and the procedures followed in the experimental programme.

Chapters V through VII present the results of the laboratory study. Chapter V compares velocity data for "wide" and "narrow" channel conditions. Velocity distribution laws (smooth and rough boundaries) are applied to those regions where the flow can be considered two-dimensional. These laws are subsequently used (chapter VI) to develop calibration curves in connection with boundary shear stress determination.

In chapter VI the effects of MT on main channel and flood plain boundary shear stress and on apparent shear stress are discussed. The techniques employed to measure these quantities are described and compared with other methods. An experimental relationship is developed through regression analysis between apparent shear stress and easily calculated geometric and hydraulic parameters of the channel. The increase in resistance to flow in the main channel is quantified by linear relationships between friction coefficients and the appropriate "single-channel" Reynolds number. These relationships are then used in an improved method developed for calculating discharge in compound channels. The method is described in later chapter.

The structure of turbulence, in particular the unique structure within the mixing regions, is presented in chapter VII. The distribution of turbulence intensities and shear stresses in the compound section are examined for both "narrow" and "wide" channel conditions. Results indicate that, if the latter condition is satisfied, the core region of the main channel flow is not affected by MT. Finally, a method for direct measurement of apparent shear stress is described.

Chapter VIII discusses the different methods available for estimating discharge in compound channels and addresses inaccuracies and questionable assumptions regarding existing stage-discharge predictors. "Single-channel" and "separate-channels" methods as well as methods based on correction factors are applied to highlight the errors incurred in discharge estimation when apparent shear stress is either ignored or only partly considered. A method based on momentum considerations is proposed which accounts for the presence of apparent shear stress and the effective increase produced in the friction factor for the main channel. The method provides superior results when compared to alternative methods currently in use.

Application of the K-ε turbulence model to assist in describing the complex flow field of a compound channel system is examined in chapter IX. While application of the model should be restricted to hydraulically "wide" channels its performance, when applied to to "narrow" compound channel conditions, was also tested using modified boundary conditions. The model produced satisfactory results for the range of conditions examined.

In the final chapter the important conclusions of the study are summarised and suggestions are offered for future research work in this area.

Chapter II

LITERATURE REVIEW

2.1 INTRODUCTION

This chapter describes the major research contributions of past years on the subject of momentum transfer in compound channels. Since these works deal with different yet related aspects of the same phenomenon, their description will be treated in a thematic rather than a chronological order.

It was also considered more appropriate to discuss past contributions on numerical modelling separately in chapter IX, where a modified numerical model based on this work is presented.

The principal experimental investigations of the past can be classified, in general terms, under 'Qualitative' or 'Quantitative' studies. The first group are those studies in which various flow visualization techniques were used to examine the large-scale interaction process between the main channel and flood plain flows. Quantitative studies, on the other hand, were concerned with developing suitable stage-discharge relationships for compound channels based on experimental observations.

2.2 PAST RESEARCH

Sellin (120) used photographic techniques to obtain qualitative information on the nature of the transfer mechanism. He dusted highly-reflective aluminum powder on the water surface of his model compound channel and photographed the surface patterns generated in the mixing regions with a camera positioned directly above these zones.

In order to highlight the secondary flow components, the camera was made to travel at a streamwise speed equal to the mean surface velocity in the junction regions. The (short-time exposure) photographic records produced in this manner were subsequently used to draw representative two-dimensional streamline patterns (a row of large eddies centered along the junction) of the surface flow.

Sellin also investigated these surface patterns with an optical system employing the Schlieren principle (121). A distribution function defining the width of and spacing between adjacent eddies was obtained using this particular technique.

Tamai and Kawahara (125) used similar flow visualisation techniques to study the complex mixing process generated in the junction regions of compound flow fields. In their experiments streak patterns on consecutive photographic plates were used to calculate longitudinal and transverse surface velocity components within the eddy structure. The hydrogen-bubble technique was also employed to measure velocity distributions at three different levels within the flood plain depth. Their stage-discharge relationship accounted for apparent shear stress acting on the main channel/ flood plain interface. The latter was related to the mean rotational velocity of the eddies (V), the scale of the eddies (L) and hydraulic characteristics of the compound channel.

Quantitative studies involve experimental measurements of such parameters as velocity, boundary shear stress and turbulence characteristics. Their main goal is the development of improved methods for better accuracy in estimating system discharge.

Hegly (43) investigated flow conditions in a canal of compound cross-section that comprised a trapezoidal main channel with a single flood plain zone. Under uniform flow conditions, water flowed independently in each section and hence discharge could be computed using conventional uniform flow formulae.

Zheleznyakov (143) performed experiments in symmetrical channels having parabolic-shaped main sections flanked by flood plain zones. He observed reductions of local and mean velocities in the main channel for conditions of low flood plain depth. At the same time, local velocities increased in that part of the flood plain zone near the main channel/ flood plain interface. He also reported on similar investigations by others on larger models in which the same general effects were noted.

In another paper (144) he introduced an important parameter which characterizes the capacity of the river channel. This is defined as the ratio of the total flow depth over the flood plain depth (n=yt/yf). Its inverse was termed the relative depth of the flood plain. He showed that for a certain value of relative depth the discharge ratio Qr/Qe (where Qr is the channel discharge) decreases to a minimum value after which it increases again. He also presented two formulae for the determination of actual discharge in natural watercourses. The first formula is based on aerial hydrometry and the second uses coefficients which account for the presence of the MT mechanism.

Sellin (120) generated stage-discharge curves for his model compound section, the isolated main channel section, the isolated flood plain zones and also for the sum of the last two components. This permitted comparison between observed and calculated discharge for the different subsections and for the system as a whole. Sellin also observed the characteristic decrease in main channel velocity associated with the "interacting" flow condition.

Rajaratnam and Ahmadi (103,104) observed velocity distributions in two compound channel systems. The first had a "narrow" main channel with two "wide" flood plain zones and the second had a "wide" main channel with a single "wide" flood plain. They found that velocities could be correlated with self-similarity laws of exponential form, (the exponents having different magnitudes for the main channel and flood plain zones). They also noted that, across much of the mixing zone, vertical velocity profiles could be calculated by the logarithmic velocity distribution (LVD) law, however the measured local shear velocity had to be used as a velocity scale. On the other hand, the LVD law did not hold in the upper portion of the main channel flow.

Ghosh (39) and Myers (73) studied the boundary shear stress distribution in both symmetrical and asymmetrical compound channels under both interacting and isolated flow conditions. They concluded that MT effectively decreases main channel boundary shear stress, while increasing flood plain boundary shear stress. Myers (71) quantified the effects of MT by expressing momentum transfer as an apparent shear force derived from the momentum equation for steady, uniform flow. The apparent shear force was found to increase with increase in flow depth to some upper value, after which it decreased. The apparent shear stress (obtained by dividing the apparent shear force by the area of channel/ flood plain interface) was found to decrease with an increase in flood plain depth. This finding supported an earlier conclusion, namely that the mechanism's effect appeared to be strongest when the channel depth just exceeded the bankfull depth.

Following these important studies it has been common practice to express MT as an apparent shear stress acting on the imaginary main channel/flood plain interface plane (either vertical, horizontal or inclined).

Ervine and Baird (30), in analysing the results of other investigators, developed a linear relationship between apparent shear stress and the differential velocity between main channel and flood plain zones.

Wormleaton et al (137) performed a multiple linear regression and expressed apparent shear stress as a function of the geometrical and hydraulic characteristics of their model channel.

A similar relationship was developed by Prinos and Townsend (92) for a compound channel comprising a trapezoidal main channel with two flood plain zones. This relationship was subsequently used in a method for estimating discharge in compound channels.

Knight and Demetriou (56) proposed a group of empirical relationships for calculating flood plain boundary shear force and apparent shear force acting on the main channel/ flood plain interface.

Because suitable instrumentation was generally not available at the time, very few past studies on this subject were concerned with the structure of turbulence in compound flow fields.

Townsend (128) studied momentum transfer phenomena in an asymmetrical compound channel, with special emphasis on the nature of turbulence in the mixing region. The turbulence field was investigated both for interacting and isolated flow conditions in the compound section. The constant-temperature anemometer method and a novel flow visualisation technique were employed to respectively measure longitudinal and cross-stream turbulence intensity levels. Townsend found that, except for the wall regions, turbulence intensities were generally much higher in the mixing zone than elsewhere in the compound flow field. At small flood plain depths maximum levels were approximately 3 times those found in the central region of the main channel flow. Moreover, although the longitudinal intensity levels in the mixing zone were found to be generally higher than the cross-stream intensity levels therein, the general increase in cross-stream intensity was found to extend much further into the flood plain zone than did the former.

Elsawy et al (29) used a Laser-Doppler anemometry (LDA) system to measure velocity distributions and turbulence characteristics in a variable-geometry compound channel. Because of the limitations of their equipment, they measured only longitudinal turbulence intensities. However, by assuming the flow was close to isotropic, they were able to compare observed normal stress in the longitudinal direction with apparent shear stress at the interface plane.

Tracy (131) also studied the structure of turbulence in a closed (pressurized) conduit of complex cross section where air was the flowing medium. He was principally concerned with the production (and effect on system efficiency) of the secondary currents in the conduit. He concluded that variation in the turbulence levels in the corner regions of the conduit was the most probable cause of the secondary motions. He also found that the transfer of air across the interface plane separating the larger from the smaller channel is small and that shear stress is also small there. Therefore methods for calculating discharge in complex channels, that are based on dividing the channel into subsections, could be used for the conditions examined.

Numerous researchers working in this area have concentrated on developing accurate stage-discharge predictors as aids in design (30,48,49,63,76,89).

Three approaches to the problem have been widely used in past studies. In the first approach the critical factor is accuracy in the estimation of hydraulic radius which is then used in an appropriate uniform flow formula (Manning, Chezy etc.). The second approach uses experimentally-derived correction factors to account for MT effects. The third is based on momentum considerations and uses a relationship incorporating the aforementioned apparent shear stress parameter.

Rice (111) and Posey (89) applied conventional methods for calculating discharge in compound channels.They divided the cross section into hydraulically homogeneous zones using various imaginary interface planes (vertical, horizontal, diagonal). The discharges were calculated separately for each zone and then summed to give total discharge. They estimated the error associated with these methods, all of which ignore the presence of the MT mechanism.

These particular methods assume no shear acting on the imaginary interface planes and hence the latter are not included in the wetted perimeter calculations. In some cases the interface was included in the main channel wetted perimeter only (implying that apparent shear stress and main channel boundary shear stress were approximately equal).

Delleur et al (24) studied uniform flow in prismatic flood plain channels that had a variety of surface roughnesses. They compared different methods of subdividing the compound cross section for the purpose of discharge computation and also compared formulae for evaluating the equivalent Manning's coefficient. None of the methods examined was considered entirely satisfactory for all possible flow conditions.

Toebes and Sooky (127) examined the hydraulics of meandering channels with flood plains. They were mainly concerned with the effects of the meander profile on system conveyance, however they also considered the junction mixing process itself. For the purpose of analysis they proposed that the composite cross section is best divided by an imaginary (fluid) boundary that is horizontal and located at the level of the flood plains zones.

Wright and Carstens (139) proposed that the interface plane should be included in the wetted perimeter calculation for the main channel only since the apparent shear stress in their channel was of the same order of magnitude as the main channel boundary shear stress. They also included apparent shear stress in the calculation of average velocity in their channel's flood plain zone. Their new method gave better results than those obtained using conventional methods.

Yen and Overton (141) established division lines of zero shear in a compound flow field, with their common origin at the junction between the deep and shallow sections. These lines need not be included in the wetted perimeter computation since the apparent shear stress is zero. They found that the inclination of the division lines varies with flood plain stage, although roughness distribution and other geometrical factors appear to have some influence on this.

Wormleaton et al (137) studied flow in channels having rough flood plain zones. They calculated the apparent shear stress for different imaginary main channel/ flood plain interfaces. Next they used an apparent shear stress ratio as a criterion in deciding whether or not to include a particular interface plane in the wetted perimeter calculation. For an apparent shear stress ratio less than 0.2 the interface plane was neglected however, when it was greater than 0.2, the plane was included in the main channel wetted perimeter calculation. For the conditions examined in their study a horizontal interface plane arrangement produced the best results.

The second approach to predicting stage-discharge relationships for compound channels employs simple correction factors derived from experimental data. These factors are then incorporated in the uniform flow calculation.

Le Van Kiyen (63) determined correction factors for both main channel and flood plain zones and then used Chezy's equation to calculate the discharge for each subsection. The correction factors were based on five empirical relationships. Their purpose was to account for the main geometrical and hydraulic factors, namely the ratio of channel to flood plain roughness, the shape of cross section and the relative depth of flow. Kiyen's method is tedious however and its application does not provide any significant improvements over other methods (93).

Karasev (49) used momentum considerations to obtain expressions involving two empirical parameters which were then combined with the Chezy equation to estimate discharge. The correction factors were derived from approximately 300 experiments and therefore can be considered quite significant from a statistical viewpoint.

James and Brown (48) determined a simple correction factor to Manning's equation based on a procedure that relates boundary roughness to certain shape properties of the channel. They named their method the "modified single- channel" approach and found that calculated discharge was very close to that observed in experiments.

Nicollet and Uan (76) proposed an empirical relationship between relative discharge in the system under interacting and isolated conditions and the system's relative roughness parameter. They also extended their discharge computation method to gradually-varied flows in compound channels.

The third approach used in the computation of system discharge incorporates apparent shear stress acting on the main channel/flood plain interface.

For smooth compound channels Ervine and Baird (30) included in their analysis a simple linear relationship between apparent shear stress and differential velocity.

A similar methodology proposed by Prinos and Townsend (93) has wider application since spatial variation in boundary roughness can be accomodated in their method.

Some of the "discharge calculation" methods referred to in this chapter were applied to the present study data for the purpose of comparing their effectiveness. The methods selected for this exercise are described, more fully, in chapter VII.

Chapter III

THEORETICAL CONSIDERATIONS

3.1 MEAN FLOW EQUATIONS

Generally flow in compound open channels is three dimensional and the fundamental equations which describe this motion are the conservation laws of mass and momentum.

For steady,incompressible flows these laws can be expressed in tensor notation as:

(1) Mass conservation (Continuity equation):

$$\frac{\partial U_i}{\partial x_i} = 0 \qquad (3.1)$$

(2) Momentum conservation (Navier-Stokes equations):

$$U_j \frac{\partial U_i}{\partial x_j} = -\frac{1}{\rho}\frac{\partial P}{\partial x_i} + \frac{\partial}{\partial x_j}\left(\nu\frac{\partial U_i}{\partial x_j} - \overline{u_i u_j}\right) \qquad (3.2)$$

where U_i U_j = components of mean velocity in x_i, x_j directions respectively ;

P = mean pressure ;

ρ = density of water ;

ν = kinematic viscosity of water ;

$-\rho\overline{u_i u_j}$ = turbulent shear stress.

Equations (3.1) and (3.2) can only be solved when the correlations between the fluctuating velocities, u u, can be determined in some way.

Physically these correlations, when multiplied by the density, represent the transport of momentum due to the fluctuating (turbulent) motion.

The quantity $-\rho\overline{u_i u_j}$ is the transport of x_i -momentum in the x_j direction (or vice versa). It acts as a stress on the fluid and is called the turbulent or Reynolds stress. In most flows and especially in fully developed flows the viscous terms of equation (3.2) are only significant in regions very close to the boundary. The turbulent shear stresses are much larger elsewhere in the flow field and hence equation (3.2) can be simplified by neglecting the viscous terms. The turbulent shear stresses $-\rho\overline{u_i u_j}$ can be determined in terms of the mean velocity using the popular concept of eddy-viscosity and Boussinesq's approximation. The above concept assumes that, in analogy to the viscous stresses in laminar flows, the turbulent stresses are proportional to the mean velocity gradients.

Using the above concept equations (3.1) and (3.2) can be written, for the longitudinal (x), vertical (y) and transverse (z) directions as :

Continuity equation:

$$\frac{\partial U}{\partial x} + \frac{\partial V}{\partial y} + \frac{\partial W}{\partial z} = 0 \qquad (3.3)$$

x - Momentum equation :

$$U\frac{\partial U}{\partial x} + V\frac{\partial U}{\partial y} + W\frac{\partial U}{\partial z} = \frac{\partial}{\partial y}(\nu_t \frac{\partial U}{\partial y}) + \frac{\partial}{\partial z}(\nu_t \frac{\partial U}{\partial z}) - g\frac{dh}{dx} + gS \qquad (3.4)$$

y - Momentum equation :

$$U\frac{\partial V}{\partial x} + V\frac{\partial V}{\partial y} + W\frac{\partial V}{\partial z} = \frac{\partial}{\partial y}(\nu_t \frac{\partial U}{\partial y}) + \frac{\partial}{\partial z}(\nu_t \frac{\partial V}{\partial z}) - \frac{1}{\rho}\frac{\partial P}{\partial y} \qquad (3.5)$$

z - Momentum equation :

$$U\frac{\partial W}{\partial x} + V\frac{\partial W}{\partial y} + W\frac{\partial W}{\partial z} = \frac{\partial}{\partial y}(\nu_t \frac{\partial W}{\partial y}) + \frac{\partial}{\partial z}(\nu_t \frac{\partial W}{\partial z}) - \frac{1}{\rho}\frac{\partial P}{\partial z} \qquad (3.6)$$

where U,V,W = components of mean velocity in x,y,z directions respectively ;

ν_t = eddy (turbulent) viscosity ;

S = slope of the channel ;

g = acceleration due to gravity ;

h = flow depth.

Equations (3.3 to 3.6) have been simplified for flows that are parabolic in the longitudinal direction. In this case the turbulent transport of momentum in the longitudinal direction is negligible and the longitudinal pressure gradient can be assumed constant over any cross section of the channel. Therefore, terms involving second derivatives with respect to x have been neglected and the original pressure term of equation (3.2) i.e $(-1/\rho \cdot \partial P/\partial x)$ has been replaced by $(-g \cdot dh/dx + gS)$.

For uniform flow conditions, equations (3.3 to 3.6) can be simplified further since terms involving the longitudinal velocity and depth gradients are zero.

3.2 DEPTH-AVERAGED MEAN FLOW EQUATIONS

In many "open channels" problems the three-dimensional portion of the flow field is of secondary importance. For example, when the channel is sufficiently "wide" (ie. the width to depth ratio is >10), it is mainly the horizontal distribution of flow quantities that is of interest and not the vertical distribution which is often nearly uniform due to strong vertical mixing induced by the bed shear.

Therefore the three-dimensional equations can be integrated over the water depth (h) assuming the pressure distribution to be hydrostatic. The resulting depth-averaged equations were derived by Kuipers and Vreugdenhil (59) as follows:

Continuity equation:

$$\frac{1}{h}\left(\frac{\partial \overline{U}h}{\partial x}\right) + \frac{\partial \overline{W}}{\partial z} = 0 \qquad (3.7)$$

x - Momentum equation :

$$\overline{U}\,\frac{\partial \overline{U}}{\partial x} + \overline{W}\,\frac{\partial \overline{U}}{\partial z} = \frac{\partial}{\partial z}\left(\overline{\nu}_t\,\frac{\partial \overline{U}}{\partial z}\right) + gS - g\frac{dh}{dx} - \frac{\tau_b}{\rho h} \qquad (3.8)$$

where $\overline{U},\overline{W}$ = depth-averaged velocities in x,z directions respectively ;

τ_b = boundary shear stress ;

$\overline{\nu}_t$ = depth-averaged eddy viscosity.

The distribution of $\overline{\nu}_t$ can be determined by a turbulence model. This model, called the depth-averaged k-ε model, is presented in chapter IX where the numerical modelling of flow in compound channels is discussed.

Equations (3.7) and (3.8) are restricted to parabolic flows only. The velocity components $\overline{U}$ and $\overline{W}$ are governed only by the continuity and the x-momentum equations. The depth-averaged (z) momentum is not needed and the vertical momentum equation is therefore reduced to the hydrostatic pressure relation. As a result of depth averaging, equation (3.8) contains the local bottom shear stress τ_b (surface shear stress is neglected) which is related to the local depth-averaged velocity $\overline{U}$ as follows:

$$\tau_b = \rho U_*^2 = \rho c_f\,\overline{U}^2 \qquad (3.9)$$

in which U_* = the local shear velocity ;

c_f = friction coefficient.

For fully developed flows the continuity equation is satisfied automatically and the x-momentum becomes

$$0 = \frac{d}{dz}\left(\overline{\nu_t}\,\frac{d\overline{U}}{dz}\right) + gS - \frac{\tau_b}{\rho h} \qquad (3.10)$$

3.3 DISCRETIZED EQUATION FOR X-MOMENTUM AND ITS APPLICATION TO COMPOUND CHANNELS

The discretized equation for x-momentum can be derived by using a control-volume formulation. With the latter, the calculation domain is divided into a number of nonoverlapping control volumes and the differential equation is integrated over each control volume. For a typical control volume (figure 1) the discretized form of x-momentum (equation 3.10) can be written as:

$$0 = (\tau_n - \tau_s)h\Delta x + \rho g S h \Delta x \Delta z - \tau_b \Delta x \Delta z \qquad (3.11)$$

where τ_n, τ_s = the apparent shear stresses acting on the n and s faces respectively ($\tau = \rho \overline{\nu_t}\, d\overline{U}/dz$).

For a symmetrical compound channel of unit length (figure 2) equation (3.11) becomes:

$$\rho g A S = \tau_c P_c + 2\tau_f P_f \qquad (3.12)$$

where A = total cross-sectional area ;
τ_c, τ_f = boundary shear stress for main channel and flood plain respectively ;
P_c, P_f = wetted perimeters of main channel and flood plain respectively.

Equation (3.12) is obtained by considering the compound channel as a control volume.

Equation (3.11) can be applied to any subsection of a compound channel. For the main channel the velocity differential between channel and flood plain generates additional internal shear, and a continuous transfer of momentum (due to turbulence diffusion) from the main channel to the flood plain zone.

Because of this interaction process equation (3.11), when applied to the main channel control volume, gives

$$\rho g A_c S = \tau_c P_c + 2\tau_a y_f \quad , \qquad (3.13)$$

where A_c = main channel cross-sectional area ;
τ_a = apparent shear stress acting on the vertical

imaginary interface ;

y_f = flow depth in the flood plain zone.

Considering the flood plain control volume (figure 2), the apparent shear stress acts in the direction of flow, hence :

$$\rho g A_f S + \tau_a y_f = \tau_f P_f \tag{3.14}$$

where A_f = flood plain cross sectional area.

Therefore equations (3.13) and/or (3.14) can be used to calculate apparent shear stress if the boundary shear stress in the main channel or the flood plain zone is known.

Similar equations can be developed for any imaginary interface plane (diagonal, horizontal etc.) by considering the appropriate "control volume" geometry. Hence apparent shear stress can be calculated for any such interface if the corresponding boundary shear stress distribution is known.

An alternative approach in the determination of apparent shear stress is its direct measurement by means of, for example, laser doppler or hot-film anemometry. The apparent shear stress for a vertical interface of a control volume (figure 2) can be written as:

$$\tau_{n,s} = \frac{1}{h}\int_{o}^{h} - \overline{\rho uw}\, dy \tag{3.15}$$

where $-\rho\overline{uw}$ = local apparent shear stress at a distance y from the boundary.

Direct measurement of uw provides local values of apparent shear stress within the flow depth and therefore its vertical distribution can be determined. The former procedure (i.e using equations (3.13) and (3.14)) does not give any information about local quantities, only a depth-averaged value. The latter, however, can be obtained from equation (3.15) and can be compared with that determined from equations (3.13) and/or (3.14). Such comparisons should indicate whether or not indirect methods for measuring boundary shear stress (e.g the Preston tube technique) can be used in complex flow fields (i.e. interaction region of compound channels) where velocity distribution laws are assumed to apply.

Direct measurement of apparent shear stress is favoured over indirect estimates (equations 3.13 and 3.14) since the latter procedure is laborious. However direct measurement has posed significant problems in the past because of difficulties associated with the use of hot-film probes in untreated water.

In this study apparent shear stress is calculated and also measured directly in the physical model using a cross-type hot-film probe. The results obtained from these two different approaches are compared in chapter VII.

Chapter IV

EXPERIMENTAL APPARATUS AND PROCEDURE

4.1 EXPERIMENTAL CHANNEL

The laboratory experiments were performed in a 12.2 m-long (plexiglass) compound channel comprising a trapezoidal shaped deep section that was flanked on either side by wide shallow berms (flood plains).

The main channel section was 10.2cm deep and its base width could be adjusted between 20.3 and 50.8 cm. The width of each flood plain section was fixed at 38.1 cm. These physical dimensions, when combined with the particular flow depths adopted in the study, produced the "narrow channel" conditions referred to in this study. A 7.2cm-high "false floor" unit was subsequently placed in the central channel section (when the latter's base width was set at 50.8cm) to produce higher width to depth ratios. Accordingly the scope of the investigation extented to "wide" as well as "narrow" channel conditions.

The flood plain zones and the channel walls were supported at 30.5cm intervals to minimize deflection. The entire channel rested on a wooden platform supported 1 m above the laboratory floor on an adjustable-slope steel frame. A general view of the channel is shown in figure 3.

The channel's inlet and outlet tanks were separate units supported on steel frames that could be easily relocated in the event of a change in channel slope. The function of the inlet tank was to supply, with minimal disturbance, smooth entrance flow to the different sections of the channel. Water entered the upstream end of the tank through a pipe fitted with a multiport diffuser. Screens and baffles were installed downstream of the diffuser to dissipate large-scale turbulence and secondary circulation in the tank. The downstream end of the tank contained a transition section which accelerated the flow smoothly from the tank to the channel. A view of the inlet tank is shown in figure 4.

The outlet tank provided a means for monitoring system discharge during the experiments. The channel flow was collected in the upstream end of the tank, it then passed through several screens and finally discharged over a calibrated weir to the main holding tank underneath the laboratory floor. Head above both the weir was measured at a manometer located an appropriate distance upstream of the weir section. A top view of the outlet tank is shown in figure 5.

An adjustable outfall weir was located at the downstream end of the channel. Its purpose was to give accurate control of the water surface in the channel since this was essential in establishing and maintaining uniform flow in the test section. The outfall weir is shown in figure 6.

4.2 MEASUREMENTS

4.2.1 Bed Slope and Water Surface Level

Precise elevation readings were taken at 30cm-intervals along the channel centreline and also along the flood plain sections. The channel bed and flood plain profiles were checked along side the "least-squares" lines fitting the data to give the effective slope. The latter was also checked by comparing it with the piezometer (static head) profile corresponding to zero discharge condition in the channel. Static head readings were taken with a cathetometer reading to 0.05mm.

Figure 7 is a sample plot of the water surface slope for a particular discharge together with the computed slope for the channel. The maximum deviation of the water surface profile from the constant (uniform) depth value did not exceed 1mm in all the experiments. Moreover this maximum deviation occurred in a section of the channel remote from the test section reach.

Local flow depth was also checked using manually-operated point gauges located at 4 measuring stations along the channel. These gauges (reading to 1mm), although not very sensitive, were very useful in the initial stages of establishing uniform-flow in the test section. The discharge control valve and the outfall weir elevation were adjusted to approximate a uniform water surface profile using the point gauges. Subsequent "fine-tuning" of the surface profile was accomplished using the precision cathetometer.

4.2.2 Boundary shear stress

Local boundary shear stress was measured by the Preston-tube technique (91). A total head tube (1.67 mm O.D.), resting on the boundary and aligned parallel to the flow, was used in conjunction with a standard static tube of the same diameter. The small diameter of the impact tube was necessary to ensure that the axis of the tube was within the "law of the wall" region, even for shallow flood plain depths. Differential pressure (between the total and static probes) was correlated with boundary shear stress using an appropriate "law of the wall". A differential pressure transducer (Validyne DP-103), of the variable reluctance type, was connected to both tubes to measure differential pressure. The main sensing component of the transducer is a thin diaphragm of magnetically permeable stainless steel, mounted symetrically between two blocks allowing only a narrow gap on either side of the diaphragm and the core. Deflection of the transducer diaphragm due to differential pressure alters the magnetic reluctance of the device. This in turn alters the value of the induction of the two coils located on either side of the diaphragm. Thin diaphragms with maximum permissible pressure 8 to 25mm of water were used for accurate measurements of low pressure in the flood plain zones.

The output voltage was displayed on a digital indicator (Validyne CD 23). Voltage readings for a given point measurement exhibited fluctuations of approximately 0.05 to 0.1

volts and were averaged over a selected number of readings using a voltmeter with a 10 secs time constant.

Prior to its use with the impact and static tubes, the transducer-indicator system was calibrated with a known static head of water. As shown in figure 8 the response of the transducer was linear up to the maximum permissible differential pressure.

When the main channel was "wide", local boundary shear stress was also measured using the velocity profile method. In applying this method local velocities in the "inner region" of the wall were measured and shear velocity and local boundary shear stress were calculated based on the "law of the wall". Both methods gave results in very close agreement (difference ±5%). A more detailed account of the methods used to measure boundary shear stress is given in chapter VI.

Water temperature was monitored at fixed time intervals during all experiments. The thermometer, which was located just downstream of the test section, indicated only minor fluctuations in temperature (up to $\pm 0.2^{\circ}$ C) during the experiments.

4.2.3 Velocity Measurements

Local velocities were measured using a commercial Pitot tube (4mm O.D) and a miniature current flowmeter system (Nixon-403) designed for measuring very low velocities. In zones of relatively low velocities the Pitot tube was also used with a precision inclined manometer (angle of inclination 10° degrees).

The calibration curve for the differential pressure transducer is shown in figure 8. The curve was checked by taking velocity measurements at the centre line of a "wide" channel, where a logarithmic velocity distribution occurred. The same procedure was repeated for the Pitot tube connected to the inclined manometer and similar results were obtained.

The Pitot tube was used to measure velocities close to both the channel boundaries and free water surface and also on the flood plain zones at low flood plain depths. Because of its greater size the propeller meter was restricted to measurements in the main body of the channel flow. It had a measuring head with a cage approximately 15mm diameter and hence measurements could not be taken closer than 7.5mm from the boundary or the free surface.

The system was highly sensitive, in that it measured velocities as low as 2.5cm/sec with an accuracy of ±5% (for the range 2.5-7.5cm/sec), ±2% (from 7.5-15cm/sec), and ±1% (from 15-150cm/sec). The measuring head of the current meter consists of a five bladed rotor mounted on a hard stainless steel spindle. The spindle terminates in fine burnished conical pivots which run in jewel bearings mounted in an open frame. Frictional torque is thus extremely low and results in a linear output over a wide range of velocities.

The head is attached to the end of a stainless steel tube containing an insulated gold wire terminating 0.1 mm away from the rotor. The probe is connected to an electronic counter via a co-axial cable.

When the rotor is immersed in flowing water, the passage of the rotor blades past the gold wire tip slightly varies the measurable impedance between the tip and the tube. This variation is used to modulate a 15Khz carrier signal generated within the indicating instrument which in turn is applied to the electronic detector circuits. Automatic compensation is made for change in liquid conductivity and following amplification and filtering of the carrier frequency a square wave signal is obtained.

In the digital indicator (type 401/412) the pulses are counted over a known time period to obtain a digital reading. The display is automatically updated every 1 or 10 seconds (depending on the selected range) but a new measuring period may be started manually by pressing the Manual Reset/start button.

A calibration chart relating frequency to linear velocity was provided by the company and was checked in the laboratory against measurements made by the Pitot tube. The probes used for boundary shear stress and velocity measurements are shown in figure 9.

4.2.4 Turbulence characteristics

A commercially available cross hot-film probe (TSI 1243-60W boundary layer probe) was used to measure turbulence characteristics in the laboratory channel (figure 10). The probe has two cylindrical elements containing thin platinum films (sensors) that are insulated from the surrounding fluid by a thin coating of quartz. The coating eliminates the chemical and electrochemical side effects arising from the use of pure platinum elements. Also, because of the strength of the film, the sensor can be cleaned without fear of damage or rapid deterioration. The 0.15mm diameter elements have 2.0mm sensing length, are 1.0mm apart and are oriented at +45 degrees to the mean flow direction.

The probe was connected to two constant-temperature anemometers (TSI 1050), an analog correlator (DISA 55D70) and two DC/RMS voltmeters (TSI 1076). The constant temperature (constant resistance) mode of operation was used. Using a feedback system, the electrical current fluctuates with the fluctuating velocity (the film's electrical resistance is kept constant). The electronic equipment used in the study is shown in figure 11.

The hot-film probe was calibrated before each experiment against a known velocity range , hence a relationship between output voltage E and velocity U was obtained for both elements (figure 12). This relationship was used to convert voltage fluctuations to velocity fluctuations assuming that the change in slope (dE/dU) of the calibration curve is small over the observed range of the velocity fluctuations. Hence the tangent to the voltage /velocity curve, at the given mean velocity, was used to convert voltage fluctuations to velocity fluctuations.

Special care is required when using hot film probes in (untreated) water system. Foreign materials in ordinary "tap" water (dust fibres, rust particles etc.) can damage the probe. Also microscopic air bubbles tend to collect on the sensors after a short period of use and these tend to produce instability in the signal. This occurs because the transient air bubbles isolate parts of the sensor from the surrounding fluid and consequently there is an uneven heat distribution on the element. To reduce the possibility of these occurrences, fine mesh filters were installed at the downstream end of the entrance tank and, before taking readings, the system was run for a long period to remove dust particles on the channel walls. Also the sensing elements were cleaned periodically during each experiment with a camel-hair brush to prevent possible buildup of air bubbles and dust particles on the sensors.

The working principle of hot-film anemometry is given in chapter VII along with an analysis of the turbulence measurements.

4.3 EXPERIMENTAL PROCEDURE

Before commencing the main experimental programme, a series of experiments was performed in the channel to locate the test section and check the flow characteristics therein. Velocity traverses were made at sections 6, 7.5 and 9 m downstream from the entrance section. The resulting isovel patterns indicated that flow over this reach of the channel was fully-developed and not influenced by either "entrance" or "outlet" effects (figure 13). As a result of these observations it was decided to locate the test section 9 m downstream from the entrance section.

Another series of experiments was performed to determine velocity and boundary shear stress distributions in the test section for different stage-discharge conditions in the channel. Observations confirmed that both distributions were essentially symmetrical about the channel centreline therefore, while periodic checks were made from time to time in the other half of the cross section, most observations were made in one or other half of the channel cross section.

Close to uniform flow was established along the test reach of the channel by fine adjustments to the supply line control valve and variable height outfall weir.

The Preston tube was used to record differential pressure at intervals of 15-25mm, along the perimeter of compound channel. A specially-developed computer program converted pressure readings to local boundary shear stress values. The same program was also used to calculate the compound channel's average value (applying the trapezoidal rule) and compare the latter with the average value estimated from energy considerations. The errors were generally small (no larger than ±4.2%) and were considered acceptable.

Point velocities were measured at 15 positions within each vertical and at 15 locations across the channel. Individual values were checked by numerical integration of the depth-averaged values over the width of the compound channel. The calculated mean section value was compared with the corresponding mean value obtained from the continuity equation. Since the error for all the experiments was less than +5% (and as this was considered as an acceptable error) no adjustments of local velocities were made.

Turbulence intensities and shear stresses were measured at 15 representative verticals of the compound section.

For measurements of the $-\rho\overline{uv}$ shear stress and the streamwise (u') and vertical (v') turbulence intensities the hot-film probe was used directly in the x-y plane vertical to the channel bed. In the case of the ($-\rho\overline{uw}$) apparent shear stress, additional inclined measurements were required with the probe axis inclined at 30° to the vertical. An indication of the accuracy of this procedure is seen by comparing streamwise turbulence intensities measured by the probe in the vertical and then in the inclined position. The maximum discrepancy between the two values amounted to ±5% only.

However, measurements taken in the "wall" regions of the flow field were subject to larger errors since the mean velocity distribution along the sensing elements is not uniform. Observations close to channel walls therefore were considered less reliable than elsewhere.

When the main channel was made hydraulically "wide", measurements taken at the centre of the compound channel were compared with similar measurements for "wide" channels of simple cross section reported by other investigators and also with theoretical values derived from the Navier-Stokes equations for two-dimensional flow. The study data was found to agree closely with the theory as well as with the observations reported by others.

For each channel base width flood plain depths varied between 10 and 50mm and different flood plain boundary roughnesses were used. The flood plain zones were artificially roughened by attaching to them different grades and patterns of wire mesh. The first two were "square grid" wire meshes (6.4 and 3.2 mm squares; 1.1 mm thick) and the third was a coarser "diamond pattern" (1.6 mm thick). A separate series of tests to determine Manning's n for the three meshes gave corresponding values of 0.014, 0.018 and 0.022. Figure 14 shows samples of the three wire meshes used in the study.

4.4 REVIEW OF ERROR ANALYSIS

An error analysis was performed for both measured and calculated parameters for the sample data associated with the first series of tests (i.e. based on "wide" channel conditions). Table 1, Appendix A lists an estimate of the error for all the variables considered. A sensitivity analysis for the main parameters of the study is included in this section.

For discharge computation based on the "single channel" method, the estimated error in discharge is approximately ±7.5% when the errors in channel slope, cross-sectional area and hydraulic radius are assumed to be ±5%, ±2.5% and ±3.5% respectively. Similar errors are obtained when other methods are used for the calculation of discharge.

For the calculation of apparent shear stress, through momentum balance considerations, the estimated error is about ±14% when the errors for the weight force, the bed shear stress and the flood plain depth are taken as ±7%, ±4% and ±3% respectively. The latter errors have been obtained from an error analysis of the primary variables associated with the above quantities.

In turbulence measurements an assumed ±6% error in $(e_1+e_2)'$ together with an estimated ±3% error in S_1 result in ±9% in u'. On the basis of these a ±11% error is assigned to longitudinal turbulence intensity u'/U. Similarly, in the calculation of the vertical turbulence intensity v'/U, an error of ±9% occurs whith errors in the measurements of $(e_1 - e_2)'$ and S_1 of ±4.5% and ±3.0% respectively.

The greatest error occurs in the calculation of shear stress - uv since signals of the same order of magnitude are squared and then subtracted. For example: ±3.0%, ±4.0% and ±3.0% errors respectively in e_1', e_2' and S_1 result in a ±20.0% error in shear stress. This indicates that, even with the most careful measurements, we should expect significant errors in the estimation of turbulent shear stress.

Chapter V

ANALYSIS OF VELOCITY MEASUREMENTS

5.1 MOMENTUM TRANSFER EFFECTS ON SYSTEM VELOCITY DISTRIBUTION

Detailed isovels patterns were plotted for both "wide" and "narrow" channel conditions in the system. Figure 15 (a and b) shows two typical patterns for a "wide" channel condition with smooth and roughened flood plain zones respectively. The relative depth in each case was 0.33. The MT mechanism was found to reduce, only slightly, local velocities in the mixing region and did not affect the central region of the channel flow nor the region of the flood plain flow remote from the junction where two-dimensional flow conditions apply. Maximum velocities were measured at the water surface for all verticals, except those near the flood plain side walls. In the latter case the maximum velocity filament was observed below the water surface.

For "wide" channel conditions the isovel pattern remained essentially unchanged for all values of relative roughness. However in subsequent experiments, when the central channel satisfied "narrow" conditions, the flow field in the central region was found to be sensitive to change in the flood plain boundary roughness. The general isovel pattern remained essentially unchanged when the relative depth was increased to 0.5 (Figure 16). MT however, is clearly weaker as a result of the reduced velocity differential between the main channel and flood plain zones.

In general, for "wide" central channel conditions, average velocities in the main channel were found to be only 2-15% less than those calculated under isolated conditions (using Manning's equation). Figure 17 indicates the decrease of actual mean channel velocity with regard to the isolated channel velocity for different relative depths. The decrease is not significant from a practical viewpoint because of the "wide" conditions and large relative depths. In the flood plain zones measured velocities, for both smooth and roughened boundary conditions were 15-30% greater than those calculated (figure 18).

The decrease of velocity in the main channel and the corresponding increase in the flood plain (with regard to the isolated flow conditions) are both seen to increase with increasing relative roughness (figures 19 and 20).

Sample isovel patterns for a "narrow" central channel reflecting both smooth and roughened flood plains, are shown in figure 21 (a and b) respectively. As expected, because of the "narrow" condition, the maximum velocity filament is depressed below the water surface. Similar experiments using different degrees of flood plain roughness demonstrate that submergence of the maximum velocity filament increases with an increase in the relative roughness parameter.

Under "narrow" channel conditions the corresponding average velocities in the main channel were found to be significantly smaller than those calculated under isolated conditions.

Figure 17 indicates the discrepancy between observed and calculated mean velocity (under isolated conditions) in the channel section for various relative depths. The discrepancy is large at small relative depths (22% decrease for a 0.089 relative depth) and becomes increasingly smaller with increasing relative depth (8 % decrease for a 0.32 relative depth). This confirms that MT becomes progressively weaker as the relative depth parameter approches unity.

A significant increase in the streamwise velocity component (with regard to isolated flow conditions) was observed in the flood plain zones, especially for low flood plain depth and high relative roughness. Figure 18 shows the ratio of observed mean flood plain velocity over mean "isolated" velocity for various relative depths indicating the increase in flood plain velocity under interacting conditions. This increase is maximum for the lowest flood plain depth (70 % for a 0.089 relative depth) indicating the highest lateral velocity gradient in the interaction region. With increasing relative depth the lateral velocity gradient decreases and hence the velocity in the flood plain zone tends to approach its undisturbed value. In this instance, the main channel/flood plain flow interaction is negligible and hence total discharge in the system can be calculated by conventional methods.

The decrease of velocity in the main channel is more pronounced with increase of relative roughness. For an increase of relative roughness of 100% the velocity is decreased by 35% and 15% for relative depths 0.089 and 0.32 respectively. This is also demonstrated in figure 19 where relative velocity is plotted versus relative roughness for various flood plain depths.

The higher lateral velocity gradient occurring between smooth channel and rough flood plains results to a greater increase of velocity in flood plains as figure 20 indicates. For an increase of relative roughness 100% we observe an increase up to 92% in flood plain mean velocity, for low relative depths.

5.2 VELOCITY DISTRIBUTION LAWS

5.2.1 Smooth Boundaries

As demonstrated by Keulegan (53), for a two-dimensional flow field the distribution of velocity in the vertical direction (outside of the viscous sublayer) is described by the Prandtl-von Karman logarithmic equation. This equation can be derived using Prandtl's concept of "mixing length" and, for hydraulically smooth boundaries, its final form is

$$\frac{u}{U_*} = 5.75 \log \frac{U_* y}{\nu} + 5.5 \qquad (5.1)$$

where u = local mean velocity ;

y = vertical distance from the boundary.

Equation (5.1) was verified through velocity measurements taken in regions of the flow field where two-dimensional flow conditions apply. These regions included the central part of the main channel flow, for "wide" channel conditions only and also those parts of the flood plain zones remote from the interaction regions and the side walls. The latter were found to lie between approximately 75mm and 125mm from the flood plain side walls for "narrow" channel conditions and between 75mm and 200mm for "wide" channel conditions.

Figure 22 indicates good agreement between the measured data and equation (5.1) for the conditions examined.

5.2.2 Rough Boundaries

When the flow is "fully rough" ($U_* K_s/\nu > 70$, where K_s is the equivalent sand grain roughness) Keulegan (53) suggests the following relationship:

$$\frac{u}{U_*} = 5.75 \log \frac{y}{K_s} + C \qquad (5.2)$$

in which $C = 8.5$.

In the transition region ($3.5 < U_* K_s/\nu < 70$) the coefficient C is not constant but depends on the value of $U_* K_s/\nu$.

Nikuradse (77) divided the transition region into the following categories with the appropriate coefficient value:

$$3.5 < \frac{U_* K_s}{\nu} < 7.1 \qquad C = 3.5 \log \frac{U_* K_s}{\nu} + 6.59 \qquad (5.3)$$

$$7.1 < \frac{U_* K_s}{\nu} < 14.1 \qquad C = 9.58 \qquad (5.4)$$

$$14.1 < \frac{U_* K_s}{\nu} < 70 \qquad C = 11.5 - 1.62 \log \frac{U_* K_s}{\nu} \qquad (5.5)$$

Equation (5.2) can be expressed in the form of equation (5.1). For example equation (5.2), with C equal to 8.5, is equivalent to

$$\frac{u}{U_*} = 5.75 \log \frac{U_* y}{\nu} - 2.11 \qquad (5.6)$$

with the substitution $U_* K_s/\nu = 70$ (which is the lower limit for fully rough turbulent flow). The form of equation (5.6) has the advantage of being independent of the roughness size and clearly indicates the various flow regimes (Figure 22). The only problem is in the determination of the correct datum from which to measure the distance y. This problem is discussed in the following section.

For those experiments involving artificially-roughened flood plains, the form of equation (5.6) was adopted and the coefficient C determined. As indicated in figure 23, a transitional flow regime prevailed for the first two flood plain roughness conditions while a fully-rough flow regime was dominant for the third boundary roughness (figure 24). The value for C was calculated for each condition examined and these values are presented in table 9 (Appendix B).

The shear velocity was calculated (equation 5.2) by plotting measured velocities against distance from the boundary (figure 25) and estimating the slope of the best-fit line. A correction of 0.15 times the Pitot tube diameter was applied to the distance measurement (y) to account for the displacement effect.

5.2.3 <u>The Zero Velocity Datum</u>

Care is required in determining the appropriate "zero velocity" datum when a total head tube is used to measure velocity and boundary shear stress close to rough surfaces.

Datum selection can be by trial and error by plotting y versus u for various datum planes until the best fit logarithmic plot is obtained. This method has been used by Hollingshead (45) in experiments on rough surfaces consisting of closely packed hemispheres. In his study the datum was considered to lie at an elevation 0.2 diameters below the tops of the hemispheres.

Nikuradse (77) defined the origin from which to measure distance from the wall as the surface of an imaginary cylinder having a volume equal to the measured volume of water contained in a known length of pipe. Schlichting (119) plotted velocity profiles from the same origin, as determined by Nikuradse, whereas Keulegan (53) used the top of the roughness elements as the origin for y.

Einstein and El-Samni (27) found that, for a surface consisting of closely packed hemispheres, the logarithmic velocity distribution law is valid if distances are measured from a hypothetical surface 0.2 diameters below the tops of the hemispheres. On the other hand Blinco and Partheniades (9) found that the hypothetical surface lies 0.27 times the average roughness height below the plane joining the tops of fairly uniform roughness particles.

Yen and Overton (141), while studying "shape" effects on resistance in flood-plain channels, determined the effective boundary by trial and error using Manning's equation. The effective boundary value was chosen so that the slope of the line of best fit would equal 1/n when the conveyance term $Q/S^{1/2}$ is plotted against the $AR^{2/3}$ term on linear graph paper.

Zippe and Graff (145), in a study on turbulent boundary layers over permeable and non-permeable surfaces, used the "velocity-defect" law to calculate the friction velocity and the law of the wall to determine the zero velocity datum.

In the present study the zero velocity datum was calculated by a trial and error procedure, similar to that used by Yen and Overton (141), using Manning's equation. The three zero datums were found to be 0.2, 0.27 and 0.41mm (measured from the top of the roughness elements) for Manning's coefficients 0.014, 0.018 and 0.022 respectively.

Chapter VI

ANALYSIS OF BOUNDARY SHEAR STRESS MEASUREMENTS

6.1 INTRODUCTION

Traditional methods for determining boundary shear stress in a two-dimensional flow field were developed based on an appropriate "law of the wall". Typical methods for smooth and rough boundary systems are described in sections 6.2 and 6.3 respectively. Their application to compound channel flow is described in section 6.4 along with certain assumptions regarding the structure of the mixing region flow field. The effect of the mixing region flow on main channel and flood plain boundary shear stress is discussed in section 6.5 and its effect on apparent shear stress (acting at the imaginary main channel/flood plain interface) is discussed in section 6.6. Finally, friction factor relationships developed for the deep section of the compound channel, are presented in the last section and are used later in the proposed method for estimating discharge in compound channels.

6.2 SMOOTH-BOUNDARY TECHNIQUES

Various direct and indirect methods are available to determine boundary shear stress distribution in smooth channels.

Direct methods have been performed in both air and water systems by measuring the shear force acting on an element of the channel boundary (12,87). The instrumentation, although simple in principle, requires precise construction and careful use. It should be noted that many of these instruments are designed to measure shear stress at a predetermined fixed point on the channel boundary and hence are generally unsuitable for determining boundary shear stress distribution.

Indirect techniques, on the other hand, are based on theoretical assumptions relating the measured quantity to boundary shear stress. One of the standard indirect methods is based on momentum balance considerations and requires measurement of the streamwise pressure gradient. The method can be applied easily to simple-geometry systems (straight uniform ducts, circular pipes) where, for fully developed flows, the boundary shear stress is essentially uniform.

Another indirect method requires measurement of apparent shear stress in the system. If shear stress is measured at two points near the wall in a turbulent boundary layer, an extrapolation based on an assumed linear variation of shear stress yields the local value of boundary shear stress. The apparent shear stress $-\rho\overline{uv}$ depends on measurements of the cross-correlation parameter uv. Such measurements in water channels introduce certain difficulties when hot-film probes are used and therefore widespread application of this method in past years has been limited.

The most commonly used indirect methods are the "velocity profile" method and the "Preston tube" technique. The first method assumes a logarithmic velocity distribution and requires measurement of velocity profiles along lines normal to the channel boundaries. The second approach, which uses a total head tube in contact with the channel boundary to measure local shear stress, was developed by Preston (91).

Both these methods are discussed in some detail in the following sections.

6.2.1 Velocity Profile Method

Equation (5.1), which describes the velocity distribution in smooth two -dimensional flow, is used in the determination of boundary shear stress. The equation can be written in the form :

$$U_* = \frac{u_2 - u_1}{5.75 \log \frac{y_2}{y_1}} \qquad (6.1)$$

where u_1 = local velocity measured at y_1 ;

u_2 = local velocity measured at y_2 .

Hence local shear stress can be calculated using two or more point velocities measured within the region where equation (5.1) is valid and evaluating the ratio on the right side of equation (6.1). While this particular method gives good results in the case of a smooth-boundary system, it has the disadvantage of being a laborious procedure.

6.2.2 Preston Tube Technique

In 1954, Preston (91) suggested a method for measuring shear stress on a smooth boundary using a total head tube resting on the boundary. The method is based on the concept of universality of the "law of the wall" in turbulent wall shear layers.

Dimensional analysis of the important parameters leads to a wall law of the form:

$$u/U_* = f\ (y\,U_*/\nu) \qquad (6.2)$$

Replacing mean velocity with the pressure difference recorded by a pitot tube resting on the wall, equation (6.2) becomes:

$$\Delta p/\tau_w = f_1\,(U_* d/\nu) \qquad (6.3)$$

where $\Delta p = p - po$ = dynamic pressure d = external diameter of the Preston tube

Finally the above relationship can be written in the form:

$$\frac{\tau_w d^2}{4\rho\nu^2} = f_2\left(\frac{\Delta p d^2}{4\rho\nu^2}\right)$$

$$\text{or} \quad \tau_{w*} = f_2(\Delta p_*) \tag{6.4}$$

This last relationship provides a convenient way to determine boundary shear stress since the latter is uniquely related to the dynamic pressure. For a pitot tube of given size, the function f_2 can be determined from experiments where the boundary shear stress is measured by another means (for example, in pipe flow experiments, boundary shear stress can be deduced from pressure drop measurements). Preston produced equations relating the above quantities, both for the case of a laminar sublayer enveloping the tube and when the tube is in a turbulent boundary layer.

In the original study by Preston, the ratio of the internal to external diameter of the tube was kept approximately equal to 0.6, however later experiments by Patel (85) and Rajaratnam and Muralidhar (107) have shown that it is not especially important to adopt this particular value.

Preston demonstrated that the maximum thickness of the region, in which dynamic similarity may be expected to apply, is approximately one-fifth of the boundary layer thickness. This finding emphasizes the importance of not exceeding the maximum thickness through the use of Preston tubes with outside diameters exceeding the former.

Over the years, many investigators (37,41,78,85) have performed experiments to check Preston's original calibrations and also extend the use of his technique to measurements in developing boundary layers etc.

In his pipe flow experiments Patel (85) published experimental calibration curves for the three regions of the boundary layer. His relationships are:

$$\log \tau_{w*} = \frac{1}{2} \log \Delta p_* + 0.037 \qquad \text{for } \log \tau_{w_*} < 1.5 \qquad (6.5)$$

$$\log \tau_{w*} = 0.8287 - 0.1381 \log \Delta p_* + 0.1437 (\log \Delta p_*)^2 - 0.006 (\log \Delta p_*)^3$$
$$\text{for } 1.5 < \log \tau_{w*} < 3.5 \qquad (6.6)$$

$$\log \Delta p_* = \log \tau_{w*} + 2 \log (1.95 \log \tau_{w*} + 4.10) \qquad (6.7)$$
$$\text{for } 3.5 < \log \tau_{w_*} < 5.3$$

These three relationships correspond roughly to the three regions in the velocity profile, namely : the viscous sublayer ($U_* y/\nu < 5.6$), the transition region ($5.6 < U_* y/\nu < 55$) and the logarithmic region ($55 < U_* y/\nu < 800$). He also deduced the values of the coefficients in the logarithmic law of the wall (for the fully turbulent region) using a displacement of the effective centre of the Pitot tube given by MacMillan (67).

Head and Ram (41) pointed out that calibrations in the form of equations (6.5) to (6.7) are somewhat inconvenient to use, particularly equation (6.7) which is implicit in the unknown parameter. They suggested a modified relationship based on the expression

$$\frac{\Delta p}{\tau_w} = F\left(\frac{\Delta p d^2}{\rho \nu^2}\right) \qquad (6.8)$$

This form has the advantage that the dependent variable varies only over a range of about 25 over the entire calibration range, whereas the parameter used by Patel varies by several orders of magnitude.

Nitsche (78), on the other hand, produced his calibration curve by numerical integration of the wall laws for turbulent "flat plate" flow and fully-developed pipe flow developed by van Driest (26). His results were found to be in close agreement with those of Patel (85).

The Preston tube technique has been widely applied in hydraulically-smooth open channel flow experiments. Ippen and Drinker (47) employed a 7th power law to extend the original relationship, developed for pipe flow, to open channel flows.

Ghosh and Roy (37) favoured the Karman-Prandtl velocity distribution for flow in channels having a depth to width ratio less than 0.5. They developed a pressure-shear relationship and also showed the differences in this relationship based on different velocity distribution laws.

Other investigators (55,71) applied Patel's experimental calibration curve directly to open channel flows. However, in these cases analysis is subject to errors arising from minor differences between the Karman-Prandtl coefficients and those derived by Patel.

This feature is demonstrated in figure 26 where a computational calibration curve, based on the Karman-Prandtl velocity distribution, is compared with the experimental calibration curves of Patel, Preston and Ghosh. The former was developed using the relationships:

$$\Delta p = \frac{1}{2}\rho u^2 \qquad (6.9)$$

$$\tau_w = \rho U_*^2 \qquad (6.10)$$

and therefore $\frac{\Delta p}{\tau_w} = \frac{1}{2}\left(\frac{u}{u_*}\right)^2$ (6.11)

or $$\frac{\Delta P_*}{\tau_{w_*}} = \frac{1}{2}\left[5.75 \log\left(\frac{u_* dk}{2\nu}\right) + 5.5\right]^2 \qquad (6.12)$$

where k is a displacement factor and equal to 1.3.

The parameter τ_{w_*} can be expressed as:

$$\tau_{w_*} = \left(\frac{U_* d}{2\nu}\right)^2 \qquad (6.13)$$

hence, combining equations (6.12) and (6.13), we obtain for the computed calibration curve :

$$\frac{\Delta p}{\tau_{w_*}} = \frac{1}{2}\,[5.75 \log(k\sqrt{\tau_{w_*}}) + 5.5]^2 \qquad (6.14)$$

Equation (6.14) and Ghosh's calibration curve are in close agreement since both utilise the same logarithmic velocity distribution law. Equation (6.14) is in close agreement with Patel's calibration for $\log(\Delta pd^2/4\rho\nu^2) > 4.4$ while the error is significant for $3.0 < \log(\Delta pd^2/4\rho\nu^2) < 4.4$.

Preliminary experiments validated the use of equation (6.14) for the conditions examined, hence it was used in the present study to convert pressure readings to local boundary shear stress values.

6.3 ROUGH-BOUNDARY TECHNIQUES

6.3.1 Velocity Profile Method for Rough Boundaries

Equation (5.2) is used to determine boundary shear stress in rough turbulent flows. It can be written in the form of equation (6.1), hence the values of C and Ks need not be known initially. It is necessary though, to determine the correct datum from which to measure y in order to plot y versus u. This problem has been discussed in detail in chapter V where the analysis of velocity measurements in compound channel flow was presented.

6.3.2 Preston Tube Technique for Rough Boundaries

For the general case of steady, two-dimensional uniform flow over a rough boundary, the dynamic pressure p measured by an impact tube is a function of the following parameters:

$$\Delta p = f(\rho, \mu, U_*, K, d) \qquad (6.15)$$

where K = roughness height.

Using dimensional analysis equation (6.15) can be expressed as:

$$\frac{\Delta p}{\tau_w} = f\left(\frac{U_* K}{\nu}, \frac{d}{K}\right) \qquad (6.16)$$

For fully rough flow the ratio $\Delta p/\tau_w$ depends only on d/K and therefore using equation (5.2) we can define the following relationship, in the determination of boundary shear stress, as:

$$\frac{\Delta p}{\tau_w} = \frac{1}{2}\left(5.75 \log \frac{y}{K_s} + 8.5\right)^2 \qquad (6.17)$$

which implies that with a fixed roughness and tube size the ratio is constant. This is not the case for the transitional flow regime since the coefficient 8.5 does not remain constant and hence the equation used must reflect the particular flow condition examined.

Different investigators have used equations similar to equation (6.17) to determine boundary shear stress on rough surfaces. Hwang and Larsen (46) used the logarithmic velocity distribution with Nikuradse's constants integrated over the area of the opening of the impact tube.

Ghosh and Roy (37), using Keulegan's resistance formula and analysing the experimental results of other investigators, derived an expression for velocity distribution in open channel flow which accounts for artificial roughness. However their results did not compare favorably with those values obtained using the velocity profile method or by direct measurement.

Hollick (44) used Nikuradse's equation for velocity distribution over a fully rough surface to develop a theoretical calibration for a Preston tube on a sand-roughened boundary. The main problem associated with this procedure is determination of the effective boundary position. He suggested the use of a square plate close to the tube's mouth for consistent positioning over the sand grains.

Hollingshead (45) used the Preston tube technique to measure boundary shear values on a boundary roughened by hemispheres at their maximum possible density. He reported fairly accurate local boundary shear stress measurements with the tube resting on the tops of the roughness elements.

6.4 BOUNDARY SHEAR STRESS IN COMPOUND OPEN CHANNELS

Determination of boundary shear stress distribution constitutes the most essential part of any research concerned with resistance to flow in compound channels. Changes in local boundary shear stress, produced by the complex mixing processes in the junction regions, can locate potential sites for excessive deposition or scouring action.

Also the average main channel and flood plain boundary shear stress are needed to quantify momentum transfer across the junction regions.

The Preston tube technique is widely employed to measure local boundary shear stress in channels of simple cross section. Moreover its use has been extended to studies dealing with flow in compound channels with excellent results.

The method assumes that the law of the wall applies in those regions close to solid boundaries, including the region near the main channel- flood plain interface where the mixing process is obviously very strong. Also, for rough surfaces the law of the wall can apply when suitable parameters describing the rough boundary have been identified. Most of the past studies on compound channel hydraulics, however, were performed in smooth boundary systems where no appreciable difficulty arises.

Ghosh and Jena (39) applied the law of the wall to hydraulically-smooth flow in a compound channel and used an integration procedure similar to that presented by Huang and

Larsen (46) to obtain an expression relating the measured dynamic pressure to the corresponding local shear stress.

Myers (73) also used the Preston tube technique to measure shear stress distributions around the periphery of an asymmetrical compound channel, consisting of a deep section and one flood plain. Myers used Patel's methodology (85) to convert differential pressure reading to boundary shear stress. He emphasized the importance of using Preston tube diameters not exceeding, even at the lowest flood plain depth, the limit of one fifth of the boundary layer thickness recommended by Preston (91). Average boundary shear stress for the compound section was found to be in close agreement with shear stress calculated from energy balance considerations.

Other investigators (56,103,104) have successfully used the Preston tube technique along with Patel's relationship to measure shear stress on smooth surfaces.

On the other hand, few studies of this type have dealt with measurements of shear stress in rough-boundary systems. Apart from the inherent difficulties associated with measurements near rough boundaries, the increased momentum transfer levels create additional problems when attempting to measure boundary shear stress in the junction regions of compound channels.

Ghosh and Jena (39) assumed that velocity distribution relationships for simple, artificially-roughened channels also apply to flow in roughened compound channels. They developed slightly modified equations relating local shear stress to dynamic pressure readings for compound systems.

In a related paper, Ghosh (38) used a modified velocity distribution developed by Nece and Smith (75), and applied this to hydraulically smooth, transitional and hydraulically rough surfaces. He determined the sand roughness height Ks from a "resistance" chart provided by McDowell (69) and used an indirect solution to determine local shear stress.

Wormleaton et al (136) reported some difficulties in their attempt to measure local boundary shear stress in roughened flood plain zones. Their approach was to calculate average flood plain boundary shear stress from momentum balance considerations once the local shear stress in the smooth main channel was known.

In present study, both the velocity profile method and the Preston tube technique were used in the determination of local boundary shear stress.

For a "wide" channel condition (smooth flood plains), both methods were applied along the perimeter of the compound section ; using equation (6.1) in the velocity profile method and equation (6.14) in the Preston tube technique. The average boundary shear stress for each subsection was then calculated using the two methods and was found to be in close agreement (Error ± 5%).

Sample boundary shear stress distributions by the two methods are presented in figure 27. Small differences between the two distributions appear in the junction regions where boundary shear stress calculated using the velocity profile method is somewhat higher. These local discrepancies are partly attributed to inaccuracies associated with estimating boundary shear stress using the velocity profile method in these regions of the cross section.

Once the calibration curve (equation 6.14) was validated for the flood plain zones and those regions near the channel walls, the Preston tube technique was extensively employed throughout the experimental program. The velocity profile method was only used to calculate shear stress in those regions where the parameters of equation (6.14) had to be estimated.

The average boundary shear stress for each subsection was then calculated and the apparent shear stress values determined from equations (3.13) and (3.14). The close agreement between the two values was a clear indication of the suitability and accuracy of the methods used in the measurement of local boundary shear stress.

When the flood plain zone was artificially roughened, measurement of local boundary shear stress therein was by the Preston tube technique using the following equation:

$$\frac{\Delta p_*}{\tau_{w_*}} = \frac{1}{2} [5.75 \log (k \sqrt{\tau_{w_*}}) + C]^2 \qquad (6.18)$$

The displacement factor K_r accounts for the distance from the zero velocity datum to the top of the roughness elements and also the displacement of the tube and takes the values 1.54, 1.62 and 1.79 for the three boundary roughness elements used in the study. The coefficient C was calculated in chapter V and its values are listed in table 8 (Appendix I). Equation (6.18) was validated by comparing values of boundary shear stress obtained from the velocity profile method with those calculated using equation (6.18).

Accordingly equation (6.18) was used to convert differential pressure measurements to boundary shear stress in the flood plain zone (assuming that two-dimensional flow conditions apply in a limited portion of the flow depth in the junction region). This assumption was checked by comparing apparent shear stress calculated separately from the flood plain and main channel measurements through equations (3.13) and (3.14). Such comparisons indicated generally good agreement.

In experiments where significant differences were found between the two apparent shear stresses, the apparent shear stress was calculated from a momentum balance in the main channel. The latter value was then adopted in subsequent calculations. Typical boundary shear stress distributions for smooth and rough flood plain conditions are shown in figure 28. In the main channel boundary shear stress decreases from a maximum value at the channel centreline to a minimum value at the channel corner. Along the inclined channel side walls shear stress increases from the channel corner to approximatelly the middle of the wall and then decreases again as the junction is approached. In the flood plain, boundary shear stress decreases continuously from a maximum value at the interface plane to a two-dimensional value and then decreases again as the flood plain side wall is approached.

6.5 MOMENTUM TRANSFER EFFECTS ON BOUNDARY SHEAR STRESS

The effect of momentum transfer on boundary shear stress distributions in the main channel and flood plain zones was investigated for different geometric and hydraulic conditions in the model. The relative depth was varied from 0.089 to 0.325 for "narrow" channel conditions and from 0.33 to 0.5 for "wide" channel conditions. Also, the relative roughness was varied from 1.0 to 2.0 for "narrow" channel conditions.

The observed (average) boundary shear stress in the main channel, divided by the value for the corresponding "isolated" conditions, is plotted against relative depth in figure 29. For smooth boundary there is a 15% to 25% decrease in boundary shear stress associated with the compound flow. The ratio's maximum value corresponds to the lowest relative depth condition. For high relative depths transverse mixing in the junction regions is clearly not very strong (e.g. resulting in only an 8.0% decrease in boundary shear stress for a relative depth of 0.33).

The decrease of main channel boundary shear stress associated with interacting flow conditions is more noticeable when the flood plain roughness is increased. For a relative roughness of 2.0, a significant decrease in the boundary shear stress was noted for low relative depths. The decrease of main channel boundary shear stress with increasing relative roughness is clearly indicated in figure 30 where relative boundary shear stress is plotted against relative roughness for different relative depths. For the lowest relative depth value, the channel boundary shear stress is seen to decrease with increasing relative roughness. The same rate of decrease can be observed for each relative depth considered.

The effect of relative width on main channel boundary shear stress was also examined (figure 31). Boundary shear stress is seen to increase with a decrease in the relative width parameter. This is a further evidence of the MT mechanism's wider zone of influence (main channel section) in the case of a "narrow" central channel condition. The rate of decrease of boundary shear stress was approximately the same for all relative depths (figure 31).

The effect of MT on flood plain boundary shear stress was also investigated for the same hydraulic conditions. Due to momentum transfer from the main channel to the flood plain zones, boundary shear stress in the latter increases significantly compared to the equivalent isolated value. Figure 32 shows that flood plain boundary shear stress increases with a decrease in relative depth. For a smooth flood plain condition, the boundary shear stress is seen to increase from 35% to 290% for relative depths decreasing from 0.325 to 0.089 respectively. The increase in boundary shear is somewhat greater for the corresponding roughened flood plain conditions. For a relative roughness of 2.0 the boundary shear stress increases from 50% to 340% for the same range of relative depths. For still greater relative depths (wide channel conditions), the increase is smaller indicating that boundary shear stress will approach its equivalent isolated value for large values of relative depth. In the latter case the shear zone generated between main channel and flood plain is very weak and its net effect on system hydraulics is negligible.

In general flood plain boundary shear stress increases with increasing relative roughness (figure 33). The increase is greatest when the relative depth value is the smallest. This is because the interaction mechanism is strongest at this point and hence the apparent shear force acting on the main channel/flood plain interface is a maximum. For a relative depth of 0.089 the flood plain boundary shear stress increases from 290% to 340% for a 100% increase in the relative roughness parameter. Similarly for a relative depth of 0.33 the corresponding increase is from 32% to 44%.

The variation of flood plain boundary shear stress as a function of relative width of the channel was also investigated for various flood plain depths (figure 34). For a smooth boundary system the increase in boundary shear stress is seen to decrease with increasing relative width. For the smallest relative depth, flood plain boundary shear stress decreases from 290% to 200% with increasing relative width. For a relative depth 0.33 it decreases from 33% to 20% with a 100% increase in relative width. The above decrease is even smaller for "wide" channel condition (figure 34) indicating that, for the latter condition, MT does not affect significantly shear stress in the compound channel.

6.6 APPARENT SHEAR STRESS AS A STRENGTH INDICATOR FOR THE INTERACTION MECHANISM

The strength of the interaction mechanism is quantified through equations (3.13) and (3.14) as an apparent shear stress acting on the vertical main channel/flood plain interface. In the analysis the depth-averaged apparent shear stress was divided by the main channel boundary shear stress, calculated from energy balance (based on isolated conditions), with imaginary interface included in the wetted perimeter of the main channel. This ratio was indicative of the relative accuracy of those methods used to estimate discharge, which normally assume that apparent shear stress and main channel boundary shear stress are of equal magnitude.

Figure 35 shows the ratio for various relative depths and boundary roughnesses. Its value increases with decreasing relative depth, which supports the earlier conclusion that the mechanism's strength is greatest when the relative depth is smallest. This is to be expected since the large velocity gradients, occuring between the main channel and flood plain zones, at small flood plain depths, generate significant apparent shear stress at the interface.

Apparent shear stress is found to increase with increasing relative roughness. This is due to the correspondingly larger velocity gradients generated. It should be noted that the ratio is close to unity for large relative depths (greater than 0.325). This suggests that conventional methods for estimating discharge, which include the imaginary interface in the wetted perimeter calculation, should only be used when relative depth is large. The assumption of zero apparent shear stress, which is common in other methods, is unrealistic as figure 35 shows. For example, at small relative depths, the apparent shear stress is an order of magnitude greater than the corresponding boundary shear stress value. A detailed analysis of the various methods used for discharge estimation and the errors associated with each method are presented in chapter IX.

The effect of variable channel width on the apparent shear stress was also examined. In figure 36 the relative apparent shear stress is plotted against relative width for various relative depths. The ratio decreases with increasing relative width and depth, which is an indication of the increased strength of the mechanism associated with smaller relative widths.

The interdependence of apparent shear stress and the velocity differential between main channel and flood plain flow was also examined in this phase of the study. Instead of plotting apparent shear stress against the velocity differential across the mixing zone only, the former was plotted against the difference in the average velocities of the main channel and flood plain flows, calculated using the "separate-channels" method. Although this may not be an adequate representation of the velocity difference existing in the mixing region, it is readily calculated and provides an empirical means of evaluating apparent shear stress. Such an approach has been developed by Ervine and Baird (30) for a system comprising a rectangular main channel with one or two flood plain zones.

Figure 37 shows the relationship between apparent shear stress and mean velocity differential for various hydraulic conditions. Apparent shear stress increases with increasing velocity difference and approaches zero for small differential velocity. Obviously both main channel and flood plain flows will have essentially the same average velocities when the flood plain depth is very large and when no appreciable velocity gradient exists at the junction.

In view of the strong dependence of apparent shear stress on relative depth, width, roughness and velocity differential, a statistical analysis was performed to furnish an empirical relationship between apparent shear stress (dependent variable) and the above parameters (independent variables). This relationship is then used in a proposed new method for estimating discharge in compound channels (chapter IX).

A multiple regression analysis was performed with the SPSS (Statistical Package for Social Sciences) program, using representative experimental data. The relationship obtained was then validated using the remaining data. Initially the analysis was performed on the relationship

$$\tau_a = A\, y_r^{B}\, W_r^{C}\, \Delta U^{D}\, n_r^{E} \qquad (6.19)$$

which resulted in the following equation:

$$\tau_a = 0.104 y_r^{-1.209}\, W_r^{-0.576}\, n_r^{0.426}\, \Delta U^{0.092} \qquad (6.20)$$

The correlation coefficient and the coefficient of determination were calculated as 0.995 and 0.990 respectively.

Since relative roughness will influence to some extent velocity differential in the compound section another regression analysis was performed with the former excluded as an independent variable. This second regression analysis gave a correlation coefficient of 0.993 and a coefficient of determination 0.987. Thus the regression analysis is marginally improved when relative roughness is included. The relationship becomes:

$$\tau_a = 0.425 y_r^{-1.15} W_r^{-0.376} \Delta U^{0.874} \quad (6.21)$$

On the other hand when relative width is excluded from the analysis the following relationship is obtained:

$$\tau_a = 0.626 y_r^{-1.131} \Delta U^{1.139} \quad (6.22)$$

which gives a correlation coefficient 0.977 and a coefficient of determination 0.955. This demonstrates the importance of relative width in the analysis.

Equations (6.21) and (6.22) indicate that apparent shear stress is proportional to ΔU and not to ΔU^2 (assuming that the mixing length hypothesis is valid). This may be attributed to the fact that apparent shear stress is not correlated to the actual differential velocity in the mixing region but to an "imaginary" differential velocity for calculation purposes. Also the calculation of apparent shear stress using the mixing length hypothesis may not be valid in the main channel/flood plain interaction region.

Equation (6.21) was used to compare observed and calculated apparent shear stress values and these were found to be in close agreement (figure 38).

Equation (6.21) was also validated for similar experimental data not included in the present analysis. The validation is presented in figure 39 which shows close agreement between observed and calculated apparent shear stress for a wide range of flow conditions.

6.7. FRICTION FACTOR RELATIONSHIPS FOR COMPOUND CHANNELS

The development of friction factor relationships for compound channels, similar to those used for simple channels, is essential for the accurate prediction of discharge. Moreover, such relationships can be used as input to mathematical models describing such systems.

The decrease of velocity and boundary shear stress in the deep section of a compound channel, caused by MT effects, results in an effective increase in the friction factor for this portion of the cross section. Hence the usual assumption of equal friction factors, for both isolated and interacting conditions, is an oversimplification and can lead to significant discrepancies between observed and calculated discharge especially for small flood plain depths. Similarly the corresponding increase in velocity and boundary shear stress produced in the flood plain zones results in decreased friction factors for these zones.

Although application of modified friction factor relationships for the flood plain zones will normally not improve system discharge estimation, this is not the case for the main channel since the latter conveys most of the flow. Therefore appropriate modified main channel friction factors represent a major improvement in the modelling process.

Myers (72) developed friction factors relationships for the rectangular deep section of his symmetrical compound channel using the Darcy-Weisbach factor f, calculated from velocity measurements only, and assuming that main channel boundary shear stress is constant under both interacting and isolated conditions. However as stated earlier, the latter assumption is unrealistic and so friction factors calculated using such relationships differ significantly from those observed under interacting conditions.

In the present study friction factors were determined for those tests where both boundary shear stress and velocities in the main channel were measured under interacting conditions. They were found to be consistently greater than their corresponding values based on isolated conditions and furthermore were found to depend on the Reynolds number of the main channel flow(figure 40). Since the latter is not readily available, unless the velocity is measured experimentally, the friction factors were related to the corresponding "single-channel" Reynolds number. Figure (41) shows the relationship between main channel friction factor and the "single-channel" Reynolds number. A single linear relationship exists between friction factor and Reynolds number since the effect of relative roughness and relative width are incorporated in the estimation of the one-dimensional velocity.

Using regression analysis, the following relationship was obtained:

$$c_f = 0.015-0.003\cdot\log(Re) \tag{6.23}$$

in which the Reynolds number is expressed as:

$$Re = U_s R_t/\nu \tag{6.24}$$

where U_s = velocity calculated from "single-channel" method ;

R_t = hydraulic radius of compound channel.

Based on the above analysis the correlation coefficient was found equal to 0.979 and the coefficient of determination 0.958.

Equation (6.23) is used in the proposed new method for predicting discharge in compound channels.

When the Darcy-Weisbach friction factor f was used in the analysis ($f = 8c_f$) and the Reynolds number was calculated from the relationship $Re=4 \cdot U \cdot R/\nu$, the regression analysis provided an equation of the form:

$$\log f = 0.131 - 0.379*\log(Re) \qquad (6.25)$$

with correlation coefficient 0.975 and coefficient of determination 0.951. Experimental results together with equation (6.25) are shown in figure 42. Clearly for the range of conditions examined in this study, equations (6.24) and (6.25) can be used to calculate friction factors c_f or f in the deep section of a symmetrical compound channel.

Chapter VII

TURBULENCE CHARACTERISTICS IN COMPOUND FLOW FIELDS

7.1 INTRODUCTION

In chapter V it was established that, under certain flow conditions, the MT feature can have a significant effect on compound channel conveyance. Since transport processes of this type are turbulence related, an in-depth study of the MT's influence on system hydraulics calls for an examination of the turbulence field generated in the mixing zones.

Accordingly an examination was made of the internal structure of the mixing region flow field, with relative depth, channel width and boundary roughness being the principal study variables. The turbulence field associated with a two-dimensional channel flow provided an important basis for comparison when studying the effects of MT under "wide" central channel conditions. In addition to this turbulence data were obtained in the mixing regions of the compound channel for "wide" and "narrow" channel conditions.

Finally direct measurement of apparent shear stress at the vertical interface plane (separating the adjacent-deep and shallow zones), provided a useful comparison for estimates based on momentum balance considerations.

7.2 WORKING PRINCIPLES OF HOT-FILM ANEMOMETRY

The working principle of a hot-film sensor is based on the convective heat transfer from a cylinder. The film is heated above the ambient temperature of the fluid by passing an electrical current through a resistance material. The flow of fluid over the heated film cools it by forced convection. The cooling of the film is a function of the flow velocity, temperature, density, viscosity, and thermal conductivity of the fluid and the temperature, diameter, thickness and length of the film material. If all but one of the fluid and film variables are kept constant, the heated film becomes a transducer for measuring the remaining variable. Mainly, the hot-film has been developed as a resistance-temperature transducer for measuring velocity fluctuations.

Two modes of operation of hot-film anemometry have been used extensively: (1) The constant-current method, in which the electrical current is kept constant and thus the film's electrical resistance fluctuates with velocity fluctuations; (2) the constant temperature (constant resistance) method, used here, in which by using an electrical feedback system, the current fluctuates with the fluctuating component.

For a constant-temperature hot-film anemometer, the heat loss from a cylinder is described by King's law (54) for potential flow which can be expressed as:

$$\frac{I^2R_w}{R_w-R_a} = A + BU^{1/2} \tag{7.1}$$

where I = electrical current ;

R_w = electrical resistance of wire at wire temperature ;

R_a = electrical resistance of wire at fluid temperature ;

A,B = coefficients.

For incompressible flow heat loss is related to mean velocity by the experimentally verified relationship:

$$\frac{I^2 R_w^2}{R_w (R_w - R_a)} = A + BU^n \quad (7.2)$$

Equation (7.2) can be written as :

$$E^2 = R_a^2\, k(k-1)(A+BU^n) \quad (7.3)$$

or

$$E^2 = A' + B'U^n \quad (7.4)$$

where E = mean voltage ;

k = overheat ratio (R_w/R_a).

To measure turbulence characteristics, the cold resistance of the film R_w is measured in the ambient fluid and then a resistance of $K \cdot R_a$ is set on one leg of the bridge in the anemometer. The fluctuating velocity causes a fluctuation in the heat transfer from the film, which serves as the opposite leg of the anemometer bridge. A feedback servo-system senses any imbalance of the bridge caused by the velocity fluctuations and keeps the resistance of the wire constant by constantly and instantaneously changing the current in the film. This fluctuating current in the feedback system is the output of the anemometer and is displayed as a voltage.

The conversion of voltage fluctuations to velocity fluctuations for a cross type hot-film probe, with two mutually perpendicular sensors set at ±45° to the main flow (Figure 43), is based on the following equations (146):

$$u' = \frac{(e_1+e_2)'}{2S_1} \tag{7.5}$$

$$v' = \frac{(e_1-e_2)'}{2S_1} \tag{7.6}$$

$$\overline{uv} \quad \frac{\overline{e_1^2} - \overline{e_2^2}}{4S_1^2} \tag{7.7}$$

where u',v' = rms of the velocity fluctuations in the longitudinal and vertical directions ;

$\overline{uv}$ = turbulent shear stress;

S_1 = slope of calibration curve ;

$(e_1+e_2)'$ = rms of the summation of both voltage fluctuations ;

$(e_1 - e_2)'$ = rms of the difference of both voltage fluctuations ;

$\overline{e_1^2}, \overline{e_2^2}$ = mean squares of the voltage fluctuations.

The above format assumes that both film calibrations have the same slope.

The conversion of voltage fluctuations to velocity fluctuations is based on the following assumptions: (1) The velocity vector U can be expressed by a mean value U and fluctuating components u,v,w. (2) The same heat transfer relationship exists for both the mean and the fluctuating quantities and therefore the relation between mean voltage and mean velocity can be used to convert voltage fluctuations to velocity fluctuations. (3) The change in the slope of the calibration curve is small over the range of the velocity fluctuations encountered during a measurement hence the tangent to the curve at the mean velocity can be used to convert voltage fluctuations to velocity fluctuations.

7.3 DERIVATION OF APPARENT SHEAR STRESS BY TENSOR ANALYSIS

The apparent shear stress $-\rho\overline{uw}$ was determined from measurements of shear stresses in a plane normal to the channel boundary and in a plane inclined at 45° to the former. The relationships among the stresses acting on these planes are derived using tensor analysis.

By rotating the system of coordinates (figure 44) about the x-axis the Reynolds stress tensor can be transformed according to the following law:

$$\overline{u_i u_j} = \overline{u_k u_l}\, e_{ik} e_{jl} \qquad (7.8)$$

where $\overline{u_i u_j}$, $\overline{u_k u_l}$ = the components of the tensor in the old (y,z) and the new (y',z') coordinate system respectively,

e_{ik} = the cosine of the angle between the ith axis of the (y,z) coordinate system and the kth axis of the (y',z') coordinate system.

Therefore equation (7.8) can be used to determine the stress components in one coordinate system given the components of the tensor in the other system.

For the selected coordinate system e_{ij} can be written in analytical form as

$$e_{ij} = \begin{vmatrix} 1 & 0 & 0 \\ 0 & \cos\theta & -\sin\theta \\ 0 & \sin\theta & \cos\theta \end{vmatrix} \qquad (7.9)$$

Thus analysing equation (7.8) for all components of the stress tensor the following relationships apply:

$$\overline{u^2} = \overline{u_\theta{}^2} \qquad (7.10)$$

$$\overline{uv} = \overline{u_\theta v_\theta}\cos\theta - \overline{u_\theta w_\theta}\sin\theta \quad (7.11)$$

$$\overline{uw} = \overline{u_\theta v_\theta}\sin\theta + \overline{u_\theta w_\theta}\cos\theta \quad (7.12)$$

Equations (7.11) and (7.12) contain two unknowns ($\overline{u_\theta w_\theta}$, $\overline{uw}$), since the other quantities can be measured and the angle is known. The above equations were used to calculate the apparent shear stress $-\rho\overline{uw}$ at the main channel/flood plain interface since the other stresses ($\overline{uv}$, $\overline{u_\theta v_\theta}$) were measured directly using the hot-film probe in planes normal and inclined at 45° to the channel bed.

The lateral turbulence intensity and other components of the stress tensor can be determined using the following equations:

$$\overline{v^2} = \overline{v_\theta^2}\cos^2\theta + \overline{w_\theta^2}\sin^2\theta - 2\,\overline{v_\theta w_\theta}\sin\theta\cos\theta \quad (7.13)$$

$$\overline{w^2} = \overline{v_\theta^2}\sin^2\theta + 2\,\overline{v_\theta w_\theta}\cos\theta\sin\theta + \overline{w_\theta^2}\cos^2\theta \quad (7.14)$$

$$\overline{vw} = \overline{v_\theta^2}\cos\theta\sin\theta + \overline{v_\theta w_\theta}\cos^2\theta - \overline{v_\theta w_\theta}\sin^2\theta - \overline{w_\theta^2}\sin\theta\cos\theta \quad (7.15)$$

However additional measurements have to be made in another (inclined) plane since the above system of equations is not closed. The above equations contain 4 unknowns and therefore 3 similar equations can be produced using another inclined plane. The system of 6 equations with 6 unknowns can then be solved to determine the remaining unknown components of the stress tensor.

Since a complete analysis of turbulence in compound channel flow would constitute a major study in itself, the present investigation was only concerned with determination of apparent shear stress based on the above analysis.

7.4 TURBULENCE MEASUREMENTS

7.4.1 Measurements in the two-dimensional flow regions

The longitudinal (u'/U_1) and) vertical (v'/U_1) turbulence intensities (U_1 is the depth-averaged velocity) and the $\overline{uv}$ shear stress were measured depthwise in those areas of the compound flow that were essentially two-dimensional in character.

Figure 45 shows the vertical distributions of u'/U_1 and v'/U_1 for the range of Reynolds number employed in the experiments. For any discharge, u'/U_1 was found to be approximatelly twice the the magnitude of v'/U_1 and both intensities increased in value as the channel bed was approached. In general the magnitude of the intensities was found to decrease with increasing Reynolds number; the decrease being somewhat greater for the longitudinal intensity. Both of these findings confirm similar conclusions reported by Laufer (60) and McQuivey and Richardson (68) among others. For example, when the present data is compared with the corresponding McQuivey and Richardson data, reasonable agreement is obtained although the latters' longitudinal intensities are somewhat smaller near the bed (46). The near-boundary discrepancy, however, is thought to be caused by high velocity gradients generated across the sensing element when the latter is positioned near the solid boundary.

The observed vertical distribution of the $-\rho\overline{uv}$ shear stress was compared with the theoretical distribution derived from the Navier-Stokes equations for a fully developed two-dimensional flow (figure 46). In this instance the equation of motion in the streamwise direction simplifies to :

$$-\rho\overline{uv} = \rho g h S\left(1 - \frac{y}{h}\right) \qquad (7.16)$$

While there is a certain amount of scatter of the data points about the theoretical (dashed) line, equation (7.16) is nevertheless considered appropriate for these conditions.

7.4.2 Measurements in the mixing regions

7.4.2.1 "Wide Channel" conditions

The transverse distribution of longitudinal and vertical turbulence intensities as well as shear stress was examined for different relative depths and relative boundary roughness. Of particular interest was the influence of these study variables on the turbulence characteristics of the mixing regions. Since the various distributions were found to be essentially symmetrical about the channel centre line, the data for the entire cross section is reduced and presented in an equivalent "half-section" format.

Figure 47 shows the variation in longitudinal turbulence intensity u'/U (U is the average velocity for the cross section) across the compound channel when the flood plain is inundated to a depth of 20mm (relative depth 0.4). If we consider only the fluid layer above the bankfull stage, the maximum value of u'/U occurs at the junction and close to the flood plain bed. Here the value of u'/U is approximately twice the value at the channel centreline. Results indicate however that the difference between the junction and centre line values decreases with increasing distance from the bed. These findings suggest that the proximity of the flood plain bed (and hence boundary roughness) plays a dominant role in the turbulence field generated at the junction. In the zone below the bankfull stage u'/U increases as the channel side walls are approached, which is the case for channels of simple cross section.

The influence of relative depth on the u'/U distribution was studied by varying the former from 0.33 to 0.5. Figure 48 shows the variation in u'/U based on 3 different relative depth values. As indicated the maximum value of u'/U at the junction corresponds to the smallest relative depth value. Moreover the relative increase in u'/U, over the corresponding centreline value, is greatest at the smallest depth ratio.

When system discharge and hence flood plain depth was increased, the u'/U maxima in the interaction region decreased noticeably and the intensities recorded across the flood plain zones were similar to those recorded near the channel centre line.

The influence of boundary roughness on longitudinal turbulence intensity was investigated using three different roughness conditions for the flood plains described earlier. Figure 49 shows the response of u'/U to an increase in relative roughness for a given flood stage. In general turbulence intensity is seen to increase with an increase in relative roughness. This is particularly true in the junction region where, for a 100% increase in relative roughness, the intensity increases by up to 60%. Also the maximum u'/U value at the junction is approximately 3 times that observed at the channel center line. It should be noted that this increase was greater than that observed for the "smooth boundary" condition (i.e. relative roughness =1.0).

The MT's influence on the v'/U distribution is less significant. Values of v'/U across the channel are approximately half the corresponding u'/U values and the increase of v'/U at the junction is only about 1.8 times the value recorded at the channel centre line (Figure 50). As was the case for the streamwise intensity levels, the vertical turbulent intensity in the junction regions increased with an increase in relative roughness and also with a decrease in relative depth (figures 51,52). However, the increases in v'/U were considerably smaller than those observed for u'/U.

The spatial variation in the cross correlation term $-\overline{uv}/U_*^2$ is shown in figure 53. Because of the high velocity gradients generated at the channel bed, $-\overline{uv}/U_*^2$ is much greater there than at the water surface. The negative values of $-\overline{uv}/U_*^2$ in the channel portion of the mixing regions are attributed to large-eddy transport of shear stresses occurring in these regions.

The distribution of the correlation coefficient $-uv/u'v'$ is shown in figure 54. It varies across the channel and has zero value at the flood plains side walls, while its maximum value is approximately 0.32.

7.4.2.2 "Narrow Channel" conditions

The MT's influence on the turbulence field, when "narrow" central channel conditions applied, was also studied. In this case the MT's influence on the flow field is very strong. Relative roughness is found to be an important factor in this instance, consequently the effect of MT on turbulence intensities and shear stresses was studied for different boundary roughness conditions. Figure 55 shows the distribution of u'/U in the compound section. In the junction regions the value of u'/U increases significantly (up to 3 times its value at the centre line). It is clear from the figure, that MT influences a wider portion of the compound flow field when the central channel is "narrow".

The effect of increased flood plain roughness on u'/U values in the interaction region is seen in figure 56. Even for a moderate increase in relative roughness (27%) the longitudinal intensity level was seen to increase by up to 45% in the junction region. In the narrow channel experiments the maximum u'/U levels in the junction regions were 4 times greater than those measured at the channel centre line.

Similar distribution profiles were obtained for the vertical turbulent intensity v'/U although actual values were approximately half those of the corresponding u'/U distributions. The value of v'/U at the junction increased by up to 2.2 times its value at the channel centre line (Figure 57). An increase in relative roughness also produced an increase in v'/U over a wide area in the vicinity of the junction, however the increase was once again smaller than that observed for u'/U (Figure 58).

The distribution of $-\overline{uv}/U$, for a smooth boundary condition, is shown in figure 59. The distribution in the vertical is similar to that observed under "wide" channel conditions. The shear stresses decrease from the system centre line to the channel side walls at a rate faster than that observed for the wide channel case. Values of uv are smaller than the average shear velocity since measurements were not taken in those regions close to the channel bed where two-dimensional flow is dominant.

The distribution of the correlation coefficient uv/u'v' is plotted in figure 60; its maximum value was found to be approximately 0.40.

7.5 APPARENT SHEAR STRESS DISTRIBUTION

Direct measurement of local apparent shear stress $-\rho\overline{uw}$ at the imaginary (vertical) channel/flood plain interface provided information about its spatial variation there, in particular its deviation from the depth-averaged value calculated from momentum balance considerations. Figure 61 compares the calculated (depth-averaged) apparent shear with actual measurements for both "wide" and "narrow" channel conditions and for various flood plain depths and roughnesses. In all cases apparent shear stress is seen to increase as the flood plain bed is approached.

There is an estimated ±10-12% difference associated with the depth- averaged values calculated from local measurements (i.e. with respect to depth-averaged values calculated from equations (3.13) and (3.14)) which is considered acceptable in view of the difficulties associated with measurements close to a solid boundary as well as errors involved in the measurement of Reynolds stresses. Since the latter is a function of the difference between two time-averaged signals, the combined error may be large when the signals are of the same order of magnitude.

Source errors of this type can be partly avoided if a cross-type hot-film probe is used, which measures the longitudinal and lateral components simultaneously. This unit permits direct measurement of apparent shear stress $-\rho\overline{uw}$ at a point.

Chapter VIII

STAGE-DISCHARGE PREDICTORS FOR COMPOUND CHANNELS

8.1 INTRODUCTION

Conventional uniform flow formulae are normally used to develop stage-discharge relationships for open channels of simple cross section and uniform boundary roughness. However, if the channel's shape is complex, this approach can lead to considerable errors (93,137). Besides the difficulty in properly accounting for sectional shape and boundary roughness effects, the conventional approach does not consider apparent shear stress acting on the main channel/ flood plain interface.

This chapter describes some of the more popular conventional stage- discharge prediction methods and examines their effectiveness by applying them to the experimental data of Myers (73), Wormleaton et al (137) and this study.

Of special interest are two powerful "correction factor" methods developed respectively by Le Van Kiyen (63) and Karasev (49). The accuracy provided by these and the other methods are then compared with that provided by a new method developed in the present study. The new method, which is based on momentum and apparent shear stress considerations, gave consistently superior results for the conditions examined.

8.2 CONVENTIONAL METHODS

8.2.1 "Single-channel" method

The problem of defining properly the effects of channel shape and boundary roughness on system discharge can be appreciated in one of the most commonly used methods for discharge computation in compound channels, namely the "single-channel" method. In this method the compound section is considered as a single channel, hence the hydraulic radius R is computed from the total flow area A divided by the total wetted perimeter P.

Therefore total discharge is calculated by means of a uniform flow formula (e.g. Manning) as follows:

$$Q_t = \frac{1}{n} A_t R_t^{2/3} S^{1/2} \qquad \text{(S.I Units)} \qquad (8.1)$$

where
Q_t = total discharge;
n = roughness coef. for compound section ;
A_t = total cross-sectional area ;
R_t = hydraulic radius for compound section.

At very small flood plain depths there is usually a very large increase in wetted perimeter compared to the corresponding increase in flow area. This, in turn, results in a sudden decrease in hydraulic radius which (theoretically) would imply a corresponding decrease in discharge. In fact this is not the case as system discharge increases with an increase in the depth of flow.

The underestimation of system discharge, in the case of a known flow depth, or the overestimation of the flow depth, in the case of a known discharge, is greater when the flood plain roughness is substantially different from that for the main channel.

Another perceived limitation of this method is the fact that it employs a single (composite) roughness coefficient for the compound section. The problem is in the relationships developed for this purpose, which rely on higly questionable assumptions regarding the nature of the flow field.

The three principal equations for calculating composite roughness are :

$$n_e = \left(\sum_{i=1}^{I} \frac{P_i n_i^{3/2}}{P}\right)^{2/3} \tag{8.2}$$

$$n_e = \left(\sum_{i=1}^{I} \frac{P_i n_i^{2}}{P^{1/2}}\right)^{1/2} \tag{8.3}$$

$$n_e = \frac{PR^{5/3}}{\sum_{i=1}^{I} \frac{P_i R_i^{5/3}}{n_i}} \tag{8.4}$$

where n_e = composite roughness coefficient ;

n_i = roughness coefficient for the ith subsection;

P_i, R_i = wetted perimeter and hydraulic radius for the ith subsection respectively ;

P = wetted perimeter for compound channel.

The assumption made in developing equation (8.2) is that each subsection has the same average velocity which is also equal to the average velocity for the entire cross section.

The assumption of equal mean velocity for different subsections of a compound channel is obviously a gross oversimplification, especially in the case of low flood-plain depths when velocities in main channel and flood plain zones differ appreciably.

With regard to equation (8.3), it is assumed that total resistance is equal to the resistance summed over all of the subsections and, for equation (8.4), it is assumed that system discharge is equal to the sum of the component discharges for each subsection. These assumptions are also questionable since they imply that the component flows are effectively independent with no momentum exchange between them.

Figure 62 indicates the underestimation of system discharge to be expected when using the "single-channel" method for the case of a "narrow" compound channel system with smooth boundaries. For the purpose of comparison the accuracy achieved for the case of a compound system having a smooth main channel with roughened flood plains is also shown in the figure. System discharge is underestimated by up to 37% which is an indication that the composite n-value suggested by equation (8.2) is too high. Similar results were obtained when equations (8.3) and (8.4) were used to determine the equivalent roughness coefficient.

For "wide" channel conditions and relative depths ranging from 0.33 to 0.5, the method underestimates discharge by up to 10% for smooth flood plains and by up to 40% for rough flood plains (figure 63).

8.2.2 "Separate-channels" method

A common method used to overcome those problems associated with the "single-channel" approach is the "separate channels" method, which treats the channel and flood plain zones as separate entities. A major advantage of this method is the fact that it provides a convenient way to account for different boundary roughnesses between the main channel and flood plain zones.

Total discharge is calculated by summing the discharges of the various subsections which are defined by imaginary (vertical) interface planes passing through the junctions between adjacent deep and shallow sections.

Therefore total discharge is given by:

$$Q_t = \sum_{i=1}^{I} \frac{1}{n_i} A_i R_i^{2/3} S_i^{1/2} \qquad (8.5)$$

It should be noted that the wetted perimeter P only comprises the physical boundaries, i.e. it does not include the imaginary interfaces.

The "separate-channels" method tends to overestimate total discharge. This is because the imaginary interface is not included in the wetted perimeter calculation (and hence no force is assumed to act there). In fact an apparent shear force does act on the imaginary interface plane and its main effect on system conveyance is to provide additional resistance to the main channel flow. This fact is especially true for conditions of small relative depths and large relative roughness where appreciable apparent shear stress acts on the channel-flood plain interface. If this stress parameter is ignored in the analysis, a serious overestimation of discharge results for a "narrow" central channel with roughened flood plains (figure 62). However, for a "wide" central channel with roughened flood plains, a maximum overestimation of discharge of only 7% was noted (figure 63).

If a vertical interface is included in the main channel wetted perimeter calculation (i.e recognizing there is a retarding force acting on the main channel flow) the method still overestimates discharge in the case of small flood plain depths. This is because the assumption of equal apparent shear stress and boundary shear stress in the main channel is not generally correct.

Figure 64 presents sample results obtained using the "separate-channels" method with a vertical imaginary interface included in the wetted perimeter calculation for the main channel. When the method is applied to "wide" channel conditions, an overestimation of 5% results for the roughest flood plain condition examined (figure 65). It would appear therefore, that the method is appropriate for conditions examined since the error produced can be considered negligible for design purposes.

Various authors have proposed alternative arrangements for the imaginary planes, including inclined and horizontal ones (136,141), but assume that there is no shear acting on these planes. Accordingly they were not included in the wetted perimeter calculation for the main channel.

The method which uses a horizontal plane as the imaginary interface has also been applied to the "narrow channel" data (figure 64). This particular approach seems to give somewhat better results than those provided by the other methods. However, for "wide" channel conditions and large relative depths, the method underestimates significantly observed discharge (figure 65). Therefore the method should only be applied in the case for small relative depths in which case it produces results that are superior to those provided by other methods.

All of the above methods involve assumptions regarding the magnitude of the apparent shear force acting on the various interface planes. In general these assumptions are not true for a wide range of hydraulic conditions and therefore a new methodology, that can properly account for apparent shear force at the interface planes, is clearly needed.

8.3 METHODS BASED ON CORRECTION FACTORS

The inability of the foregoing methods to properly account for MT effects led to the development of relatively simple design methods based on experimentally-derived correction factors. These correction factors account for the adverse effects that small flood plain depth conditions have on system conveyance.

James and Brown (48) determined a simple correction factor (K) to the "single-channel" method, namely:

$$Q_t = \phi \frac{1}{n} A_t R_t^{2/3} S^{1/2} \qquad (8.6)$$

where $$\phi = f\left(\frac{n}{n_b}\right)^{-1} \qquad (8.7)$$

The correction factor was obtained from a curve-fitting technique which was applied to plots of n/n_b versus relative width for various relatives depths.They named their method the "modified single-channel" method and they reported good agreement between calculated and observed discharge for the conditions examined in their study.

On the basis of approximately 300 experiments Le Van Kiyen (63) produced correction factors for his system and then used the "separate-channel" method as follows

$$Q_t = \sum_{i=1}^{I} K_i \frac{1}{n_i} A_i R_i^{2/3} S_i^{1/2} \qquad (8.8)$$

in which K_i = correction factor for the ith subsection.

Five empirical relationships were used to determine the correction factors. The relationships included the following important parameters: degree of asymmetry and shape of cross section, relative depth of flow and relative roughness.

Karasev (49) used the momentum equation to obtain expressions incorporating two empirical parameters and noted that his method had a significant advantage over the empirical relationships used by Le Van Kiyen (63) which gave less accurate results.

The last two "correction factor" methods were applied to the present data for the "narrow" channel experiments and both produced results that were considered superior to those obtained by the other methods (figure 66).

8.4 PROPOSED METHOD

A method was developed in this study which uses the apparent shear stress parameter (estimated from equation(6.21)) in the calculation of discharge. Equation (6.21) has been shown to agree closely with observed data. Average boundary shear stress and velocity in the main channel are related through the following equation:

$$U_c^2 = \frac{\tau_c}{\rho c_f} \qquad (8.9)$$

Average channel boundary shear stress can be obtained from the momentum equation (3.13) as follows:

$$\tau_c = \gamma R_c S - \frac{2\tau_a y_f}{P_c} \qquad (8.10)$$

Using equations (8.9) and (8.10) and solving for average velocity we have

$$U_c^2 = \frac{1}{\rho c_f} (\gamma R_c S - \frac{2\tau_a y_f}{P_c}) \qquad (8.11)$$

Similarly on the flood plain

$$U_f^2 = \frac{1}{\rho c_f} (\gamma R_f S + \frac{\tau_a y_f}{P_f}) \qquad (8.12)$$

Hence total discharge, for a channel with two flood plains, is given by

$$Q_t = A_c U_c + 2A_f U_f \qquad (8.13)$$

Although apparent shear stress is accounted for in this method, system discharge is overestimated in the case of low relative depths (figure 67). This is because the method assumes the same friction coefficients under both "interacting" and "isolated" conditions. This assumption is not generally true since the values of both channel and flood plain boundary roughness coefficients change under interacting conditions.

When the friction factor relationship for the main channel (equation (6.23)) is used to estimate friction in equation (8.11), both friction factor and apparent shear stress are accounted for in the method and hence improved results are obtained, especially for low relative depths (figure 68).

8.5 APPLICATION OF DISCHARGE ESTIMATION METHODS TO NATURAL WATERCOURSES

The development and calibration of methods for predicting discharge in compound open channels has been based largely on laboratory observations; their application to natural rivers or artificial canals has therefore been limited. However, a meaningful extrapolation can be made from the laboratory results through the governing hydraulic and geometric parameters.

MT effects, similar to those observed in the present study, have also been observed in the field (7,49) and therefore discharge estimation methods developed from laboratory studies can be extended to natural channels, assuming similar boundary conditions apply.

In the case of "wide" rivers, stage-discharge relationships can be developed from the traditional "separate-channels" method, with a vertical interface between the deep and shallow regions included in the main channel wetted perimeter calculation. This is because MT effects only become significant when the main channel is "narrow", i.e. they do not affect the central region of "wide" river channels. Also, for "wide" river channels and small relative depths (y_r <0.3) the same method can be used with a horizontal interface not included in the main channel wetted perimeter calculation.

For "narrow" channels with relative widths of 5 or less the estimation of discharge for the compound section should be based on more refined methods which take into account the strong MT effects on system velocity and discharge. The effective increase noted in the laboratory main channel resistance to flow, at small flood plain depths, would also occur in the field, therefore methods employing modified friction factor relationships are appropriate. The methodoly developed in this study can be extended to "narrow" river channels using empirical relationships for modified friction factors and apparent shear stress. Since the latter is difficult to measure in the field it can be assumed greater than the main channel boundary shear stress and the proposed method can be applied with friction factor relationships developed for this purpose.

Chapter IX

NUMERICAL MODELLING CONSIDERATIONS

9.1 PAST WORK

In past years most of the numerical models developed for flow in compound channels are either finite element (FE) or finite difference (FD) solutions of the equations of motion.

Radojkovic and Ivetic (99) applied a numerical model to "fully-developed" flow in compound channels. The governing equations were simplified by combining convection and shear stresses in an "effective shear stress" parameter, the latter being calculated from a length-scale model. The resulting differential equation was then solved by a FE technique.

Vreughenhill and Wijbenga (134) used a FD method, of the alternating-direction-implicit (ADI) type, to solve the appropriate shallow-water equations. The eddy viscosity was not prescribed in advance but was calculated as part of the calibration process, thereby having a numerical rather than a physical sense. (It should be noted that secondary flow was not simulated in their model). The authors, in applying their model to prototype conditions, attribute its poor performance to boundary roughness effects among other things.

Demuren (25) used a three-dimensional numerical procedure for "developing" flow in channels with flood plains. The partial differential equations governing the steady-state turbulent flow field were solved in conjuction with the standard K-ε model of turbulence. The model was incapable of predicting turbulence-induced secondary currents, however for "developing flows", this was not considered a serious defect. The model was applied to Rajaratnam's data (104) and gave satisfactory results, but it was found to be computationally very expensive.

Prinos and Townsend (94) used a FE model based on the classical Ritz or Galerkin method to determine isovel patterns in their compound channel. The method is based on a variational technique in which the governing function for steady turbulent flow is minimized with respect to velocity. With this approach the distribution of longitudinal velocity U in the vertical (y) and lateral (z) directions can be obtained. For "wide" central channel conditions, differences between predicted and observed velocity distributions were considered unimportant from a practical viewpoint. However, when the main channel was made "narrow", the mathematical model did not reproduce the observed isovel patterns satisfactorily. This modelling deficiency was attributed to MT effects which were only partly accounted for in the model.

9.2 DEPTH-AVERAGED "K-ε" MODEL OF TURBULENCE

In chapter III the mean flow equations were presented and the related depth-averaged, x-momentum equation for fully developed flow derived (equation 3.10). The prediction of velocity distribution through equation(3.10) is possible once the eddy viscosity distribution is known. The latter can be calculated from simple algebraic expressions and/or differential equations (e.g. the K-ε model).

In most computational methods the turbulent or eddy viscosity is assumed constant over the flow field and therefore this was adjusted to suit a particular condition after calibration. Clearly this procedure limited the effectiveness of these methods.

Puri and Kuo (95) used a constant eddy viscosity distribution to determine the velocity field associated with a side discharge into an open channel. The results did not show a clearly defined deflection region and the accompanying recirculation zone was suppressed. They obtained better results using a variable eddy viscosity distribution based upon the Prandtl "mixing length" hypothesis and an assumed seventh power law velocity profile. The expression used was:

$$\bar{\nu}_t = 1.67 \frac{g}{C^2} h(\bar{U}^2 + \bar{W}^2)^{1/2} \qquad (9.1)$$

where C=Chezy's roughness coefficient ;

$\overline{U},\overline{W}$ =depth-averaged velocities in longitudinal and lateral directions respectively.

For the same problem Rodi (114) used a constant eddy viscosity ($\nu_t = 200\nu$) and obtained results very similar to those obtained using the K-ε model.

Lean and Weare (62) used an expression for viscosity derived from two-dimensional shear layer concepts, first proposed by Rodi (113), namely:

$$\overline{\nu}_t = 0.01\,\delta\,|U_{max} - U_{min}| \tag{9.2}$$

where δ =width of the shear layer ;

$U_{max}-U_{min}$=velocity difference across the layer.

Application of equation (9.2) requires a reasonably accurate estimation of the shear layer width. Vreugdenhil and Wijbenga (135) propose the latter to be of the order of 6(D-d), for a main river channel of depth D with flood plain depth d. It should be noted that this equation applies only to the free shear flow region and not to those regions where the channel boundary has a dominant influence on both turbulence and eddy viscosity.

Booij (10) adopted values for an effective viscosity based on the following relationship suggested by Fischer et al (31) :

$$\overline{\nu}_t = \alpha U_* h \tag{9.3}$$

where a= 0.15-0.60 (depending on channel geometry). Equation (9.3) is used in those regions of the flow field where turbulence is largely influenced by bed roughness.

The method applied in this study determines eddy-viscosity at each point in the flow field. This is achieved by means of a turbulence model that accounts for both bottom and free shear influences on the eddy viscosity distribution and therefore permits a much wider range of flows to be calculated without changing the empirical parameters involved.

The method employs the depth-averaged "K-ε" model which characterizes the local (depth-averaged) state of turbulence by two parameters, namely the turbulence kinetic energy $\overline{K}$ and the rate of dissipation of turbulence kinetic energy $\overline{\varepsilon}$. The eddy viscosity can then be related to these parameters by dimensional analysis

$$\overline{\nu}_t = c_\mu \frac{\overline{k}^2}{\overline{\varepsilon}} \tag{9.4}$$

where c_μ is a constant.

The variation of the turbulence parameters K and E is determined from the transport equations

$$\overline{U}\frac{\partial\overline{k}}{\partial x}+\overline{W}\frac{\partial\overline{k}}{\partial z} = \frac{\partial}{\partial x}\left(\frac{\overline{\nu_t}}{\sigma_k}\frac{\partial\overline{k}}{\partial x}\right)+\frac{\partial}{\partial z}\left(\frac{\overline{\nu_t}}{\sigma_k}\frac{\partial\overline{k}}{\partial z}\right) + G + P_{kv} - \overline{\varepsilon} \qquad (9.5)$$

$$\overline{U}\frac{\partial\overline{\varepsilon}}{\partial x}+\overline{W}\frac{\partial\overline{\varepsilon}}{\partial z} = \frac{\partial}{\partial x}\left(\frac{\overline{\nu_t}}{\sigma_\varepsilon}\frac{\partial\overline{\varepsilon}}{\partial x}\right)+\frac{\partial}{\partial z}\left(\frac{\overline{\nu_t}}{\sigma_\varepsilon}\frac{\partial\overline{\varepsilon}}{\partial z}\right) + c_1\frac{\overline{\varepsilon}}{\overline{k}}G + P_{\varepsilon v} - c_2\frac{\overline{\varepsilon}^2}{\overline{k}} \qquad (9.6)$$

where $\sigma_k, \sigma_\varepsilon, c_1, c_2$ = empirical constants ;

G = production of turbulence energy K due to interaction of turbulent stresses with horizontal mean velocity gradients;

P_{kv} = production of k due to bed shear;

$P_{\varepsilon v}$ = production of ε due to bed shear.

G is given by the equation:

$$G = \overline{\nu_t}\ \left[2\left(\frac{\partial\overline{U}}{\partial x}\right)^2 + 2\left(\frac{\partial\overline{W}}{\partial z}\right)^2 + \left(\frac{\partial\overline{U}}{\partial x}+\frac{\partial\overline{U}}{\partial z}\right)^2\right] \qquad (9.7)$$

Equations (9.5) and (9.6) can be considered depth-averaged forms of the three dimensional K and ε equations when all terms originating from non-uniformity of vertical profiles are assumed to be absorbed in the source terms Pkv, $P_{\varepsilon v}$. The latter terms have been added to equations (9.5) and

(9.6) to account for the significant turbulence production by the interaction mechanism. This energy production is in addition to the production G due to horizontal velocity gradients (i.e. terms with $(\partial U/\partial z)^2$), which depends strongly on the bottom roughness. Because they are governed by the near-bottom region, the additional vertical energy production terms are related to the bottom shear stress through the friction velocity U_* (108). Hence :

$$P_{kv} = c_k \frac{U_*^3}{h} \qquad P_{\varepsilon v} = c_\varepsilon \frac{U_*^4}{h^2} \qquad (9.8)$$

where c_k, c_ε = empirical constants.

The friction velocity (and hence boundary shear stress) is calculated by adjusting the friction coefficient to give the average boundary shear stress for the cross section.

The empirical constants c_k and c_ε were determined by Rastogi and Rodi (108) using the following relationship:

$$c_k = \frac{1}{\sqrt{c_f}} \qquad c_\varepsilon = 3.6 \frac{c_2}{c_f^{3/4}} \sqrt{c_\mu} \qquad (9.9)$$

The values of the various empirical constants used in the present study were adopted from Launder and Spalding (61). It should be emphasised that none of the empirical constants was adjusted to suit the particular conditions examined herein, but rather they are generally accepted values reported in the literature.

For fully-developed flow, the system of partial differential equations becomes a system of ordinary differential equations :

$$\frac{d}{dz}\left(\frac{\overline{\nu}_t}{\sigma_k}\frac{d\overline{k}}{dz}\right) + G + P_{kv} - \overline{\varepsilon} = 0 \qquad (9.10)$$

$$\frac{d}{dz}\left(\frac{\overline{\nu}_t}{\sigma_\varepsilon}\frac{d\overline{\varepsilon}}{dz}\right) + c_1\frac{\overline{\varepsilon}}{\overline{k}}G + P_{\varepsilon v} - c_2\frac{\overline{\varepsilon}^2}{\overline{k}} = 0 \qquad (9.11)$$

and those are then solved together with equations (3.10) and (9.4).

9.3 BOUNDARY CONDITIONS

The above system of equations can be solved to obtain velocity distributions when boundary conditions are specified at the centreline and the flood plain side wall.

For "wide" channel conditions, the depth-averaged velocity at the system centreline is obtained from the Karman-Prandtl velocity distribution integrated over the total depth or directly from the momentum equation (3.10) as follows:

$$\rho g h S - \rho c_f \overline{U}^2 = 0 \qquad (9.12)$$

Similarly equations (9.10) and (9.11) are simplified at the system centreline and therefore the turbulence quantities $\overline{K}$ and $\overline{\varepsilon}$ can be calculated there using the following equations:

$$G + P_{kv} - \overline{\varepsilon} + 0 \qquad (9.13)$$

$$c_1 \frac{\overline{\varepsilon}}{\overline{k}} G + P_{\varepsilon v} - c_2 \frac{\overline{\varepsilon}^2}{\overline{k}} = 0. \qquad (9.14)$$

For "narrow" channel conditions the velocity at the centre line is influenced by wall effects and hence observed values were employed in the analysis. Although this approach limits the predictive ability of the model, it was used to study the model's effectiveness in the interaction region.

The boundary condition at the flood plain side wall can be defined through 3 different approaches. The first uses the no-slip condition at the wall (U=0), the second uses the "wall function" method of Launder and Spalding (61) and the third uses the logarithmic velocity distribution in the region of the flood plain zone where two-dimensional flow conditions apply. In the second approach it is necessary to assume that shear stress is constant in a region near the wall and the logarithmic velocity law is valid. Therefore the law of the wall can be expressed as:

$$\frac{U_r}{U_*} = \frac{1}{k} \ln (E_1 z^+) \qquad (9.15)$$

where z^+ = normalised distance from the side wall;

U_r = resultant velocity ;

k = von Karman constant ;

E_1 = wall roughness parameter.

Also, within the wall region, the production G and dissipation $\bar{\varepsilon}$ of turbulent kinetic energy are assumed to be approximately in balance. Also the turbulent shear stress is assumed to be constant and equal to the wall shear stress. Acordingly $\bar{K}$ and $\bar{\varepsilon}$ take the following values:

$$\bar{k}_w = \frac{U_*^2}{\sqrt{c_\mu}} \qquad \bar{\varepsilon}_w = \frac{U_*^3}{kz_w} \qquad (9.16)$$

which then become boundary conditions for $\bar{K}$ and $\bar{\varepsilon}$ at the point nearest the wall.

Using the third approach the problem becomes similar to the mixing of two free streams with significantly different velocities, with the exception that boundary effects play a dominant role in the distibution of velocity across the test section.

Velocity predictions in the interaction region were not affected significantly by the choice of the boundary conditions since bed-generated turbulence was the major influence in those regions of the flow field.

9.4 COMPUTATIONAL PROCEDURE

Since these equations have the same form, the final set of differential equations is solved by the same numerical scheme:

$$0 = \frac{d}{dz}\left(\Gamma\frac{d\phi}{dz}\right) + S_\phi \qquad (9.17)$$

where ϕ = dependent variable ($\bar{U}$, $\bar{K}$ or $\bar{E}$) ;

S_ϕ = volumetric source term.

The algebraic equations (also called discretization equations) involving the unknown values of ϕ at selected grid points are derived from equation (9.17) employing the grid-point cluster shown in figure 69. Referring to grid point P, which has the grid points N and S as its neighbours, equation (9.17) is integrated over the control volume bounded by the two faces n and s as follows:

$$\left(\Gamma\frac{d\phi}{dz}\right)_n - \left(\Gamma\frac{d\phi}{ds}\right)_s + \int_s^n S\phi dz = 0 \qquad (9.18)$$

If the derivatives $d\phi/dz$ in equation (9.18) are evaluated from the "piecewise linear" profile, the resulting equation will be:

$$\frac{\Gamma_n(\phi_N-\phi_P)}{(\delta z)_n} - \frac{\Gamma_s(\phi_P-\phi_S)}{(\delta z)_s} + \bar{S}\,\Delta z = 0 \qquad (9.19)$$

where $\overline{S}$ = the average value of $S\phi$ over the control volume.

Equation (9.19) can take the following form:

$$\alpha_P \phi_P = \alpha_N \phi_N + \alpha_S \phi_S + b \qquad (9.20)$$

where
$$\alpha_N = \frac{\Gamma_n}{(\delta z)_n} \qquad (9.21)$$

$$\alpha_S = \frac{\Gamma_s}{(\delta z)_s} \qquad (9.22)$$

$$\alpha_P = \alpha_N + \alpha_S \qquad (9.23)$$

and
$$b = \overline{S}\Delta x \qquad (9.24)$$

The source term $\overline{S}$ is a function of the dependent variable itself and therefore is "linearised" to produce an equation which can be solved by known methods. Therefore the average value $\overline{S}$ is expressed as:

$$\overline{S} = S_c + S_p \phi_P \qquad (9.25)$$

where Sc = constant part of $\overline{S}$;

Sp = coefficient of ϕ.

When the source S is not a linear function of ϕ, then the coefficients in the discretization equation (9.18) depend on ϕ and an iteration process has to be applied based on the following procedure:

1. Values of the dependent variable ϕ are estimated at all grid points.

2. Values of the coefficients in the discretization equation are calculated based on the assumed values (step 1).
3. The set of algebraic equations is solved to obtain new values for ϕ.
4. The process is repeated from step 2 until no significant changes are noted in the values of ϕ.

The solution of the discretization equations can be obtained by the standard Gaussian-elimination method which is sometimes called the Thomas algorithm or the TDMA (TriDiagonal-Matrix Algorithm). The designation TDMA refers to the fact that when the matrix of the coefficients of these equations is written, all the non zero coefficients align themselves along these diagonals of the matrix. It is a very powerful and convenient algorithm whenever the algebraic equations can be represented in the form of equation (9.17). Furthermore it requires computer time and storage proportional only to N (where N number of grid points) rather than to N^2 or N^3. A full description of the algorithm can be found elsewhere (84).

9.5 APPLICATION OF THE MODEL

The model was applied to a series of test data representative of both "wide" and "narrow" channel conditions. The first two "wide" channel tests were performed with a smooth flood plain condition (relative roughness 1.0) and relative depths of flow of 0.33 and 0.50 respectively. (In a companion set of tests the relative depth values remained the same but the relative roughness was increased by 100%).

As stated earlier, when comparing the "compound channel" data with the equivalent "separate channel" data, MT was found to reduce local velocities in the mixing regions but not affect the central region of the main channel flow. At the channel centerline the logarithmic velocity distribution was found to apply over approximately 60% of the total depth (chapter V). Consequently the model's effectiveness was best judged on the accuracy achieved in simulating the complex flow field in the junction regions of the cross section.

Figures 70,71,72,73 compare observed with predicted depth-averaged velocities for the conditions examined. The model appears to work satisfactorily, although underestimating slightly velocities in the flood plain region near the junction. MT was responsible for the observed increase in velocity near the junction. This is more apparent for the roughened flood plain case since the turbulent shear interaction produces much higher velocities in the flood plain portion of the mixing region.

Also shown in the figures are the predicted depth-averaged velocities based on two simple turbulence models. The first model, which assumes a constant eddy-viscosity ($\overline{\nu}_t = 200\nu$), appears to work satisfactorily some of the time, however it tends to underestimate velocity in both the main channel and flood plain zones. This is a major limitation of this and similar models which assume a uniform eddy viscosity distribution throughout the flow field.

The second model assumes variable eddy-viscosity distribution as suggested by Fischer et al (31). It has been modified slightly in that local shear velocity U_* is used instead of the average shear velocity for a particular subsection. Results based on this slightly modified model are in close agreement with those obtained using the $\overline{K}-\overline{\varepsilon}$ model. This is a clear indication that wall effects, rather than free shear effects, are dominant in the weak shear zone (junction region) for the conditions examined. Therefore, it would appear that a simple turbulence model can be used satisfactorily in those instances where turbulence and eddy viscosity are governed primarily by the wall effect.

The $\overline{K}-\overline{\varepsilon}$ model was also applied to representative tests based on "narrow" channel conditions. Because of the radical change in channel dimensions, the relative depth values employed in this series of tests were considerably smaller than those used in the previous series. For relative depth values up to 0.28 the MT's effect on the mixing region flow field was a general increase in streamwise velocity in the flood plain portion of the mixing region and a decrease in same in the main channel portion. As stated earlier this redistribution of mean velocity in the cross section at small relative depths was found to have an adverse effect on system conveyance. Finally, comparisons between the corresponding "smooth" and "roughened flood plain" data clearly indicated that these system responses were magnified with an increase in relative boundary roughness.

For "narrow" channel conditions (figures 74 to 77) the $\overline{K}$-$\overline{\varepsilon}$ model gave results similar to those obtained using Fischer's model. Although velocities in the flood plain portion of the mixing region are somewhat smaller using the $\overline{K}$-$\overline{\varepsilon}$ model, general agreement between the two models is particularly good in this region of the flow field. While both models overestimate velocity in the main channel portion of the mixing region, the $\overline{K}$-$\overline{\varepsilon}$ model gives generally better results. This is because wall and free shear effects are equally important in this particular zone and the Fischer model ignores the free shear effect, which becomes important at small flood plain depths. Also presented in the figures 74 to 77 are the predicted velocities based on a constant eddy viscosity concept. As indicated in the figures this approach is acceptable for few conditions examined.

9.6 APPLICATION OF NUMERICAL MODELS TO NATURAL WATERCOURSES

Mathematical models for the computation of discharge and flow characteristics in natural rivers have been used by hydraulic engineers since the late 1950's. These models are based either on the energy equation (HEC-2 model) or the continuity and momentum equations (St. Venant equations). Their primary objective is to maintain an acceptable accuracy in the calculated results from a practical viewpoint. However, both categories of models ignore the influence of turbulent shear stresses on MT and hence the accurate prediction of compound channels flow characteristics by such models is questionable.

The primary consideration in applying the HEC-2 model to determine water surface profiles in natural rivers involves converting hydraulic parameters, which are distributed across the compound section, into averages. This conversion is achieved through the velocity head correction factor a which accounts for the non-uniform velocity distribution in the lateral direction. However, calculation of a is based on subdividing the compound channel with a vertical main channel/flood plain interface and assuming that no shear acts on this plane. This assumption is not valid as experiments have shown and hence satisfactory prediction of water surface elevation, especially for low flood plain depths, is questionable.

For a better prediction of flow depth the estimation of a should be based on subdividing the cross section with inclined or horizontal interface planes and assuming that no shear force acts there.

Another important consideration in the application of the HEC-2 model is the use of appropriate roughness values which can vary greatly across a prototype-scale compound section. The use of modified friction factor relationships, which take into account MT effects on flow characteristics, in conjunction with the above energy approach would undoubtly give superior results.

Similar problems arise from the use of the St. Venant equations for the prediction of flow in a compound river channel. A momentum correction factor M is calculated based on subdividing the compound section with a vertical interface and selecting roughness coefficients on the basis of isolated flow conditions. Also the net momentum flux produced by the lateral discharges is prescribed and this limits the model's predictive ability. A more refined modelling of the flow is achieved by applying the two-dimensional St. Venant equations, even though these ignore MT effects. An improved flow prediction can be achieved with the use of appropriately modified friction factior relationships and momentum correction factors.

The proposed $\overline{K}$-$\overline{\varepsilon}$ model overcomes these problems with the prediction of turbulent shear stress through the eddy-viscosity concept. Accordingly it is considered the best alternative among the various models used in such studies. Also the eddy-viscosity is not assumed constant, nor is it estimated from empirical relationships. It is determined using the $\overline{K}$- and $\overline{\varepsilon}$- transport equations, which is an additional advantage over the usual "shallow-water" equations approach, which uses constant eddy-viscosity. Generally the use of the $\overline{K}$-$\overline{\varepsilon}$ model is recommended for flow prediction in rivers with flood plains.

Chapter X

CONCLUSIONS AND RECOMMENDATIONS FOR FUTURE RESEARCH

This theoretical and experimental study examines the momentum transfer phenomenon associated with flow in compound channels and investigates its influence on system hydraulics for different channel widths and relative boundary roughnesses.

It has been established elsewhere that, when MT between adjacent deep and shallow zones of a compound cross section is strong, large discrepancies occur between the estimated and actual system discharge. This results from the fact that MT is not properly accounted for in the traditional discharge computation methods developed for flow in channels of simple cross section. Accordingly direct application of these methods to compound channel systems is only appropriate when the relative depth parameter for the cross section is large ($y_r > 0.4$ say), i.e. when MT is weak.

One of the main goals of this study was the development of a procedure for estimating discharge in compound channels when momentum transfer effects are significant, i.e. when the relative depth parameter is small. To accomplish this MT's effect on velocity and boundary shear stress distribution in compound flows was studied extensively in a model compound channel with the channel dimensions, relative depth and relative boundary roughness being the principal study variables.

Since fluid transport mechanisms in fully-developed flows are largely turbulence related, an important feature of the study was the measurement and analysis of turbulence characteristics in the mixing regions of the physical system.

The other important aspect of this study was the review of current numerical modelling techniques for flow in compound channels and their limitations. The modified $\bar{K}-\bar{\epsilon}$ model developed in the present study accounts for the presence of MT at small flood plain depths. It is considered an improvement over two-dimensional models based on the St. Venant equations, which ignore MT and its adverse effect on system conveyance.

The following main conclusions of the study are presented in the same order as the related subject matter appears in the text:

1. The isovel patterns obtained from the detailed velocity traverses clearly define the zones of influence of MT for the particular geometric and hydraulic conditions examined. When the main channel was "wide" the central region of the channel flow was not affected by MT, but displayed an essentially two-dimensional flow pattern throughout. On the other hand, when the main channel was "narrow", the complex

three-dimensional flow field characterising MT influenced the entire main channel flow. In addition to distorting the isovels in the junction areas the MT mechanism's presence depressed the channel's maximum velocity filament below the bankfull elevation. The degree of submergence was subsequently found to depend on the section's relative depth and relative roughness parameters. While MT's influence extended well into the flood plain zones, a portion of the flood plain flow was nevertheless found to be essentially two-dimensional in character throughout the various experiments.

2. Velocity distribution laws (smooth and rough boundaries) were developed for those regions of the compound flow field that could be characterised as being essentially two-dimensional. The logarithmic velocity distribution law proved to be appropriate for the "smooth" data. However, when the flood plain zones were artificially roughened, the flow was in the "turbulent transitional" and "fully rough" regimes and the laws developed for these particular experiments reflected this.

3. Under conditions of small relative depth and for large relative roughness and width MT was found to have a significant effect on the system's transverse velocity distribution. The severe lateral velocity

gradient that is generated in the mixing region at small flood plain depths, produces a noticeable decrease in local velocity in the main channel portion of the mixing region and a corresponding increase in local velocity in the flood plain portion.

Furthermore, it was noted that the local increase (flood plain zone) and decrease (channel zone) in the streamwise velocity within the mixing regions increased with an increase in relative roughness. This occurred as a result of the increased apparent shear stress acting on the main channel/flood plain interface.

In the case of a "narrow" central channel condition, these local changes in the velocity distribution reduced mean velocity in the main channel below the corresponding theoretical value for the given stage. On the other hand, for a "wide" channel arrangement, the discrepancy between the actual and theoretical values was such that it could be essentially ignored for all practical purposes.

4. Under conditions of small relative depth and for large relative roughness and relative width, MT decreased boundary shear stress in the main channel portion of the mixing region while increasing bed shear stress in the flood plain portion. This resulted in a net decrease (up to 35%) in the average

boundary shear stress for the main channel and an increase (up to 320%) in the average boundary shear stress for the flood plain zone.

5. The aforementioned changes in average velocity and boundary shear stress for the main channel and flood plain zones translated into adjusted friction factors for these same regions. Friction factor relationships were developed for the main channel by correlating the observed friction factor with the equivalent "single-channel" Reynolds number. A unique relationship was developed for all conditions examined.

6. The strength of MT was quantified through momentum balance considerations and the apparent shear stress, acting on the vertical main channel/flood plain interface, was found to depend on relative depth, width, roughness and velocity differential between the deep and shallow sections.

Apparent shear stress was found to decrease with increasing relative depth and width and found to increase with increasing relative roughness and differential velocity. This is due to the fact that high cross-stream velocity gradients exist at conditions of small relative depth and large relative roughness. An empirical relationship was developed between apparent shear stress and easily calculated geometric and hydraulic characteristics of the compound channel. This relationship was subsequently used in a new methodology for predicting discharge in compound channels.

7. The effects of MT on system turbulence characteristics were studied for both "wide" and "narrow" channel conditions. Under "wide" channel conditions the central region of the main channel was essentially a 2-dimensional region in character wherein turbulence intensities and shear stress were in close agreement with theoretical values and the experimental results of other investigators.

In the mixing regions the highest longitudinal and vertical turbulence intensities corresponded to the conditions of smallest relative depth and largest relative roughness. An increase in relative depth produced lower turbulence levels. For a 50% increase in relative depth both longitudinal and vertical turbulence intensities decreased up to 45%. On the other hand an increase in the relative roughness parameter resulted in higher turbulence levels in the mixing regions due to higher cross-stream velocity gradients. In general the cross-stream distribution of longitudinal turbulence intensity was found to be approximately twice the value of the vertical intensity.

8. Large eddy transport of shear stress in the main channel portion of the mixing region resulted in negative shear stress in this particular zone even though no negative velocity gradients occur there. This indicates that the eddy-viscosity concept is not valid in these regions of the cross section and therefore the numerical modelling of shear stress should be based on all physical processes that influence the shear stress.
9. A method for the direct measurement of apparent shear stress was developed using a cross hot-film probe in both vertical and inclined planes to the channel boundary and applying tensor analysis to the observed data. The results compared favorably with those based on momentum balance considerations, indicating that the proposed method is an improvement over other (indirect) methods.
10. The strong influence of MT on system discharge at conditions of small relative depth and large relative roughness was examined by comparing observed discharge with that calculated by conventional methods. Since the latter do not properly account for MT effects, an overestimation of system discharge (in some cases up to 45%) occurred at small relative depths.

A comparison of the different "separate channels" methods suggested by other investigators clearly identified the one using the "horizontal interface plane" arrangement as being the most accurate among those considered.

11. The novel discharge prediction method developed in this study is based on momentum balance considerations and employs two empirical relationships to properly account for MT effects. Even for the severest compound channel condition excellent agreement (error ±15%) was obtained between estimated and observed discharge using this method.

12. The numerical modelling of MT effects utilises both the $\overline{K}-\overline{\epsilon}$ model of turbulence and the eddy viscosity concept to account for both bed and shear generated turbulence characteristics.

For a "wide" channel condition the model predicts the depth-averaged velocity distribution in the trasverse direction satisfactorily. However, when the central channel is "narrow", MT has a significant effect on velocity profiles with the result that velocity is overestimated slightly in the main channel and underestimated in the flood plain zones.

In general the results indicate that the mathematical model is useful in predicting the effects of MT on the flow in a compound channel. It should be noted at this point that none of the empirical coefficients used in the mathematical model was adjusted to match the experimental results. Their values were those reported in the literature.

13. Two relatively simple models were also considered as possible alternatives to the $\overline{K}-\overline{\epsilon}$ model. The first, which is based on bed generated turbulence, produced better results than the $\overline{K}-\overline{\epsilon}$ model in the flood plain zones (where the flow is governed by bed generated turbulence). However this model significantly overestimated the velocity in the main channel, indicating that free shear turbulence is dominant in this region of the mixing zone.

    The second model used a constant eddy-viscosity distribution and although it appeared to work well some of the time, it was clearly not universally applicable. Because of these limitations the two (simpler) models were not considered acceptable alternatives.

The following topics are suggested for future consideration by researchers working in this area:

1. An obvious extension of this work would be to examine the nature of momentum transfer phenomena occurring in a bend of a compound channel and eventually in meandering compound channels. Clearly the strong sec-

ondary currents associated with flow in river bends will play an important role in the MT process and past studies on the topic have not addressed this important question.

2. The internal structure of compound flows should be analysed in much greater detail to better rationalise the effects of the complex transfer mechanism on system hydraulics. Turbulence studies (spectra, microscale, macroscale), the identification of any coherent structures in the flow field and the large eddy transport of shear stress, are possible topics for consideration.
3. To the author's knowledge no detailed investigation has yet been undertaken regarding the hydraulics of compound duct flow. Comparisons between "duct" and "open channel" studies would, among other things, isolate free surface effects on momentum transfer in the case of the latter.
4. Accurate prediction of isovel patterns as well as the three-dimensional nature of flow in compound channels are crucial in modelling effectively momentum transfer phenomena. The strong secondary motion and the depression of the maximum velocity filament below the free surface ("narrow channel" conditions) can be predicted by highly sophisticated models which properly reflect the complex three-dimensional flow

field. The complete set of Navier-Stokes equations must be used in conjuction with an appropriate turbulence model. The latter should not be based on the eddy-viscosity concept but on all the physical processes (i.e. convection,diffusive transport, turbulence production, viscous dissipation etc.) that influence the Reynolds stresses. A full stress equation model or an algebraic stress model should be used for a realistic simulation of flow under "narrow" channel conditions. This is clearly an important area for future research.

REFERENCES

1. Acharya,M. and Escudier, , "Measurements of the Wall Shear Stress in Boundary-layer Flows," Proceedings of 4th international Symposium on Turbulent Shear Flows Karlsruhe,September 1983,pp. 15.7-15.11.

2. Allen, J., "Significance of the Boundary Shear Stress/Momentum Flux Ratio," Proceedings I.C.E., Vol. 71, 1981, pp. 269-271.

3. Allen, J. and Ullah, M.I., "The Flow of Water through Smooth Open Channels with Narrow Rectangular and T-shaped Cross-sections," Proceedings I.C.E., Vol. 36,February 1967, pp. 325-349.

4. Bagnold, R.A., "Some Flume Experiments on Large Grains but Little Denser than the Transporting Fluid and their Implications." Proc. I.C.E. 4, Part 3, 174, 1955.

5. Bathurst, J.C., "Flow Resistance of Large-Scale Roughness," Journal of Hydraulics division,ASCE,Vol.104,No. HY12,December 1978, pp. 1587-1603

6. Belt, C. B. Jr, "The 1973 Flood and Man's Constriction of the Mississippi River" Science, v. 189 (4204) : pp 681-684.

7. Bhowmik, N.G. and Demissie,M., "Carrying Capacity of Flood Plains" Journal of the Hydraulics Division, ASCE, No. HY3, March 1982, pp. 443-453.

8. Blalock, M.E. and Sturm, T.W., "Minimum Specific Energy in Compound Open Channel" Journal of the Hydraulics Division, ASCE, No. HY6, June 1981, pp. 699-717.

9. Blinco, P. and Partheniades, E., "Turbulence Characteristics in Free Surface Flows over Smooth and Rough Boundaries." Journal of Hydraulic Research, IAHR, Vol. 9, No. 1, 1971.

10. Booij, R., Discussion on "Computation of flow patterns in rivers" Journal of Hydraulics Division, ASCE, January 1984, HY1, pp. 87-90.

11. Brown, D.C. and Joubert, P.N., "The Measurement of Skin Friction in Turbulent Boundary Layers with Adverse Pressure Gradients." Journal of Fluid Mechanics, Vol. 35, Part 4, 1969.

12. Bursali, T.S., "Bottom Shear Measurements in an Open Channel Flow." Proceeding, 12th Congress IAHR, 1967.

13. Chiu, C.L., Hsiung, D.E. and Lin, H.C., "Three-dimensional Open Channel Flow," Journal of the Hydraulics Division, ASCE, Vol. 104, No. HY8, August 1978, pp. 1119-1136.

14. Chiu, C.L. and Hsiung, D.E., "Secondary Flow, Shear Stress and Sediment Transport," Journal of Hydraulics Division, ASCE, Vol. 107, No HY7, July 1981, pp. 879-898.

15. Chiu, C.L. and Lin, H.C and Kazumasa,M., "Simulation of Hydraulic Process in Open Channels," Journal of the Hydraulics Division, ASCE, Vol. 102, No. HY2, February 1976, pp. 185-206.

16. Chow, V.T., "Open Channel Hydraulics," McGraw-Hill Book Co., New York, 1959.

17. Chow, V.T., "Handbook of Applied Hydrology," McGraw-Hill Book Co., New York, 1964.

18. City of Winnipeg Flood Channel Works.

19. Clark, J.A. and Markland, E., "Flow Visualization in Free Shear Layers," Journal of Hydraulics Division, ASCE, Vol. 99, No. HY11, November 1973, pp. 1897-1913.

20. Clayton, B.R. and Massey, B.J., "Flow Visualization in Water; a Review of Techniques," Journal of Scientific Instrumentation, Vol. 44, 1967, pp. 2-11.

21. Coleman, N.L., and Alonso, C.V. "Two Dimensional Channel Flows over Rough Surfaces," Journal of Hydraulics Division, ASCE, Vol. 109, No. 2, Feb. 1983, pp. 225-184.

22. Cruff, R.W., "Cross-Channel Transfer of Linear Momentum in Smooth Rectangular Channels," U.S. Geological Survey, Water Supply, 1965, p. 1592-B.

23. Davidian, J. and Cahal, D.I., "Distribution of Shear in Rectangular Channels," U.S. Geological Survey, Prof. Paper 475-C, Art. 113, 1963, pp. C206-C208.

24. Delleur, J.W. and Toebes, G.H. and Udeozo, B.C., "Uniform Flow in Idealized Channel-Flood Plain Geometries," Proceedings 12th International Conference of IAHR, Fort Collins, Colorado, USA, 1967,pp.218-225.

25. Demuren, A.O., "Prediction of Flow in Channels with Flood Plains," Proceedings of Engineering Mechanics Conference, ASCE, May 1983, Lafayette, Indiana, Vol. 2, pp. 1212-1215.

26. vanDriest, E.R., "On Turbulent Flow Near a Wall" Journal of Aerospace Science , 23, 1007.

27. Einstein, and El-Samni "Hudrodynamic forces on a rough Wall" Rev. Mod. Physics, Vol. 21, 1949

28. Elsawy, E.M. and Crory, P.M., "Effects of Interaction on a Channel with One Flood Plain," International Conference on Water Resources Engineering, Bangkok, Thailand, January 1978, pp. 597-608.

29. Elsawy, E.M, McKee, M.P and McKeogh, E.J., "Application of LDA Techniques to Velocity and Turbulence Measurements in Open Channel of Compound Section" Proceedings of Inter. Conf. of IAHR,Vol. B, Moscow Sep. 1983, pp. 255-263.

30. Ervine, D.A. and Baird J.I., "Rating Curves for Rivers with Overbank Flow," Proceedings of I.C.E., Part 2, Vol. 73, 1982, pp. 465-472.

31. Fischer, H. B., et al., "Mixing in Inland and Coastal Waters " Academic Press, New York, N.Y., 1979

32. Gaddini, B. and Morganti, M., "Turbulent Shear-Stresses and Velocity Distribution in Open-Channel Flows," La Houlle Blanche, No. 4, 1982, pp. 309-325.

33. Gerard, R., "Momentum Transfer Model for Reynolds Stresses," Journal of the Hydraulics Division, ASCE, Vol. 103, No. HY10, October 1977, pp. 1232-1237.

34. Gessner, F.B. and Jones, J.B., "On Some Aspects of Fully Developed Turbulent Flow in Rectangular Channel," Journal of Fluid Mechanics, Vol. 23, Part 4, 1965, pp. 689-713.

35. Ghosh, S.N., "Boundary Shear Distribution in Channels with Varying Wall Roughness," Proceedings of I.C.E.,Part 2,53,December 1972,pp.529-544.

36. Ghosh, S.N. and Kar, S.K., "River Flood Plain Interaction and Distribution of Boundary Shear Stress in a Meander Channel with Flood Plain," Proc. of I.C.E., Part 2,59, December 1975, pp. 805-811.

37. Ghosh, S.N. and Roy, N., "Boundary Shear Distribution in Open Channel Flows," Journal of Hydraulics Division, ASCE, Vol. 96, April 1970, pp. 967-994.

38. Ghosh, S.N., "Boundary Shear Distribution in Rough Compound Channel," Synopsis, Proc. of I.C.E., Vol. 55, June 1973, p. 487.

39. Ghosh, S.N. and Jena, S.B., "Boundary Shear Distribution in Open Channel Compound," Proceeding of I.C.E., Vol. 49, August 1971, pp. 417-430.

40. Ghosh, S.N. and Mehta, P.J., "Boundary Shear Distribution in a Compound Channel with Varying Roughness Distribution," Proceedings of ICE, Part 2, 57, March 1974, pp. 158-163.

41. Head, M.R. and Ram, V.V., "Simplified presentation of Preston tube calibration," Aeronautical Quarterly, 22, 1971, pp. 295-300.

42. Head, M.R. and Rechenberg, I., "The Preston Tube as a Means of Measuring Skin Friction," Journal of Fluid Mechanics, Vol. 14, Part 1, 1962.

43. Hegly, V.M, "Flow in Eastern Canals of Compound Cross-section" Transactions of ASCE,November 1937, pp. 36-48.

44. Hollick, M., "Boundary Shear Stress Measurement by Preston Tube," Journal of Hydraulic Division, ASCE, Technical Notes,Vol. 101, July 1976, pp. 1053-1057.

45. Hollingshead, A.B. and Rajaratnam, N., "A Calibration Chart for the Preston Tube," Journal of Hydraulics Research, 18 (1980), No. 4, pp. 313-326.

46. Hwang, L.S. and Laursen, E.M., "Shear Measurement Techniques for Rough Surfaces," Journal of Hydraulics Division, ASCE, Vol. 89, March 1963, pp. 19-37.

47. Ippen, A. and Drinker, P.A., "Boundary Shear Stress in Curved Trapezoidal Channels," Journal of Hydraulics Division, ASCE, Vol. 88, September 1962, pp. 143-179.

48. James, M. and Brown, B., "Geometric Parameters that Influence Floodplain Flow," Research Report H-77-1, U.S. Army Eng. District, Kansas City, Missouri 64106, 1977.

49. Karasev, I.F., "Influence of the Banks and Flood Plain on Channel Conveyance," Soviet Hydrology: Selected Paper, Issue No. 5., 1969.

50. Kartha, V.C. and Leutheusser, H.J., "Distribution of Tractive Force in Open Channels," Journal of Hydraulics Division, ASCE, No. HY7, July 1970, pp. 1469-1483.

51. Kazemipour, A.K. and Apelt, C.J., "Shape Effects on Resistance to Uniform Flow in Open Channels," Journal of Hydraulic Research, Vol. 17, No. 2, 1979, pp. 129-147.

52. Kennedy, R.J. and Fulton, J.F., "The Effect of Secondary Currents Upon the Capacity of a Straight Open Channel," Transactions of E.I.C., Vol. 5, No. 1, 1961.

53. Keulegan, G.H., "Laws of Turbulent Flow in Open Channels," Journal of Research of the National Bureau of Standards, Vol. 21, December 1938, pp. 707-741.

54. King, L.V., "On the Convection of Heat from Small Cylinders in a Stream of a fluid-Determination of the Convection Constants of Small Platinum Wires With Application to Hot-Wire Anemometry" Philosophical Transactions, Royal Society, London, Series A, Vol.214, 1914, pp. 373-472.

55. Knight, D.W., "Boundary Shear in Smooth and Rough Channels," Journal of the Hydraulics Division, ASCE, Vol. 107, No. HY7, July 1981, pp. 839-851.

56. Knight, D.W. and Demetriou, J.D., "Flood Plain and Main Channel Flow Interaction," Journal of Hydraulics Division, ASCE, Vol. 108, No. HY8, August 1983, pp. 1073-1092.

57. Knight, D.W. and MacDonald, J.A., "Hydraulic Resistance of Artificial Strip Roughness," Journal of Hydraulics Division, ASCE, Vol. 105, No. HY6, June 1979, pp. 675-690.

58. Knight, D.W. and MacDonald, J.A., "Open Channel Flow with Varying Bed Roughness," Journal of Hydraulics Division, ASCE, Vol. 105, No. HY9, Sept. 1979, pp. 1167-1183.

59. Kuipers, J. and Vreugdenhil, C.B., "Calculations of Two-Dimensional Horizontal Flow" Delft Hydraulics Laboratory Report S 163, part I, 1973

60. Laufer, J., "Investigation of Turbulent Flow in a Two-Dimensional Channel" NACA, Report 1053, 1951.

61. Launder, B.E. and Spalding, D.B., "The Numerical Computations of Turbulent Flow," Computer Methods in Applied Mechanics and Engineering, 1974, 3, pp. 269-289.

62. Lean, G.H. and Weare, T.J, "Modelling Two-Dimensional Circulating Flow" Journal of the Hydraulics Division, ASCE, Vol. 105,No. HY1,1979,pp. 17-26.

63. Le Van Kiyen, "Hydraulic Computation of Flood Plain Channels," Soviet Hydrology: Selected Papers, Issue No. 4, 1968.

64. Liggett, J.A. and Chiu, C.L., Secondary Currents in a Corner," Journal of the Hydraulics Division, ASCE, Vol. 91, No. HY6, November 1965, pp. 99-117.

65. Li, Ruh-Ming and Schall, James D. and Simmons, Daryl B., "Turbulence Prediction in Open Channel Flow," Journal of the Hydraulics Division, ASCE, Vol. 106, No. HY4, April 1980, pp. 575-587.

66. Lundgren, H. and Jonson, I.G., "Shear and Velocity Distribution in Shallow Channels," Journal of Hydraulics Division, ASCE, January, 1964.

67. MacMillan, F.A., "Experiments on Pitot Tubes in Shear Flow." Aeronautical Research Council Reports and Memoranda No. 3028, 1957.

68. McQuivey, R.S. and Richardson, E.V., "Some Turbulence Measurements in Open-Channel Flow," Journal of the Hydraulics Division, January 1969, pp. 209-223.

69. McDowell, D.M., "Scale Effects in Models of Shallow Tidal Waters," Proceedings of I.C.E., Paper No. 72095, Supplementary Volume 1969.

70. Maggiolo, O.J., Fuarga, Rand and Borghi, J., "A New Method for Measuring Shear Stresses in a Hydraulically Rough Flow," Journal of Hydraulic Research, IAHR, Vol. 8, No. 2, 1970.

71. Myers, W.R.C., "Momentum Transfer in a Compound Channel," Journal of Hydraulic Research, IAHR, Vol. 16, No. 2, 1978, pp. 139-150.

72. Myers, W.R.C., "Friction Factor Relationships in Compound Channels" Proceedings of the International Conf.

73. Myers, W.R.C. and Elsawy, E.M., "Boundary Shear in Channel with Flood Plain," Journal of the Hydraulics Division, ASCE, Vol. 101, July 1975, pp. 933-946.

74. Naot, D. and Rodi, W., "Calculation of Secondary Currents in Channel Flow," Journal of the Hydraulics Division, ASCE, August 1982, pp. 948-968.

75. Nece, R.E. and Smith, J.D., "Boundary Shear Stress in Rivers and Estuaries," Journal of the Waterways and Harbours Division, ASCE, WW2, May 1970, pp. 335-358.

76. Nicollet G. and Uan, M., "Continuous Free-Surface Flow over Composite Beds," La Houille Blanche (in French), No. 1, 1979, pp. 21-30.

77. Nikuradse, J., "Laws of Flow in Rough Pipes." Translation, Technical memorandum, NACA, 1933.

78. Nitsche, W., "Measuring Skin Friction with Preston Tubes in Boundary-Layer Flows with Additional Parameters," Translated by NRC, TT-1989, Ottawa 1981.

79. Nitsche, W., Thunker, R., and Haberland, C., "A Computational Preston Tube Method," Proceedings of the 4th International Symposium on Turbulent Shear Flows, Karlsruhe, Sept. 1983.

80. Noutsopoulos, G. and Hadjipanos,P., "Discharge computations in compound channels" Proceedings of Intern. Conf. of IAHR, Vol. D, Moscow Sep. 1983,pp.173-180.

81. O'Loughlin, E.M. and Annambhotla, V.S., "Flow Phenomena Near Rough Boundaries," Journal of Hydraulic Research, Vol. 7, No. 2, 1969, pp. 231-250.

82. O'Loughlin, E.M. and MacDonald, E.G., "Some Roughness Concentration Effects on Boundary Resistance," La Houille Blanche, No. 7, 1964.

83. Pasche, E., Evers, P. and Rouve,G., "Investigations on Hydraulic Effects of Vegetated Flood Plains in Compound Cross-Section and their Influences on Discharge Capacity" Proceedings of Intern. Conf. of IAHR, Vol. D, Moscow Sep.1983, pp. 489-497.

84. Patankar, S., "Numerical Heat Transfer and Fluid Flow," Series in Computational Methods in Mechanics and Thermal Sciences, McGraw Hill Co., 1980.

85. Patel, C., "Calibration of the Preston Tube and Limitations on its use in Pressure Gradients," Journal of Fluid Mechanics, Vol. 23, 1965, pp. 185-208.

86. Petryk, S. and Grant, E.U., "Critical Flow in Rivers with Flood Plains," Journal of the Hydraulics Division, ASCE, Vol. 104, No. HY5, May 1978, pp. 583-593.

87. Petryk, S. and Shen, H.W., "Direct Measurement of Shear Stress in a Flume," Journal of Hydraulics Division, ASCE, Vol. 97, No. HY6, June 1971, pp. 883-887.

88. Perry, A.E., Schofield, W.H. and Joubert, P.N., "Rough Wall Turbulent Boundary Layers," Journal of Fluid Mechanics, Vol. 37, No. 2, 1969, pp. 383-413.

89. Posey, C.J., "Computation of Discharge including Over-Bank Flow," Civil Engineering, ASCE, April 1967, pp. 62-63.

90. Progress Report of the Task Force on Friction Factors in Open Channels of the Committee on Hydromechanics of the Hydraulics Division. "Friction Factors in Open Channels," Journal of the Hydraulics Division, ASCE, Vol. 89, No. HY2, March 1963, pp. 97-143.

91. Preston, J.H., "The Determination of Turbulent Skin Friction by Means of Pitot Tubes," Journal of Royal Aeronautical Soc., Vol. 54, pp. 109-121.

92. Prinos, P. and Townsend, D.R., "Estimating Discharge in Compound Open Channels," Proceedings of 6th Canadian Hydrotechnical Conference, Vol. 1, June 1983, pp. 129-146.

93. Prinos, P. and Townsend, D.R., "A Comparison of Methods for Predicting Discharge in Compound Open Channels" Presented in the Intern. Conf. on Hydraulic Design in Water Resources Engineering:Channel and Channel Control Structures. To be published in Advances in Water Resources, Dec. 1984.

94. Prinos, P. and Townsend, D.R., "Prediction of Main Channel/Flood plain Flow interaction with FEM" Proceedings of 6th International Conf. on Finite Elements in Water Resources, Vermont, 1984,pp. 509-519.

95. Puri, A.N and Kuo, C.Y "Penalty Function FEM for 2-D Hydrodynamic Model" Proceedings of Hydraulics Div. Special Conference on Frontiers in Hydraulic Engineering,ASCE, MIT 1983, pp.356-361

96. Pyle, R. and Novak, P., "Coefficient of Friction in Conduits with Large Roughness," Journal of Hydraulic Research, IAHR, Vol. 19, No. 1, 1981.

98. Radojkovic, M., "Mathematical Modeling of Rivers with Flood Plains," 3rd Annual Symposium of the Waterways, Harbours and Coastal Eng. Div., ASCE, Vol. 1, Rivers 1976, pp. 55-64.

99. Radojkovic, M. and Ivetic, M., "Finite Element Analysis of Momentum Transfer in Rivers of Complex Cross-Section," Proceedings 4th Int. Conference on Finite Element in Water Resources, Hanover 1982.

100. Raichlen, F., "Some Turbulence Measurements in Water," Journal of Engineering Mechanics Division, ASCE, Vol. 93, No. EM2, April 1967, pp. 73-79.

101. Rajaratnam, N., "A Theoretical Calibration Curve for the Preston Tube on Smooth Boundaries for Large Reynolds Numbers." Journal of the Royal Aeronautical Society, 1965.

102. Rajaratnam, N., "On the Preston Tube with a Hemispherical Nose;" Civil Engineering and Public Works Review, November 1965.

103. Rajaratnam, N. and Ahmadi, R.M., "Interaction between Main Channel and Flood Plain Flows," Journal of the Hydraulics Division, ASCE, Vol. 105, No. HY5, May 1979, pp. 573-588.

104. Rajaratnam, N. and Ahmadi, R., "Hydraulics of Channels with Flood Plains," Journal of Hydraulic Research, IAHR, Vol. 19, No. 1, 1981.

105. Rajaratnam, N., "Turbulent Jets," Elsevier Sc. Publ. Co., Amsterdam, 1976, p. 304.

106. Rajaratnam, N. and Muralidhar, D., "The Prandl Tube as a Preston Tube," Civil Engineering and Public Works Review.

107. Rajaratnam, N. and Muralidhar, D., "Boundary Shear Stress Distribution in Rectangular Open Channels," La Houille Blance, Grenoble, France, No. 6, 1969, pp. 603-609.

108. Rastogi, A.K. and Rodi, W., "Predictions of Heat and Mass Transfer in Open Channels," Journal of the Hydraulic Division, ASCE, 104, No. HY3, 1978, pp. 397-420.

109. Replogle, J.A. and Ghow, V.T., "Tractive Force Distribution in Open Channels," Journal of the Hydraulics Division, ASCE, Vol. 92, No. HY2, March 1966, pp. 169-191.

110. Resch, F.J., "Hot-Film Turbulence Measurements in Water Flow," Journal of Hydraulics Division, ASCE, Vol. 96, No. HY3, March 1970, pp. 787-800.

111. Rice, C.E., "Hydraulics of Main Channel Flood Plain Flows," Research Project Technical Completion Report, Oklahoma State Univ, 1974.

112. Richardson, E.V. and McQuivey, R.S., "Measurement of Turbulence in Water," Journal of the Hydraulics Division, ASCE, March 1968, pp. 411-430.

113. Rodi, W., "Turbulence Models and their Applications in Hydraulics: A State-of-the-Art Review," IAHR Book Publication, 1980, Delft.

114. Rodi, W., Testing and Calibration of Turbulence Models for Transport and Mixing Proc. of hydraulics Div. Special Conference on Applying Research to Hydraulic Practice, Jackson, 1982 pp.584-593.

115. Rotta, J.C., "Turbulent Boundary Layers in Incompressible Flow," Progress in Aeronautical Sciences, 2, 1962, London: Pergamon Press.

116. Rouse, H., "Critical Analysis of Open-Channel Resistance," Journal of the Hydraulics Division, ASCE, Vol. 91, No. HY4, July 1965, pp. 1-25.

117. Sarma, K.V.N., Lakshminarayana, P. and Rao, N.S.L., "Velocity Distribution in Smooth Rectangular Open Channels," Journal of Hydraulics Division, ASCE, Vol. 109, No. 2, Feb. 1983, pp. 270-293.

118. Schlichting, H., "Boundary-Layer Theory," McGraw Hill Book Co. Inc., New York, 1968, 6th Edition.

119. Schlichting, H., "Experimental Investigation of Surface Roughness" Translation, Technical Memorandum 823, NACA, 1936.

120. Sellin, R.H., "A Laboratory Investigation into the Interaction between the Flow in the Channel of a River and that over its Flood Plain," La Houille Blanche, Grenoble, France, No. 7, 1964, pp. 793-802.

121. Sellin, R.H.J., "A Technique based on the Schlieren Principle for Studying the Surface of a liquid" Journal of Scientific Instrumentation, Vol. 40, July 1963, pp. 355-357.

122. Sill, B.L., "New Flat Plate Turbulent Velocity Profiles," Journal of Hydraulics Division, ASCE, Vol. 108, No. HY1, Jan. 1982, pp. 1-15.

123. Smith, C.D., "Effect of Channel Meanders on Flood Stage in Valley," Journal of the Hydraulics Division, ASCE, Vol. 104, No. HY1, January 1978, pp. 49-58.

124. "South Nation " Study ; H. G. Acres Co. Ltd. (for the S. N. Water Conservation Authority)

125. Tamai, N. and Kawahara, Y., "Resistance Law of a Flow in Composite Cross Sections," 3rd Congress Asian and Pacific Regional Division of IAHR Boundary, Vol. B, Paper B & C, August 1982, pp. 42-51.

126. Tingsanchali, T. and Ackermann, N.L., "Effects of Overbank Flow in Flood Computations," Journal of the Hydraulics Division, ASCE, Vol. 102, No. HY7, July 1976, pp. 1013-1025.

127. Toebes, G.H. and Sooky, A.A., "Hydraulics of Meandering Rivers with Flood Plains," Journal of Waterways and Harbours, ASCE, Vol. 93, May 1967, pp. 213-236.

128. Townsend, D.R., "An Investigation of Turbulence Characteristics in a River Model of Complex Cross Section," Proc. Inst. of Civil Engineers, Vol. 40, June 1968, pp. 155-175.

129. Townsend, D.R., "An Investigation of Turbulence Characteristics in a Region of High Shear Flow" Ph.D thesis, Queen's University,Civil Eng. Dep., Belfast 1967.

130. Tracy, H.J., "Turbulent Flow in a Three-Dimensional Channel," Journal of the Hydraulics Division, ASCE, Vol. 91, No. HY6, November 1965, pp. 9-35.

131. Tracy, H.J., "The Structure of a Turbulent Flow in a Channel of Complex Shape" U.S. Geological Syrvey, Prof. Paper 983,1976,25p.

132. Tracy, H.J. and Lester, C.M., "Resistance Coefficients and Velocity Distribution, Smooth Rectangular Channel," U.S. Geological Survey,Water Supply Paper 1592-A,18p.

133. Weiss, H.W. and Midgley, D.C., "Suite of Mathematical Flood Plain Models," Journal of the Hydraulics Division, ASCE, Vol. 104, No. HY3, March 1978, pp. 361-376.

134. Vreugdenhil, C.B. and Wijbenga, J.H.A., "Computation of Flow Patterns in Rivers," Journal of the Hydraulics Division, ASCE, November 1982, HY11, pp. 1296-1309.

135. Vreugdenhil, C.B. and Wijbenga, J.H.A., Closure on "Computation of Flow Patterns in Rivers," Journal of the Hydraulics Division, ASCE, January 1984, HY1, pp. 90-91

136. Wormleaton, P.R. and Allen, J. and Hadjipanos, P., "Effects of Shear Stresses in Compound Channels," Proceedings of the International Conference on Water Resources Development, Taipei, Taiwan, Republic of China, May 12-14, 1980.

137. Wormleaton, P.R. and Allen, J. and Hadjipanos, P., "Discharge Assessment in Compound Channel Flow," Journal of the Hydraulics Division, ASCE, Vol. 108, No. HY9, September 1982, pp. 975-993.

138. Wormleaton, P.R. and Allen, J. and Hadjipanos, P., "Apparent Shear Stresses in Compound Channel Flow," IAHR Symposium on River Engineering and its Interaction with Hydrological and Hydraulics Research, Belgrade, Yugoslavia, May 1980.

139. Wright, R.R. and Carstens, M.R., "Linear-Momentum Flux to Overbank Sections," Journal of the Hydraulics Division, ASCE, Vol. 96, No. HY9., September 1970, pp. 1781-1793.

140. Yen, B.C., "Open-Channel Flow Equations Revisited," Journal of the Engineering Mechanics Division, ASCE, Vol. 99, No. EM5, October 1973, pp. 979-1009.

141. Yen, C.L. and Overton, D.E., "Shape Effects on Resistance in Flood-Plain Channels," Journal of the Hydraulics Division, ASCE, Vol. 99, No. HY1, January 1973, pp. 219-238.

142. Yen, C.L. and Overton, D.E., "A Method for Flow Computation in Floodplain Channels," Proceedings, International Symposium on Stochastic Hydraulics, University of Pittsburgh, 1971.

143. Zheleznyakov, G.V., "Relative Deficit of Mean Velocity of Instable River Flow, Kinematic Effect in River Beds with Flood Plains," Proceedings of International Association for Hydraulic Research, Eleventh International Congress, Vol. 345, Leningrad 1965.

144. Zheleznyakov, G.V., "Interaction of Channel and Flood Plain Streams," Proceeding of the International Association for Hydraulic Research Congress, Vol. 5, Paris, France, 1971, pp. 144-148.

145. Zippe, H., and Graf, W., "Turbulent Boundary-Layer Flow over Permeable and Non-Permeable Rough Surfaces" Journal of Hydraulic Research, IAHR, 21,1983,No. 1, pp. 51-60.

146. TSI, Technical Bulletin no. 5, "Hot-film and hot-wire anemometry, Theory and Application"

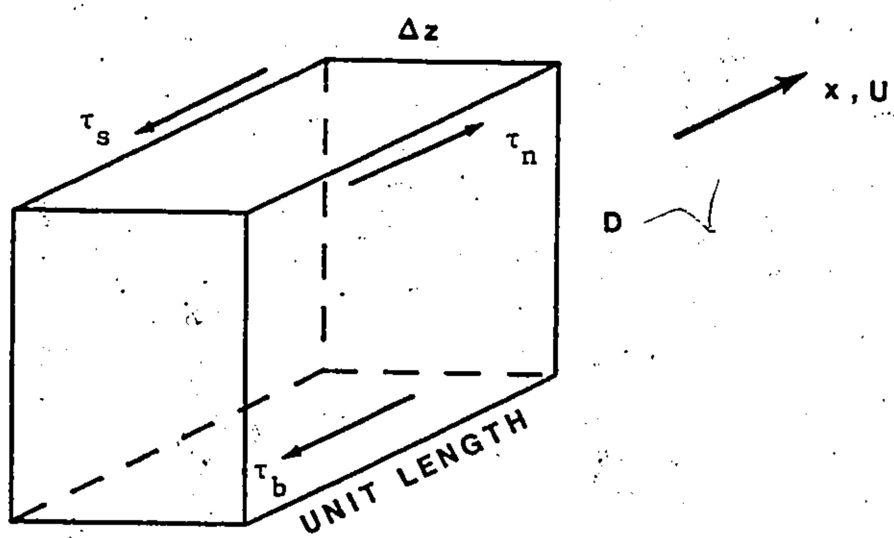

FIG. 1 : TYPICAL CONTROL VOLUME

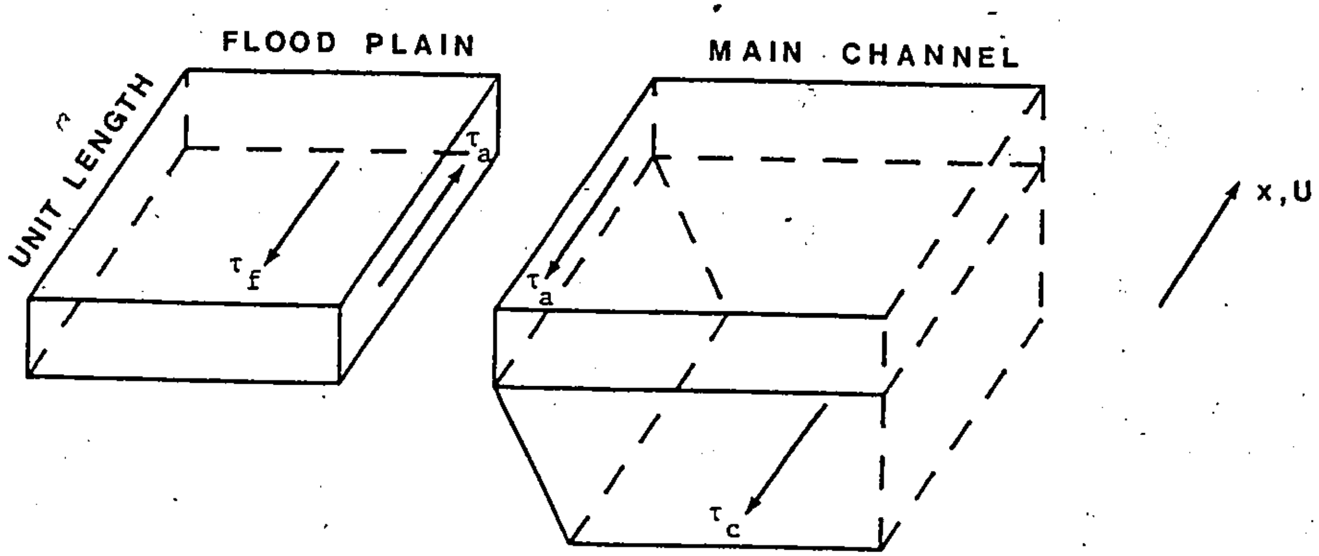

FIG. 2 : MAIN CHANNEL AND FLOOD PLAIN CONTROL VOLUMES

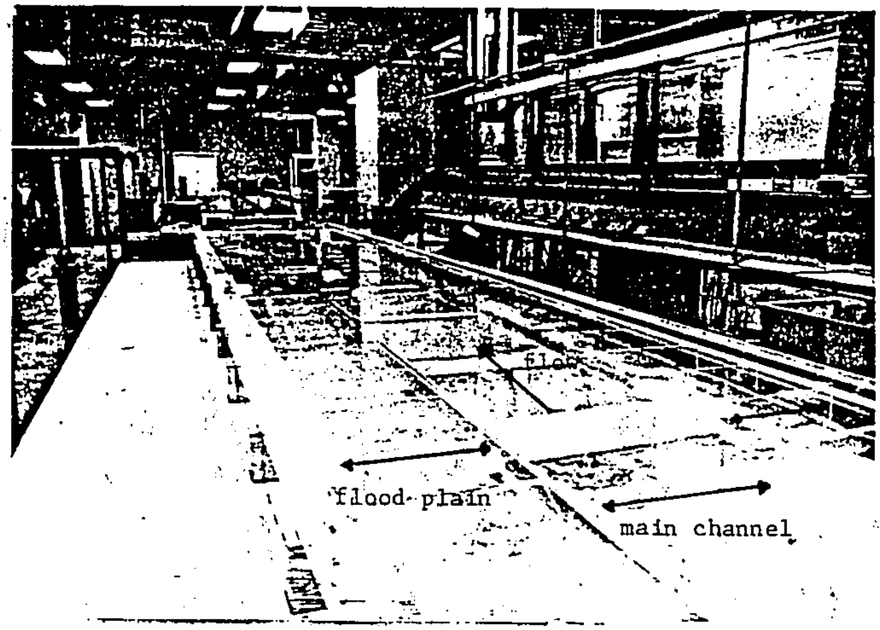

FIG. 3 : GENERAL VIEW OF THE EXPERIMENTAL CHANNEL

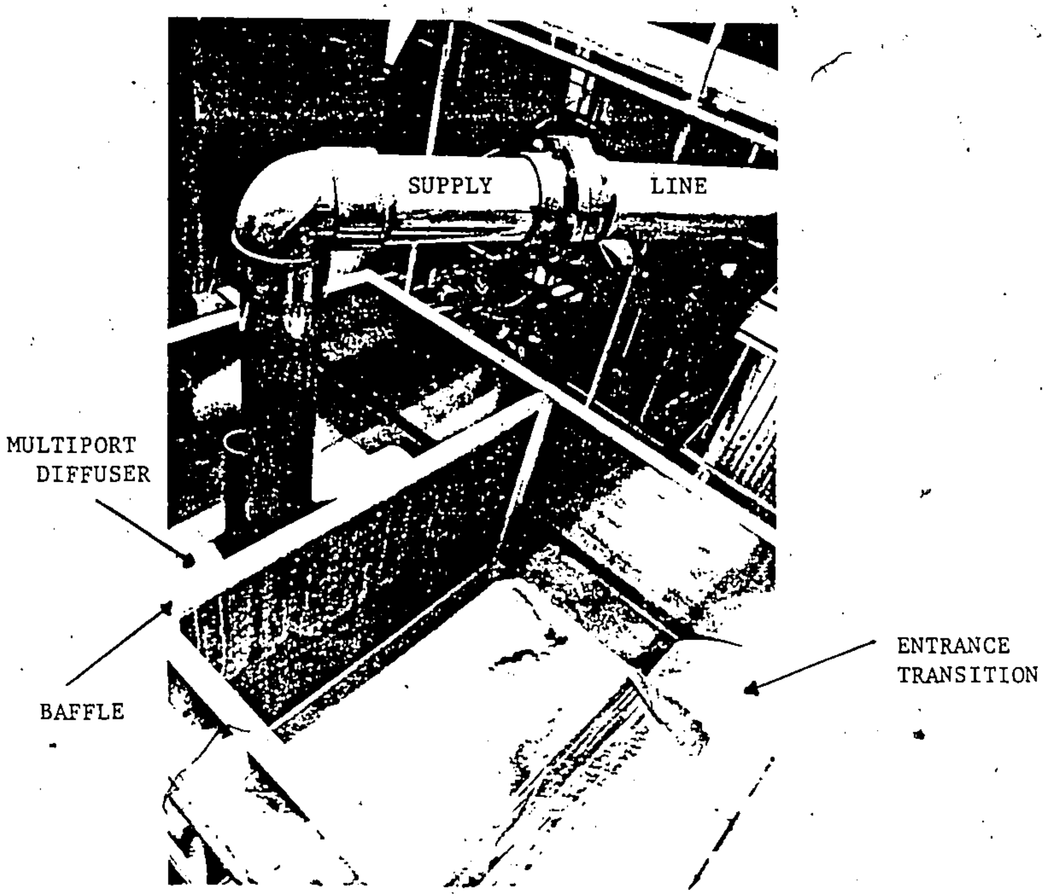

FIG. 4 : VIEW OF THE INLET TANK

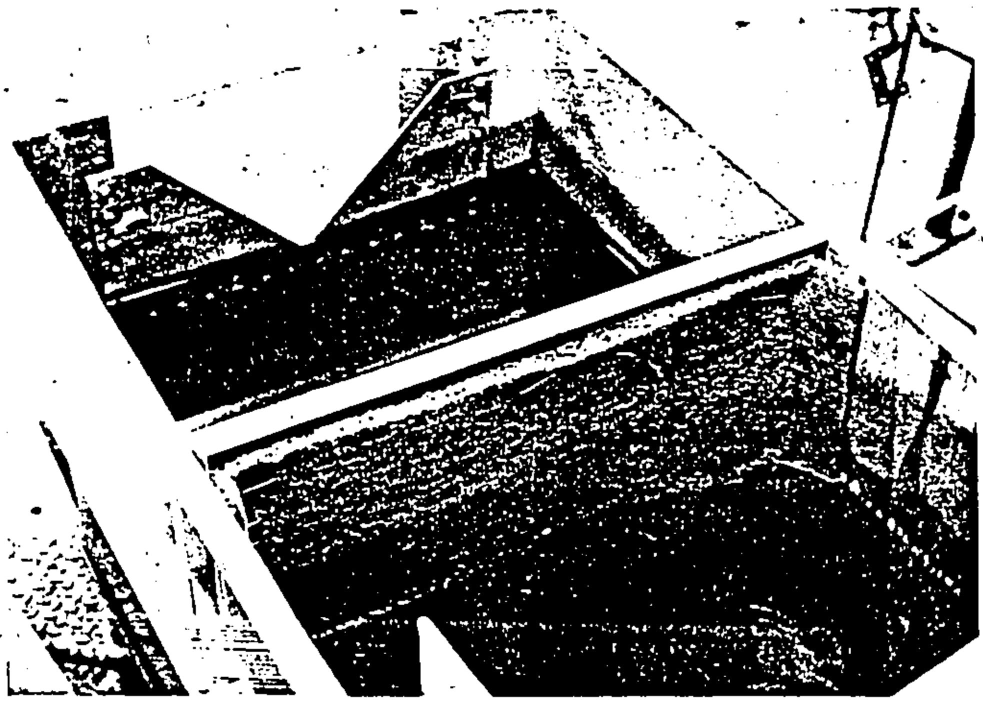

FIG. 5 : TOP VIEW OF THE OUTLET TANK

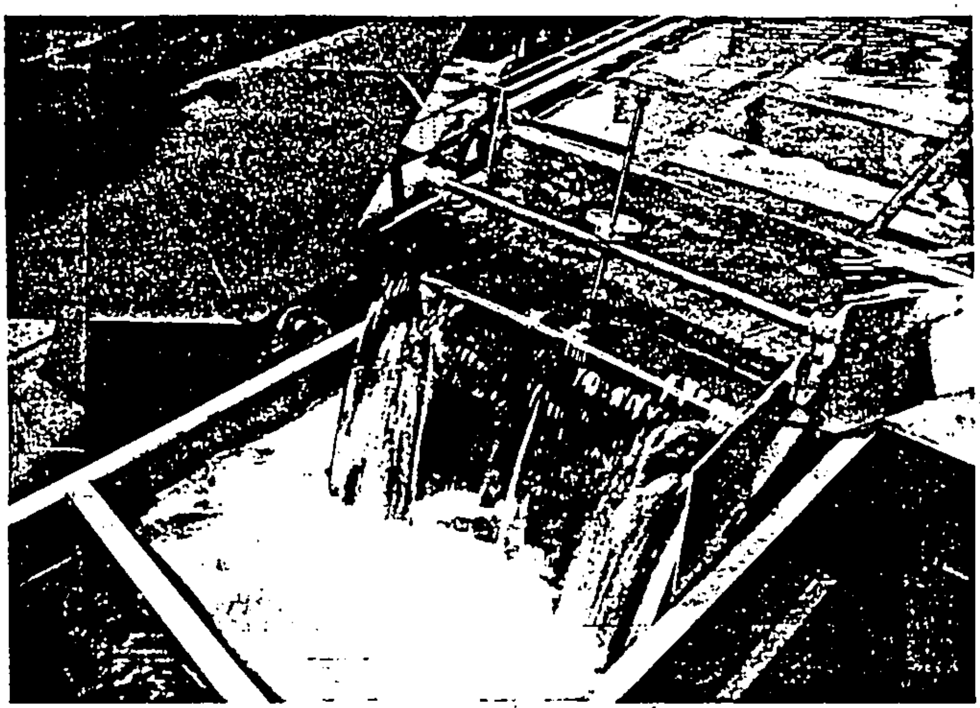

FIG.6 : OUTFALL WEIR

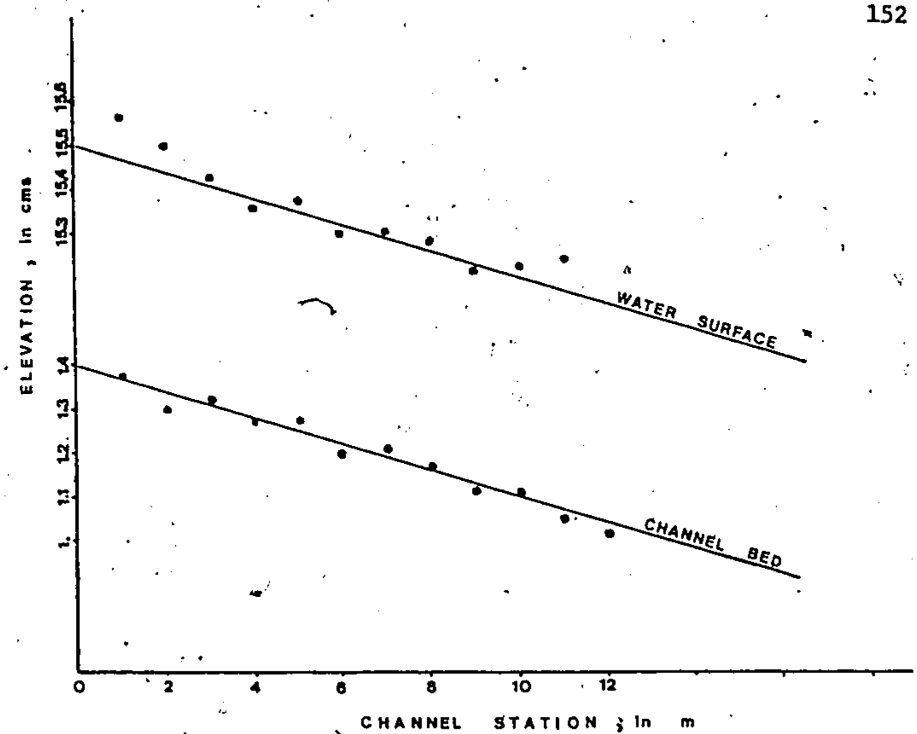

FIG. 7 : A PLOT OF THE WATER SURFACE PROFILE AND CHANNEL SLOPE

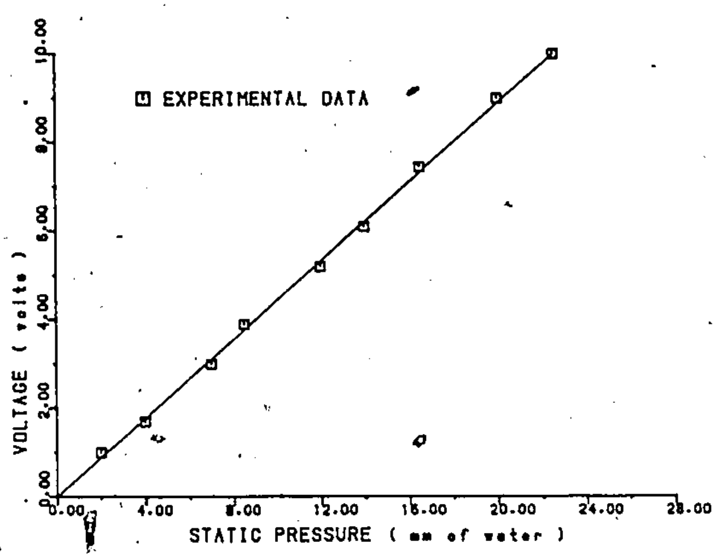

FIG. 8 : TRANSDUCER CALIBRATION WITH STATIC PRESSURE HEAD

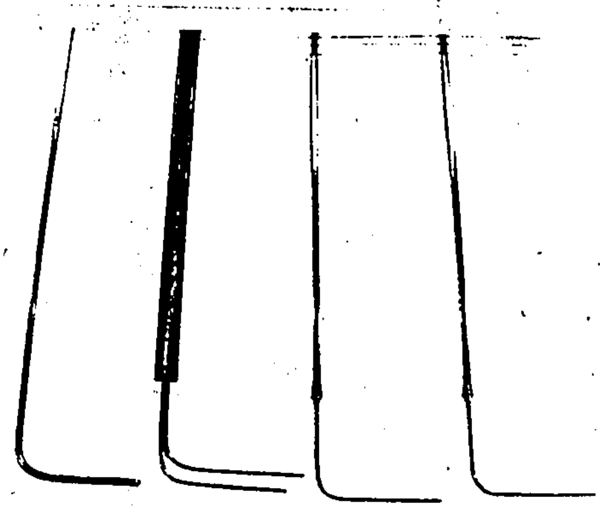

FIG. 9 : VARIOUS PROBES USED IN THE EXPERIMENTAL PROGRAM

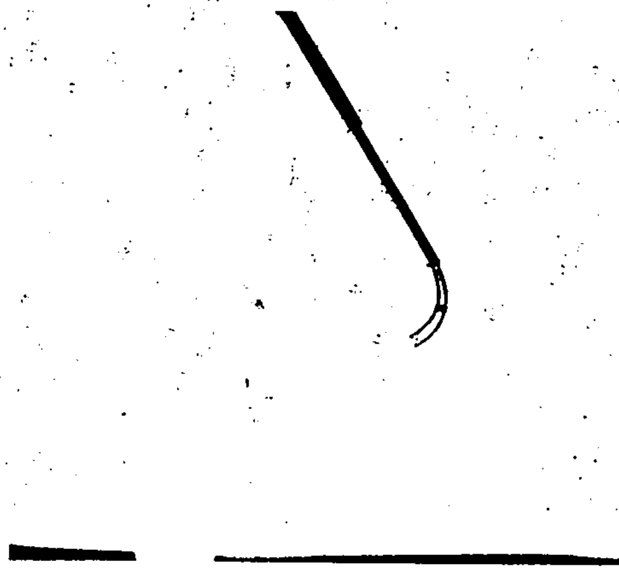

FIG. 10: CROSS HOT-FILM PROBE (MODEL TSI 1243-60W)
USED IN THE TURBULENCE MEASUREMENTS

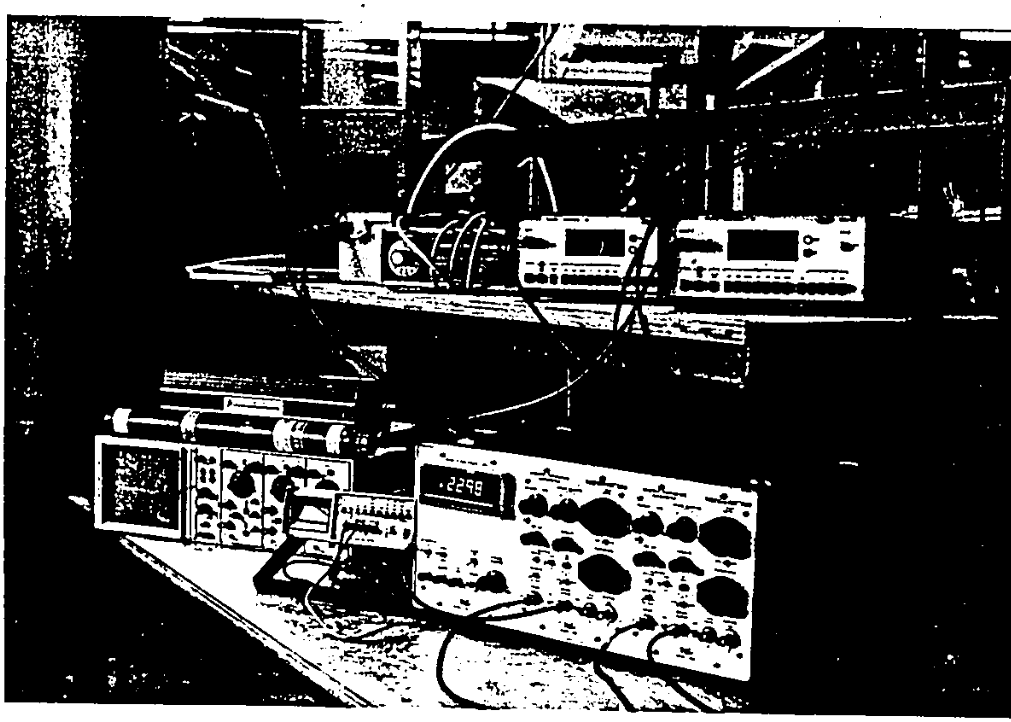

FIG. 11: ELECTRONIC EQUIPMENT USED IN THE TURBULENCE MEASUREMENTS

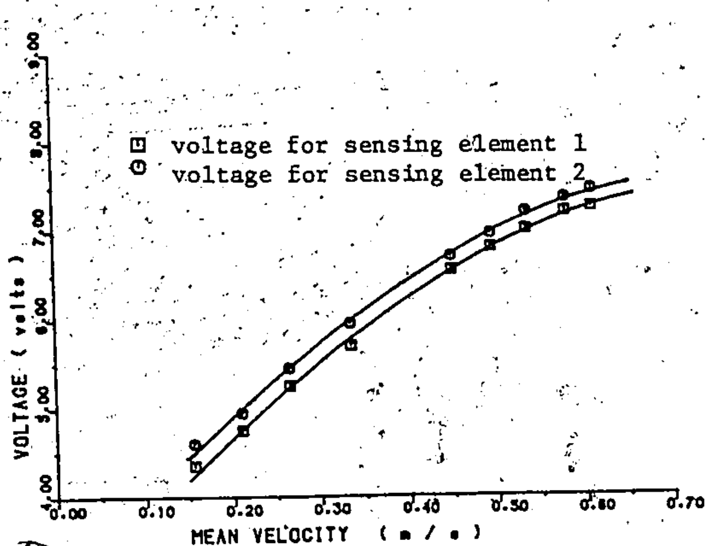

FIG.12: VOLTAGE-VELOCITY CURVE FOR CROSS HOT-FILM PROBE

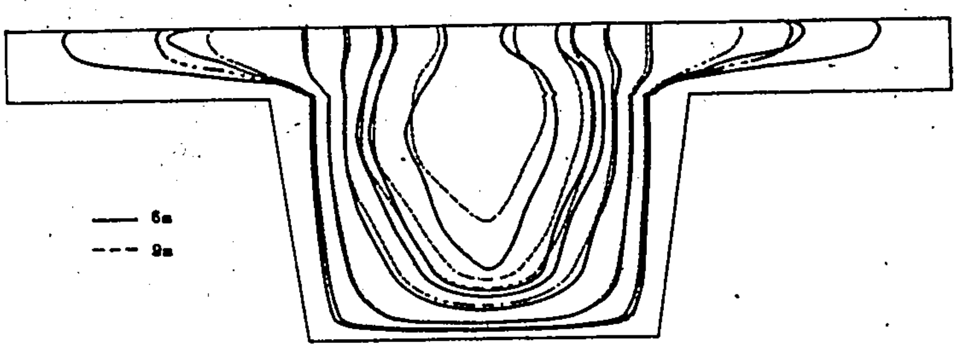

FIG 13: ISOVEL PATTERNS AT MEASURING STATIONS 6 and 9m FROM THE CHANNEL ENTRANCE

(a) (b) (c)

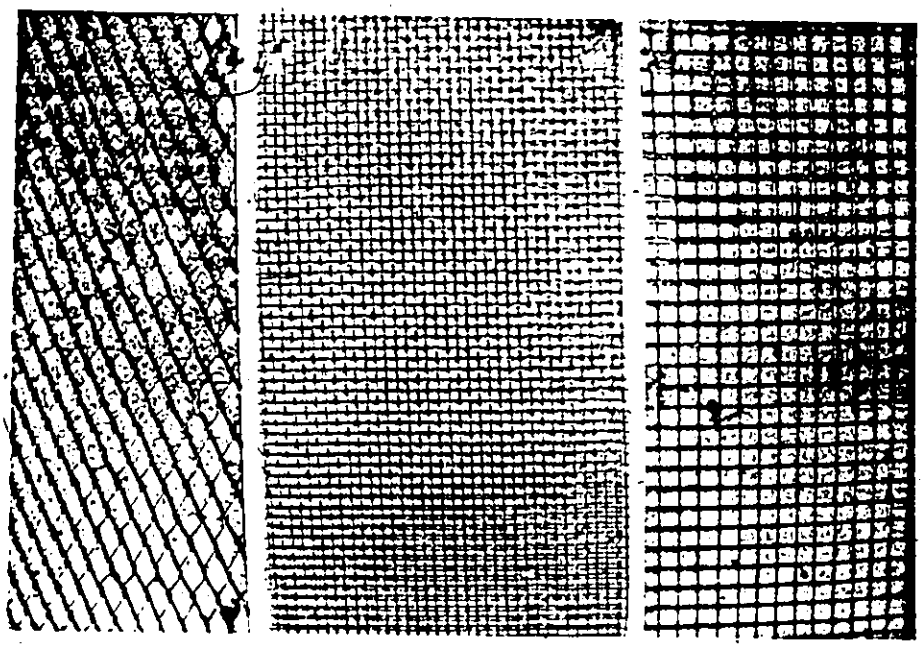

FIG. 14 : WIRE MESHES USED TO INCREASE FLOOD PLAIN ROUGHNESS

(a) "diamond pattern" expanded metal mesh
(1.5 cm longer diagonal, 1.6 mm thick)

(b) "square grid" wire mesh
(3.2 mm square, .1 mm thick)

(c) "square grid" wire mesh
(6.4 mm square, 1.1 mm thick)

y_r = relative depth

W_r = relative width

n_r = relative roughness

Q_t = total discharge

S = slope of the channel

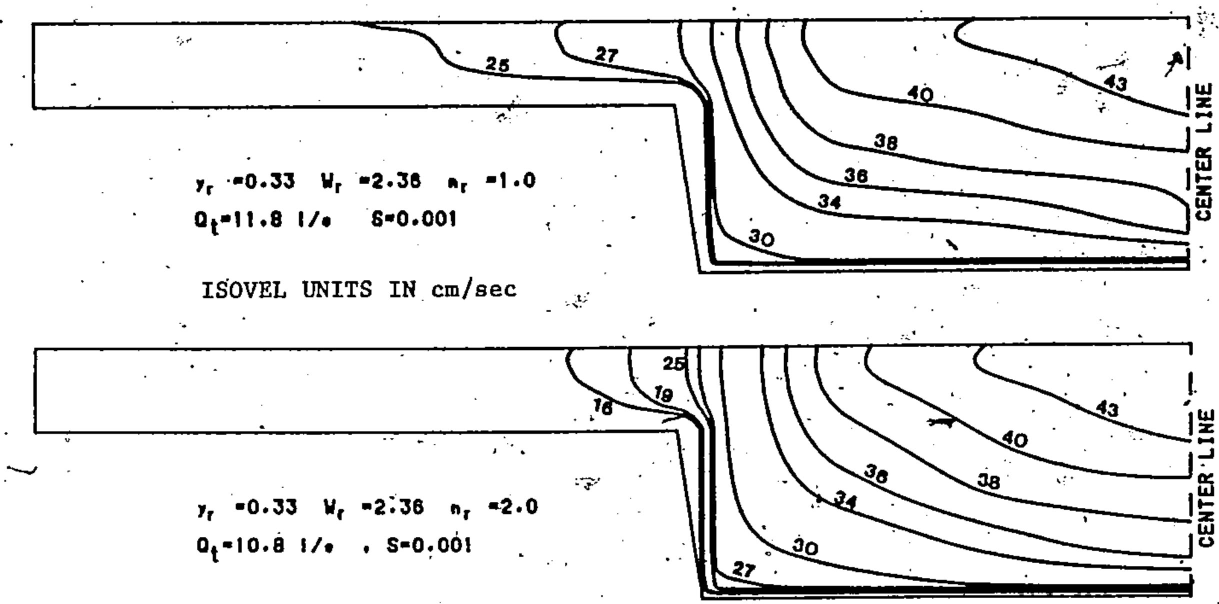

FIG.15 : ISOVEL PATTERNS FOR A "WIDE" CHANNEL CONDITION

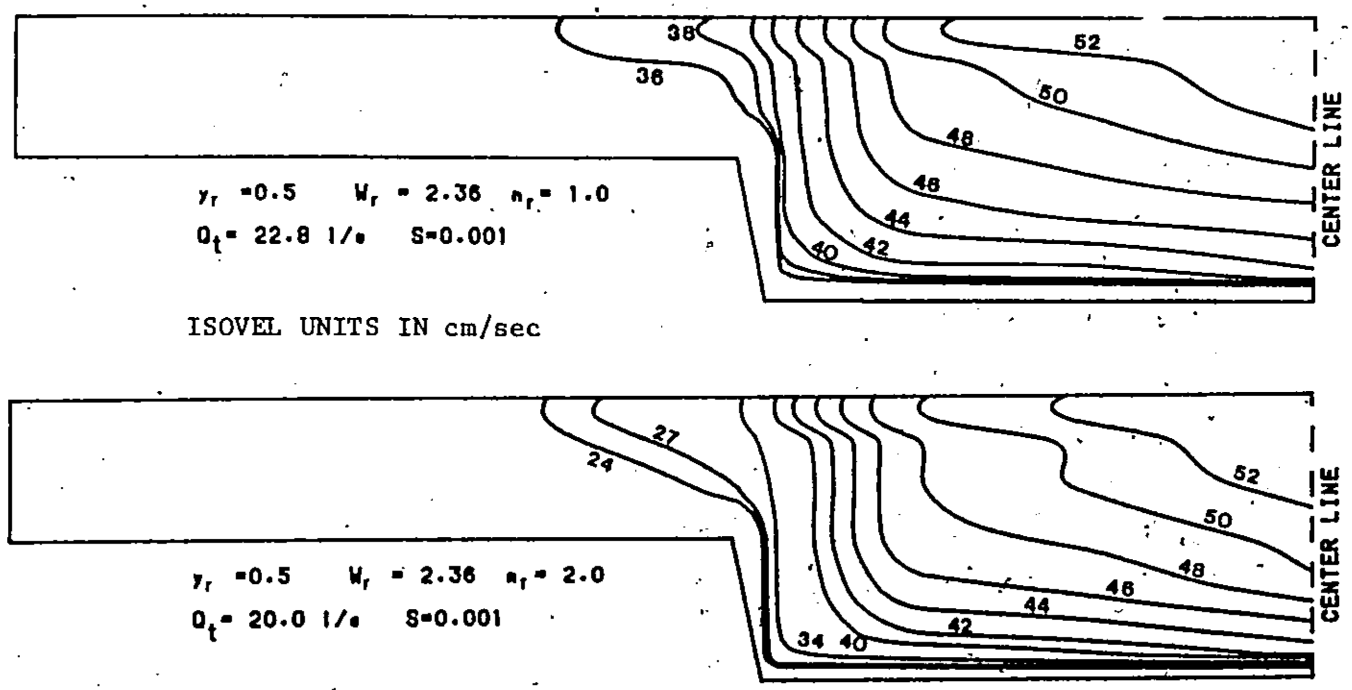

FIG 16: ISOVEL PATTERNS FOR A "WIDE" CHANNEL CONDITION

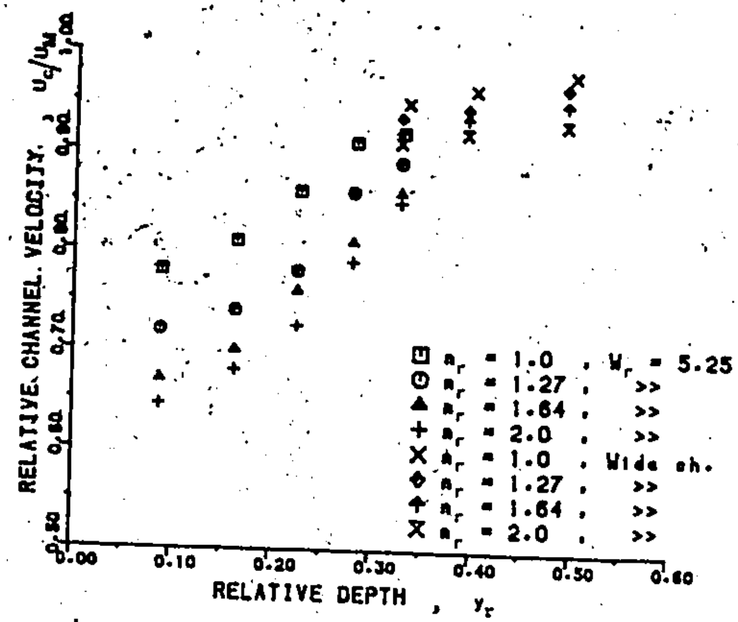

FIG.17: RELATIVE CHANNEL VELOCITY VERSUS RELATIVE DEPTH

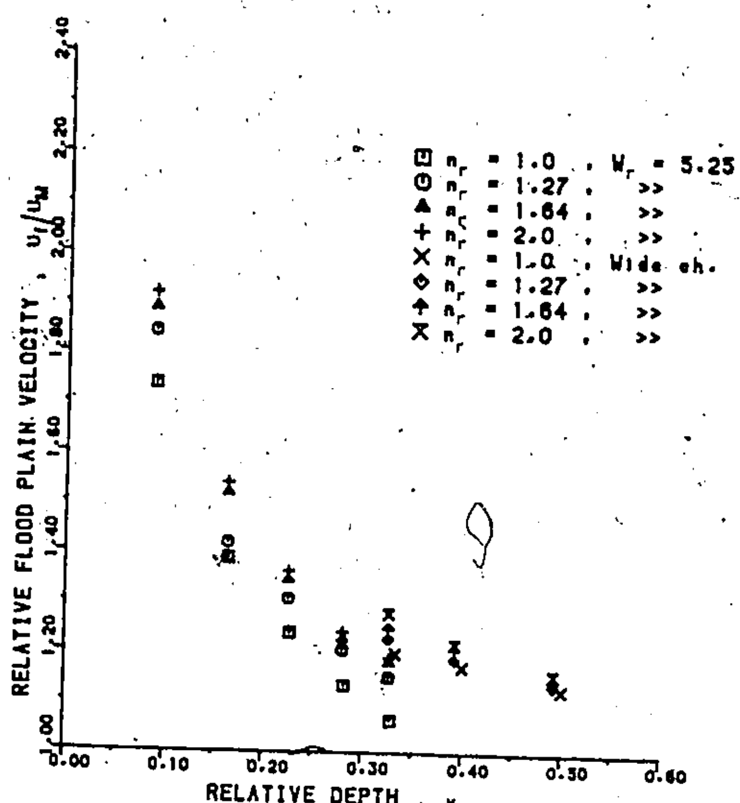

FIG.18: RELATIVE FLOOD PLAIN VELOCITY VERSUS RELATIVE DEPTH

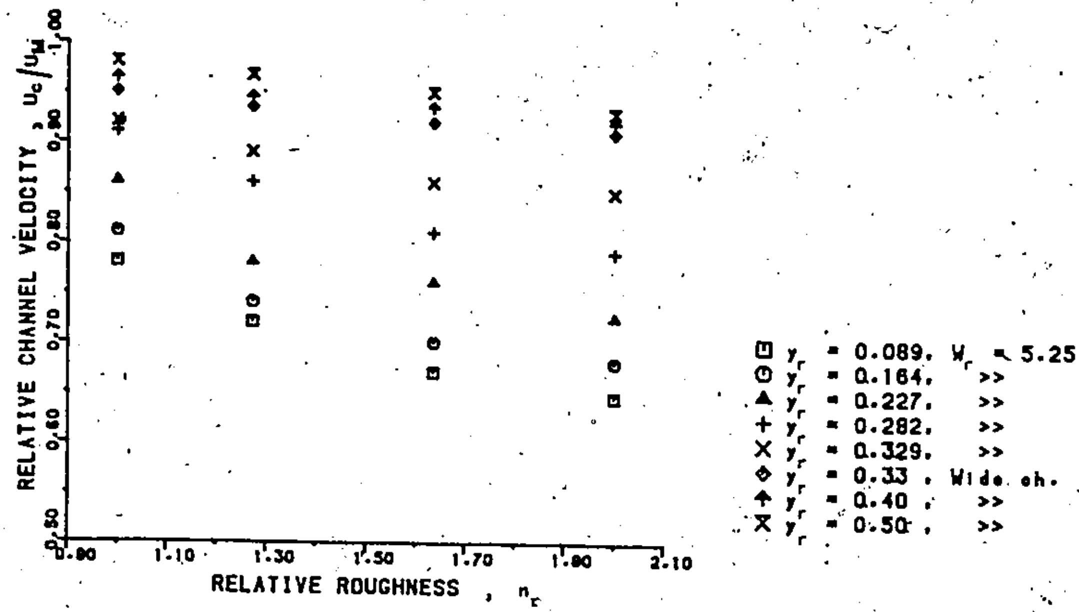

FIG.19: RELATIVE CHANNEL VELOCITY VERSUS RELATIVE ROUGHNESS

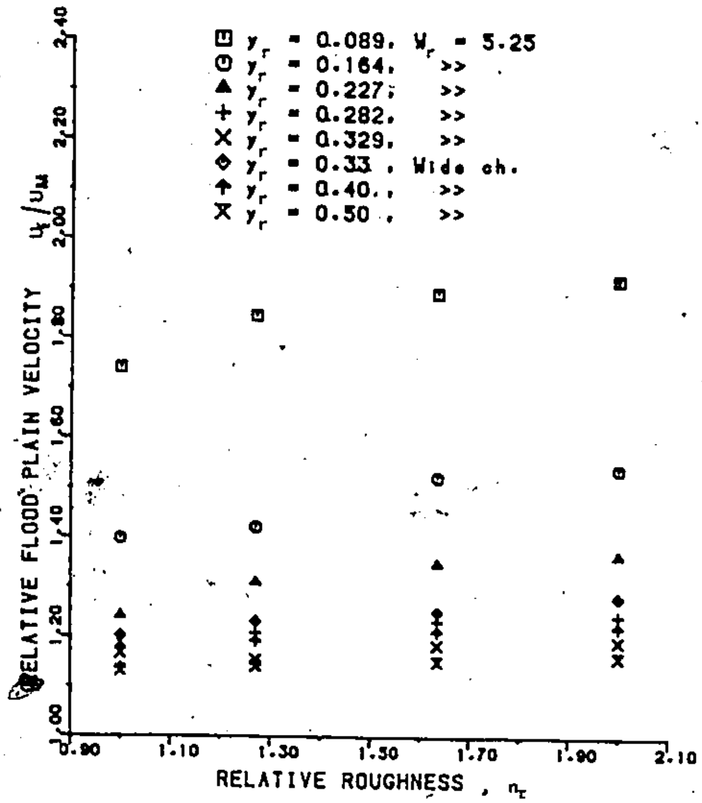

FIG.20: RELATIVE FLOOD PLAIN VELOCITY VERSUS RELATIVE ROUGHNESS

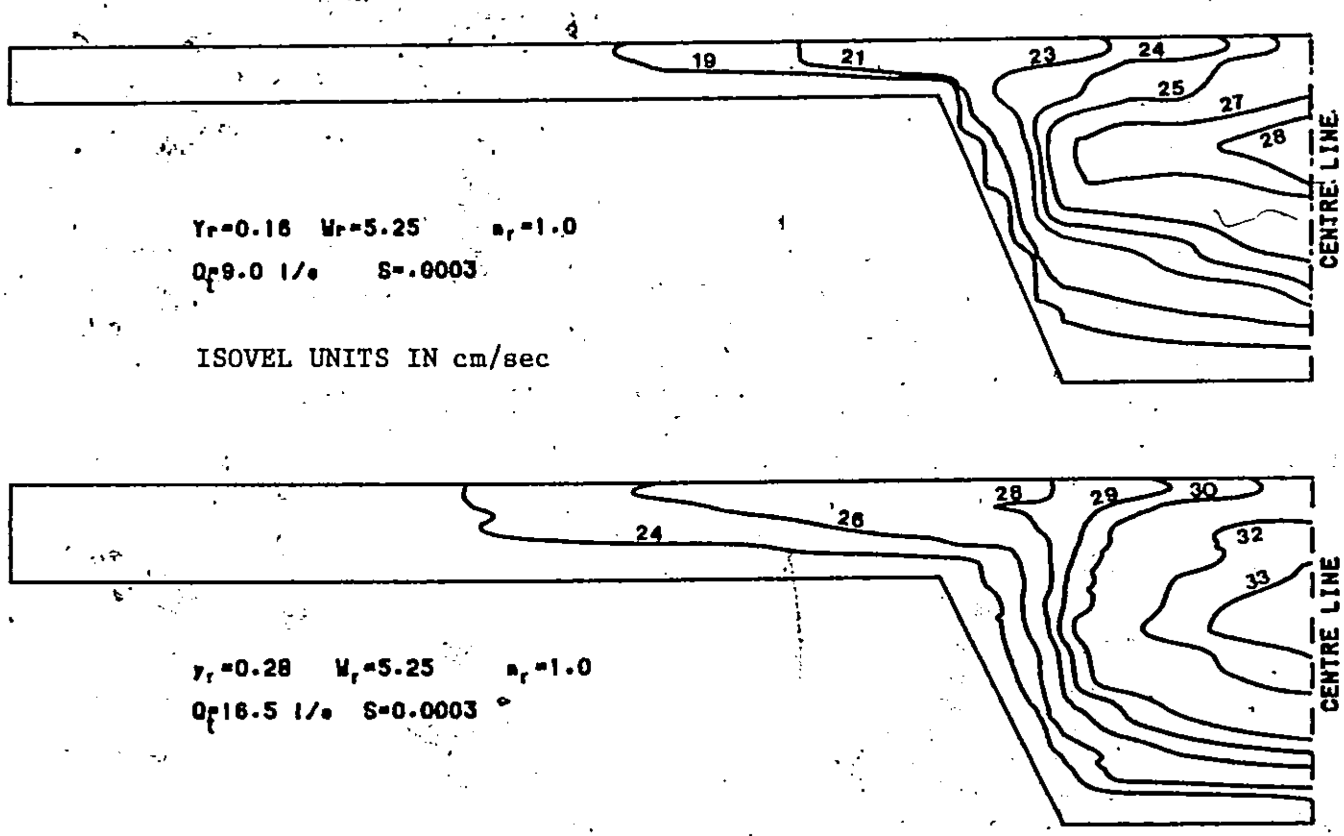

FIG. 21: ISOVEL PATTERNS FOR A "NARROW" CHANNEL CONDITION

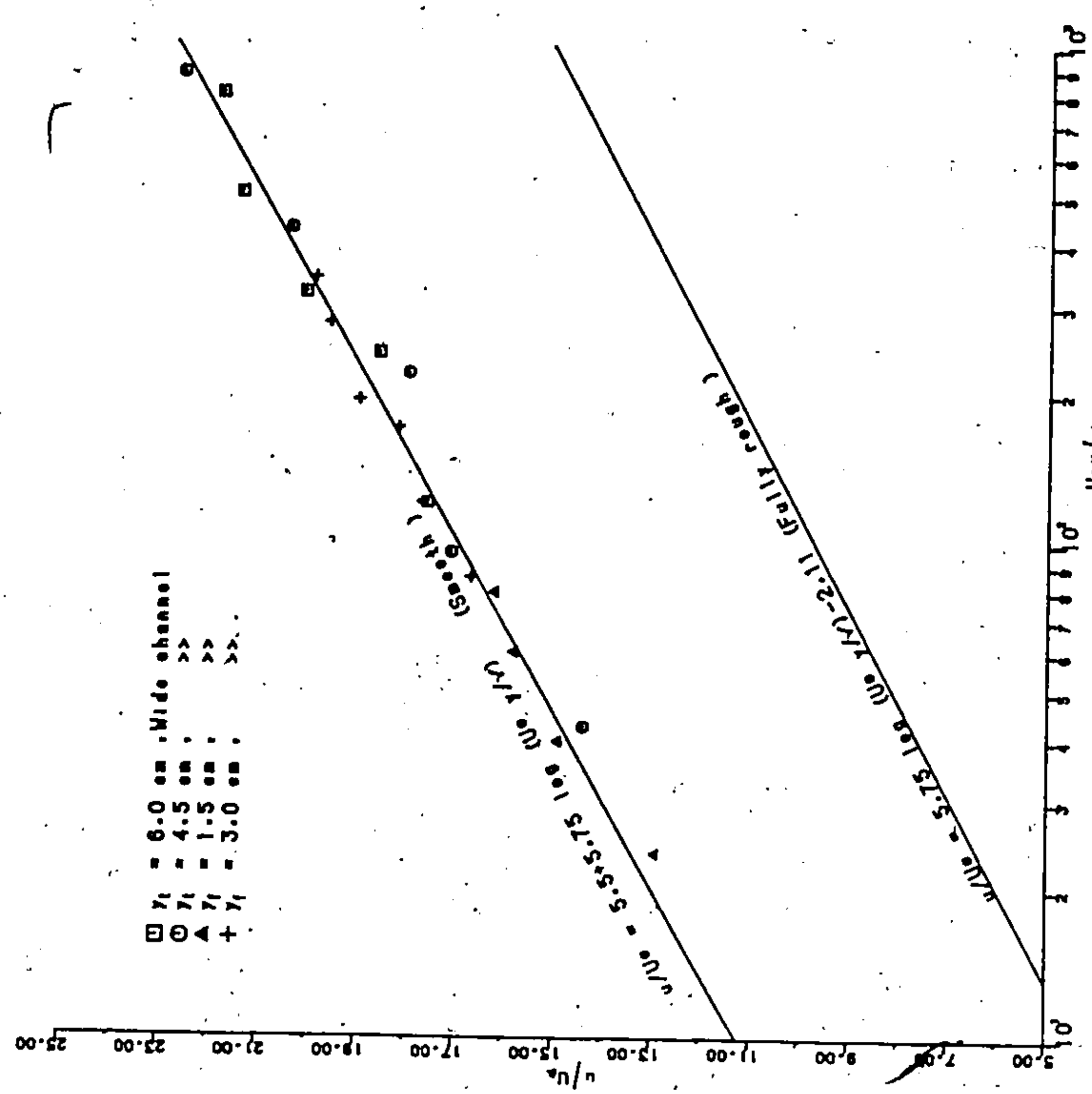

FIG.22: LOGARITHMIC VELOCITY DISTRIBUTION FOR SMOOTH TWO-DIMENSIONAL FLOW

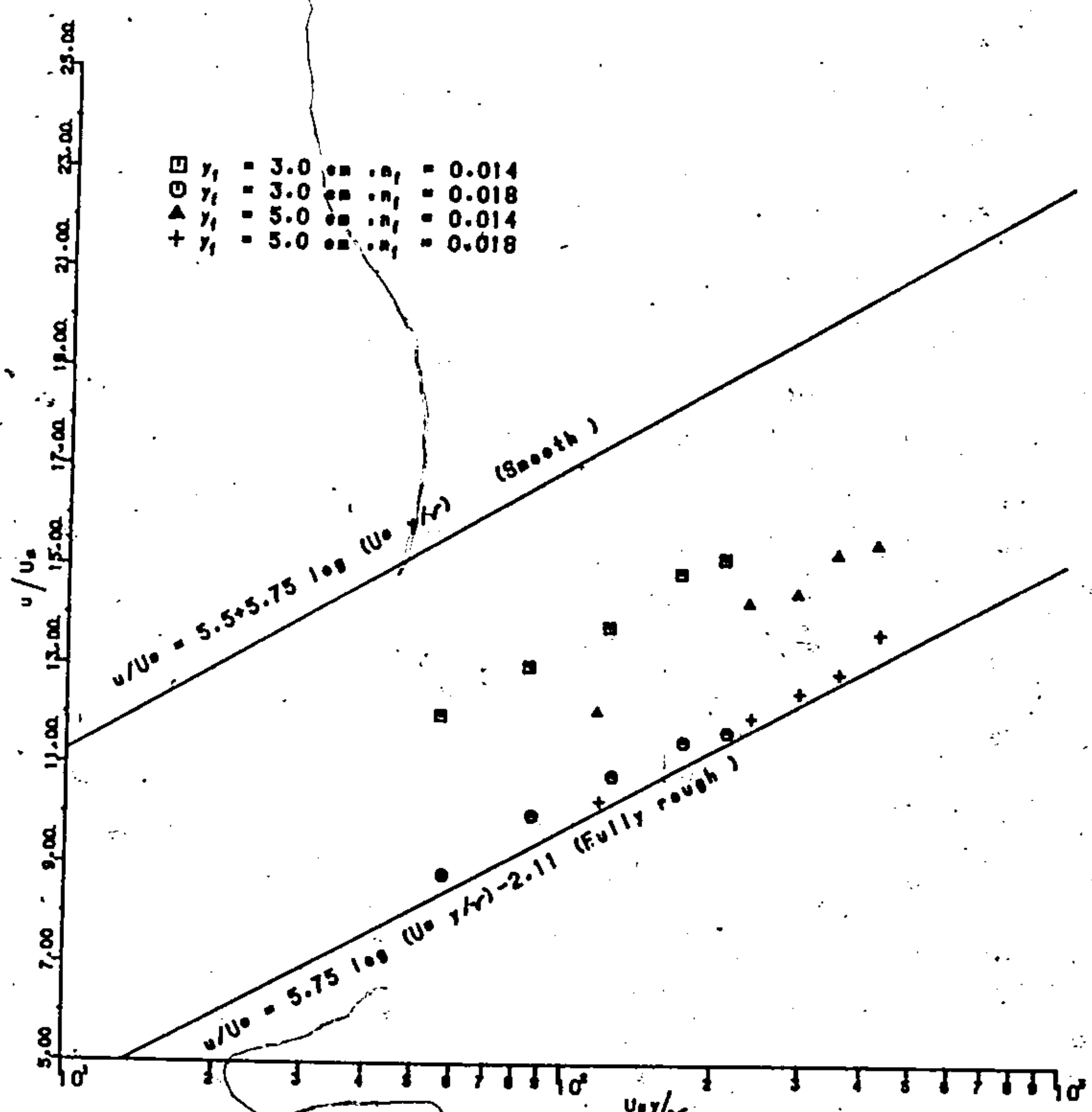

FIG. 23: LOGARITHMIC VELOCITY DISTRIBUTION FOR TRANSITIONAL TWO-DIMENSIONAL FLOW

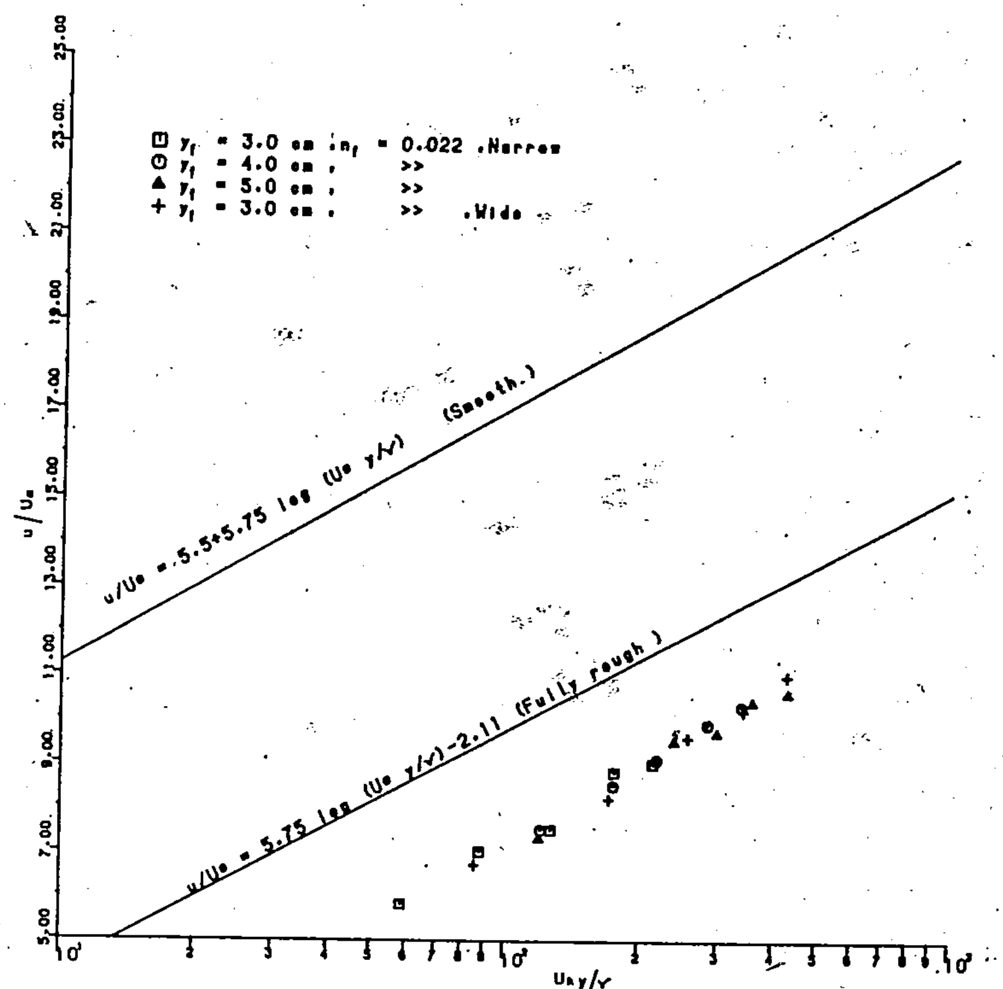

FIG.24: LOGARITHMIC VELOCITY DISTRIBUTION FOR FULLY ROUGH TWO-DIMENSIONAL FLOW

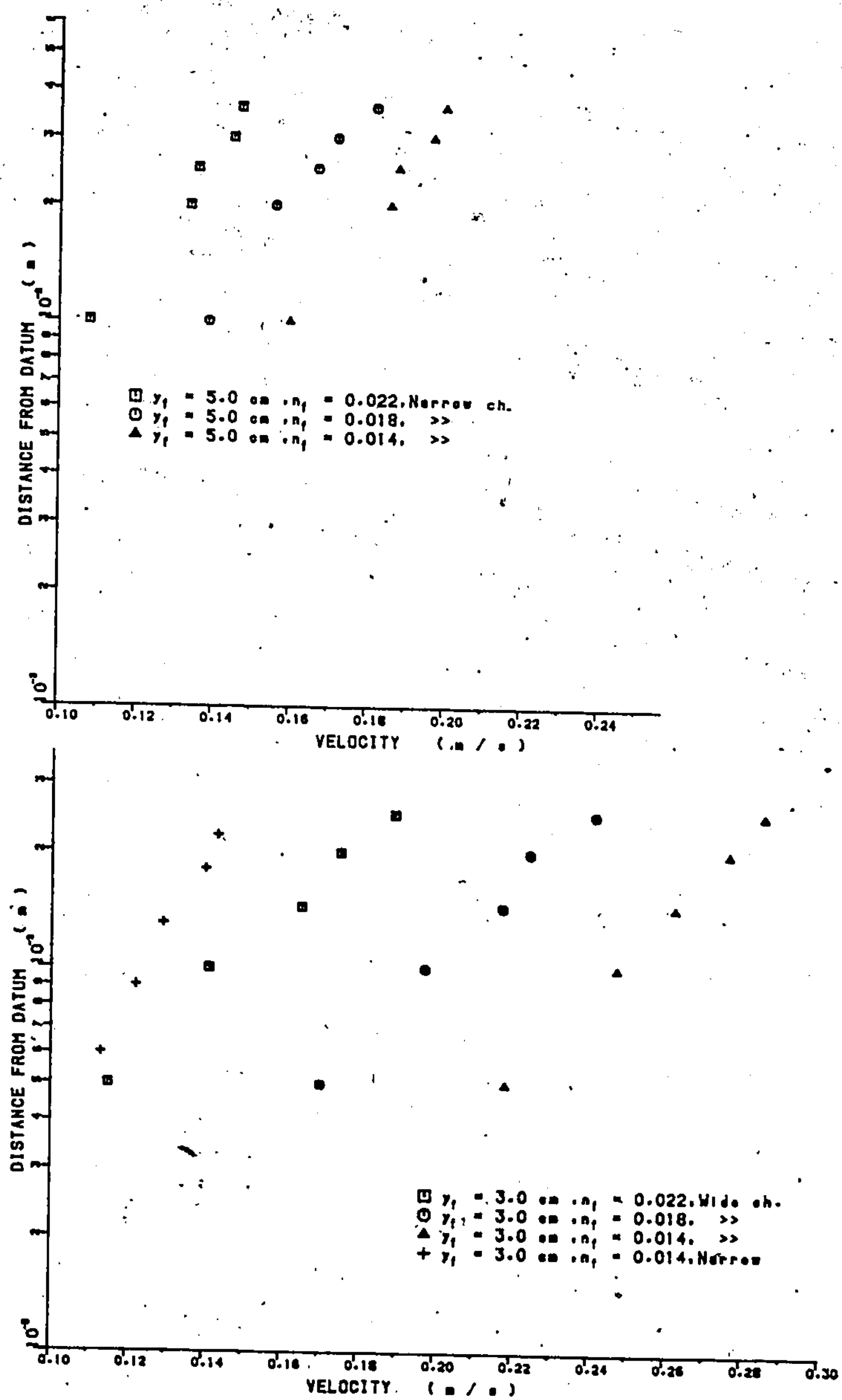

FIG. 25: VERTICAL VELOCITY DISTRIBUTION FOR TWO-DIMENSIONAL FLOW

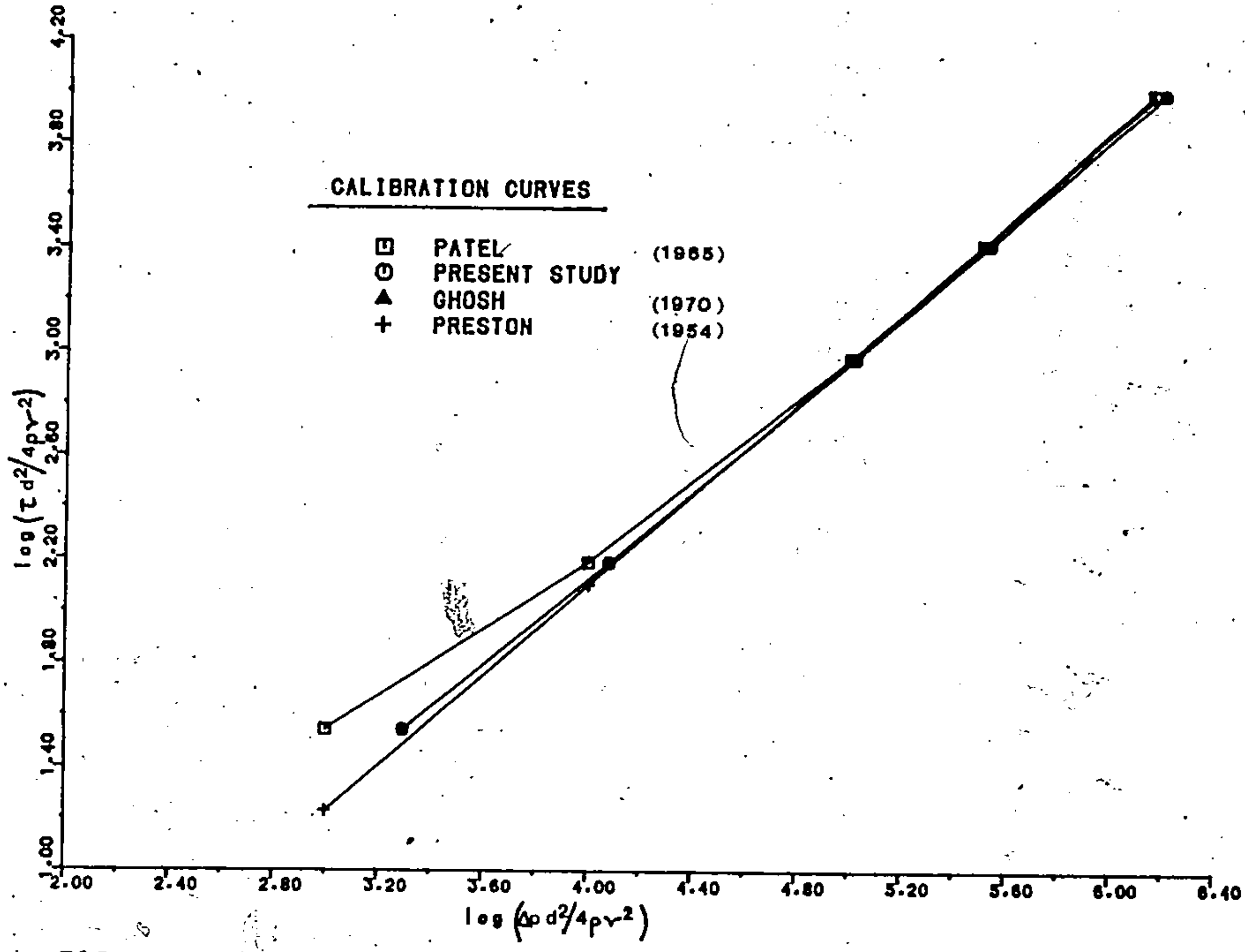

FIG. 26: CALIBRATION CURVES FOR BOUNDARY SHEAR STRESS MEASUREMENT

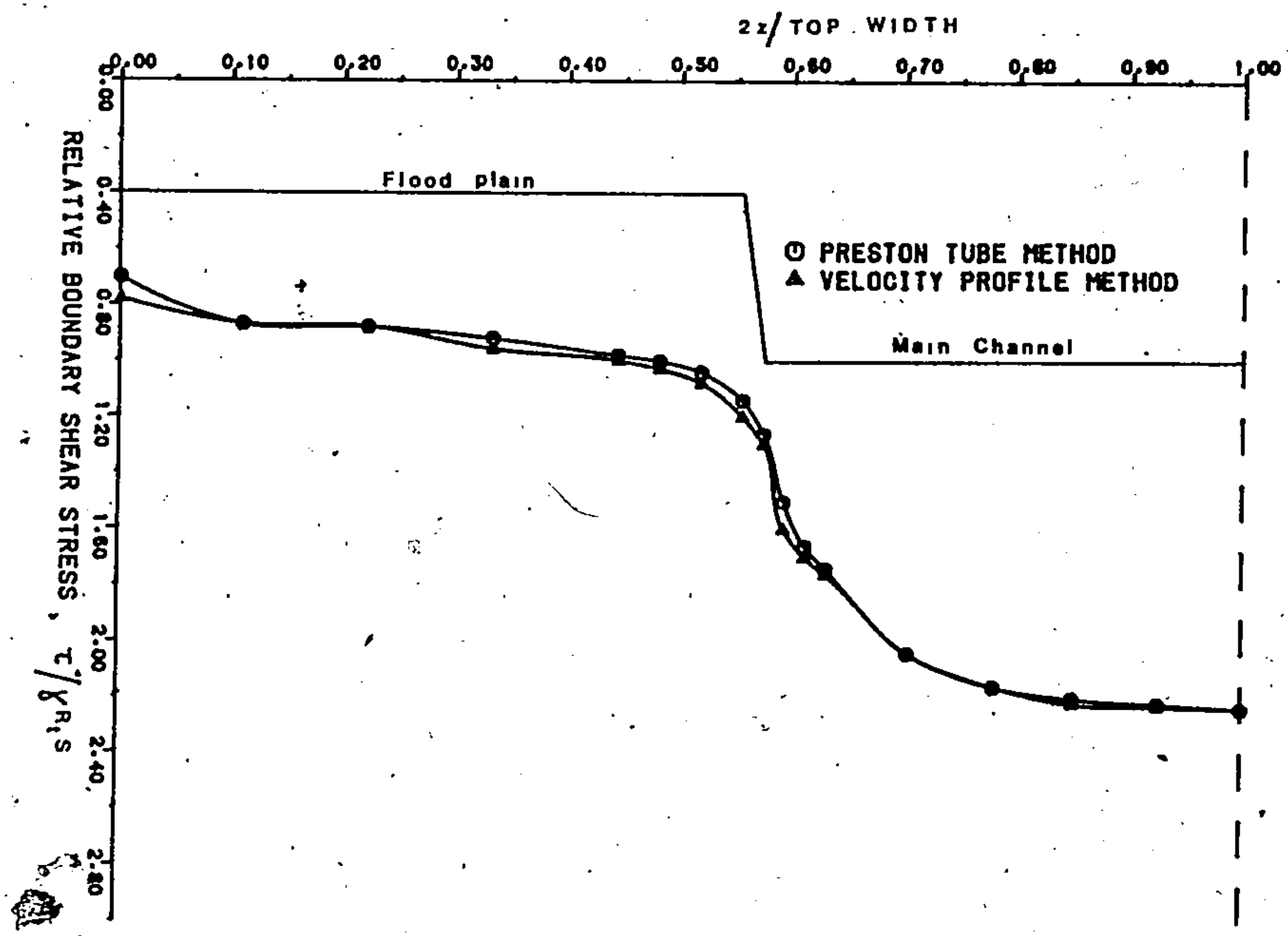

FIG. 27: BOUNDARY SHEAR STRESS DISTRIBUTION USING PRESTON TUBE AND VELOCITY PROFILE METHODS

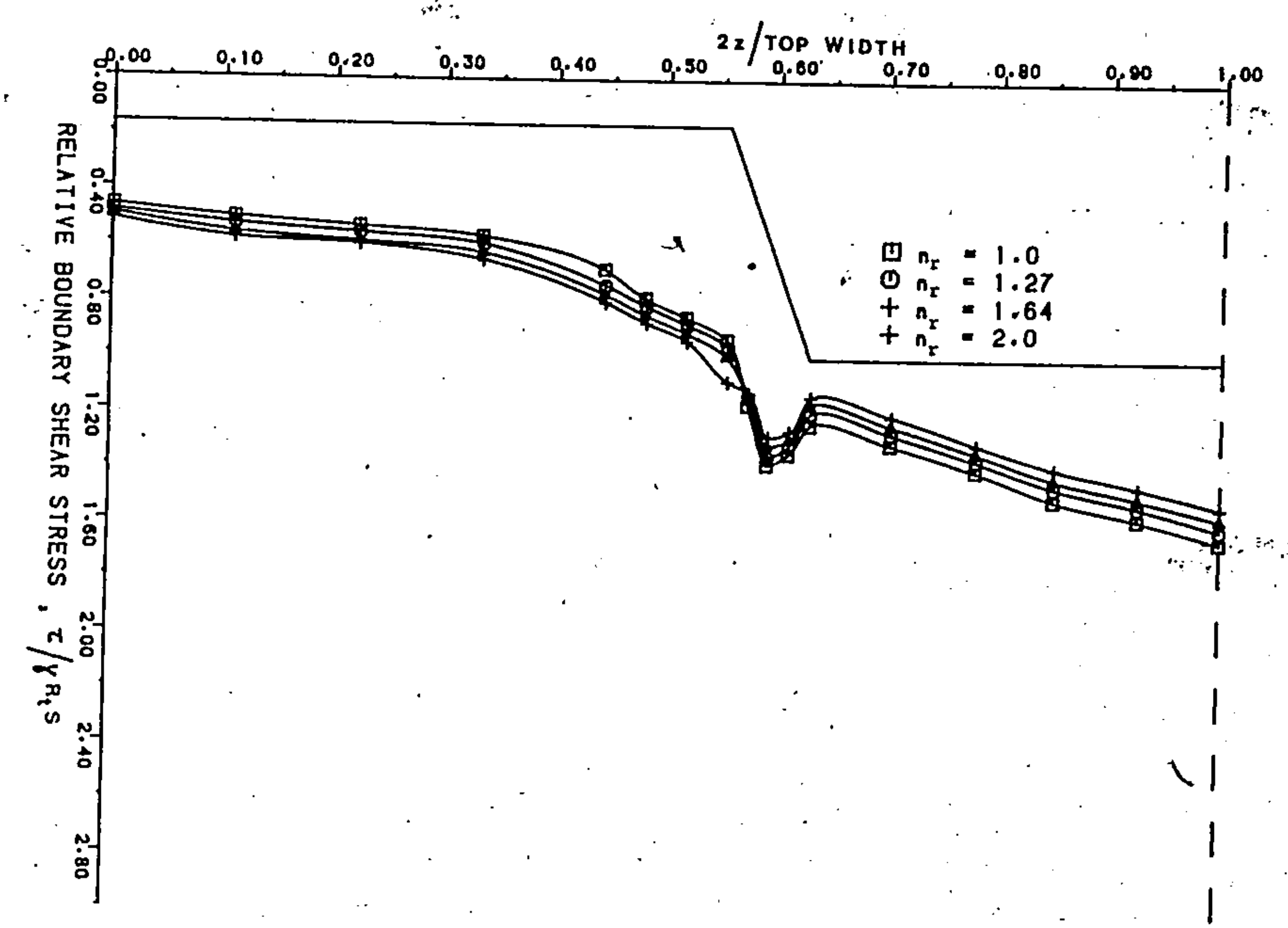

FIG. 28: BOUNDARY SHEAR STRESS DISTRIBUTION IN THE COMPOUND OPEN CHANNEL

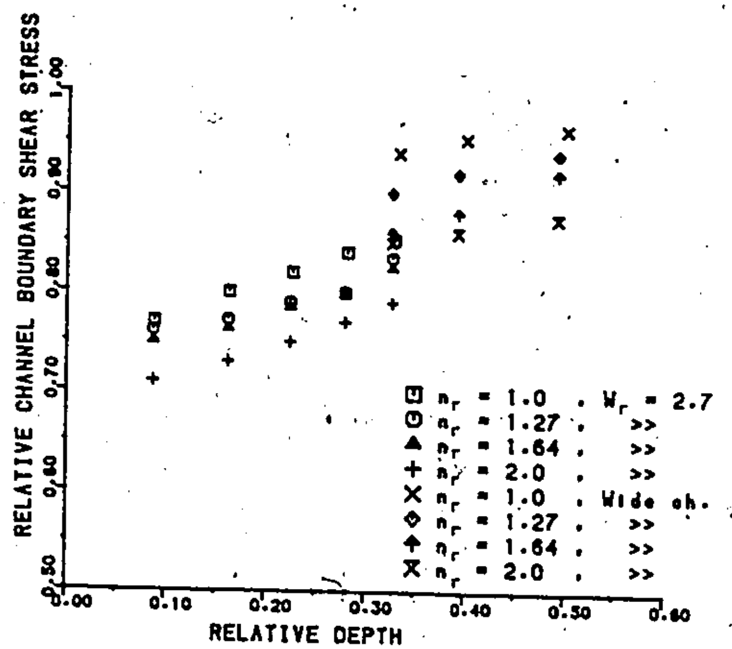

FIG.29: RELATIVE CHANNEL BOUNDARY SHEAR STRESS VERSUS RELATIVE DEPTH

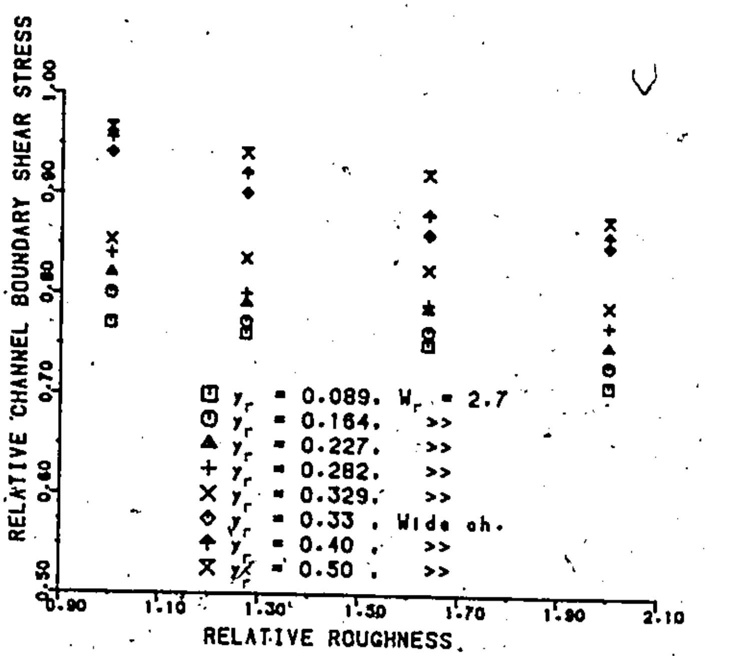

FIG.30: RELATIVE CHANNEL BOUNDARY SHEAR STRESS VERSUS RELATIVE ROUGHNESS

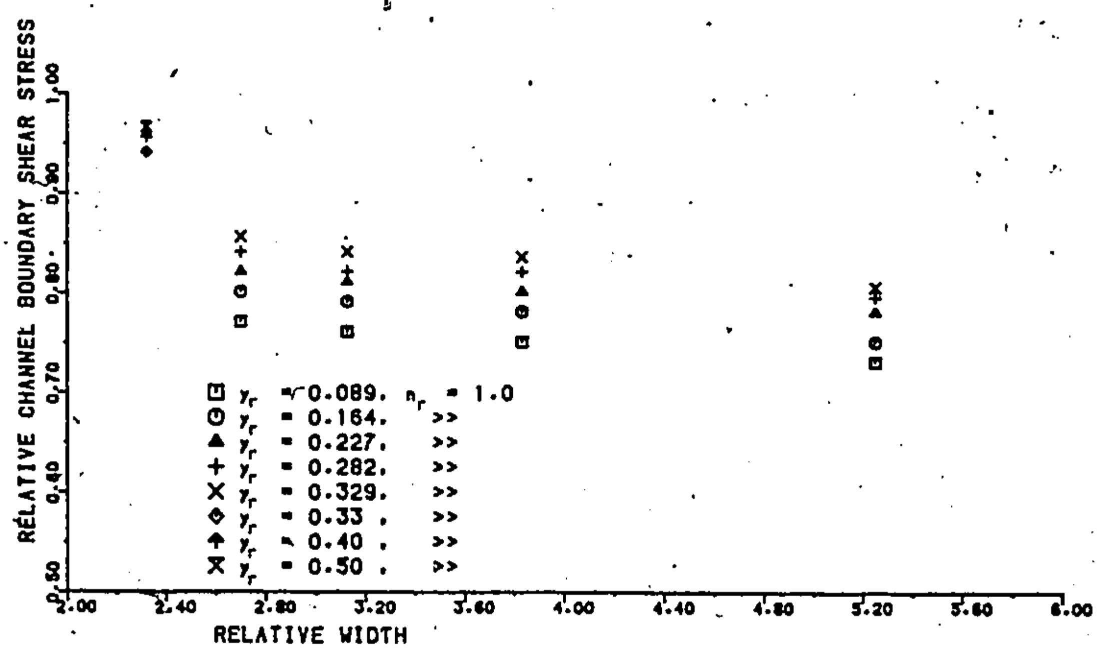

FIG.31: RELATIVE CHANNEL BOUNDARY SHEAR STRESS VERSUS RELATIVE WIDTH

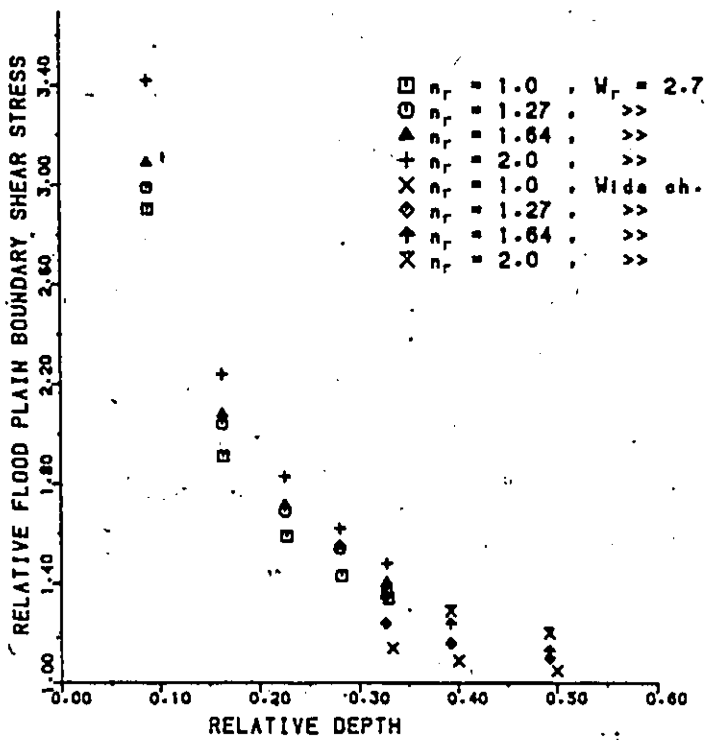

FIG.32: RELATIVE FLOOD PLAIN BOUNDARY SHEAR STRESS VERSUS RELATIVE DEPTH

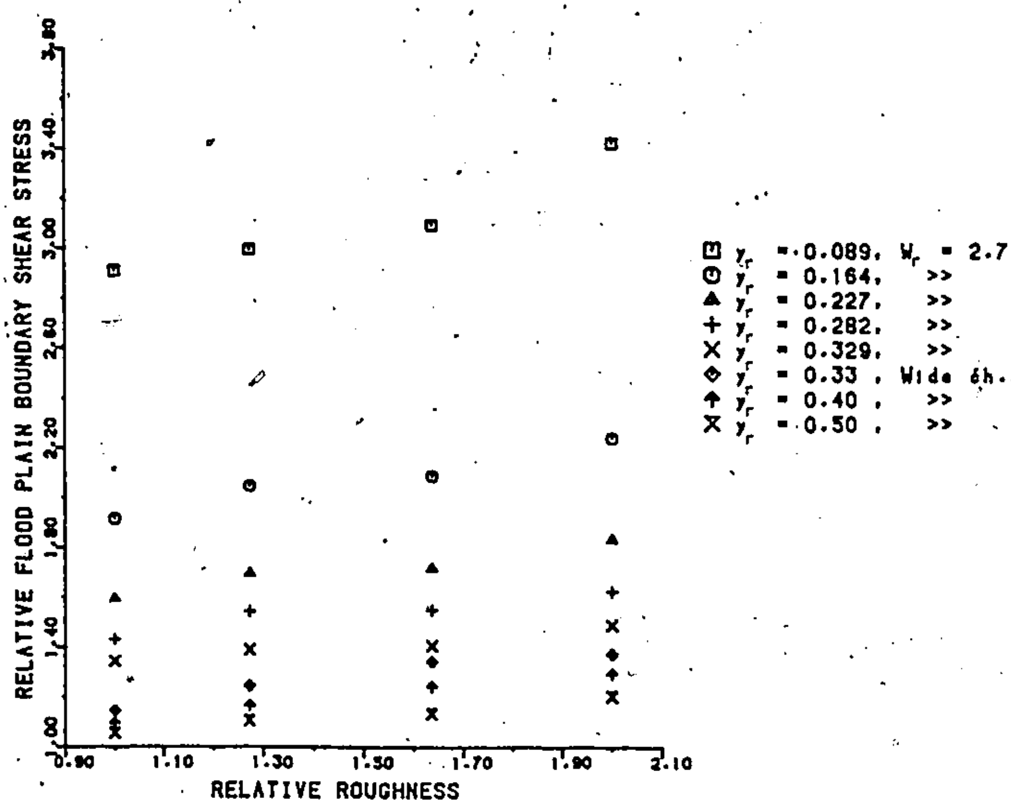

FIG. 33: RELATIVE FLOOD PLAIN BOUNDARY SHEAR STRESS VERSUS RELATIVE ROUGHNESS

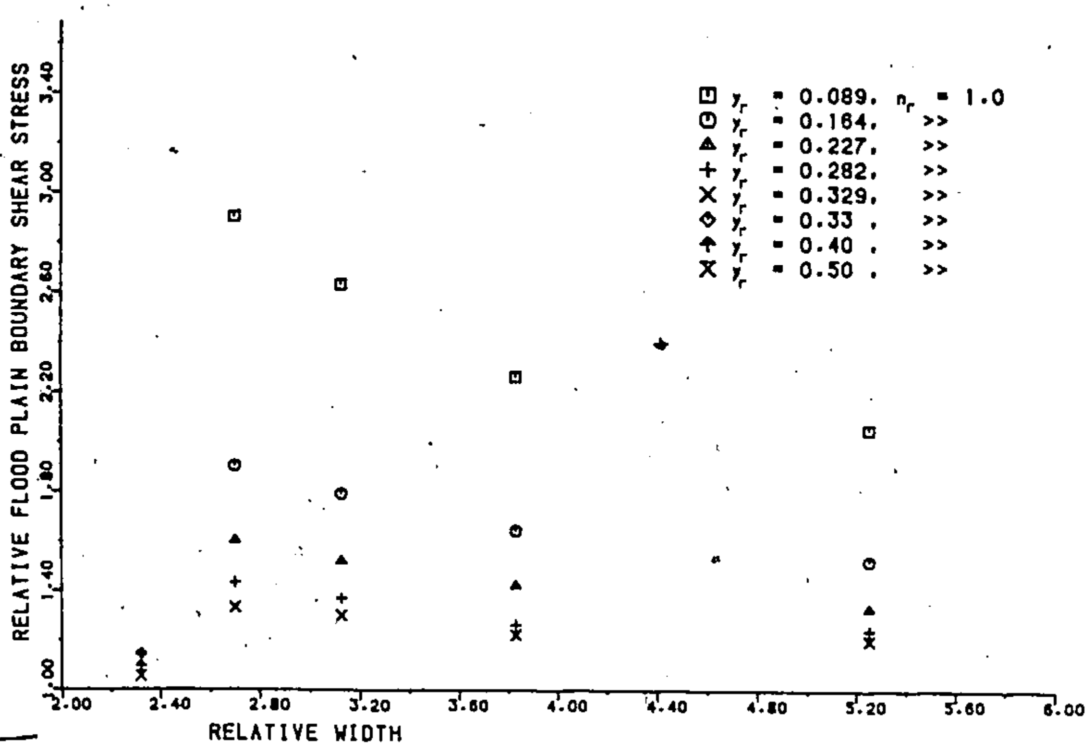

FIG. 34: RELATIVE FLOOD PLAIN BOUNDARY SHEAR STRESS VERSUS RELATIVE WIDTH

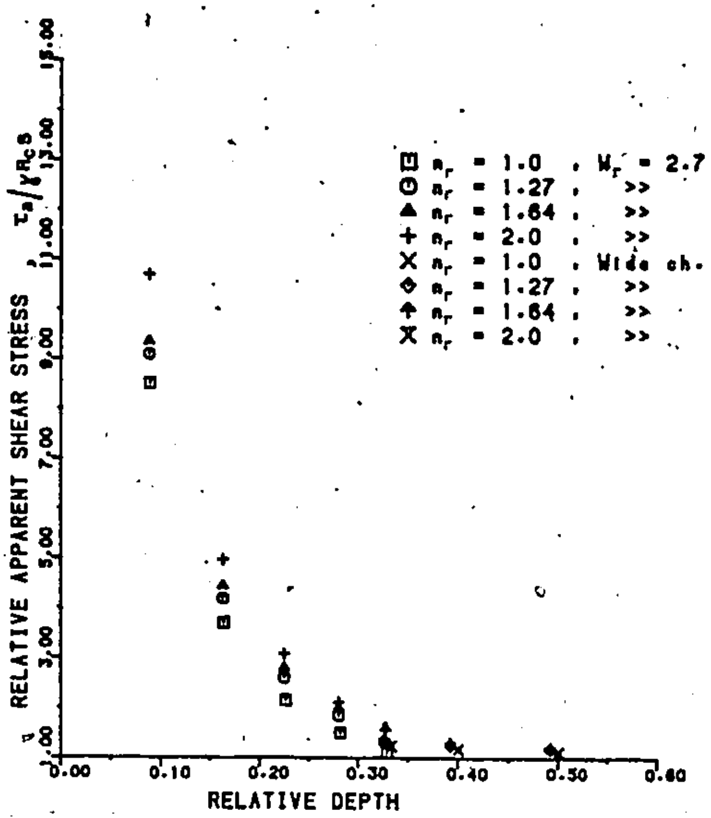

FIG. 35: RELATIVE APPARENT SHEAR STRESS VERSUS RELATIVE DEPTH

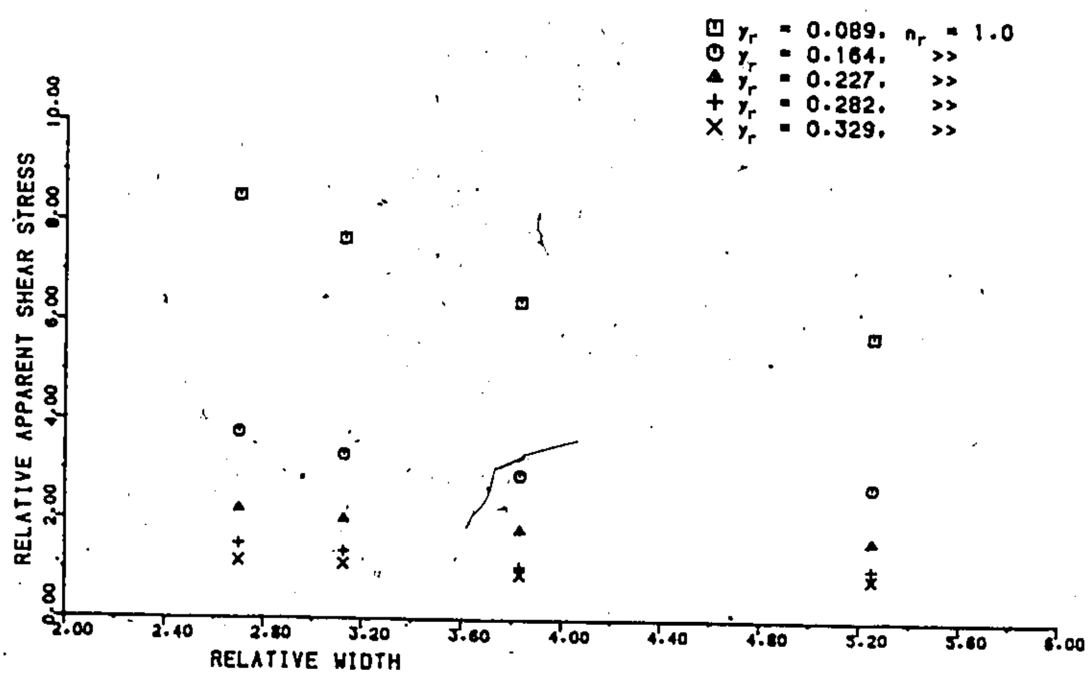

FIG. 36: RELATIVE APPARENT SHEAR STRESS VERSUS RELATIVE WIDTH

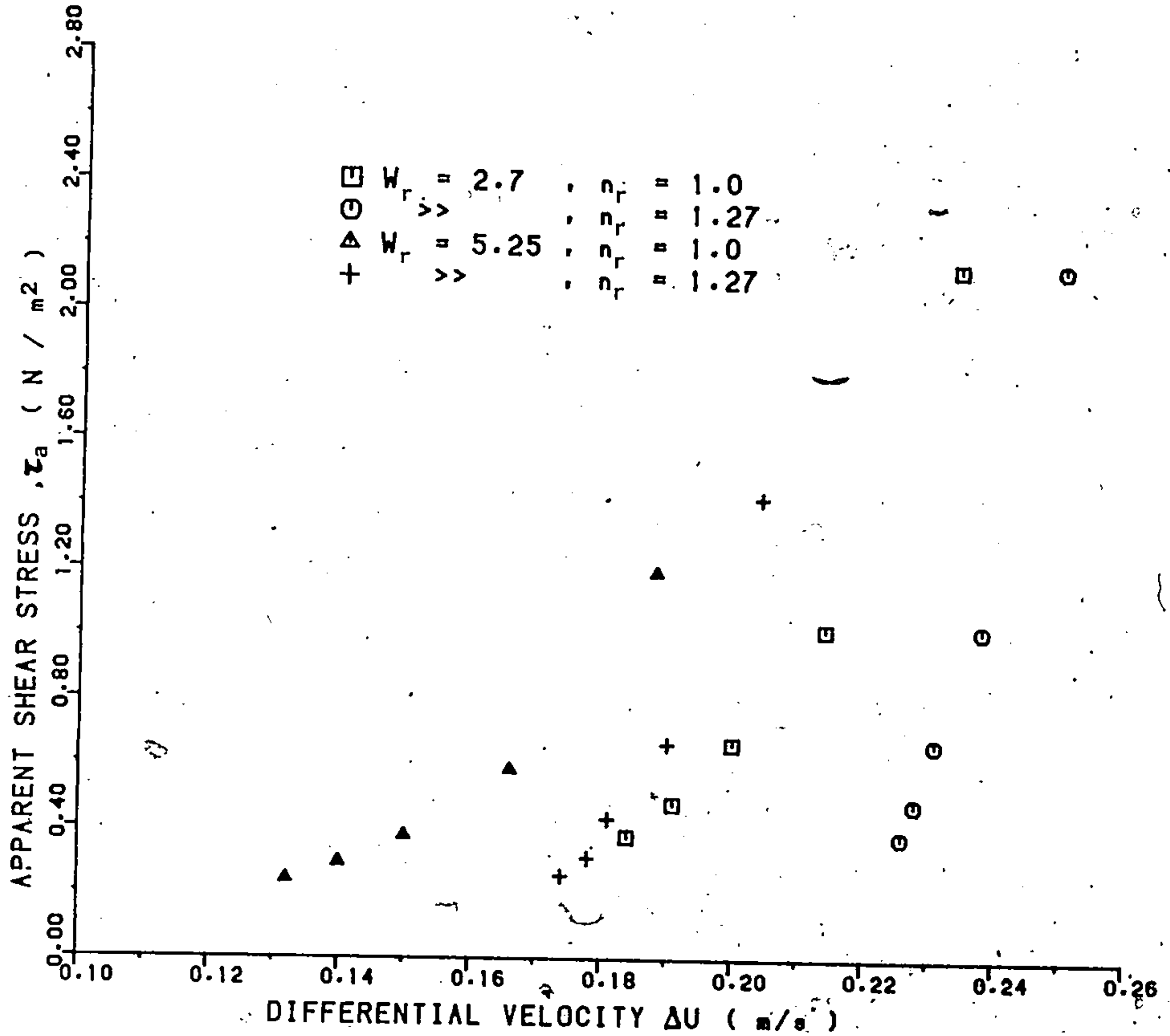

FIG. 37: APPARENT SHEAR STRESS VERSUS DIFFERENTIAL VELOCITY

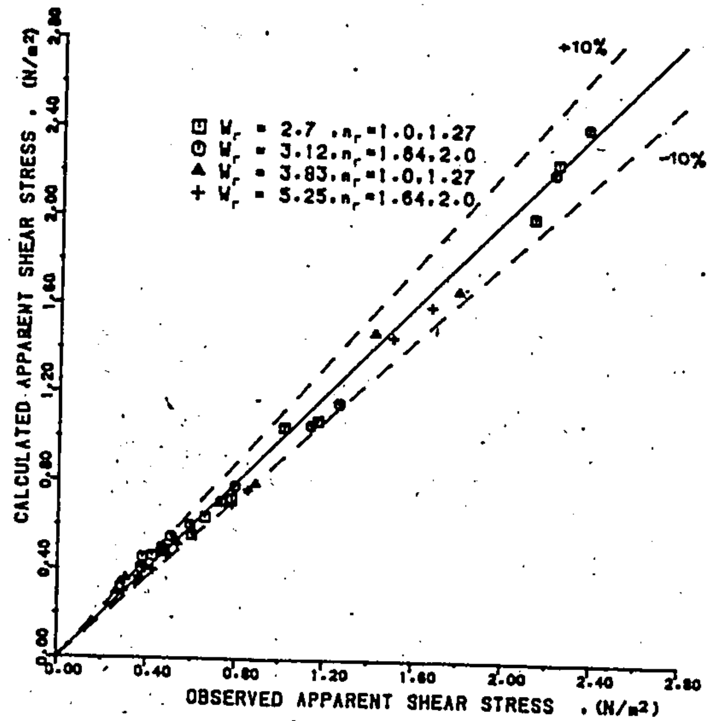

FIG.38: OBSERVED VERSUS CALCULATED APPARENT SHEAR STRESS

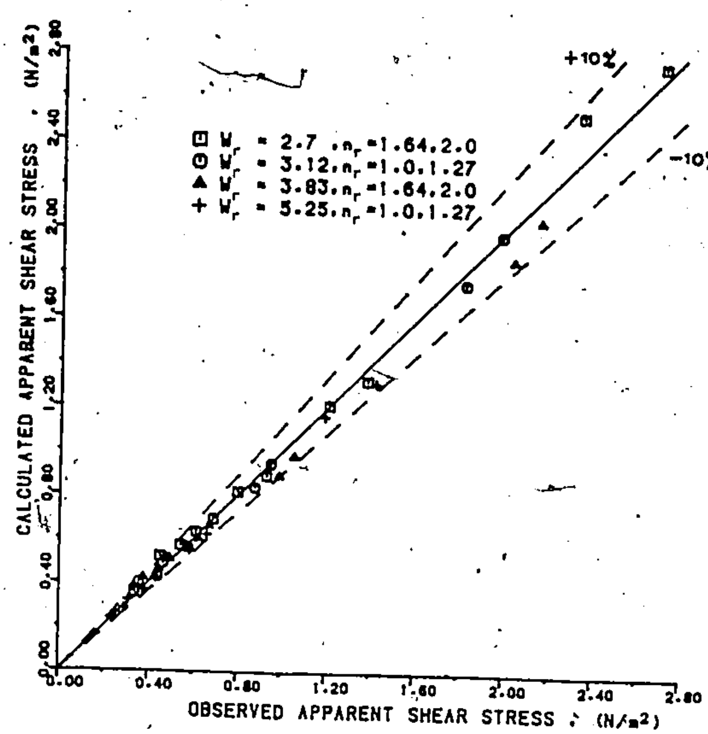

FIG.39: VALIDATION OF EMPIRICAL RELATIONSHIP FOR ESTIMATION OF APPARENT SHEAR STRESS

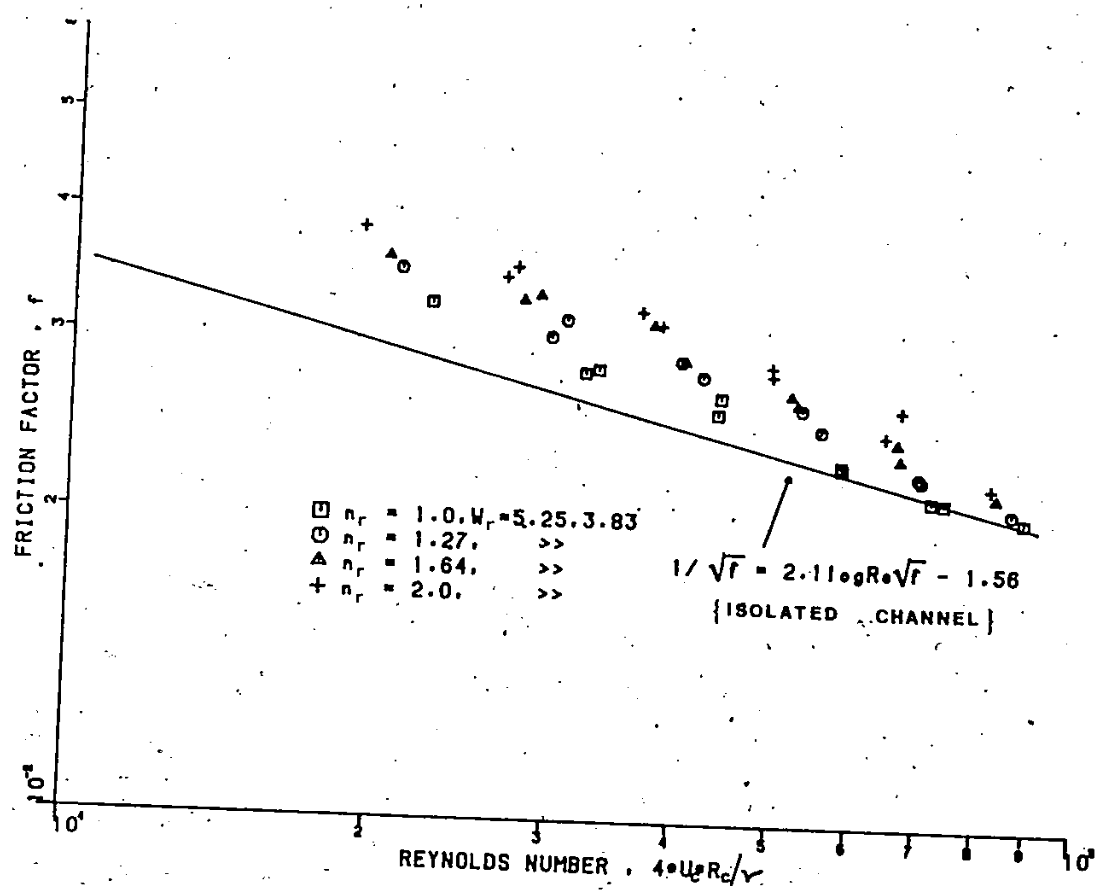

FIG. 4 : CHANNEL FRICTION FACTOR f VERSUS REYNOLDS NUMBER

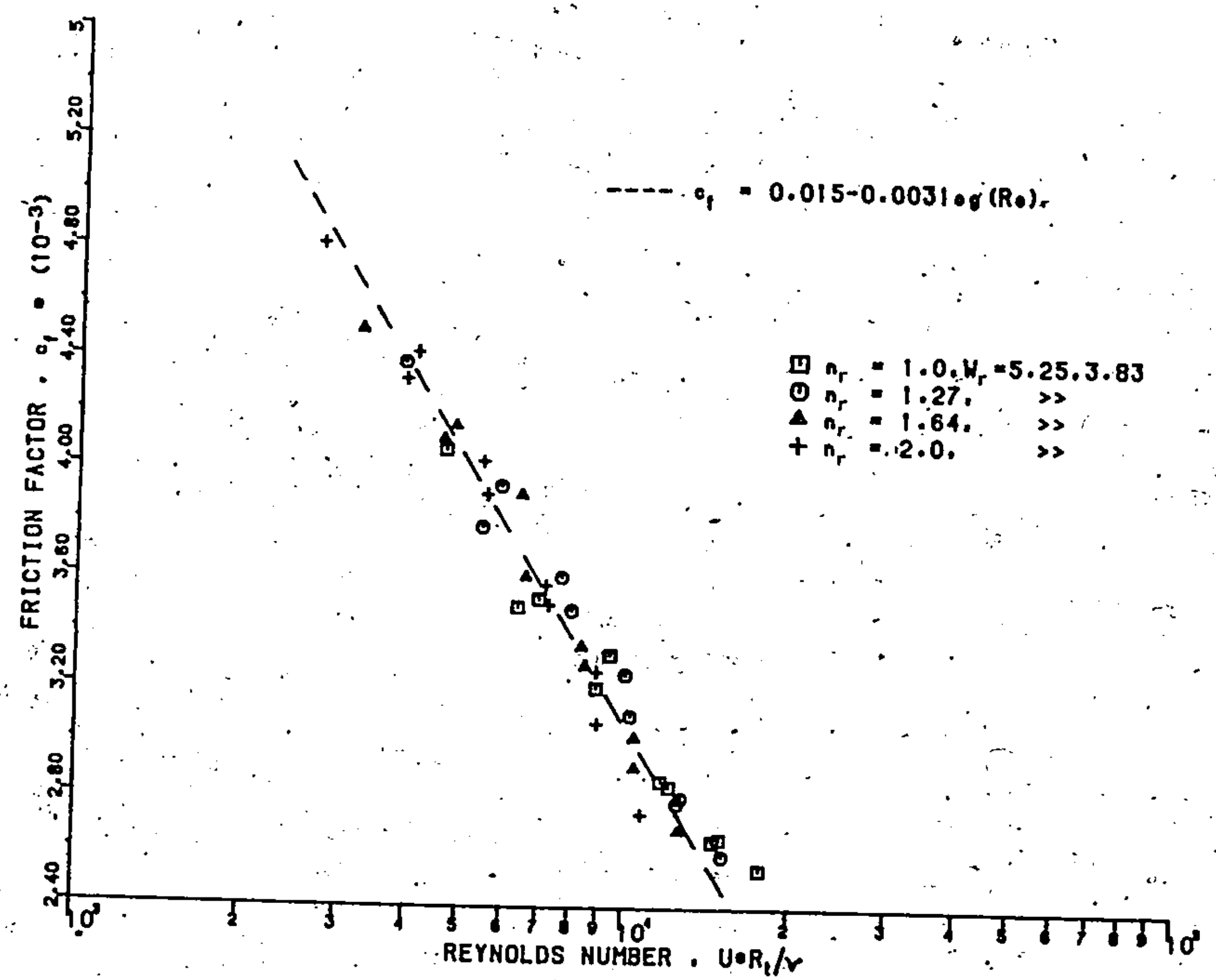

FIG.41 : CHANNEL FRICTION FACTOR c_f VERSUS "SINGLE-CHANNEL" REYNOLDS NUMBER

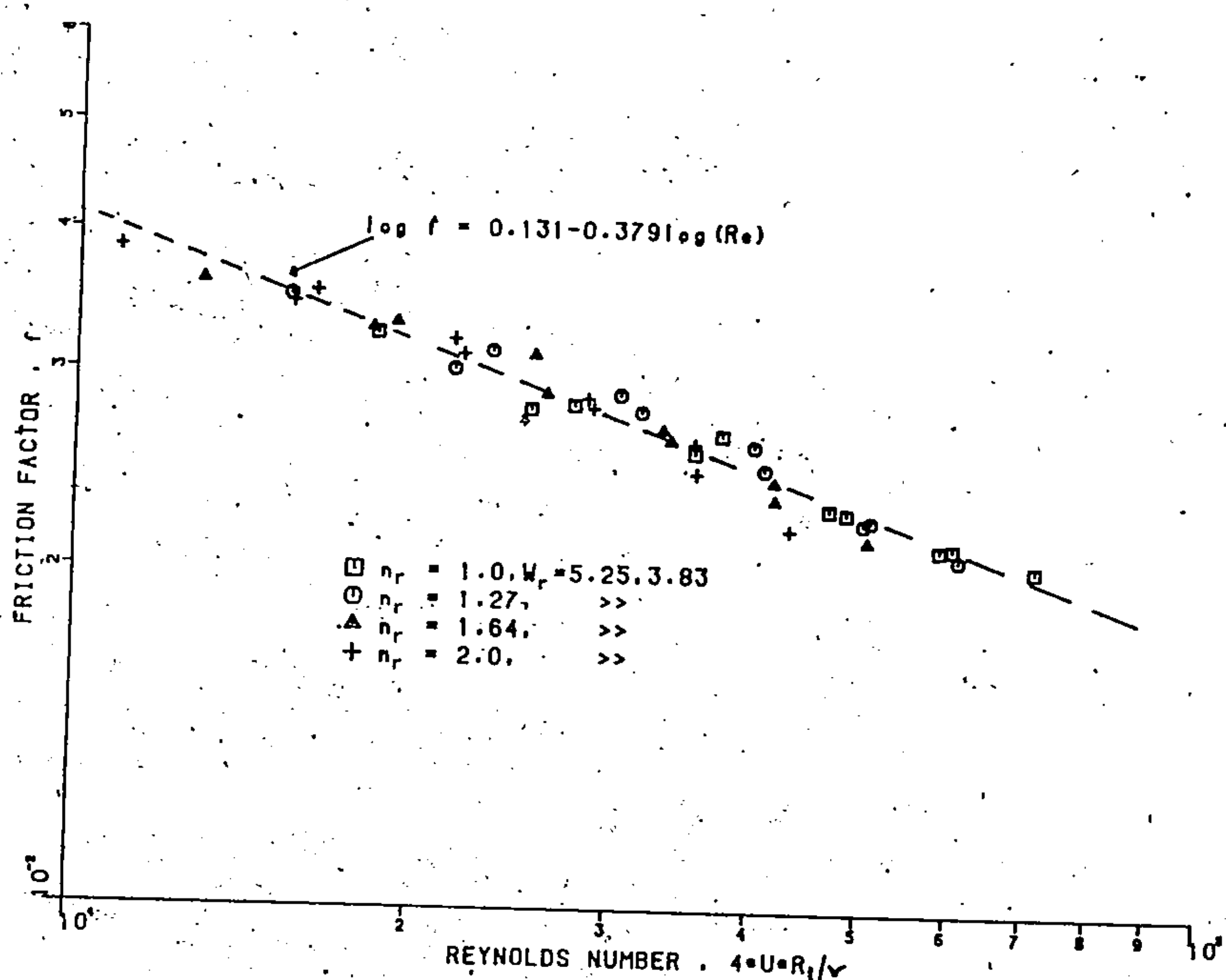

FIG.4 CHANNEL FRICTION FACTOR f VERSUS "SINGLE-CHANNEL" REYNOLDS NUMBER

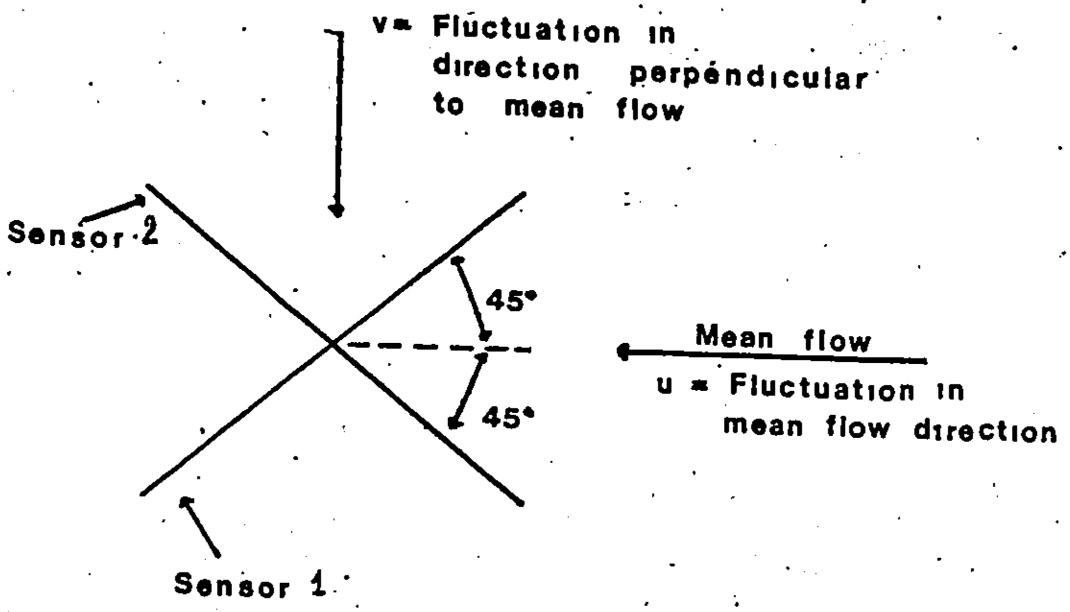

FIG. 43: STANDARD X-ARRAY CONFIGURATION FOR THE HOT FILM PROBE

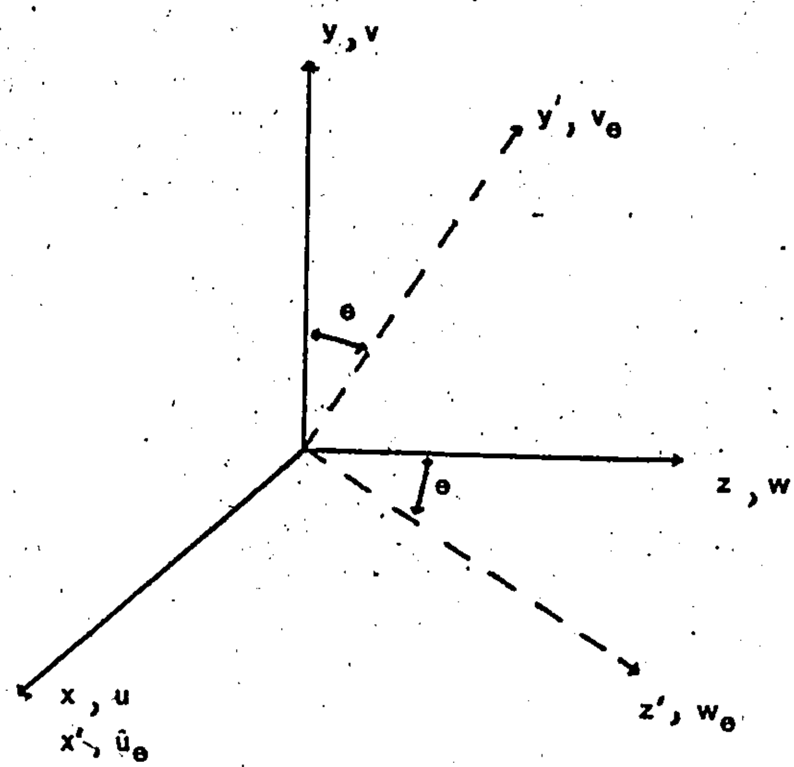

FIG. 44: TRANSFORMATION OF COORDINATES SYSTEM

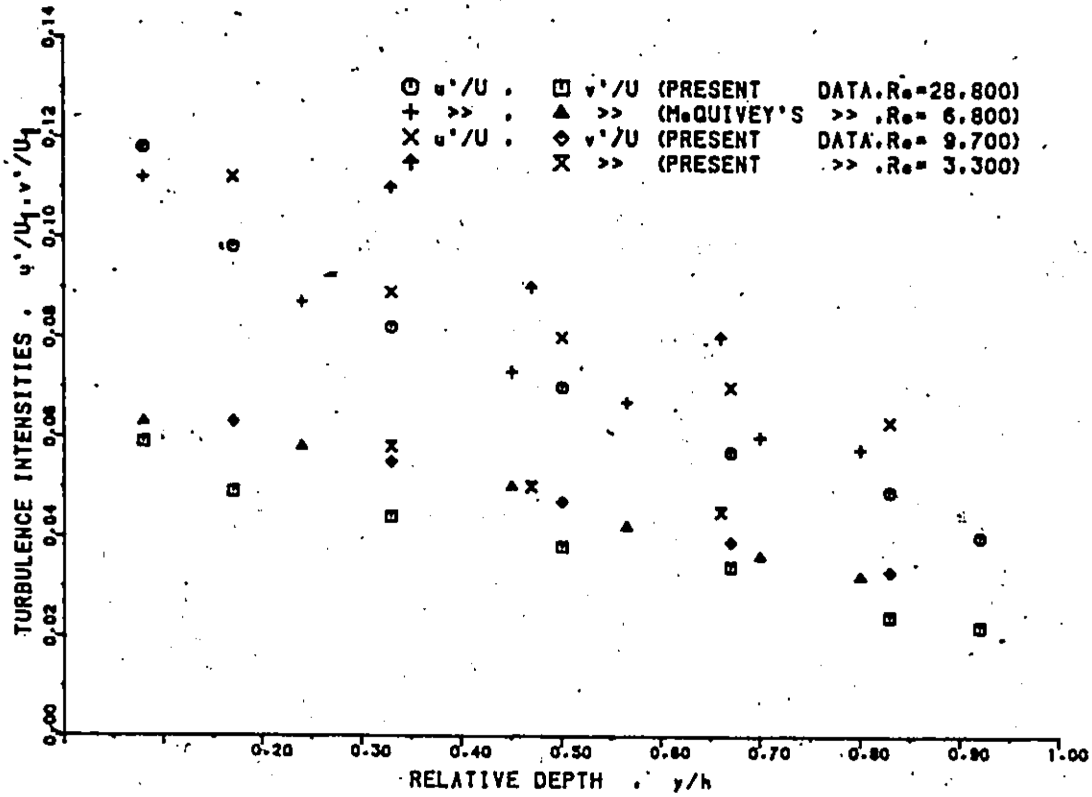

FIG.45: VERTICAL DISTRIBUTION OF u' AND v' FOR 2-DIMENSIONAL FLOW

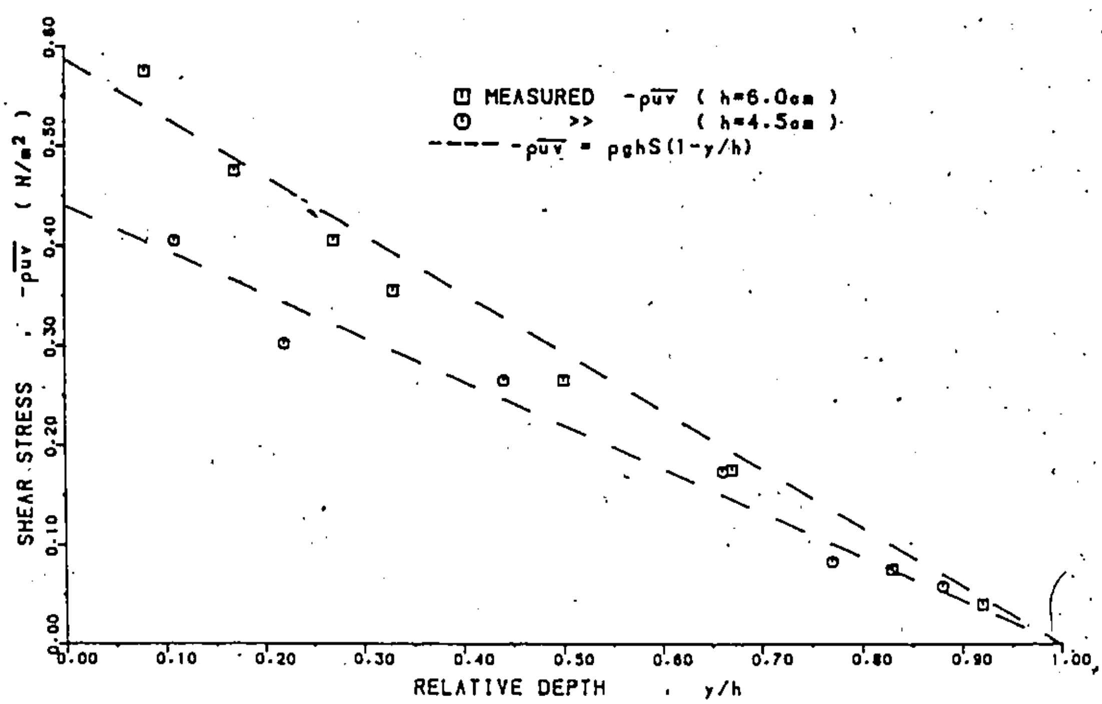

FIG.46: MEASURED AND THEORETICAL DISTRIBUTION OF SHEAR STRESS FOR 2-DIMENSIONAL FLOW

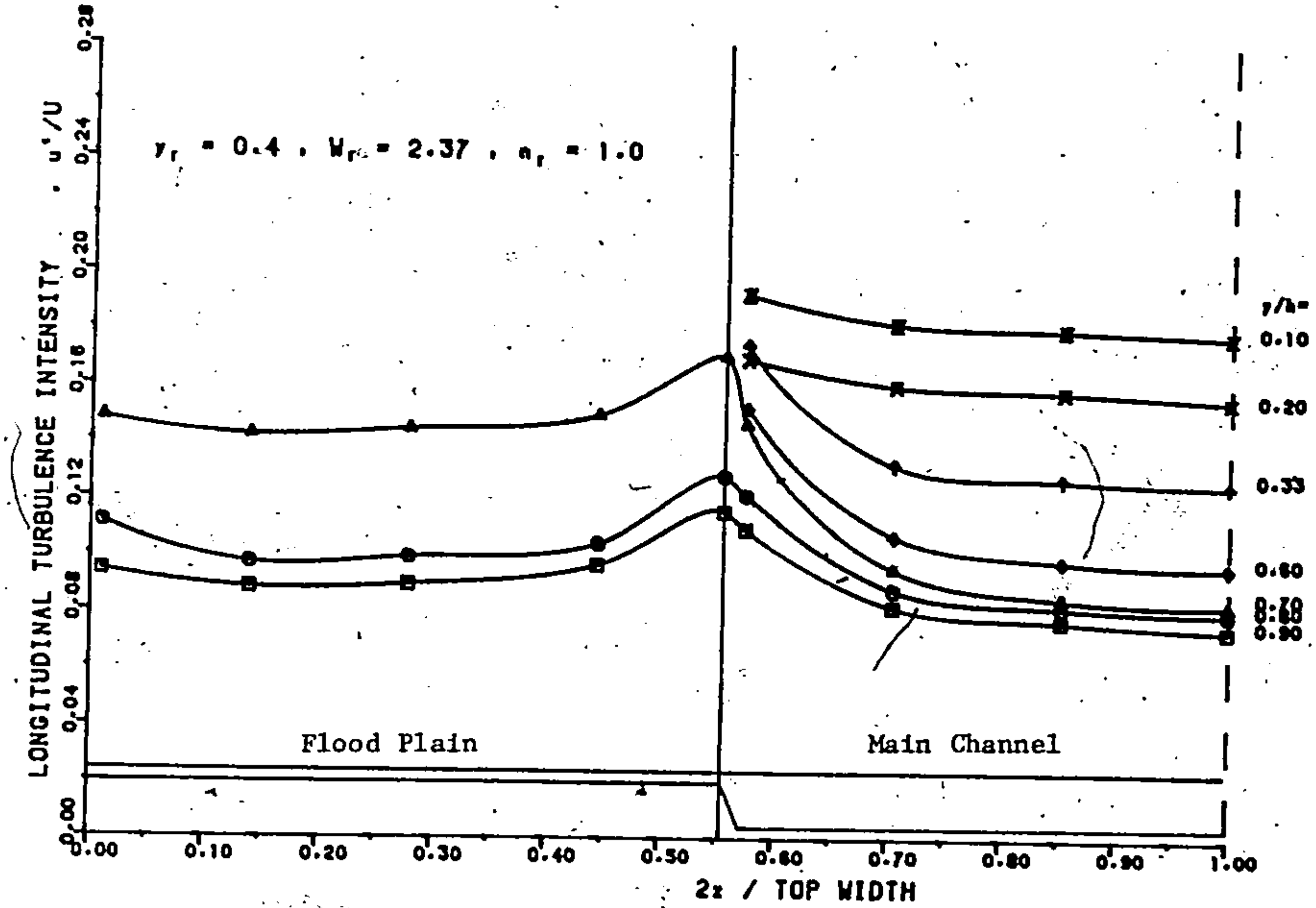

FIG. 47 : CROSS-STREAM DISTRIBUTION OF u' (WIDE CHANNEL)

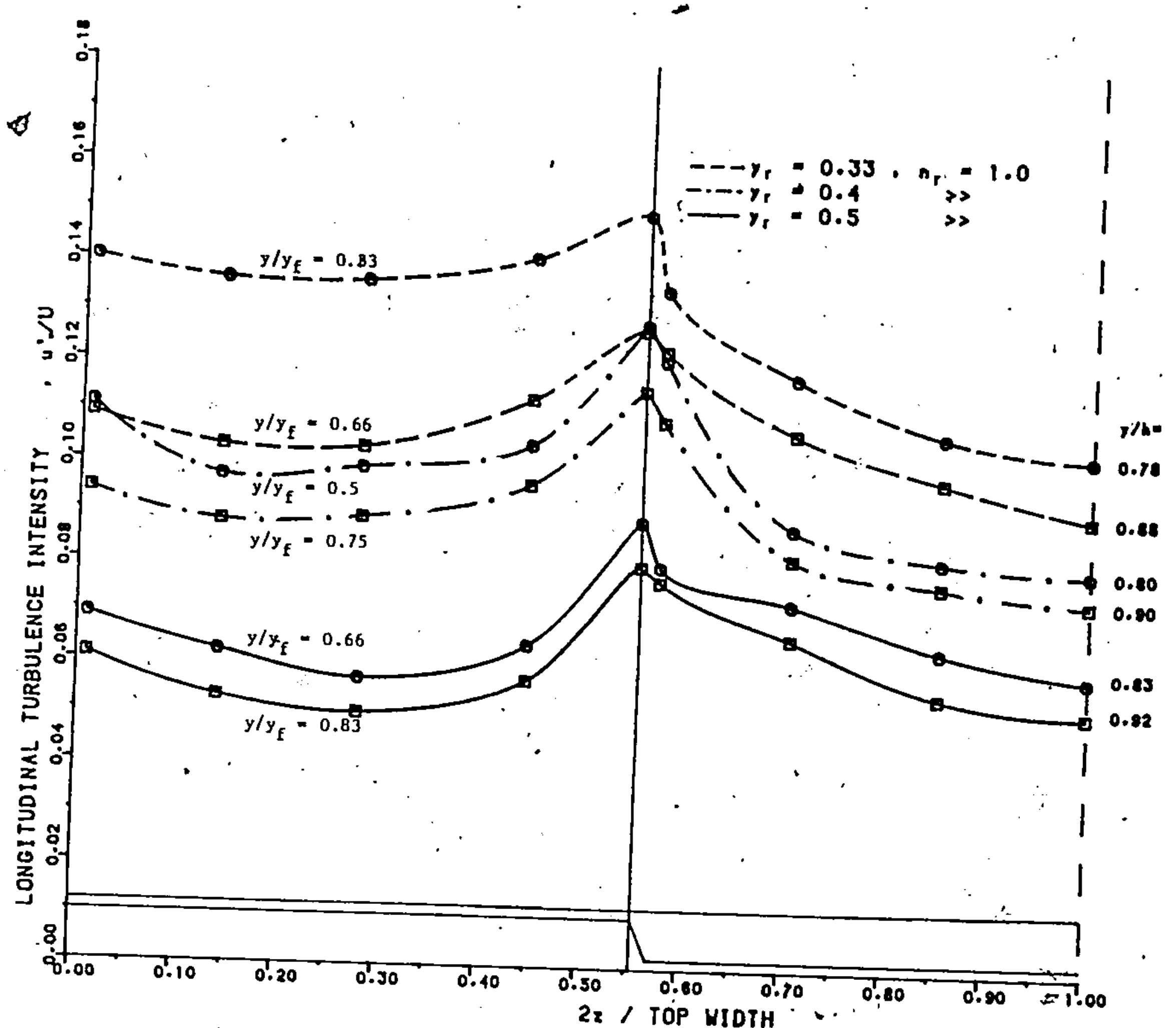

FIG. 4 : CROSS-STREAM DISTRIBUTION OF u' FOR VARIOUS RELATIVE DEPTHS (WIDE CHANNEL)

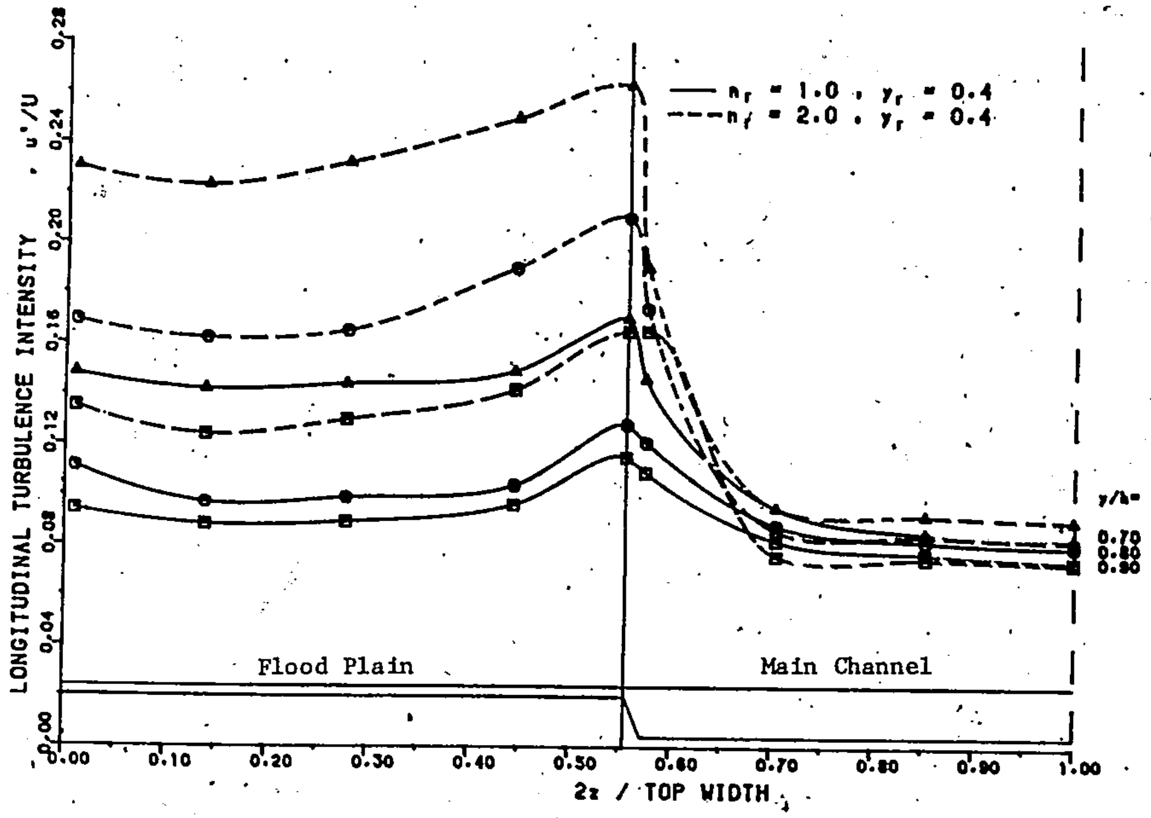

FIG. 45: CROSS-STREAM DISTRIBUTION OF u' FOR 2 RELATIVE ROUGHNESSES (WIDE CHANNEL)

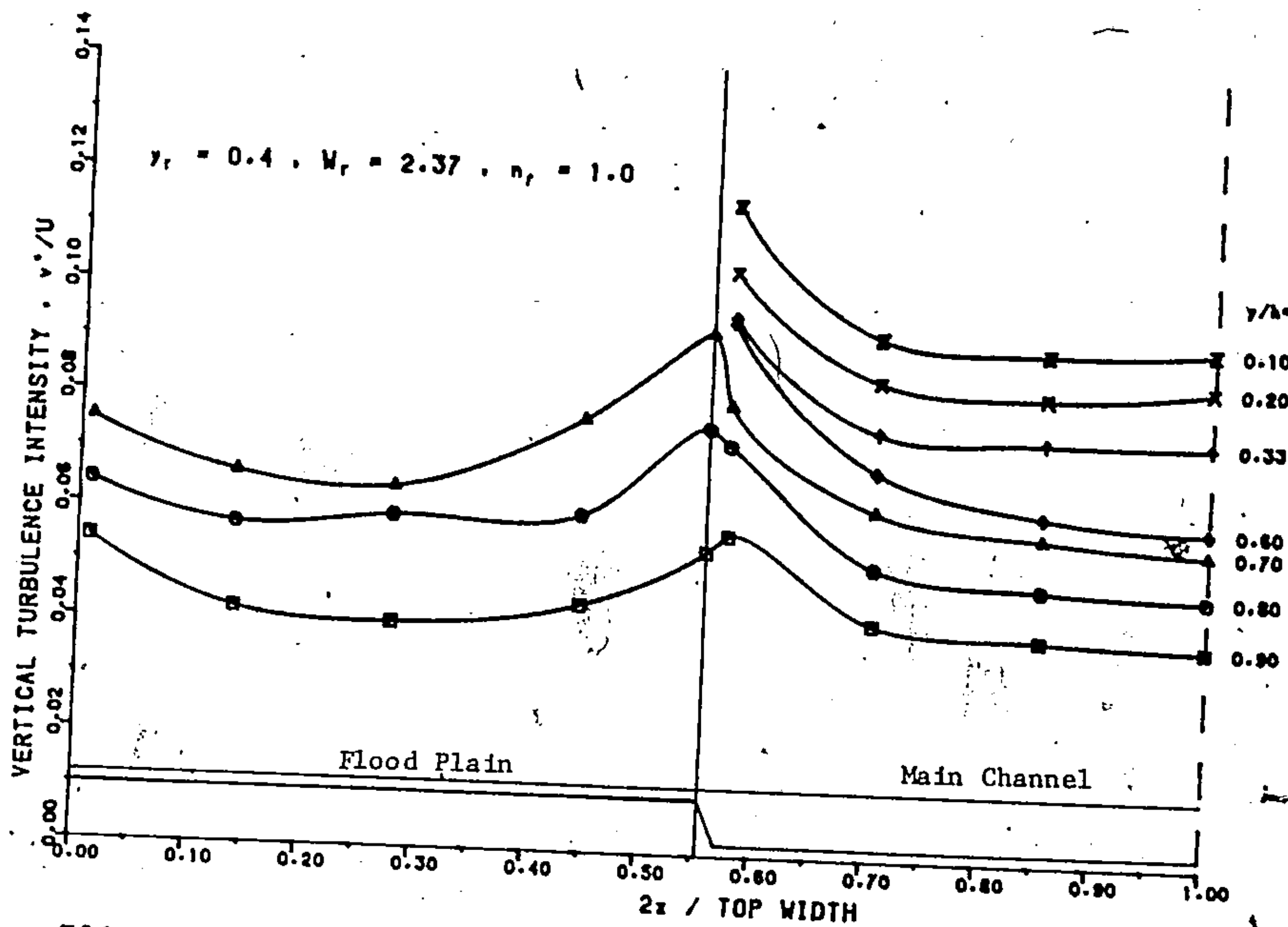

FIG. 50 : CROSS-STREAM DISTRIBUTION OF v' (WIDE CHANNEL)

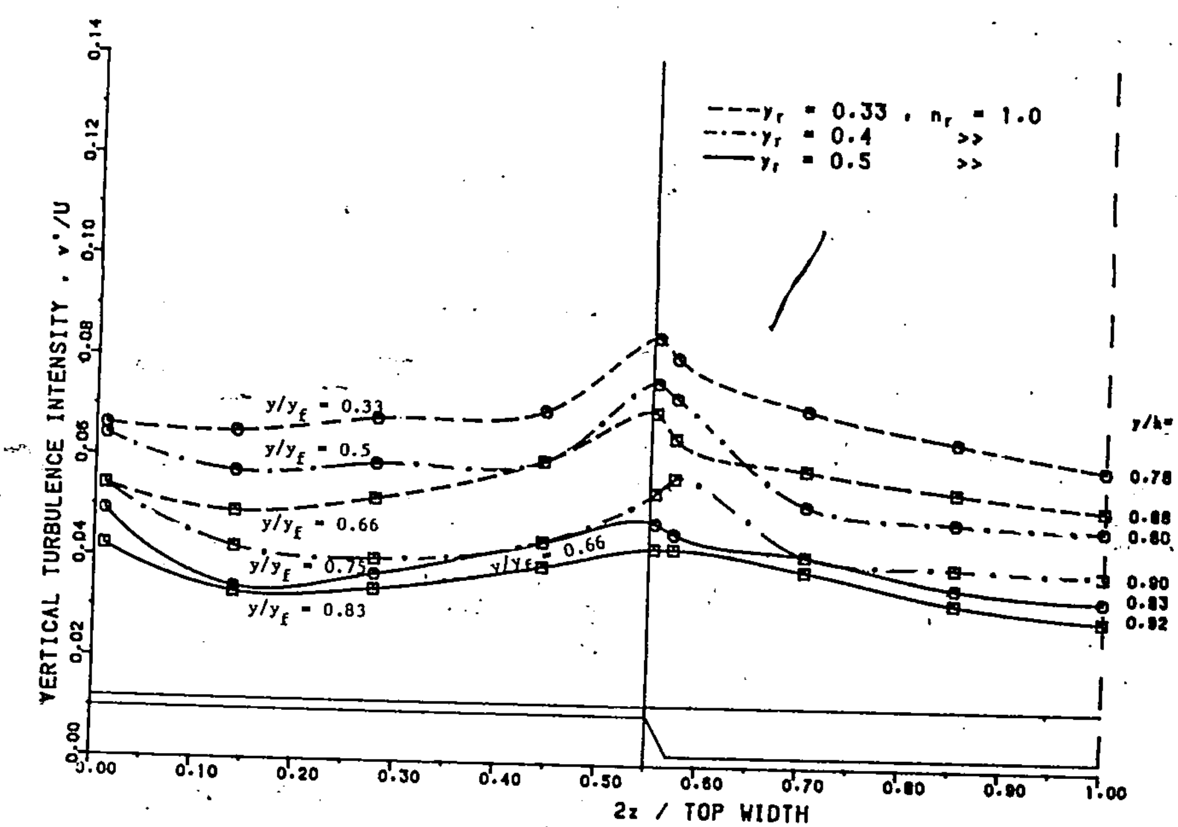

FIG. 51 : CROSS-STREAM DISTRIBUTION OF v' FOR VARIOUS RELATIVE DEPTHS (WIDE CHANNEL)

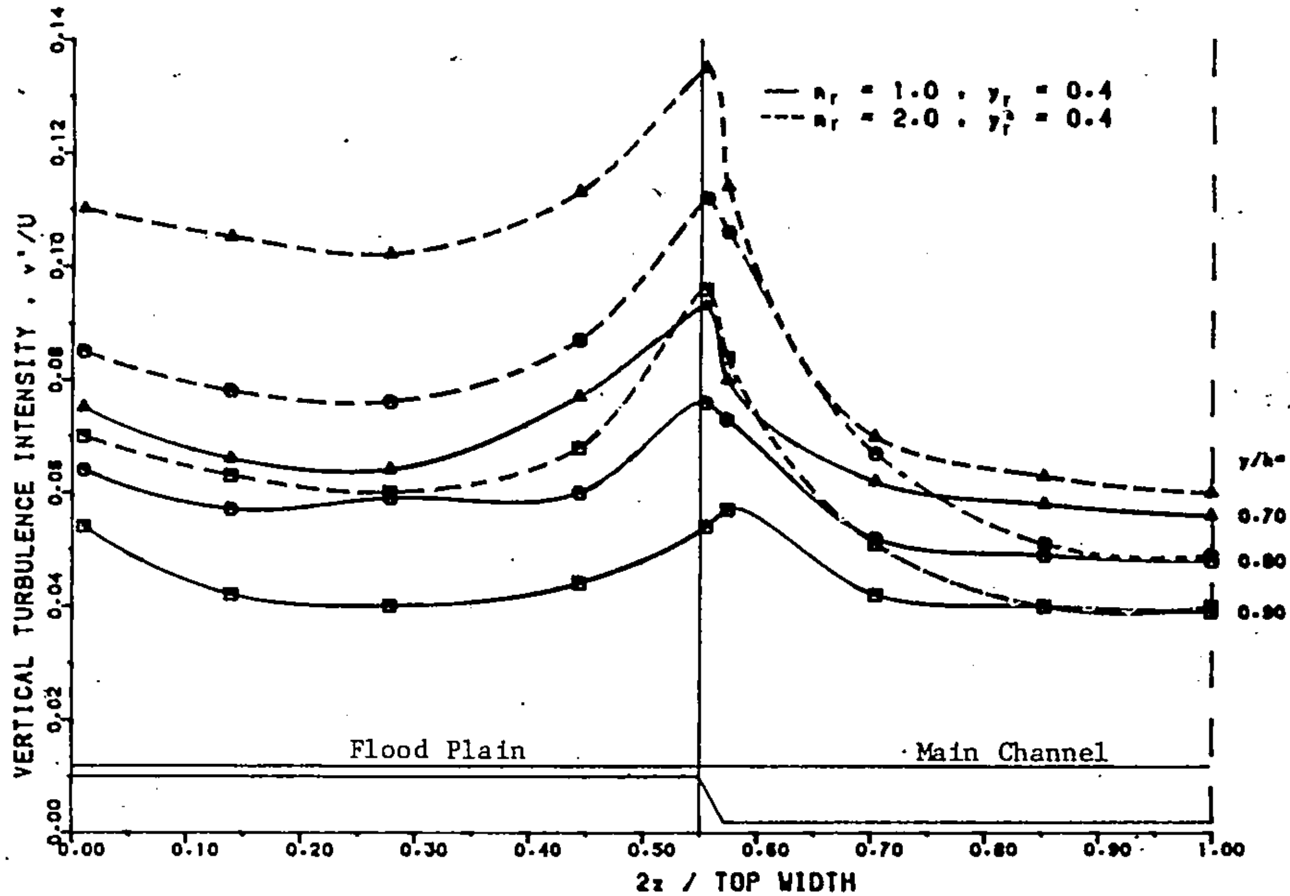

FIG. 5 : CROSS-STREAM DISTRIBUTION OF v' FOR 2 RELATIVE ROUGHNESSES (WIDE CHANNEL)

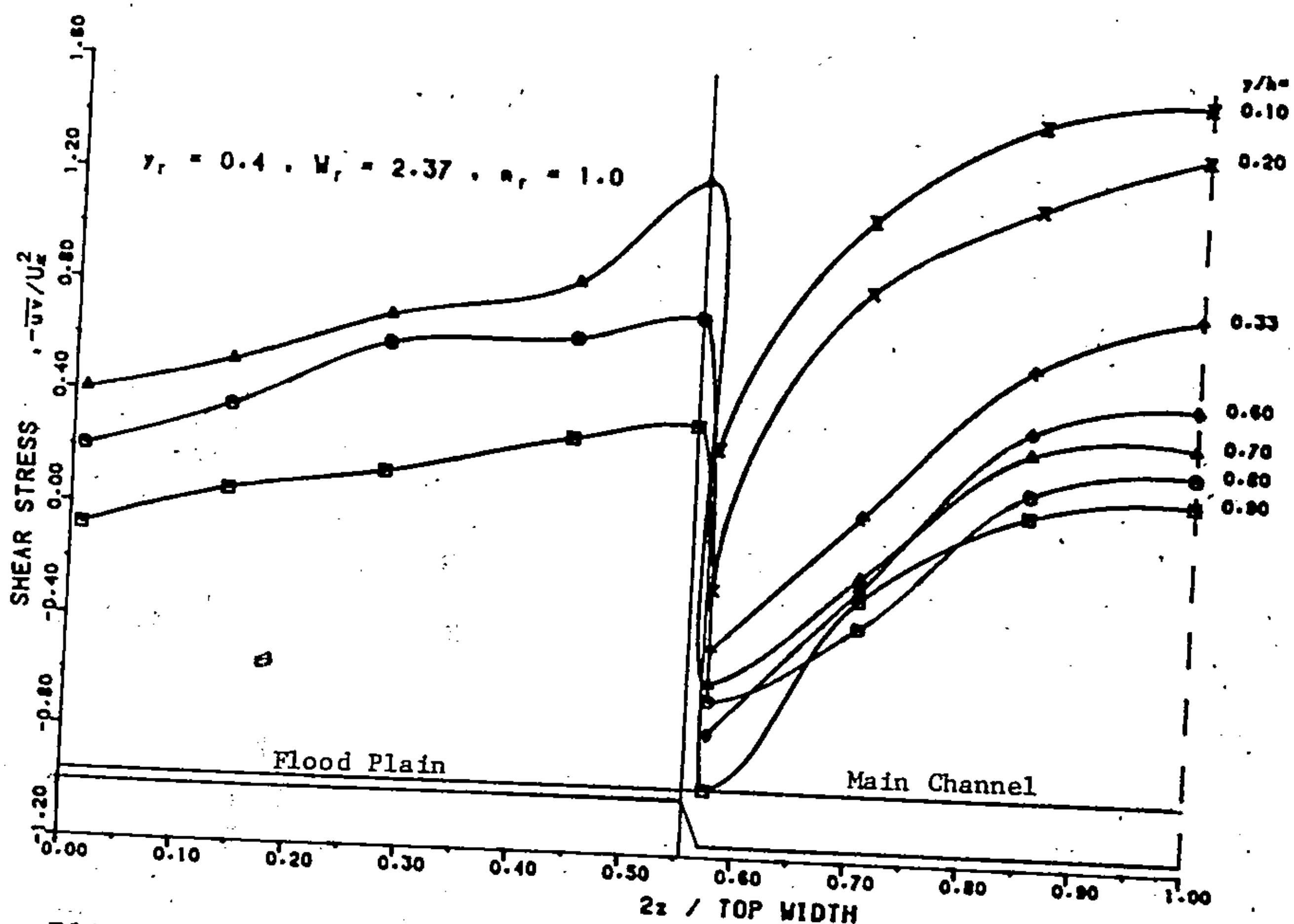

FIG. : CROSS-STREAM DISTRIBUTION OF SHEAR STRESS (WIDE CHANNEL)

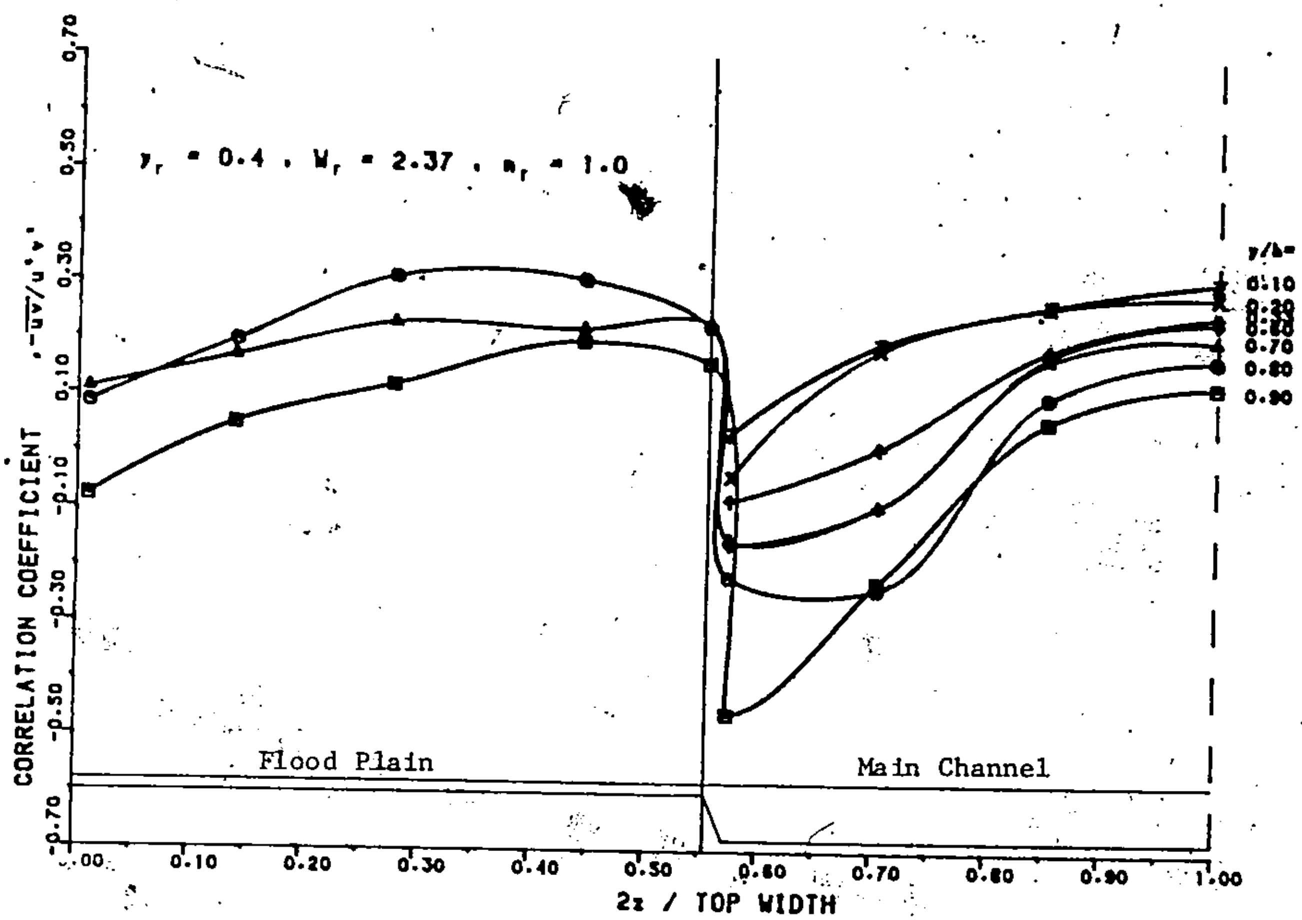

FIG. 54: CROSS-STREAM DISTRIBUTION OF CORRELATION COEFFICIENT (WIDE CHANNEL)

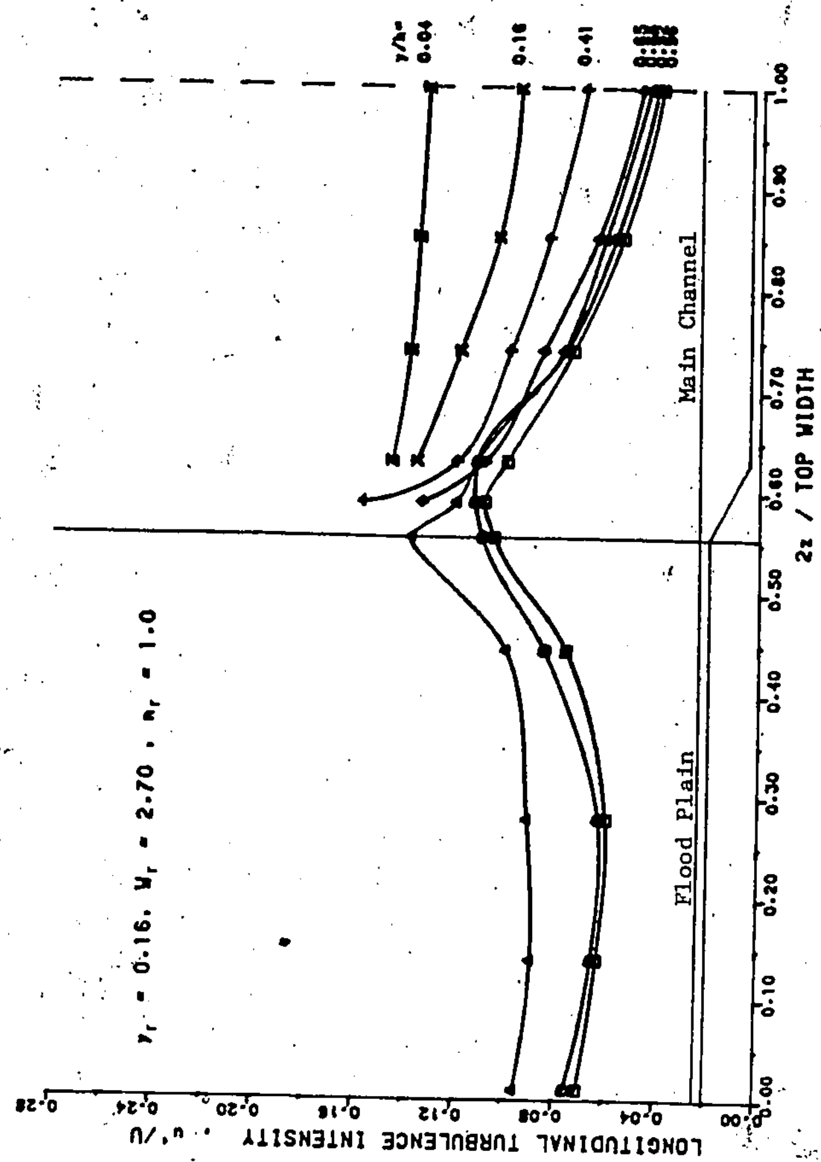

FIG. 55: CROSS-STREAM DISTRIBUTION OF u' (NARROW CHANNEL)

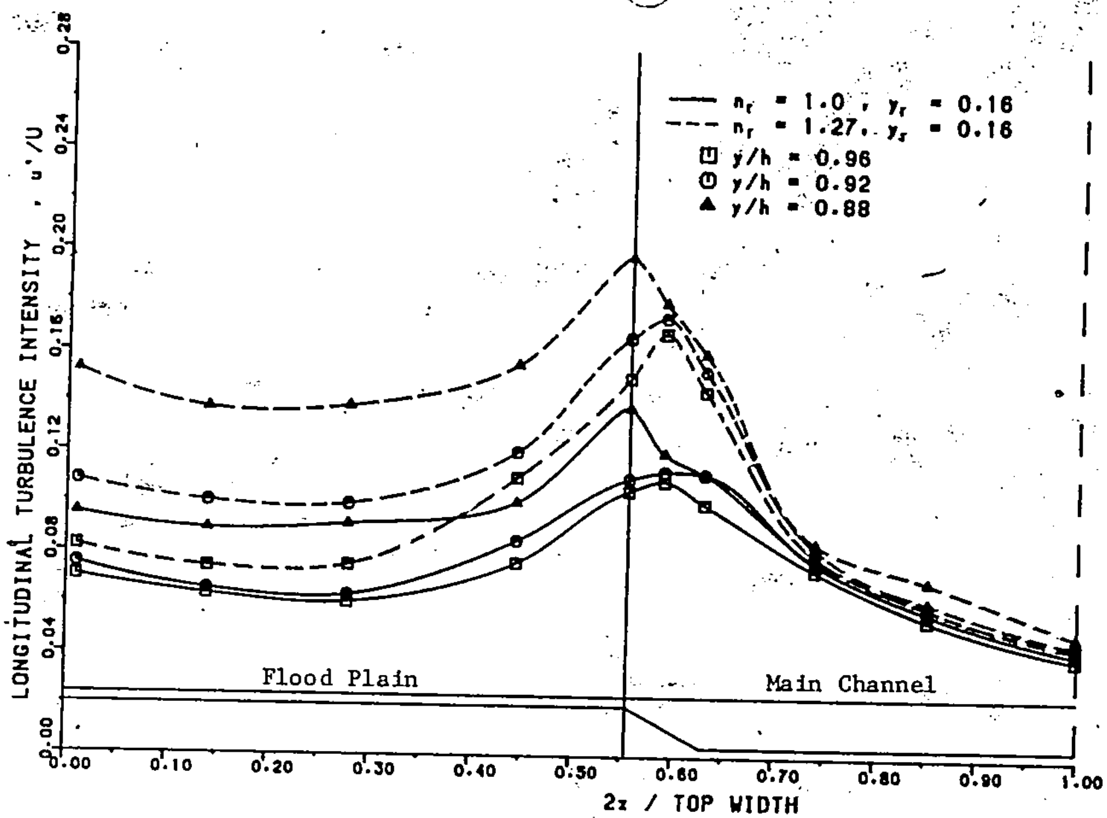

FIG. 5: CROSS-STREAM DISTRIBUTION OF u' FOR TWO RELATIVE ROUGHNESSES (NARROW CHANNEL).

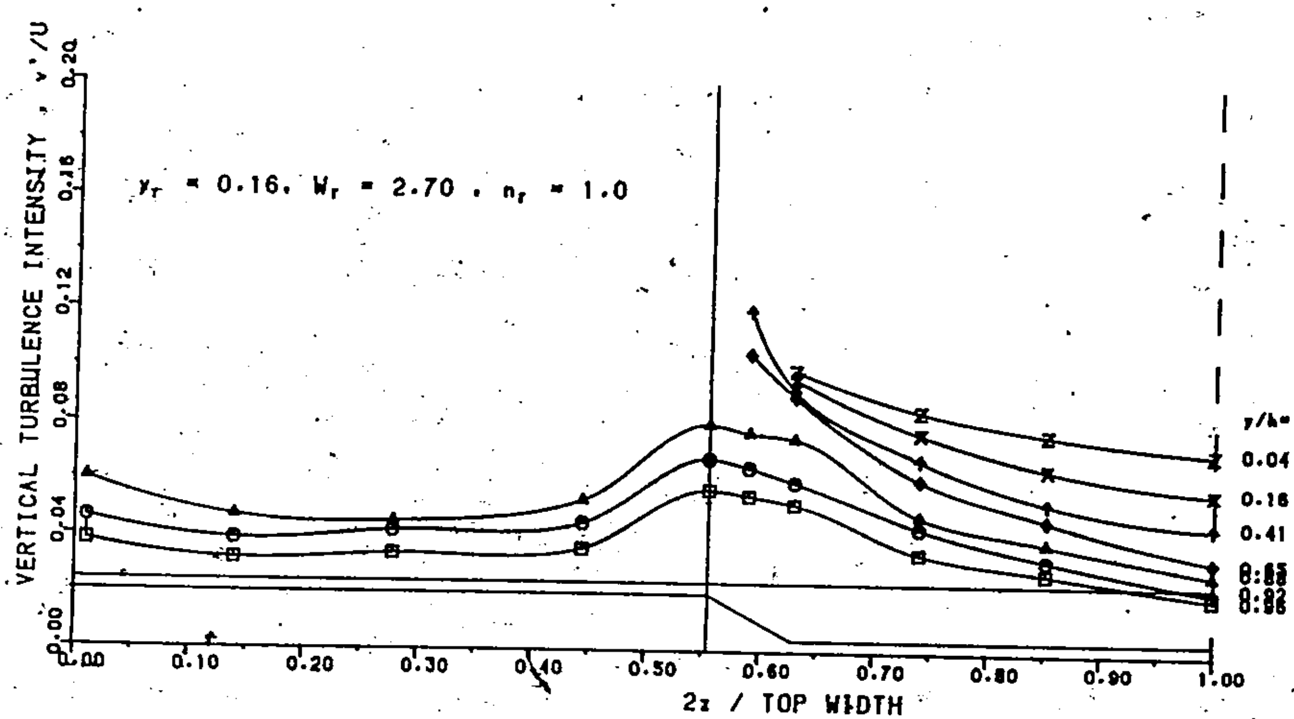

FIG. 57: CROSS-STREAM DISTRIBUTION OF v' (NARROW CHANNEL)

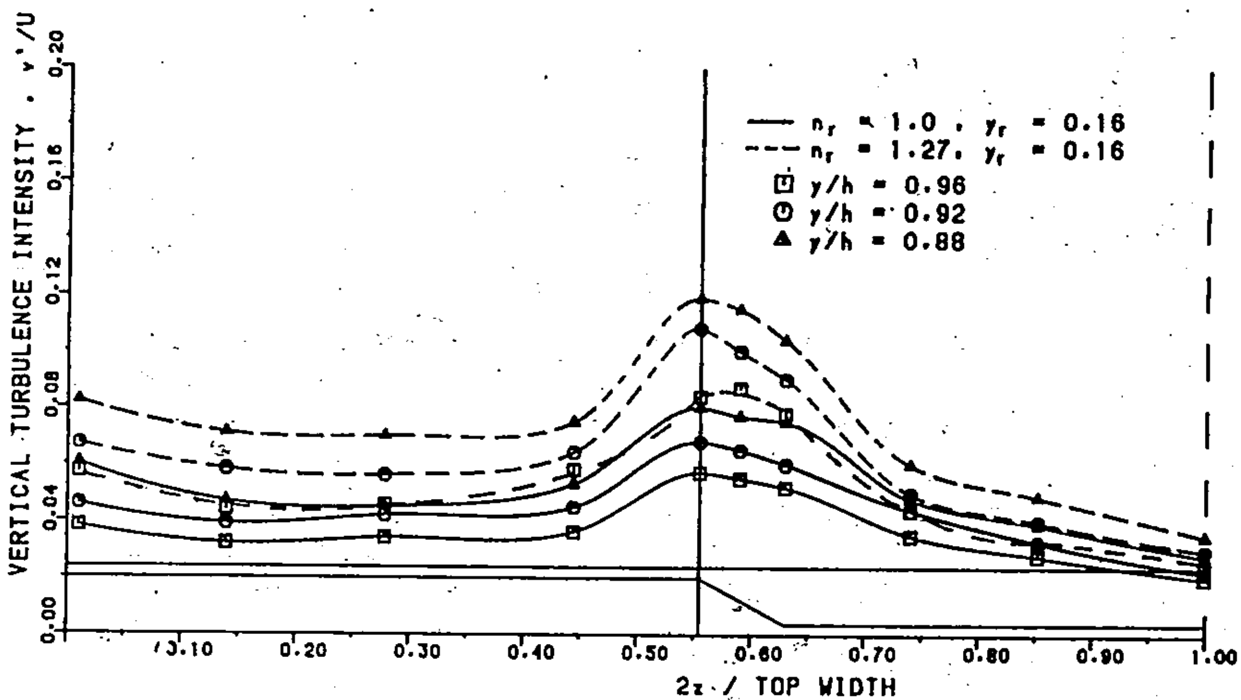

FIG. 58: CROSS-STREAM DISTRIBUTION OF v' FOR 2 RELATIVE ROUGHNESSES (NARROW CHANNEL)

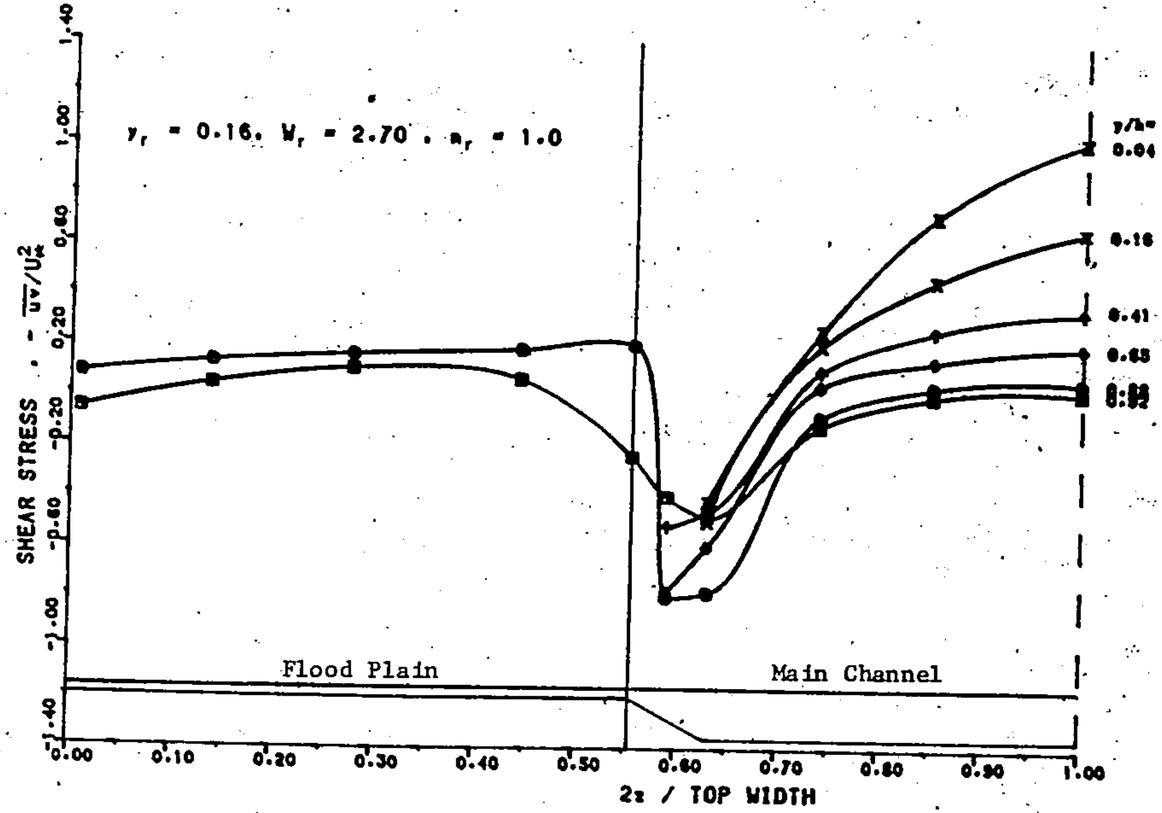

FIG. 59: CROSS-STREAM DISTRIBUTION OF SHEAR STRESS
(NARROW CHANNEL)

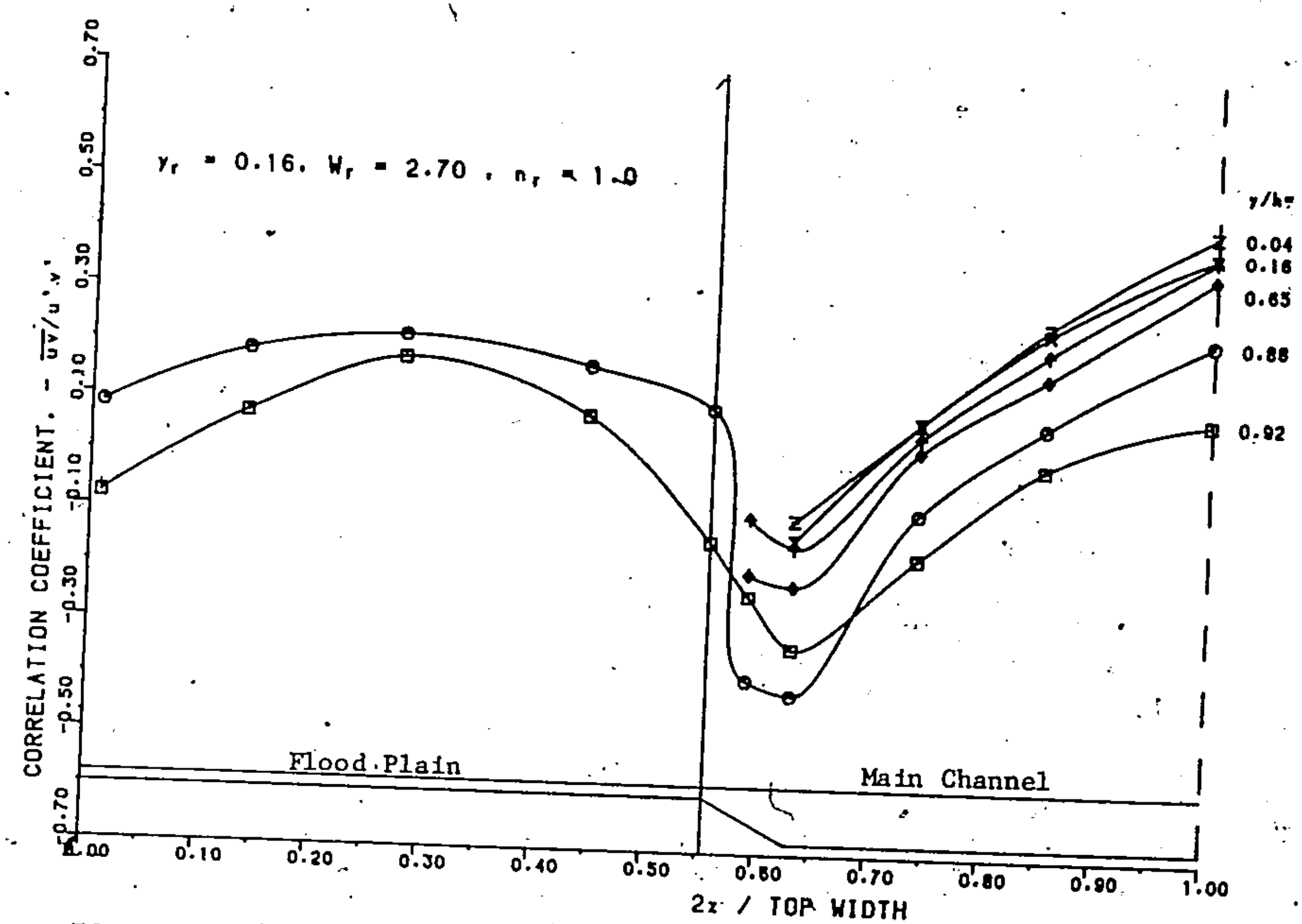

FIG. 60: CROSS-STREAM DISTRIBUTION OF CORRELATION COEFFICIENT (NARROW CHANNEL)

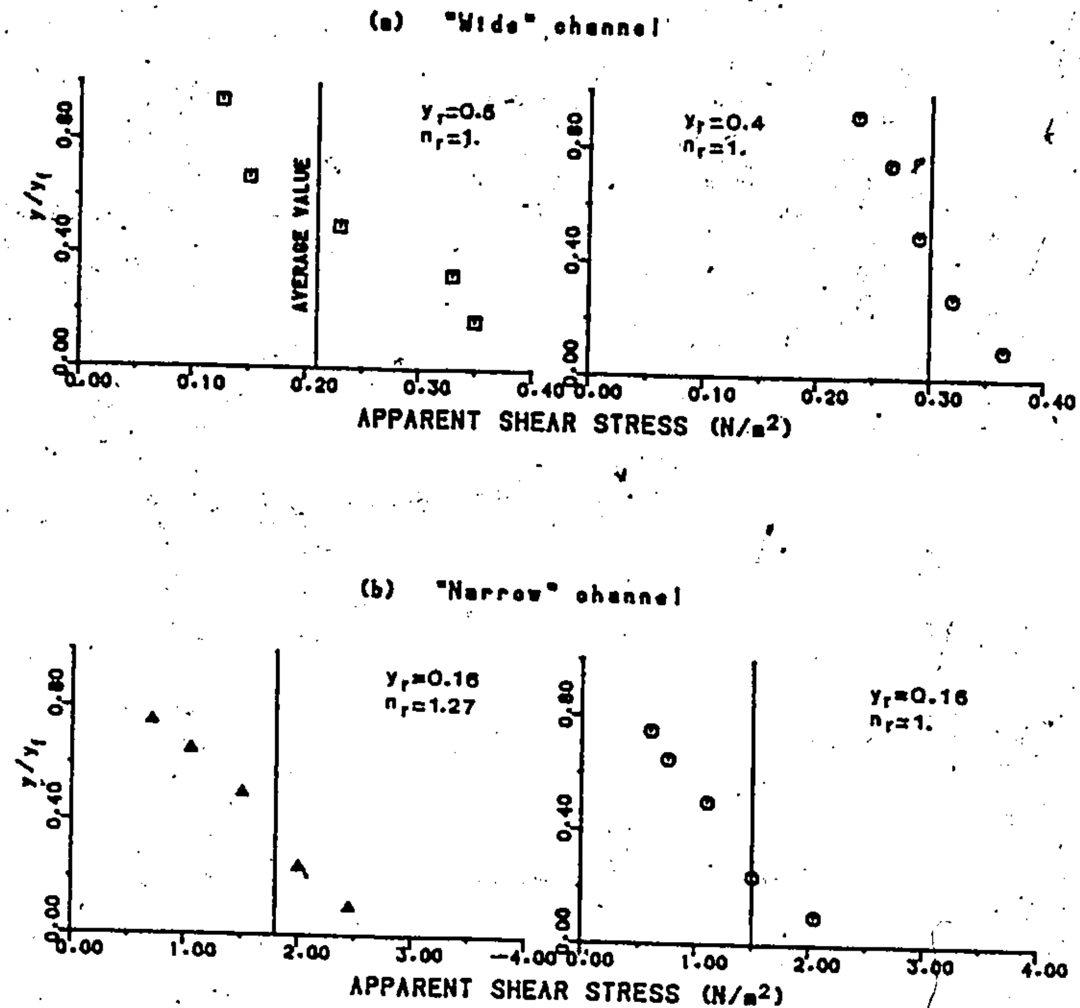

FIG.61: VERTICAL DISTRIBUTION OF APPARENT SHEAR STRESS

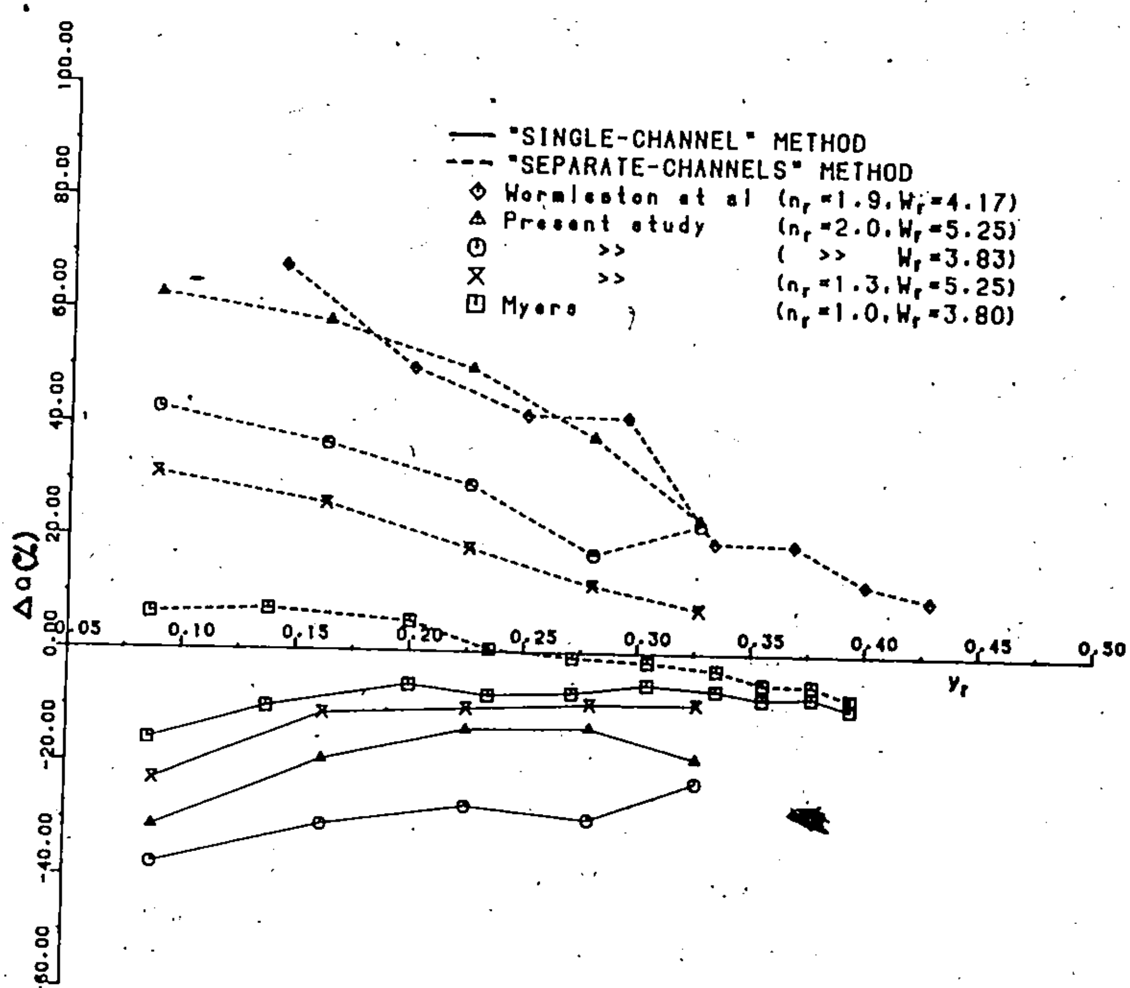

FIG. 6 : ERROR IN DISCHARGE ESTIMATION BY "SINGLE-CHANNEL" AND "SEPARATE-CHANNELS" METHODS

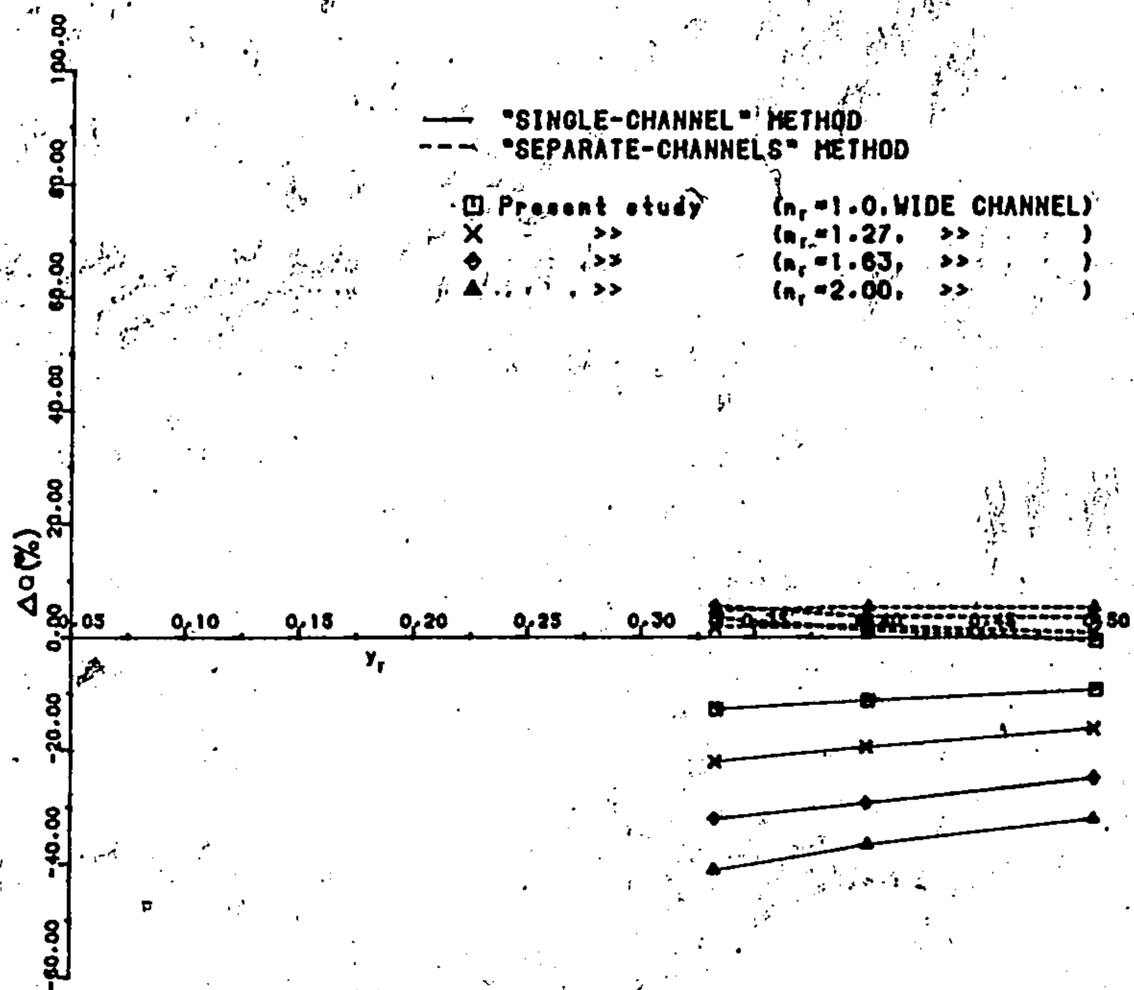

FIG.63: ERROR IN DISCHARGE ESTIMATION BY "SINGLE-CHANNEL" AND "SEPARATE-CHANNELS" METHODS

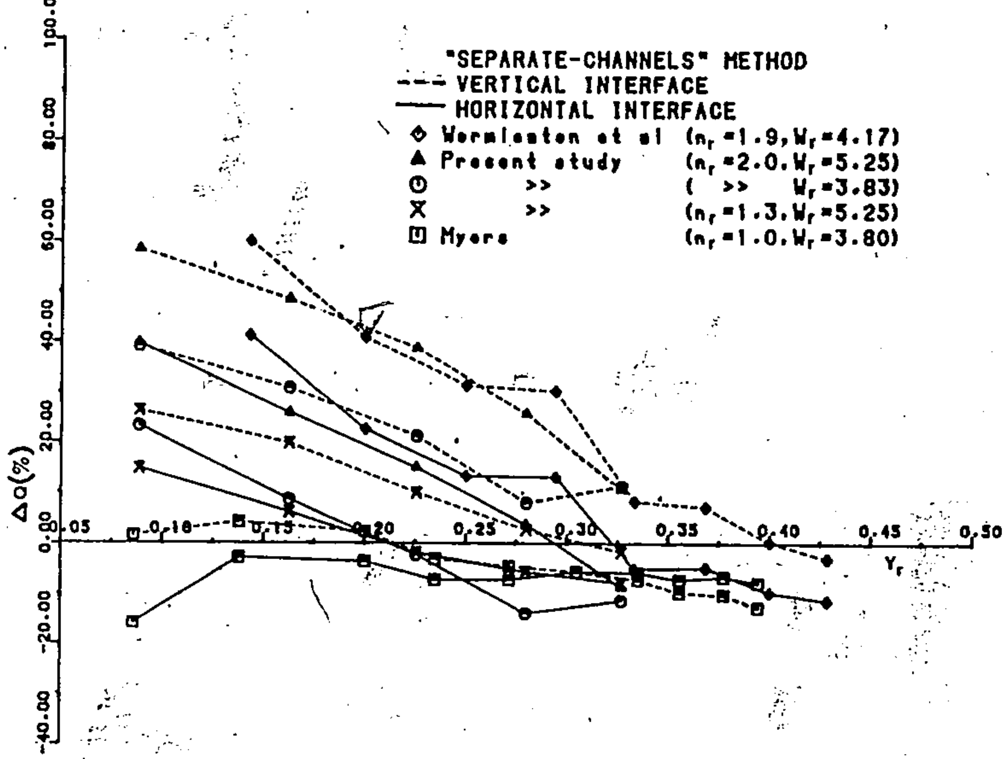

FIG. 6 : ERROR IN DISCHARGE ESTIMATION BY "SEPARATE CHANNELS" METHOD

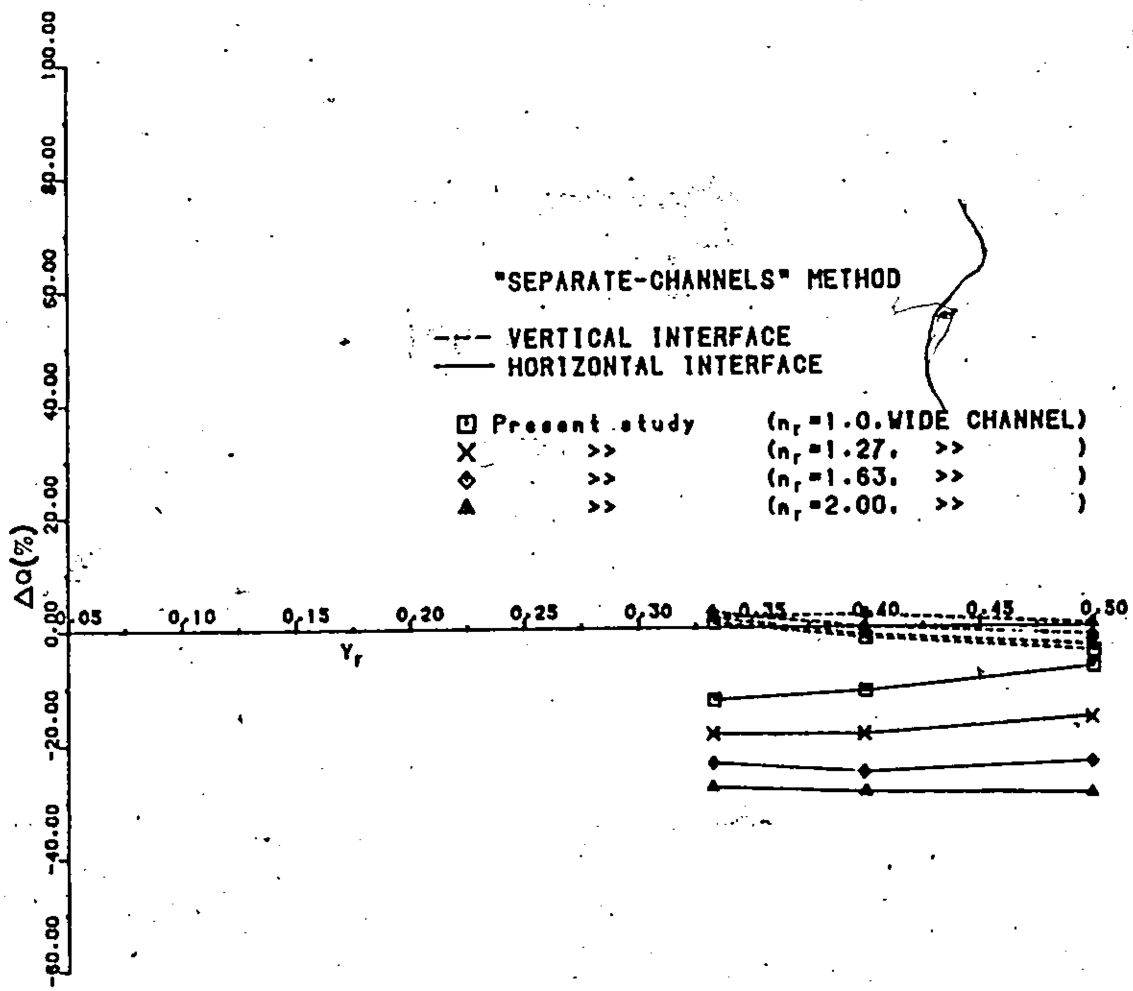

FIG.65: ERROR IN DISCHARGE ESTIMATION BY "SEPARATE CHANNELS" METHOD

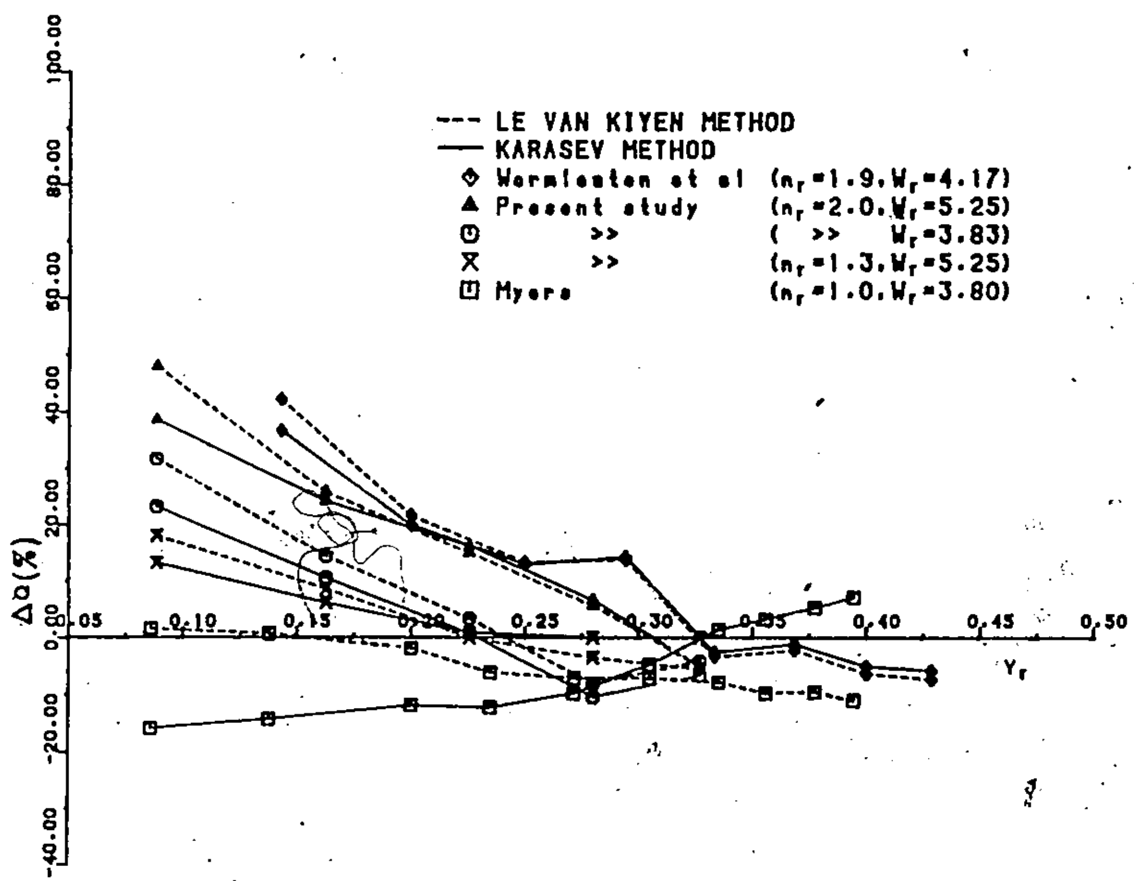

FIG. 66: ERROR IN DISCHARGE ESTIMATION BY METHODS BASED ON CORRECTION FACTORS

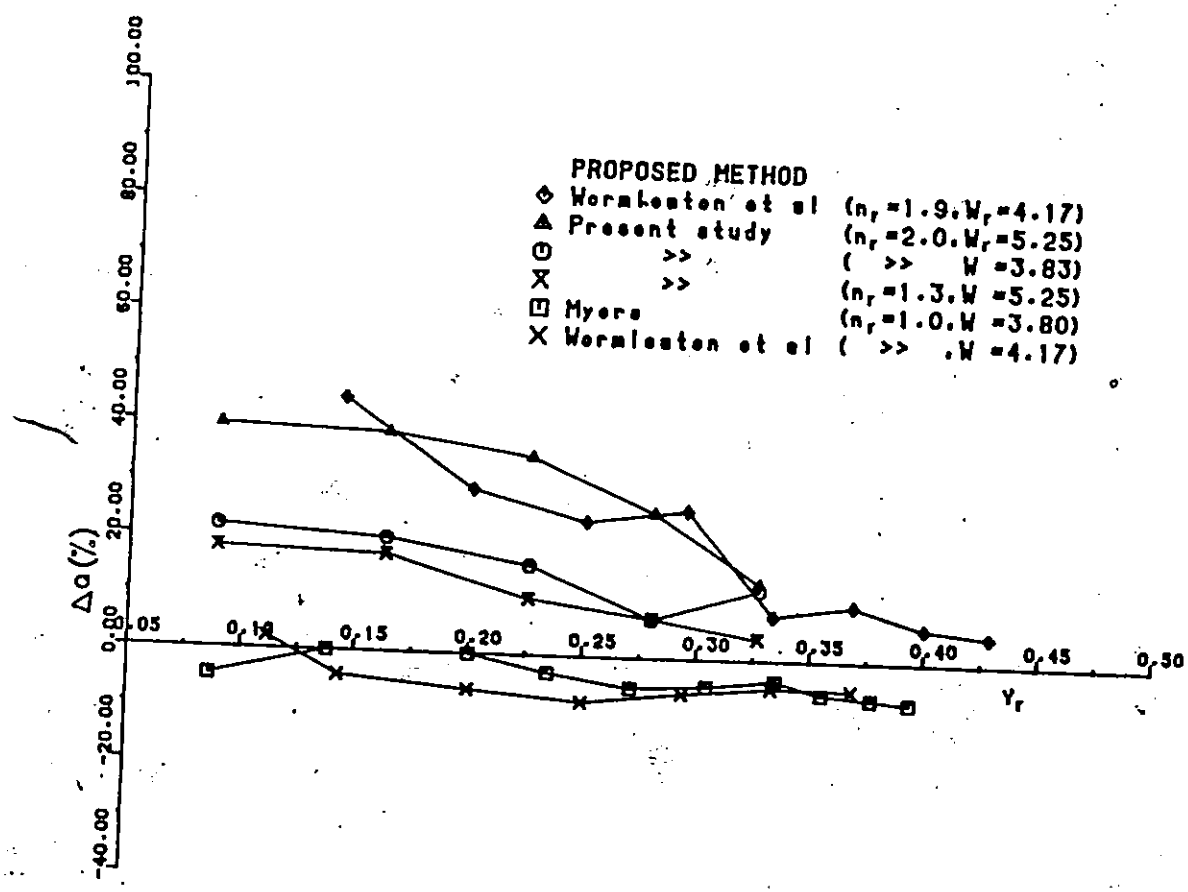

FIG. 6: ERROR IN DISCHARGE ESTIMATION BY PROPOSED METHOD

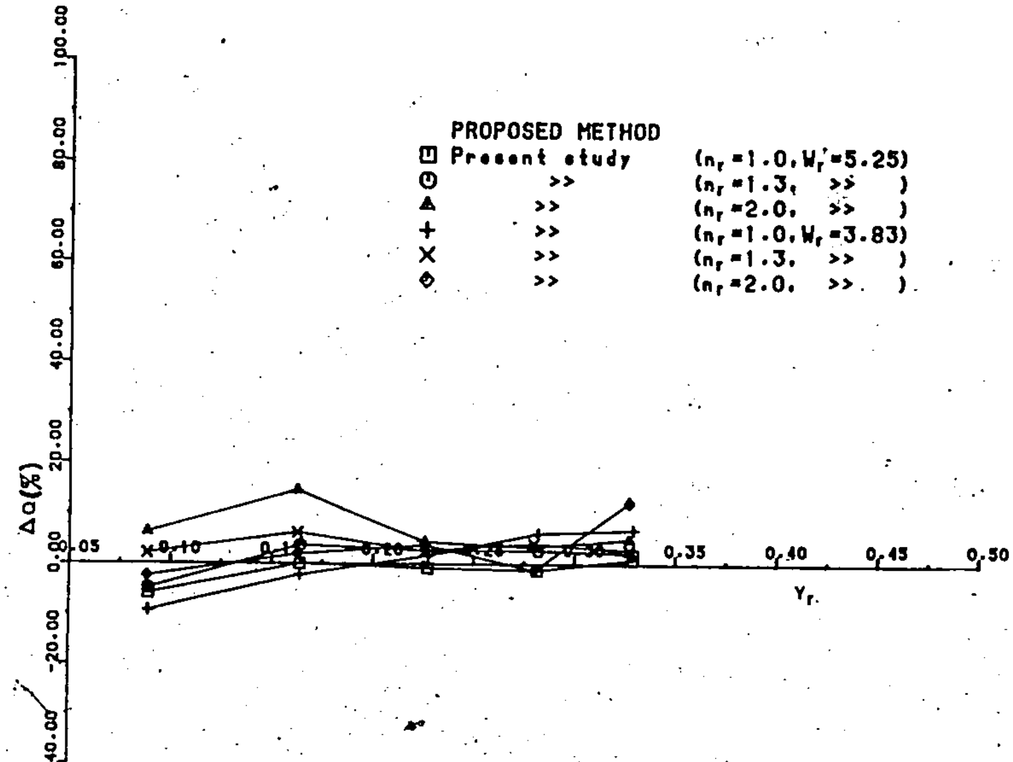

FIG. 68: ERROR IN DISCHARGE ESTIMATION BY PROPOSED METHOD WITH EQUATION 6.25

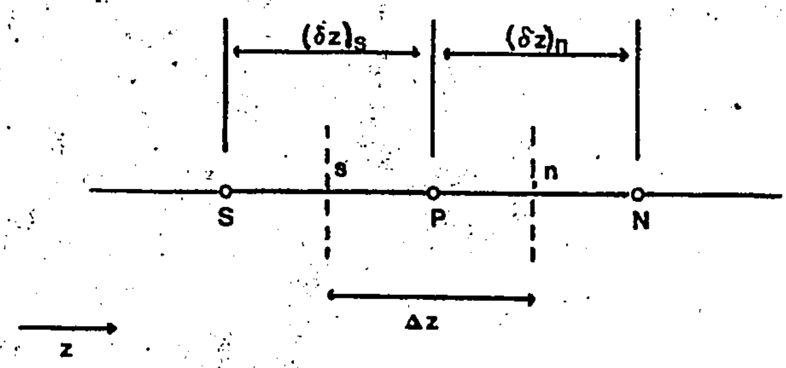

FIG. 69 : GRID-POINT CLUSTER FOR THE ONE-DIMENSIONAL PROBLEM

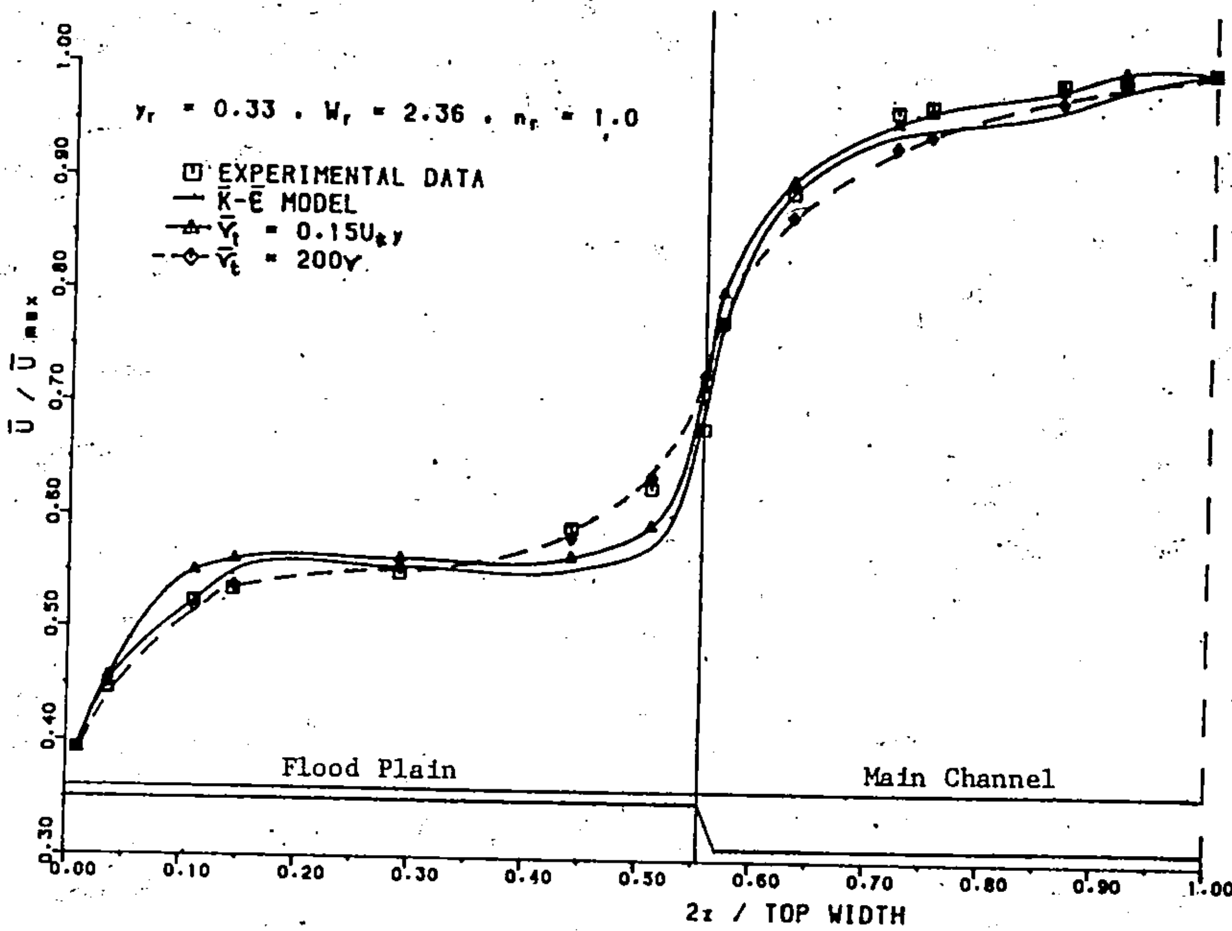

FIG.7C: OBSERVED AND PREDICTED DEPTH-AVERAGED VELOCITY (WIDE CHANNEL)

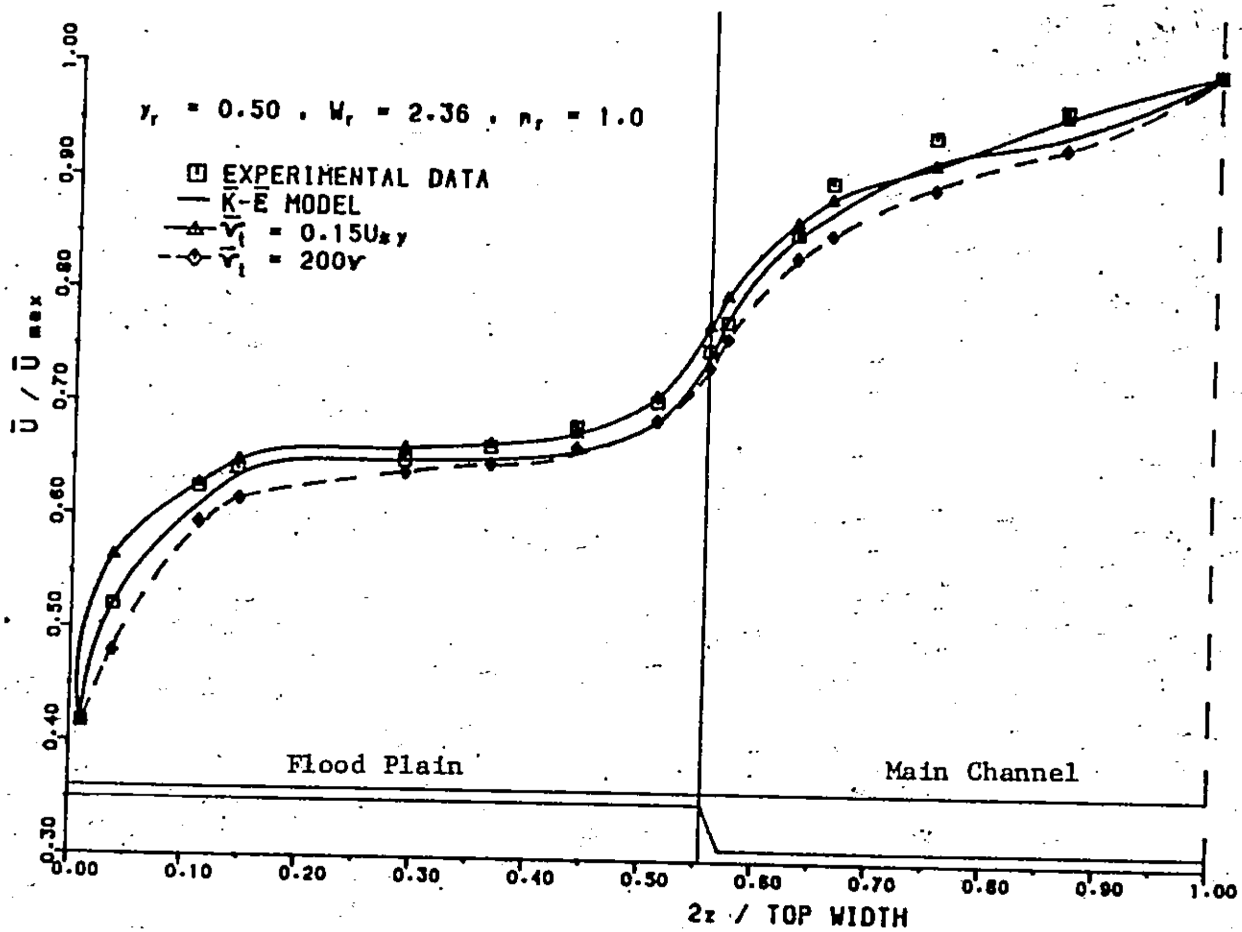

FIG. 71: OBSERVED AND PREDICTED DEPTH-AVERAGED VELOCITY (WIDE CHANNEL)

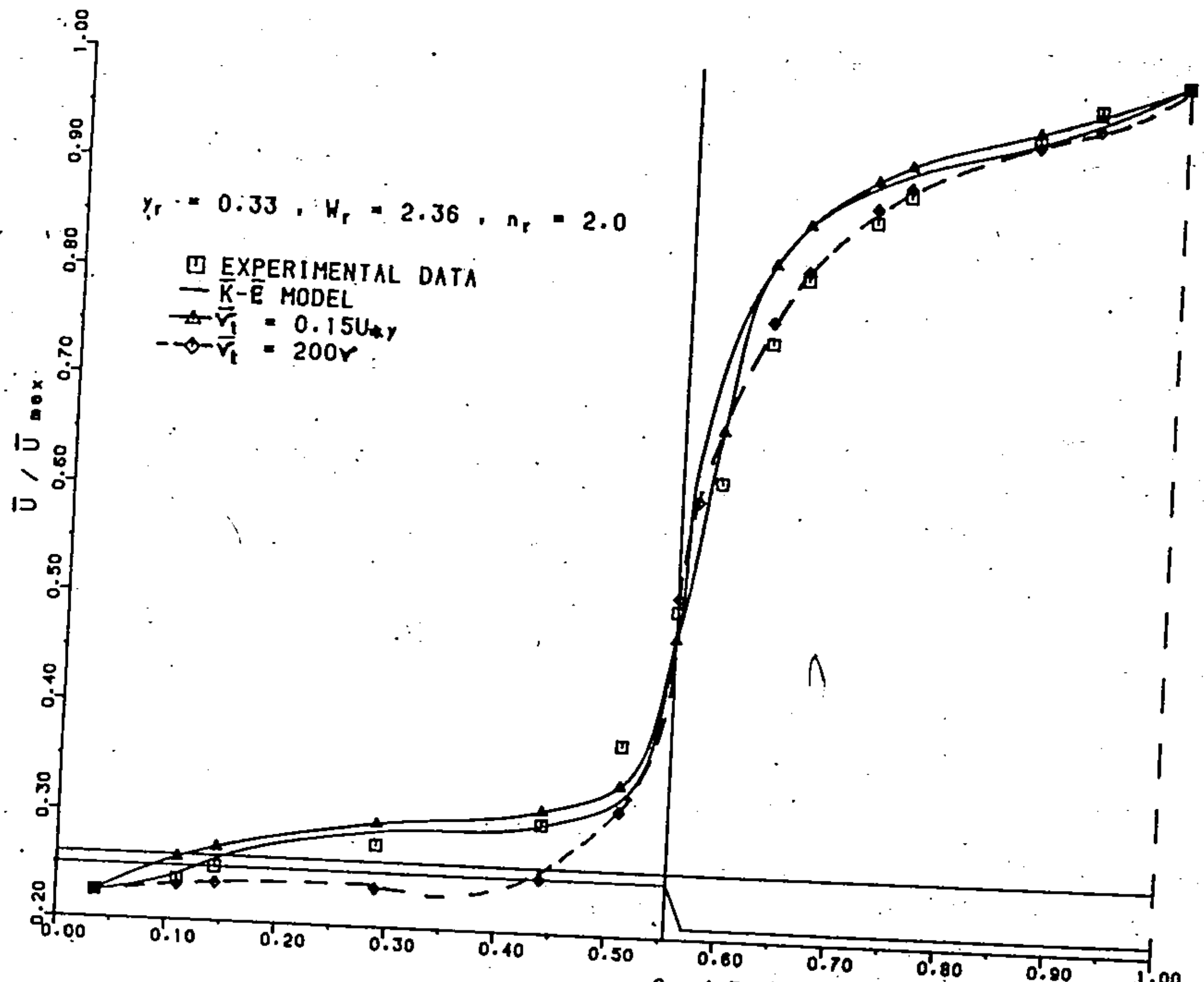

FIG.72: OBSERVED AND PREDICTED DEPTH-AVERAGED VELOCITY (WIDE CHANNEL)

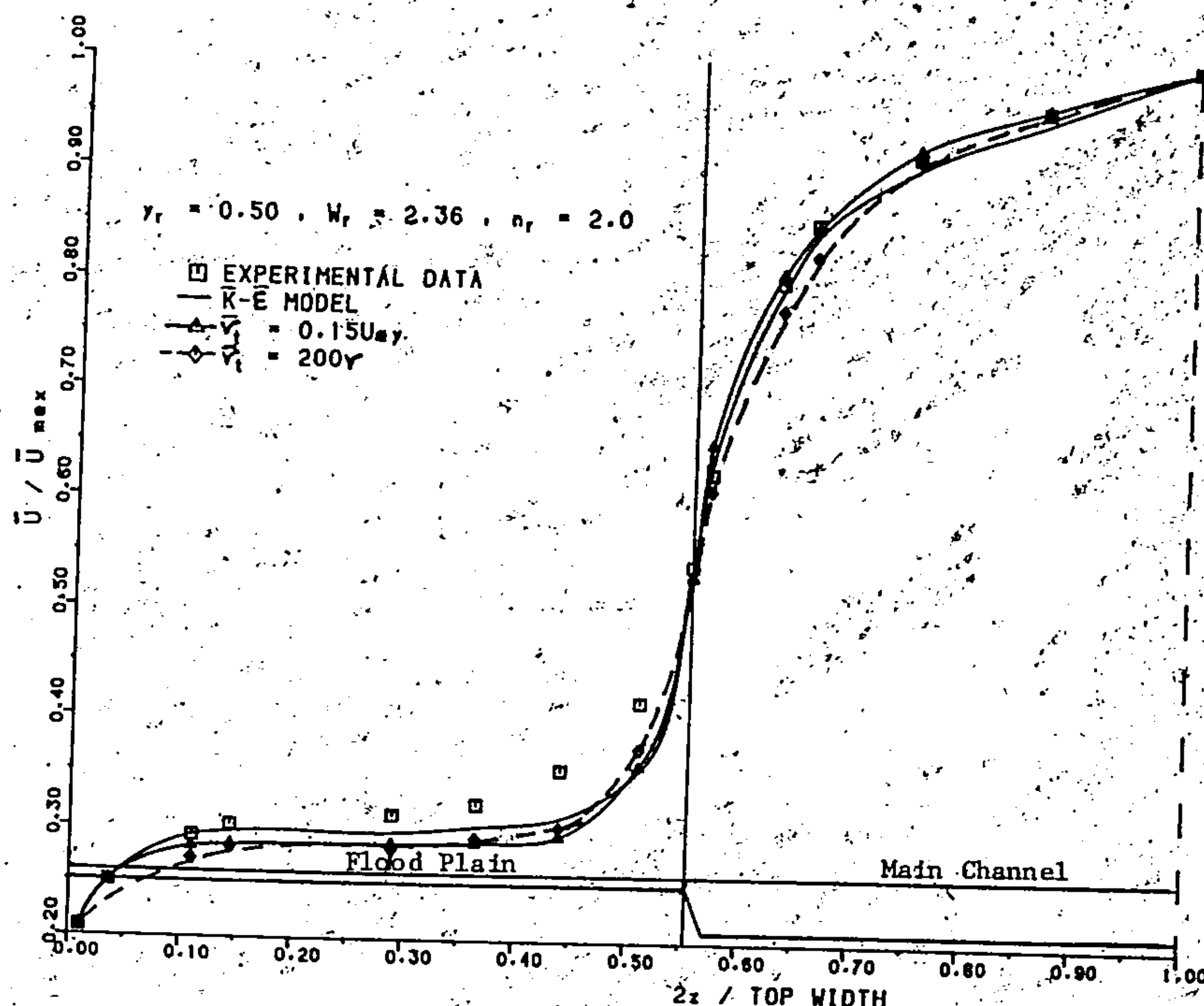

FIG. : OBSERVED AND PREDICTED DEPTH-AVERAGED VELOCITY (WIDE CHANNEL)

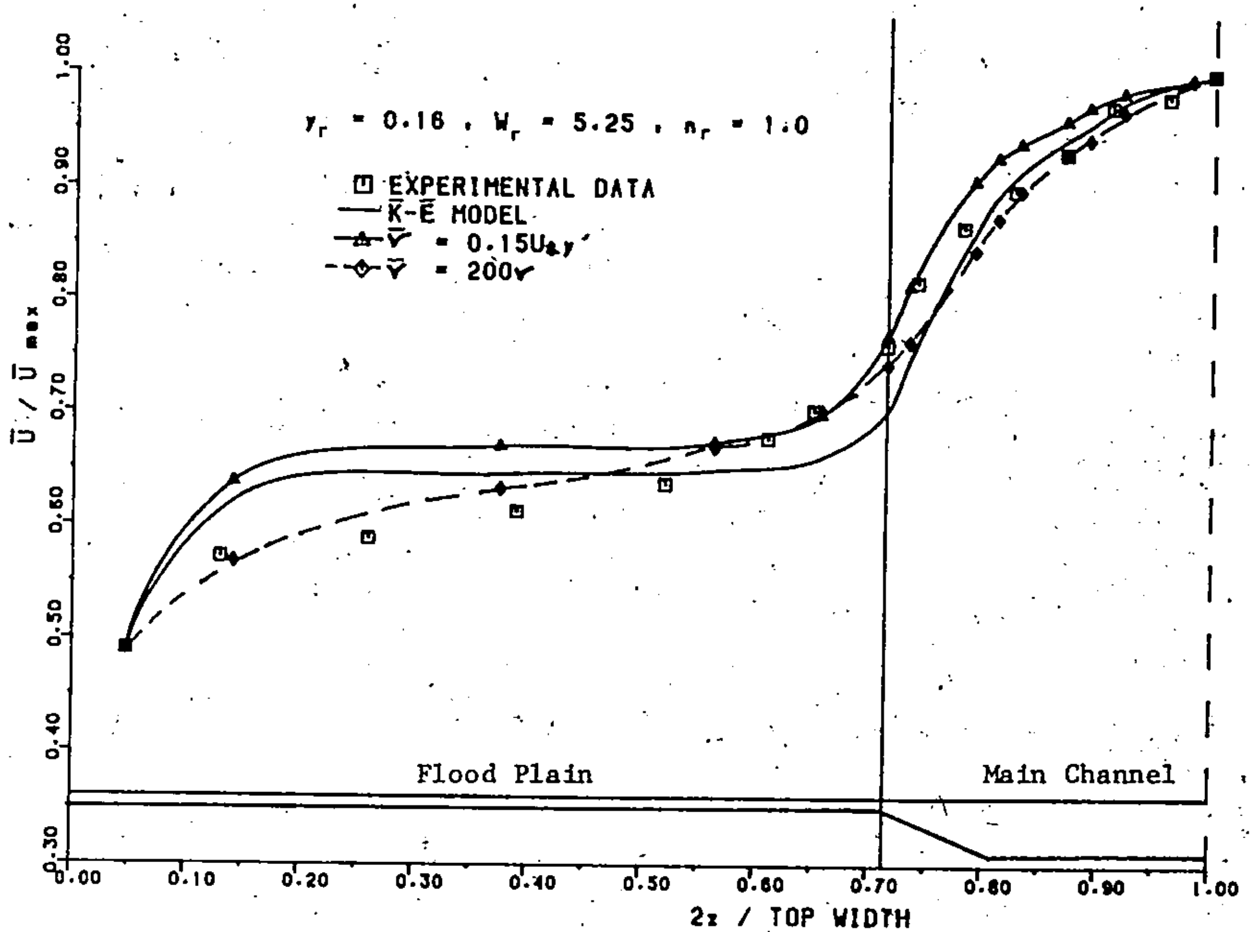

FIG. 74: OBSERVED AND PREDICTED DEPTH-AVERAGED VELOCITY (NARROW CHANNEL)

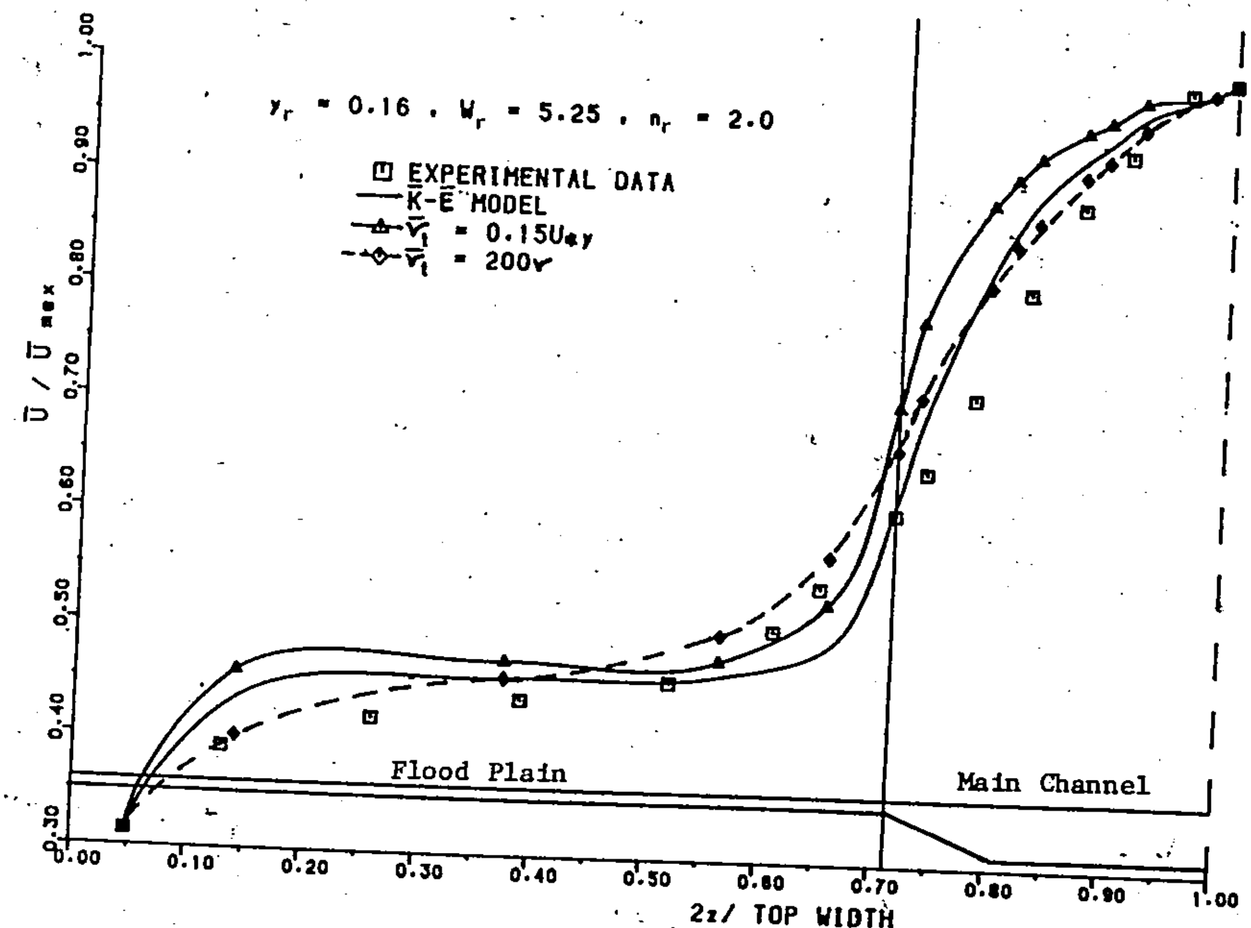

FIG. /F: OBSERVED AND PREDICTED DEPTH-AVERAGED VELOCITY (NARROW CHANNEL)

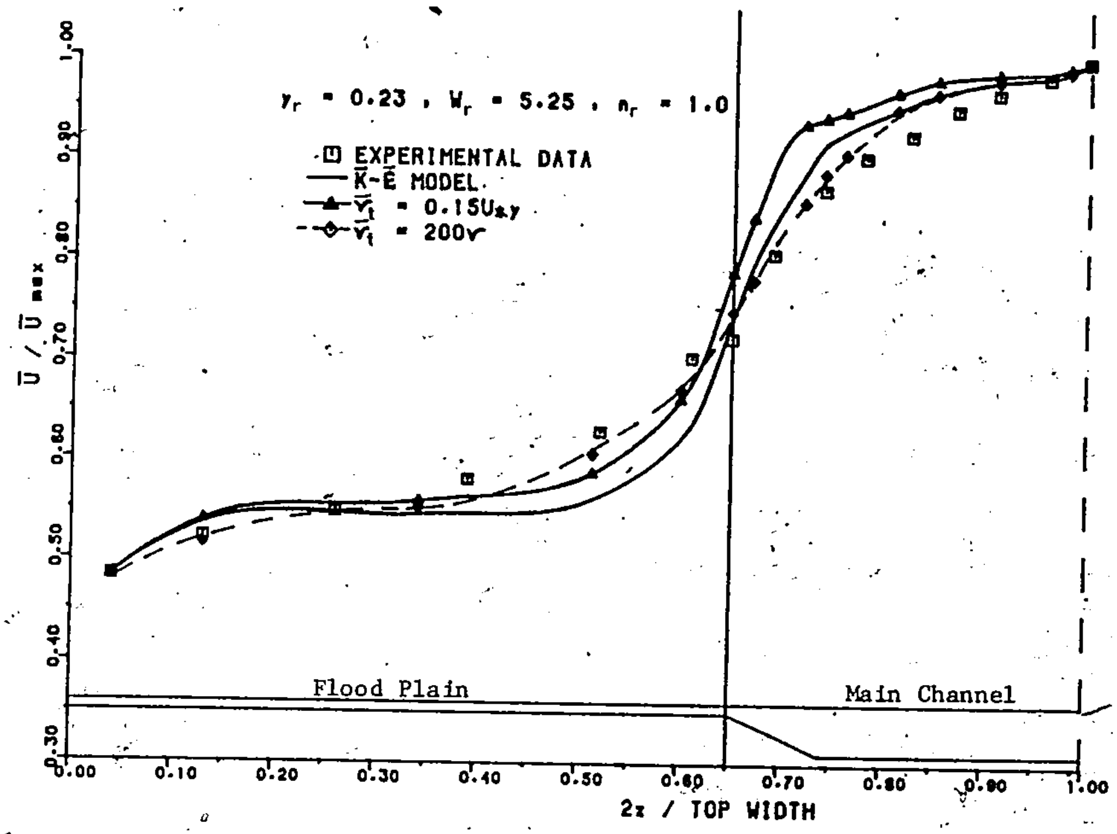

FIG.7n: OBSERVED AND PREDICTED DEPTH-AVERAGED VELOCITY (NARROW CHANNEL)

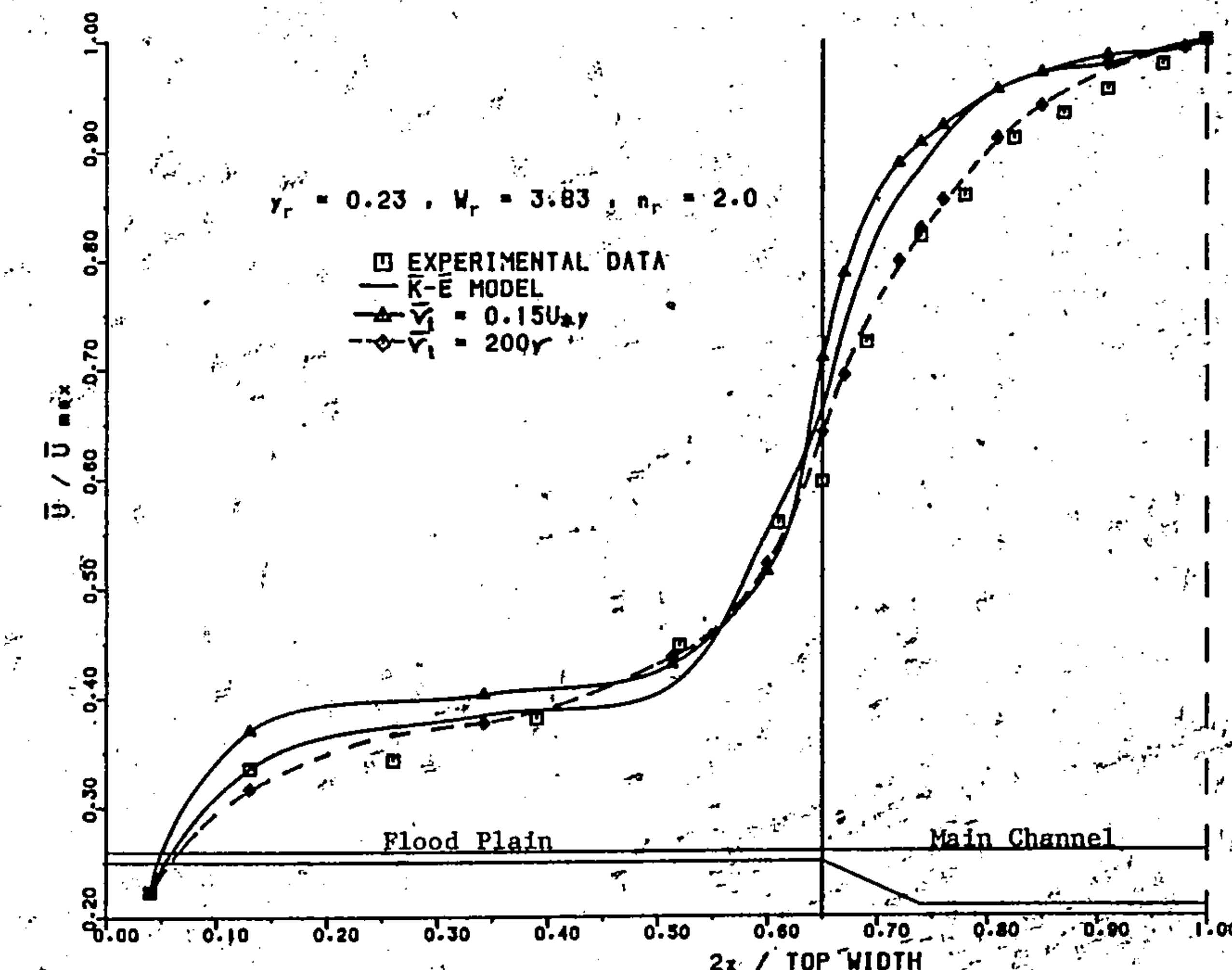

FIG. 77: OBSERVED AND PREDICTED DEPTH-AVERAGED VELOCITY (NARROW CHANNEL)

Appendix A

ERROR ANALYSIS

TABLE 1

Estimated experimental errors

Parameter	Symbol	Value	Units	Error
Channel flow depth	y_c	45.0	mm	±0.5
Flood plain depth	y_f	15.0	mm	±0.5
Relative depth	y_r	0.333		±0.015
Discharge	Q_t	11.8	l/s	±0.2
Channel slope	S	0.001		±0.00005
Flood plain width	B_f	0.381	m	±0.0005
Channel base width	B_c	0.580	m	±0.0005
Wetted perimeter	P_t	1.44	m	±0.01
Total area	A_t	0.038	m	±0.001
Hydraulic radius	R_t	0.026	m	±0.0009
Differential head	Δh	1 to 11.3	mm	±0.035
Local velocity	u	0.15 to 0.47	m/s	±0.0026
Integrated mean velocity	U	0.320	m/s	±0.005
Bulk velocity	Q/A	0.310	m/s	±0.013
2D- shear stress	τ_{2D}	0.438	N/m^2	±0.02
Integrated s. stress	τ_t	0.248	N/m^2	±0.01
Average shear stress	$\gamma R_t S$	0.255	N/m^2	±0.021
Apparent shear stress	τ_a	0.538	N/m^2	±0.07
Discharge from single-channel method	Q_s	9.6	l/s	±0.7
Slope of voltage/ velocity curve	S_1	1.85	V/m/s	±0.06
rms of (e_1+e_2) at y=5mm of ℄	$\frac{1}{2}(e_1+e_2)'$	82.0	mV	±5.0
rms of (e_1-e_2)	$\frac{1}{2}(e_1-e_2)'$	44.0	mV	±2.0
rms of voltage fluct.	e_1'	121.0	mV	±4.0
rms of voltage fluct.	e_2'	95.0	mV	±4.0
rms of velocity fluct.	u'	0.044	m/s	±0.004
longitudinal intensity	u'/U	0.137		±0.015
rms of velocity fluct.	v'	0.024	m/s	±0.0018
vertical intensity	v'/U	0.06		±0.0054
shear stress	$-\rho\overline{uv}$	0.41	N/m^2	±0.08

Appendix B

MAIN EXPERIMENTAL RESULTS

TABLE 2

Experimental results for Wr=5.25

Flood plain depth	Relative roughness	Discharge	Boundary shear stress		Apparent shear stress
y	n_r	Q_t	τ_c	τ_f	τ_a
(mm)		(l/s)	(N/m^2)		(N/m^2)
10	1.0	6.6	0.142	0.059	1.19
20	1.0	9.0	0.164	0.085	0.582
30	1.0	12.5	0.186	0.109	0.377
40	1.0	16.5	0.205	0.134	0.293
50	1.0	20.5	0.224	0.158	0.241
10	1.27	6.1	0.133	0.065	1.42
20	1.27	8.1	0.157	0.089	0.663
30	1.27	11.0	0.179	0.113	0.432
40	1.27	14.3	0.203	0.136	0.31
50	1.27	18.0	0.222	0.159	0.255
10	1.64	5.5	0.129	0.067	1.502
20	1.64	7.0	0.146	0.095	0.782
30	1.64	9.6	0.171	0.117	0.493
40	1.64	12.0	0.192	0.141	0.366
50	1.64	16.1	0.212	0.164	0.298
10	2.0	4.8	0.121	0.071	1.674
20	2.0	6.2	0.140	0.098	0.853
30	2.0	9.0	0.165	0.121	0.536
40	2.0	11.5	0.181	0.147	0.429
50	2.0	14.0	0.199	0.164	0.352

TABLE 3

Experimental results for Wr=3.83

Flood plain depth	Relative roughness	Discharge	Boundary shear stress		Apparent shear stress
y	n_r	Q_t	τ_c	τ_f	τ_a
(mm)		(l/s)	(N/m²)		(N/m²)
10	1.0	10.6	0.169	0.065	1.42
20	1.0	13.4	0.191	0.091	0.717
30	1.0	17.1	0.214	0.116	0.470
40	1.0	21.0	0.243	0.135	0.308
50	1.0	26.0	0.262	0.161	0.266
10	1.27	9.6	0.156	0.075	1.794
20	1.27	11.3	0.179	0.100	0.888
30	1.27	15.6	0.203	0.120	0.526
40	1.27	19.5	0.231	0.144	0.398
50	1.27	24.5	0.259	0.183	0.285
10	1.64	8.7	0.147	0.081	2.034
20	1.64	11.0	0.172	0.105	0.987
30	1.64	14.2	0.198	0.127	0.622
40	1.64	18.3	0.224	0.149	0.447
50	1.64	22.5	0.250	0.169	0.335
10	2.0	8.2	0.143	0.084	2.153
20	2.0	10.4	0.167	0.108	1.052
30	2.0	13.2	0.193	0.131	0.670
40	2.0	17.3	0.216	0.153	0.495
50	2.0	21.0	0.247	0.170	0.376

TABLE 4

Experimental results for Wr=3.125

Flood plain depth	Relative roughness	Discharge	Boundary shear stress		Apparent shear stress
y	n_r	Q_t	τ_c	τ_f	τ_a
(mm)		(l/s)	(N/m^2)		(N/m^2)
10	1.0	13.2	0.182	0.075	1.82
20	1.0	16.5	0.207	0.099	0.874
30	1.0	21.4	0.232	0.123	0.574
40	1.0	27.0	0.254	0.148	0.442
50	1.0	33.8	0.280	0.169	0.338
10	1.27	12.4	0.178	0.079	1.98
20	1.27	15.8	0.204	0.103	0.949
30	1.27	20.0	0.230	0.126	0.610
40	1.27	25.4	0.252	0.151	0.467
50	1.27	31.0	0.278	0.171	0.359
10	1.64	11.8	0.171	0.089	2.220
20	1.64	15.1	0.193	0.112	1.134
30	1.64	19.0	0.218	0.135	0.732
40	1.64	24.0	0.247	0.154	0.507
50	1.64	29.0	0.274	0.174	0.383
10	2.0	10.9	0.166	0.089	2.372
20	2.0	14.0	0.185	0.119	1.260
30	2.0	18.2	0.213	0.139	0.792
40	2.0	22.4	0.236	0.163	0.593
50	2.0	28.0	0.261	0.184	0.468

TABLE 5

Experimental results for Wr=2.70

Flood plain depth	Relative roughness	Discharge	Boundary shear stress		Apparent shear stress
y	n_r	Q_t	τ_c	τ_f	τ_a
(mm)		(l/s)	(N/m^2)		(N/m^2)
10	1.0	18.0	0.194	0.083	2.13
20	1.0	21.5	0.221	0.106	1.015
30	1.0	26.0	0.246	0.130	0.663
40	1.0	32.6	0.272	0.152	0.478
50	1.0	38.0	0.297	0.173	0.377
10	1.27	17.8	0.193	0.086	2.234
20	1.27	20.6	0.214	0.114	1.167
30	1.27	25.0	0.238	0.138	0.779
40	1.27	29.5	0.261	0.163	0.601
50	1.27	36.0	0.292	0.179	0.426
10	1.64	16.9	0.190	0.088	2.336
20	1.64	19.4	0.212	0.116	1.214
30	1.64	24.0	0.237	0.140	0.798
40	1.64	28.5	0.260	0.164	0.610
50	1.64	34.0	0.289	0.182	0.452
10	2.0	15.5	0.180	0.098	2.710
20	2.0	18.5	0.202	0.125	1.382
30	2.0	23.1	0.226	0.149	0.928
40	2.0	27.2	0.251	0.172	0.692
50	2.0	32.0	0.276	0.193	0.543
* 20	1.0	36.0	0.840	0.261	1.50
* 20	1.27	33.1	0.821	0.276	1.8
* 20	1.64	30.2	0.81	0.288	2.05
* 20	2.0	28.4	0.806	0.293	2.14

* Slope of the channel is 0.001

TABLE 6

Experimental results for Wide Channel (S = 0.001)

Flood plain depth	Relative roughness	Discharge	Boundary shear stress		Apparent shear stress
y	n_r	Q_t	τ_c	τ_f	τ_a
(mm)		(l/s)	(N/m^2)		(N/m^2)
15	1.0	11.8	0.384	0.161	0.537
20	1.0	15.2	0.434	0.203	0.336
30	1.0	22.8	0.528	0.287	0.210
15	1.27	11.3	0.375	0.176	0.910
20	1.27	14.4	0.425	0.216	0.609
30	1.27	21.2	0.521	0.299	0.365
15	1.64	10.9	0.358	0.190	1.281
20	1.64	13.7	0.407	0.231	0.907
30	1.64	19.7	0.510	0.307	0.487
15	2.0	10.7	0.354	0.193	1.370
20	2.0	13.1	0.397	0.239	1.070
30	2.0	18.7	0.485	0.327	0.760

TABLE 7

Observed main channel and flood plain average velocities

Flood plain depth	Relative roughness	Wr=5.25 Channel Velocity	Wr=5.25 Flood Plain Velocity	Wr=3.83 Channel Velocity	Wr=3.83 Flood Plain Velocity
y	n_r	U_c	U_f	U_c	U_f
(mm)		(m/s)		(m/s)	
10	1.0	0.187	0.129	0.22	0.125
20	1.0	0.218	0.150	0.244	0.146
30	1.0	0.237	0.186	0.281	0.173
40	1.0	0.269	0.205	0.304	0.195
50	1.0	0.291	0.227	0.320	0.210
10	1.27	0.174	0.109	0.203	0.103
20	1.27	0.200	0.138	0.223	0.125
30	1.27	0.227	0.155	0.250	0.148
40	1.27	0.256	0.171	0.288	0.163
50	1.27	0.282	0.185	0.316	0.179
10	1.64	0.169	0.087	0.190	0.083
20	1.64	0.187	0.108	0.209	0.103
30	1.64	0.218	0.122	0.243	0.118
40	1.64	0.242	0.135	0.272	0.129
50	1.64	0.278	0.150	0.305	0.142
10	2.0	0.159	0.076	0.182	0.069
20	2.0	0.178	0.091	0.204	0.086
30	2.0	0.206	0.102	0.232	0.098
40	2.0	0.228	0.112	0.265	0.107
50	2.0	0.247	0.120	0.300	0.117

TABLE 8

Observed main channel and flood plain average velocities

Wide Channel

Flood plain depth	Relative roughness	Channel	Flood Plain
		Velocity	
y	n_r	U_c	U_f
(mm)		(m/s)	
15	1.0	0.361	0.206
20	1.0	0.392	0.238
30	1.0	0.450	0.298
15	1.27	0.355	0.164
20	1.27	0.385	0.191
30	1.27	0.446	0.237
15	1.64	0.350	0.130
20	1.64	0.381	0.151
30	1.64	0.439	0.185
15	2.0	0.346	0.109
20	2.0	0.375	0.125
30	2.0	0.427	0.155

TABLE 9

Shear Velocity and Constant C for Rough Flood Plains

Flood plain depth	Relative roughness	Narrow Channel Shear Vel.	Narrow Channel Constant	Wide Channel Shear Vel.	Wide Channel Constant
y	n_r	U_*	C	U_*	C
(mm)		(m/s)		(m/s)	
20	1.27	0.0078	3.050	0.0137	3.050
30	1.27	0.0094	2.250	0.0168	2.250
40	1.27	0.0106	1.550		
50	1.27	0.0116	1.050		
20	1.64	0.0081	0.200	0.0139	0.200
30	1.64	0.0096	-0.750	0.017	-0.750
40	1.64	0.0108	-1.000		
50	1.64	0.0118	-1.205		
20	2.0	0.0083	-4.080	0.0143	-4.080
30	2.0	0.0098	-4.080	0.0172	-4.080
40	2.0	0.011	-4.080		
50	2.0	0.012	-4.080		

Appendix C

LISTING OF THE COMPUTER PROGRAM

```
C*************************************************************************
C
C            DEPTH-AVERAGED VERSION OF THE K-E MODEL
C               FOR FULLY DEVELOPED FLOWS
C               P. PRINOS, UNIV. OF OTTAWA
C*************************************************************************
C
      DIMENSION HEDU(9),HEDV(9),HEDP(9),HEDT(9),HEDK(9),HEDD(9),HEDM(9)
     1          ,HEDA(9),HEDB(9),HEDQ(9),HEDR(9),HEDG(9),HEDE(9)
      COMMON
     1/UVEL/RESORU,NSWPU,URFU,DXEPU(32),DXPWU(32),SEWU(32),U1(30)
     1/VVEL/RESORV,NSWPV,URFV,DYNPV(32),DYPSV(32),SNSV(32),RCV(32)
     1/PCOR/RESORM,NSWPP,URFP,DU(30,30),DV(30,30),IPREF,JPREF
     1/TEN/RESORK,NSWPK,URFK
     1/TDIS/RESORE,NSWPD,URFE
     1/VAR/U(30,30),V(30,30),P(30,30),PP(30,30),TE(30,30),ED(30,30)
     1/ALL/IT,JT,NI,NJ,NIM1,NJM1,GREAT,ALPHA(32),UU(32),TB(32)
      COMMON
     1/GEOM/INDCOS,X(32),Y(32),DXEP(32),DXPW(32),DYNP(32),DYPS(32),
     1       SNS(32),SEW(32),XU(32),YV(32),R(32),RV(32),H1(32),Y1(32)
     1/FLUPR/URFVIS,VISCOS,DENSIT,PRANDT,DEN(30,30),VIS(30,30),
     2        VISD(30,30),TE1(32),ED1(32),U2(32)
     1/PROB1/UIN,TEIN,EDIN,FLOWIN,ALAMDA,
     2       RSMALL,RLARGE,AL1,AL2,JSTEP,ISTEP,JSTP1,JSTM1,ISTP1,ISTM1,
     3    NITER,US
     1/TURB/GEN(30,30),CD,CMU,C1,C2,CAPPA,ELOG,PRED,PRTE,CF(50),
     2      CK(50),C5,CE1(50)
     1/WALLF/YPLUSN(30,30),XPLUSW(30,30),TAUN(30,30),TAUW(30,30)
     1/COEF/AP(30,30),AN(30,30),AS(30,30),AE(30,30),AW(30,30),SU(30,30),
     1      SP(30,30)
      COMMON
     1/SUS/SU1(30,30),SU2(30,30),SU3(30,30),SU4(30,30)
     1/SUSP/SUKD(30,30),SPKD(30,30)
     1/TEMP/T(30,30),GAMH(30,30),RESORT,NSWPT,URFT,PRANDL,PFUN,
     2     TWALLN,TIN,GAMQ(30,30),TBOTOM
     1/MSTF/QE(30,30),PRQE,CQ1,CQ2,RESQE,URFQ,BETA,GRAVTY,C3,C4,NSWPQ,
     1       SUQE(30,30),GENQ(30,30),SPQE(30,30),RESORQ
     1/AREA1/INCT
     1/FINAL/ALNULH(32),ALNULR(32),ALNUTH(32),ALNUTR(32),
     2       VAVR(30,30),RA(30,30),ANGLE(30,30),UAVR(30,30),FENRG(30,30)
      LOGICAL INCALU,INCALV,INCALP,INPRO,INCALK,INCALD,INCALM,INCALA,
     1    INCALB,INCALT,INCT,INCALQ,INCALR,INCALG,INCAFE
      REAL NU
      READ(5,010)HEDU,HEDV,HEDP,HEDT,HEDK,HEDD,HEDM,HEDA,HEDB,HEDQ
     1,HEDR,HEDG,HEDE
  010 FORMAT(9A4)
C    *************           'TEACH - T'          **************        C
CHAPTER  1  1 . 1  1  1  PARAMETERS AND CONTROL INDICES  1  1  1  1  1  1
C
C-----GRID
      I=1
      GREAT=1.E30
      NITER=0
      IT=30
      JT=30
```

```
      NSWPU=1
      NSWPV=3
      NSWPP=5
      NSWPT=3
      NSWPK=1
      NSWPD=1
      NSWPQ=3
      NI=1
      NJ=25
      NIM1=NI-1
      NJM1=NJ-1
      IMAX=NI
      JMAX=NJ
      JSTEP=NJ-3
      JSTM1=JSTEP+1
      JSTP1=4
      INDCOS=2
C     DY=0.0075
C     DX=0.004
      Y(1)=0.00
      Y(2)=0.025
      Y(3)=.0750
      Y(4)=.1000
      Y(5)=.2000
      Y(6)=.2500
      Y(7)=.300
      Y(8)=.350
      Y(9)=.380
      Y(10)=.382
      Y(11)=.386
      Y(12)=.3910
      Y(13)=.394
      Y(14)=.3960
      Y(15)=.3970
      Y(16)=.4330
      Y(17)=.453
      Y(18)=.4730
      Y(19)=.493
      Y(20)=.513
      Y(21)=.553
      Y(22)=.593
      Y(23)=.633
      Y(24)=.685
      Y(25)=.686
      H1(1)=.015
      H1(2)=.015
      H1(3)=.015
      H1(4)=.015
      H1(5)=.015
      H1(6)=.015
      H1(7)=.015
      H1(8)=.015
      H1(9)=.015
      H1(10)=.017
      H1(11)=.025
```

```
H1(12)=.035
H1(13)=.041
H1(14)=.045
H1(15)=.045
H1(16)=.045
H1(17)=.045
H1(18)=.045
H1(19)=.045
H1(20)=.045
H1(21)=.045
H1(22)=.045
H1(23)=.045
H1(24)=.045
H1(25)=.045
S0=.001
TE1(1)=8.95E-5
TE1(2)=1.0E-4
TE1(3)=1.09E-4
TE1(4)=1.19E-4
TE1(5)=1.20E-4
TE1(6)=1.21E-4
TE1(7)=1.23E-4
TE1(8)=1.243E-4
TE1(9)=1.256E-4
TE1(10)=1.27E-4
TE1(11)=1.363E-4
TE1(12)=1.456E-4
TE1(13)=1.55E-4
TE1(14)=1.26E-3
TE1(15)=1.26E-3
TE1(16)=1.26E-3
TE1(17)=1.26E-3
TE1(18)=1.26E-3
TE1(19)=1.26E-3
TE1(20)=1.26E-3
TE1(21)=1.26E-3
TE1(22)=1.26E-3
TE1(23)=1.26E-3
TE1(24)=1.26E-3
TE1(25)=1.26E-3
ED1(1)=2.06E-4
ED1(2)=2.1E-4
ED1(3)=2.12E-4
ED1(4)=2.16E-4
ED1(5)=2.19E-4
ED1(6)=2.22E-4
ED1(7)=2.35E-4
ED1(8)=2.49E-4
ED1(9)=2.543E-4
ED1(10)=2.689E-4
ED1(11)=2.756E-4
ED1(12)=2.823E-4
ED1(13)=3.09E-4
ED1(14)=4.04E-4
ED1(15)=4.04E-4
```

```
      ED1(16)=4.04E-4
      ED1(17)=5.04E-4
      ED1(18)=5.04E-4
      ED1(19)=5.04E-4
      ED1(20)=6.04E-4
      ED1(21)=6.04E-4
      ED1(22)=7.04E-4
      ED1(23)=7.04E-4
      ED1(24)=8.04E-4
      ED1(25)=9.04E-4
C-----DEPENDENT VARIABLE SELECTION
      INCALU=.TRUE.
      INCALD=.TRUE.
      INCALK=.TRUE.
      INPRO=.TRUE.
C-----FLUID PROPERTIES
      DENSIT=997.0
      VISCOS=0.89E-6
      PRANDL=2.330
      TK=0.16
      CPP=1002.3
      BETA=6.72E-4
      NU=VISCOS/DENSIT
      PRANDL=CPP*VISCOS/TK
C-----TURBULENCE CONSTANTS
      CMU=0.09
      CD=1.00
      C5=3.6
      DO 30 J=1,NJ
      Y1(J)=Y(J)
      IF (Y1(J).GT..381) GO TO 50
      CF(J)=.00380
      CK(J)=1./SQRT(CF(J))
      CE1(J)=C5*1.92*SQRT(CMU)/(CF(J)**(3./4.))
      GO TO 30
   50 CF(J)=.00380
      CK(J)=1./SQRT(CF(J))
      CE1(J)=C5*1.92*SQRT(CMU)/(CF(J)**(3./4.))
      C1=1.44
      C2=1.92
      C3=1.44
      C4=0.5
      CAPPA=.4187
      ELOG=9.000
      PRED=1.3
      PRTE=1.0
      PRANDT=0.9
      PFUN=PRANDL/PRANDT
      PFUN=9.24*(PFUN**0.75-1.)
C-----BOUNDARY VALUES
C
      UIN=0.1E-9
      U1(1)=.07
      U1(2)=.073
      U1(3)=.078
      U1(4)=.105
```

```
      U1(5)=.113
      U1(6)=.122
      U1(7)=.137
      U1(8)=.1472
      U1(9)=.150
      U1(10)=.155
      U1(11)=.158
      U1(12)=.161
      U1(13)=.164
      U1(14)=.165
      U1(15)=.173
      U1(16)=.179
      U1(17)=.181
      U1(18)=.182
      U1(19)=.19
      U1(20)=.194
      U1(21)=.196
      U1(22)=.198
      U1(23)=.199
      U1(24)=.2
      U1(25)=.2
      TURBIN=.03
      TEIN=1.E-6
      QEIN=0.001*TURBIN
      ALAMDA=0.005
      EDIN=1.E-4
C-----PRESSURE CALCULATION
      JPREF=9
      IPREF=9
      TIN=300.
C-----PROGRAM CONTROL AND MONITOR
      MAXIT=20
      IMON=4
      JMON=4
      URFU=0.5
      URFV=0.5
      URFP=1.0
      URFT=1.0
      URFE=0.7
      URFK=0.7
      URFQ=0.7
      URFVIS=0.7
      TWALLN=323.
      TBOTOM=288.
      INDPRI=100
      SORMAX=0.01
      GRAVTY=9.807
C
CHAPTER  2  2  2  2  2  2  INITIAL OPERATIONS  2  2  2  2  2  2  2  2  2
C
C-----CALCULATE GEOMETRICAL QUANTITIES AND SET VARIABLES TO ZERO
      CALL INIT
C------SPECIFY INLET CONDITIONS
C      PLUG FLOW CONDITIONS SPECIFIED IN THIS EXAMPLE
      DO 202 J=1,NJ
```

```
      TE(I,J)=TE1(J)
      ED(I,J)=ED1(J)
  202 U(I,J)=U1(J)
      CALL PROPS
C-----INITIAL OUTPUT
      IF(INCALU) CALL PRINT(2,2,NI,NJ,IT,JT,XU,Y,U,HEDU)
      IF(INCALK) CALL PRINT(2,2,NI,NJ,IT,JT,X,Y,TE,HEDK)
      IF(INCALD) CALL PRINT(2,2,NI,NJ,IT,JT,X,Y,ED,HEDD)
C---------CALCULATE RESIDUAL SOURCE-NORMALIZATION FACTORS------------
C
CHAPTER  3  3  3  3  3  3  3  ITERATION LOOP  3  3  3  3  3  3  3  3  3
C
      WRITE(6,310) IMON,JMON
  300 NITER=NITER+1
C-----UPDATE MAIN DEPENDENT VARIABLES
      IF(INCALD) CALL CALCED
      IF(INCALK) CALL CALCTE
      IF(INPRO) CALL PROPS
      IF(INCALU) CALL CALCU
C-----INTERMEDIATE OUTPUT
      WRITE(6,399) NITER
  399 FORMAT(I4)
      WRITE(6,3333) RESORU,RESORK,RESORE
 3333 FORMAT(2X,F20.5)
C     DUMMY=0.0
      DUMMY=T(IMON,JMON)
      IF(NITER.LE.150) GO TO 301
      IF(MOD(NITER,50).NE.0) GO TO 301
      WRITE(6,311) NITER,RESORU,RESORV,RESORM,RESORT,RESORK,RESORE
     1             ,U(IMON,JMON),V(IMON,JMON),P(IMON,JMON),DUMMY,
     1               TE(IMON,NJM1),ED(IMON,NJM1)
      IF(INCALU) CALL PRINT(2,2,NI,NJ,IT,JT,XU,Y,U,HEDU)
      IF(INCALK) CALL PRINT(2,2,NI,NJ,IT,JT,X,Y,TE,HEDK)
      IF(INCALD) CALL PRINT(2,2,NI,NJ,IT,JT,X,Y,ED,HEDD)
      IF(NITER.LE.25) GO TO 301
      WRITE(6,310) IMON,JMON
  301 CONTINUE
C-----TERMINATION TESTS
      SORCE=AMAX1(RESORU,RESORK,RESORE)
C     IF(NITER.EQ.20.AND.SORCE.GT.1.0E4*SORMAX) GO TO  302
C     IF(NITER.EQ.MAXIT) GO TO 302
C     GO TO 300
  302 CONTINUE
C
CHAPTER  4  4  4  4  4  4  FINAL OPERATIONS AND OUTPUT  4  4  4  4  4  4
C
      IF(INCALU) CALL PRINT(2,2,NI,NJ,IT,JT,XU,Y,U,HEDU)
      IF(INCALV) CALL PRINT(2,2,NI,NJ,IT,JT,X,YV,V,HEDV)
      IF(INCALP) CALL PRINT(2,2,NI,NJ,IT,JT,X,Y,P,HEDP)
      INCT=.TRUE.
      IF(INCALT) CALL PRINT(2,2,NI,NJ,IT,JT,X,Y,T,HEDT)
      INCT=.FALSE.
      IF(INCALK) CALL PRINT(2,2,NI,NJ,IT,JT,X,Y,TE,HEDK)
      IF(INCALD) CALL PRINT(2,2,NI,NJ,IT,JT,X,Y,ED,HEDD)
      IF(INPRO ) CALL PRINT(2,2,NI,NJ,IT,JT,X,Y,VIS,HEDM)
```

```
      IF(INCALQ) CALL PRINT(2,2,NI,NJ,IT,JT,X,Y,QE,HEDQ)
C     IF(NITER.LT.MAXIT.AND.SORCE.LT.1.0E1*SORMAX) GO TO 500
      IF(NITER.EQ.MAXIT) GO TO 500
      GO TO 300
      STOP
C-----FORMAT STATEMENTS
  310 FORMAT(1H0,4HITER,4X,106HI------------ABSOLUTE RESIDUAL SOURCE SU
     1S------------I            I-------FIELD VALUES AT MONITORING LOCATION
     2      1H(,I2,1H,,I2,1H),9H--------I/2X,2HNO,6X,4HUMOM,6X,4HVMOM,6X
     34HMASS,6X,4HENER,6X,4HTKIN,6X,4HDISP,10X,1HU,9X,1HV,9X,1HP,9X,1HT
     49X,1HK,9X,1HD/)
  311 FORMAT(1H ,I3,4X,1P6E10.3,3X,1P6E10.3)
      END
      SUBROUTINE INIT
C
CHAPTER  0  0  0  0  0  0  0  0  PRELIMINARIES  0  0  0  0  0  0  0  0
C
      COMMON
     1/UVEL/RESORU,NSWPU,URFU,DXEPU(32),DXPWU(32),SEWU(32),U1(30)
     1/VVEL/RESORV,NSWPV,URFV,DYNPV(32),DYPSV(32),SNSV(32),RCV(32)
     1/PCOR/RESORM,NSWPP,URFP,DU(30,30),DV(30,30),IPREF,JPREF
     1/VAR/U(30,30),V(30,30),P(30,30),PP(30,30),TE(30,30),ED(30,30)
     1/ALL/IT,JT,NI,NJ,NIM1,NJM1,GREAT,ALPHA(32),UU(32),TB(32)
      COMMON
     1/GEOM/INDCOS,X(32),Y(32),DXEP(32),DXPW(32),DYNP(32),DYPS(32),
     1      SNS(32),SEW(32),XU(32),YV(32),R(32),RV(32),H1(32),Y1(32)
     1/FLUPR/URFVIS,VISCOS,DENSIT,PRANDT,DEN(30,30),VIS(30,30),
     2       VISD(30,30),TE1(32),ED1(32),U2(32)
     1/PROB1/UIN,TEIN,EDIN,FLOWIN,ALAMDA,
     2       RSMALL,RLARGE,AL1,AL2,JSTEP,ISTEP,JSTP1,JSTM1,ISTP1,ISTM1,
     3    NITER,US
     1/TURB/GEN(30,30),CD,CMU,C1,C2,CAPPA,ELOG,PRED,PRTE,CF(50),
     2      CK(50),C5,CE1(50)
     1/COEF/AP(30,30),AN(30,30),AS(30,30),AE(30,30),AW(30,30),SU(30,30),
     1      SP(30,30)
     1/TEMP/T(30,30),GAMH(30,30),RESORT,NSWPT,URFT,PRANDL,PFUN,
     2     TWALLN,TIN,GAMQ(30,30),TBOTOM
     1/MSTF/QE(30,30),PRQE,CQ1,CQ2,RESQE,URFQ,BETA,GRAVTY,C3,C4,NSWPQ,
     1        SUQE(30,30),GENQ(30,30),SPQE(30,30),RESORQ
C
      DO 100 J=1,NJ
      R(J)=H1(J)
  100 IF(INDCOS.EQ.1)R(J)=1.0
      DYPS(1)=0.0
      DYNP(NJ)=0.0
      DO 102 J=1,NJM1
      DYNP(J)=Y(J+1)-Y(J)
  102 DYPS(J+1)=DYNP(J)
      SNS(1)=0.0
      SNS(NJ)=0.0
      DO 104 J=2,NJM1
  104 SNS(J)=0.5*(DYNP(J)+DYPS(J))
      YV(1)=0.0
      RV(1)=0.0
      DO 108 J=2,NJ
```

```
      RV(J)=0.5*(R(J)+R(J-1))
      I=1
      RCV(J)=0.5*(RV(J)+RV(J-1))
  108 YV(J)=0.5*(Y(J)+Y(J-1))
      DYPSV(1)=0.0
      DYPSV(2)=0.0
      DYNPV(NJ)=0.0
      DO 109 J=2,NJM1
      DYNPV(J)=YV(J+1)-YV(J)
  109 DYPSV(J+1)=DYNPV(J)
      SNSV(1)=0.0
      SNSV(2)=0.0
      SNSV(NJ)=0.0
      DO 110 J=3,NJM1
  110 SNSV(J)=0.5*(DYNPV(J)+DYPSV(J))
C
CHAPTER  2  2  2  2  2  2  SET VARIABLES TO ZERO  2  2  2  2  2  2
C
C
      DO 200 I=1,NI
      DO 200 J=1,NJ
      U(I,J)=U1(J)
      V(I,J)=0.0
      P(I,J)=0.0
      PP(I,J)=0.0
      TE(I,J)=TE1(J)
      ED(I,J)=ED1(J)
      QE(I,J)=1.E-20
      DEN(I,J)=DENSIT
      ALPHA(I)=0.0
      VIS(I,J)=VISCOS
      WRITE (6,119) VIS(I,J)
  119 FORMAT (2X,F10.8)
      GAMH(I,J)=VISCOS/PRANDL
      GAMQ(I,J)=VISCOS/PRANDL
      DU(I,J)=0.0
      DV(I,J)=0.0
      SU(I,J)=0.0
      SP(I,J)=0.0
  200 CONTINUE
      RETURN
      END
      SUBROUTINE PROPS
C
CHAPTER  0  0  0  0  0  0  0  0  PRELIMINARIES  0  0  0  0  0  0  0  0
C
      COMMON
     1/GEOM/INDCOS,X(32),Y(32),DXEP(32),DXPW(32),DYNP(32),DYPS(32),
     1      SNS(32),SEW(32),XU(32),YV(32),R(32),RV(32),H1(32),Y1(32)
     1/FLUPR/URFVIS,VISCOS,DENSIT,PRANDT,DEN(30,30),VIS(30,30),
     2      VISD(30,30),TE1(32),ED1(32),U2(32)
     1/VAR/U(30,30),V(30,30),P(30,30),PP(30,30),TE(30,30),ED(30,30)
     1/ALL/IT,JT,NI,NJ,NIM1,NJM1,GREAT,ALPHA(32),UU(32),TB(32)
     1/TURB/GEN(30,30),CD,CMU,C1,C2,CAPPA,ELOG,PRED,PRTE,CF(50),
     2      CK(50),C5,CE1(50)
     1/TEMP/T(30,30),GAMH(30,30),RESORT,NSWPT,URFT,PRANDL,PFUN,
```

```
     2       TWALLN,TIN,GAMQ(30,30),TBOTOM
C
CHAPTER   1   1   1   VISCOSITY   1   1   1
C
      PRQE=0.9
      I=1
      DO 100 J=1,NJ
      VISOLD=VIS(I,J)
      VIS(I,J)=(CMU*TE(I,J)**2/ED(I,J))+VISCOS
      GO  TO  103
  102 VIS(I,J)=VISCOS
C101  VIS(I,J)=URFVIS*VIS(I,J)+(1.-URFVIS)*VISOLD
  103 WRITE (6,109) VIS(I,J)
  109 FORMAT (2X,F10.8)
      GAMH(I,J)=VISCOS/PRANDL+(VIS(I,J)-VISCOS)/PRANDT
      GAMQ(I,J)=VISCOS/PRANDL+(VIS(I,J)-VISCOS)/PRQE
C-----UNDER-RELAX VISCOSITY
  100 CONTINUE
      UT=0.0
      DO 105 J=1,NJ
      IF (Y1(J).GT..381.AND.Y1(J).LT..396) GO TO 50
      U2(J)=CF(J)*(U(I,J)**2)*SNS(J)
      GO TO 101
   50 U2(J)=CF(J)*(U(I,J)**2)*SNS(J)/0.447
  101 CONTINUE
      UT=UT+U2(J)
  105 WRITE (6,109) UT
      DO 160 J=1,NJ
      IF (UT.EQ.1.88E-4) GO TO 60
      CC=1.88E-4/UT
      CF(J)=CC*CF(J)
      GO TO 160
   60 CF(J)=CF(J)
  160 WRITE (6,312) CF(J)
  312 FORMAT (3F12.5)
      RETURN
      END
      SUBROUTINE CALCU
C
CHAPTER  0  0  0  0  0  0  0  0  PRELIMINARIES  0  0  0  0  0  0  0  0
C
      COMMON
     1/UVEL/RESORU,NSWPU,URFU,DXEPU(32),DXPWU(32),SEWU(32),U1(30)
     1/PCOR/RESORM,NSWPP,URFP,DU(30,30),DV(30,30),IPREF,JPREF
     1/VAR/U(30,30),V(30,30),P(30,30),PP(30,30),TE(30,30),ED(30,30)
     1/ALL/IT,JT,NI,NJ,NIM1,NJM1,GREAT,ALPHA(32),UU(32),TB(32)
     1/TURB/GEN(30,30),CD,CMU,C1,C2,CAPPA,ELOG,PRED,PRTE,CF(50),
     2       CK(50),C5,CE1(50)
      COMMON
     1/GEOM/INDCOS,X(32),Y(32),DXEP(32),DXPW(32),DYNP(32),DYPS(32),
     1       SNS(32),SEW(32),XU(32),YV(32),R(32),RV(32),H1(32),Y1(32)
     1/FLUPR/URFVIS,VISCOS,DENSIT,PRANDT,DEN(30,30),VIS(30,30),
     2       VISD(30,30),TE1(32),ED1(32),U2(32)
     1/COEF/AP(30,30),AN(30,30),AS(30,30),AE(30,30),AW(30,30),SU(30,30),
     1       SP(30,30)
```

```
      1/PROB1/UIN,TEIN,EDIN,FLOWIN,ALAMDA,
      2       RSMALL,RLARGE,AL1,AL2,JSTEP,ISTEP,JSTP1,JSTM1,ISTP1,ISTM1,
      3    NITER,US
      1/TEMP/T(30,30),GAMH(30,30),RESORT,NSWPT,URFT,PRANDL,PFUN,
      2      TWALLN,TIN,GAMQ(30,30),TBOTOM
      1/MSTF/QE(30,30),PRQE,CQ1,CQ2,RESQE,URFQ,BETA,GRAVTY,C3,C4,NSWPQ,
      2      SUQE(30,30),GENQ(30,30),SPQE(30,30),RESQRQ
C
CHAPTER  1  1  1  1  1  1  ASSEMBLY OF COEFFICIENTS  1  1  1  1  1  1  1
C
      DO 101 J=2,NJM1
      I=1
C-----COMPUTE AREAS AND VOLUME
      Y1(J)=Y(J)
      VOL=R(J)*SNS(J)
C-----CALCULATE DIFFUSION COEFFICIENTS
      VISN=0.50*(VIS(I,J)+VIS(I,J+1))
      VISS=0.50*(VIS(I,J)+VIS(I,J-1))
C-----ASSEMBLE MAIN COEFFICIENTS
      AN(I,J)=RV(J+1)*VISN/DYNP(J)
      AS(I,J)=RV(J)*VISS/DYPS(J)
      SU(I,J)=0.0
      SU(I,J)=SU(I,J)+(GRAVTY*R(J)*.001*SNS(J))
      SP(I,J)=0.
      IF (Y1(J).GT..381.AND.Y1(J).LT..396) GO TO 50
      SP(I,J)=SP(I,J)-(CF(J)*U(I,J)*SNS(J))
      GO TO 100
   50 SP(I,J)=SP(I,J)-(CF(J)*U(I,J)*SNS(J)/.447)
  100 CONTINUE
  101 CONTINUE
C
CHAPTER  2  2  2  2  2  2  2  PROBLEM MODIFICATIONS  2  2  2  2  2  2  2
C
      CALL MODU
C
CHAPTER  3  FINAL COEFF. ASSEMBLY AND RESIDUAL SOURCE CALCULATION  3  3
      RESORU=0.0
C     DO 300 I=3,NIM1
      DO 301 J=2,NJM1
      I=1
      AP(I,J)=AN(I,J)+AS(I,J)-SP(I,J)
C     DU(I,J)=DU(I,J)/AP(I,J)
      RESOR=AN(I,J)*U(I,J+1)+AS(I,J)*U(I,J-1)
     1      -AP(I,J)*U(I,J)+SU(I,J)
      VOL=R(J)*SNS(J)
      SORVOL=GREAT*VOL
      IF(-SP(I,J).GT.0.5*SORVOL)  RESOR=RESOR/SORVOL
      RESORU=RESORU+ABS(RESOR)
C-----UNDER-RELAXATION
C     AP(I,J)=AP(I,J)/URFU
C     SU(I,J)=SU(I,J)+(1.-URFU)*AP(I,J)*U(I,J)
C     DU(I,J)=DU(I,J)*URFU
  301 CONTINUE
  300 CONTINUE
C
```

```
CHAPTER  4  4  4  SOLUTION OF DIFFERENCE EQUATION  4  4  4  4  4  4  4
C
      DO 400 N=1,NSWPU
  400 CALL LISOLV(3,2,NI,NJ,IT,JT,U)
      RETURN
      END
      SUBROUTINE CALCTE
C
CHAPTER  0  0  0  0  0  0  0  PRELIMINARIES  0  0  0  0  0  0  0
C
      COMMON
     1/TEN/RESORK,NSWPK,URFK
     1/VAR/U(30,30),V(30,30),P(30,30),PP(30,30),TE(30,30),ED(30,30)
     1/ALL/IT,JT,NI,NJ,NIM1,NJM1,GREAT,ALPHA(32),UU(32),TB(32)
      COMMON
     1/GEOM/INDCOS,X(32),Y(32),DXEP(32),DXPW(32),DYNP(32),DYPS(32),
     1      SNS(32),SEW(32),XU(32),YV(32),R(32),RV(32),H1(32),Y1(32)
     1/FLUPR/URFVIS,VISCOS,DENSIT,PRANDT,DEN(30,30),VIS(30,30),
     2       VISD(30,30),TE1(32),ED1(32),U2(32)
     1/COEF/AP(30,30),AN(30,30),AS(30,30),AE(30,30),AW(30,30),SU(30,30),
     1      SP(30,30)
     1/TURB/GEN(30,30),CD,CMU,C1,C2,CAPPA,ELOG,PRED,PRTE,CF(50),
     2      CK(50),C5,CE1(50)
     1/WALLF/YPLUSN(30,30),XPLUSW(30,30),TAUN(30,30),TAUW(30,30)
     1/PROB1/UIN,TEIN,EDIN,FLOWIN,ALAMDA,
     2       RSMALL,RLARGE,AL1,AL2,JSTEP,ISTEP,JSTP1,JSTM1,ISTP1,ISTM1,
     3    NITER,US
     1/SUSP/SUKD(30,30),SPKD(30,30)
     1/MSTF/QE(30,30),PRQE,CQ1,CQ2,RESQE,URFQ,BETA,GRAVTY,C3,C4,NSWPQ,
     1       SUQE(30,30),GENQ(30,30),SPQE(30,30),RESORQ
C
CHAPTER  1  1  1  1  1  1  ASSEMBLY OF COEFFICIENTS  1  1  1  1  1  1
C
      PRTE=1.0
      DO 101 J=2,NJM1
      I=1
C-----COMPUTE AREAS AND VOLUME
      Y1(J)=Y(J)
      VOL=R(J)*SNS(J)
C-----CALCULATE DIFFUSION COEFFICIENTS
      GAMN=0.5*(VIS(I,J)+VIS(I,J+1))/PRTE
      GAMS=0.5*(VIS(I,J)+VIS(I,J-1))/PRTE
C-----SOURCE TERMS
      CP=0.0
      CPO=CP
      DUDY=((U(I,J)+U(I,J+1))/2.-(U(I,J)+
     1U(I,J-1))/2.)/SNS(J)
      GEN(I,J)=(DUDY**2)*VIS(I,J)
C-----ASSEMBLE MAIN COEFFICIENTS
      AN(I,J)=GAMN/DYNP(J)
      AS(I,J)=GAMS/DYPS(J)
      SU(I,J)=CPO*TE(I,J)
      SUKD(I,J)=SU(I,J)
      SU(I,J)=SU(I,J)+GEN(I,J)*SNS(J)
      SP(I,J)=-CP
```

```
      SPKD(I,J)=SP(I,J)
      SP(I,J)=SP(I,J)-(CD*CMU*TE(I,J)*SNS(J)/VIS(I,J))
      IF (Y1(J).GT..381.AND.Y1(J).LT..396) GO TO 50
      SU(I,J)=SU(I,J)+(CF(J)*(U(I,J)**3)*SNS(J)/R(J))
      GO TO 100
   50 SU(I,J)=SU(I,J)+(CF(J)*(U(I,J)**3)*SNS(J)/(.3*R(J)))
  100 CONTINUE
  101 CONTINUE
C
CHAPTER  2  2  2  2  2  2  PROBLEM MODIFICATIONS  2  2  2  2  2  2
C
      CALL MODTE
C
CHAPTER 3 FINAL COEFFICIENT ASSEMBLY AND RESIDUAL SOURCE CALCULATION 3
C
      RESORK=0.0
      DO 301 J=2,NJM1
      AP(I,J)=AN(I,J)+AS(I,J)-SP(I,J)
      RESOR=AN(I,J)*TE(I,J+1)+AS(I,J)*TE(I,J-1)
     1       -AP(I,J)*TE(I,J)+SU(I,J)
      VOL=R(J)*SNS(J)
      SORVOL=GREAT*VOL
      IF(-SP(I,J).GT.0.5*SORVOL)  RESOR=RESOR/SORVOL
      RESORK=RESORK+ABS(RESOR)
C-----UNDER-RELAXATION
C     AP(I,J)=AP(I,J)/URFK
C     SU(I,J)=SU(I,J)+(1.-URFK)*AP(I,J)*TE(I,J)
  301 CONTINUE
  300 CONTINUE
C
CHAPTER  4  4  4  4  4  SOLUTION OF DIFFERENCE EQUATIONS  4  4  4  4  4
C
      DO 400 N=1,NSWPK
  400 CALL LISOLV(2,2,NI,NJ,IT,JT,TE)
      RETURN
      END
      SUBROUTINE CALCED
C
CHAPTER  0  0  0  0  0  0  0  PRELIMINARIES  0  0  0  0  0  0  0
C
      COMMON
     1/TDIS/RESORE,NSWPD,URFE
     1/ALL/IT,JT,NI,NJ,NIM1,NJM1,GREAT,ALPHA(32),UU(32),TB(32)
      COMMON
     1/GEOM/INDCOS,X(32),Y(32),DXEP(32),DXPW(32),DYNP(32),DYPS(32),
     1      SNS(32),SEW(32),XU(32),YV(32),R(32),RV(32),H1(32),Y1(32)
     1/FLUPR/URFVIS,VISCOS,DENSIT,PRANDT,DEN(30,30),VIS(30,30),
     2         VISD(30,30),TE1(32),ED1(32),U2(32)
     1/COEF/AP(30,30),AN(30,30),AS(30,30),AE(30,30),AW(30,30),SU(30,30),
     1      SP(30,30)
     1/TURB/GEN(30,30),CD,CMU,C1,C2,CAPPA,ELOG,PRED,PRTE,CF(50),
     2      CK(50),C5,CE1(50)
     1/WALLF/YPLUSN(30,30),XPLUSW(30,30),TAUN(30,30),TAUW(30,30)
     1/SUSP/SUKD(30,30),SPKD(30,30)
     1/VAR/U(30,30),V(30,30),P(30,30),PP(30,30),TE(30,30),ED(30,30)
```

```
     1/PROB1/UIN,TEIN,EDIN,FLOWIN,ALAMDA,
     2        RSMALL,RLARGE,AL1,AL2,JSTEP,ISTEP,JSTP1,JSTM1,ISTP1,ISTM1,
     3    NITER,US
     1/MSTF/QE(30,30),PRQE,CQ1,CQ2,RESQE,URFQ,BETA,GRAVTY,C3,C4,NSWPQ,
     1        SUQE(30,30),GENQ(30,30),SPQE(30,30),RESORQ
C
CHAPTER  1  1  1  1  1  1  ASSEMBLY OF COEFFICIENTS  1  1  1  1  1  1
C
      DO 101 J=2,NJM1
      I=1
C-----COMPUTE AREAS AND VOLUME
      Y1(J)=Y(J)
      VOL=R(J)*SNS(J)
C-----CALCULATE DIFFUSION COEFFICIENTS
      GAMN=0.5*(VIS(I,J)+VIS(I,J+1))/PRED
      GAMS=0.5*(VIS(I,J)+VIS(I,J-1))/PRED
C-----SOURCE TERMS
      CP=0.0
      CPO=CP
C-----ASSEMBLE MAIN COEFFICIENTS
      AN(I,J)=GAMN/DYNP(J)
      AS(I,J)=GAMS/DYPS(J)
      SU(I,J)=CPO*ED(I,J)
      SUKD(I,J)=SU(I,J)
      DUDY=((U(I,J)+U(I,J+1))/2.-(U(I,J)+U(I,J-1))/2.)/SNS(J)
      GEN(I,J)=(DUDY**2)*VIS(I,J)
      SU(I,J)=SU(I,J)+C1*CMU*GEN(I,J)*SNS(J)*TE(I,J)/VIS(I,J)
      SP(I,J)=-CP
      SPKD(I,J)=SP(I,J)
      SP(I,J)=SP(I,J)-(C2*ED(I,J)*SNS(J)/TE(I,J))
      QEPTE=QE(I,J)/TE(I,J)
      IF (Y1(J).GT..381.AND.Y1(J).LT..396 ) GO TO 50
      SU(I,J)=SU(I,J)+(CE1(J)*(CF(J)**2)*(U(I,J)**4)*SNS(J)/(R(J)**2))
      GO TO 100
   50 SU(I,J)=SU(I,J)+(CE1(J)*(CF(J)**2)*(U(I,J)**4)*SNS(J)/(.2*R(J)**2
     1))
  100 CONTINUE
  101 CONTINUE
C
CHAPTER  2  2  2  2  2  2  PROBLEM MODIFICATIONS  2  2  2  2  2  2
C
      CALL MODED
C
CHAPTER 3 FINAL COEFFICIENT ASSEMBLY AND RESIDUAL SOURCE CALCULATION 3
      RESORE=0.0
C
      DO 301 J=2,NJM1
      AP(I,J)=AN(I,J)+AS(I,J)-SP(I,J)
      RESOR=AN(I,J)*ED(I,J+1)+AS(I,J)*ED(I,J-1)
     1      -AP(I,J)*ED(I,J)+SU(I,J)
      VOL=R(J)*SNS(J)
      SORVOL=GREAT*VOL
      IF(-SP(I,J).GT.0.5*SORVOL)  RESOR=RESOR/SORVOL
      RESORE=RESORE+ABS(RESOR)
C-----UNDER-RELAXATION
```

```
C       AP(I,J)=AP(I,J)/URFE
C       SU(I,J)=SU(I,J)+(1.-URFE)*AP(I,J)*ED(I,J)
  301 CONTINUE
  300 CONTINUE
C
CHAPTER  4  4  4  4  4  SOLUTION OF DIFFERENCE EQUATIONS  4  4  4  4  4
C
      DO 400 N=1,NSWPD
  400 CALL LISOLV(2,2,NI,NJ,IT,JT,ED)
      RETURN
      END
      SUBROUTINE LISOLV(ISTART,JSTART,NI,NJ,IT,JT,PHI)
C
CHAPTER  0  0  0  0  0  0  0  0  PRELIMINARIES  0  0  0  0  0  0  0  0
C
      DIMENSION PHI(IT,JT),A(32),B(32),C(32),D(32)
      COMMON
     1/COEF/AP(30,30),AN(30,30),AS(30,30),AE(30,30),AW(30,30),SU(30,30),
     1      SP(30,30)
     1/VAR/U(30,30),V(30,30),P(30,30),PP(30,30),TE(30,30),ED(30,30)
     1/GEOM/INDCOS,X(32),Y(32),DXEP(32),DXPW(32),DYNP(32),DYPS(32),
     1      SNS(32),SEW(32),XU(32),YV(32),R(32),RV(32),H1(32),Y1(32)
     1/TURB/GEN(30,30),CD,CMU,C1,C2,CAPPA,ELOG,PRED,PRTE,CF(50),
     2      CK(50),C5,CE1(50)
      LOGICAL INCT
C     INCT=.TRUE.
      NIM1=NI-1
      NJM1=NJ-1
      JSTM1=JSTART-1
      A(JSTM1)=0.0
C-----COMMENCE W-E SWEEP
      C(JSTM1)=PHI(1,JSTM1)
C-----COMMENCE S-N TRAVERSE
      DO 101 J=JSTART,NJM1
C-----ASSEMBLE TDMA COEFFICIENTS
      A(J)=AN(1,J)
      B(J)=AS(1,J)
      C(J)=SU(1,J)
      D(J)=AP(1,J)
C-----CALCULATE COEFFICIENTS OF RECURRENCE FORMULA
      TERM=1./(D(J)-(B(J)*A(J-1)))
      A(J)=A(J)*TERM
      C(J)=(C(J)+B(J)*C(J-1))*TERM
  101 CONTINUE
  109 FORMAT (5X,I10,8(1PE12.3,3X))
C-----OBTAIN NEW PHI'S
      DO 102 JJ=JSTART,NJM1
      I=1
      J=NJ+JSTM1-JJ
      PHI(I,J)=A(J)*PHI(I,J+1)+C(J)
  102 CONTINUE
  105 FORMAT (F12.5)
  100 CONTINUE
C     INCT=.FALSE.
      RETURN
```

```
      END
      SUBROUTINE PRINT(ISTART,JSTART,NI,NJ,IT,JT,X,Y,PHI,HEAD)
      COMMON
     1/AREA1/INCT
      DIMENSION PHI(IT,JT),X(IT),Y(JT),HEAD(9),STORE(50)
      DIMENSION F(7),F4(11)
      LOGICAL INCT
      DATA F/4H(1H ,4H,A4,,4HI3, ,4H11I ,4H10, ,4H7X, ,
     14HA6) /
      DATA F4/4H 1I ,4H 2I ,4H 3I ,4H 4I ,4H 5I ,4H 6I ,
     1        4H 7I ,4H 8I ,4H 9I ,4H10I ,4H11I /
      DATA HI,HY/4H  I=,4H Y =/
      ISKIP=1
      JSKIP=1
      WRITE(6,110)HEAD
      ISTA=ISTART
  100 CONTINUE
C     ISTA=ISTA+12
      IEND=ISTA
      IEND=MIN0(NI,IEND)
      F(4)=F4(IEND-ISTA)
      WRITE(6,F) HI, (I,I=ISTA,IEND,ISKIP), HY
      WRITE(6,112)
      DO 101 JJ=JSTART,NJ,JSKIP
      J=JSTART+NJ-JJ
C     DO 120 I=ISTA,IEND
      A=PHI(1,J)
      IF(ABS(A).LT.1.E-20) A=0.0
  120 STORE(1)=A
      IF(INCT) GO TO 200
      WRITE(6,113)  J,(STORE(1)),Y(J)
      GO TO 300
  200 WRITE(6,150)  J,(STORE(1)),Y(J)
  300 CONTINUE
  101 CONTINUE
C     WRITE(6,114) (X(I),I=ISTA,IEND,ISKIP)
C-----------------------------------------------------------
      IF(IEND.LT.NI)GO TO 100
      RETURN
  110 FORMAT(1H0,20(2H*-),7X,9A4,7X,20(2H-*))
  112 FORMAT(3H  J)
  113 FORMAT(1H ,I3,1P1E10.2,0PF7.3)
  114 FORMAT(6H0X=    ,F7.3,11F10.3)
  150 FORMAT(1H ,I3,1P1E10.3,0PF7.3)
      RETURN
      END
      SUBROUTINE PROMOD
C
CHAPTER  0  0  0  0  0  0  0  PRELIMINARIES  0  0  0  0  0  0  0  0  0
C
      DIMENSION PHI(IT,JT),A(32),B(32),C(32),D(32)
      COMMON
     1/VVEL/RESORV,NSWPV,URFV,DYNPV(32),DYPSV(32),SNSV(32),RCV(32)
     1/UVEL/RESORU,NSWPU,URFU,DXEPU(32),DXPWU(32),SEWU(32),U1(30)
     1/PCOR/RESORM,NSWPP,URFP,DU(30,30),DV(30,30),IPREF,JPREF
```

```
      1/VAR/U(30,30),V(30,30),P(30,30),PP(30,30),TE(30,30),ED(30,30)
      1/ALL/IT,JT,NI,NJ,NIM1,NJM1,GREAT,ALPHA(32),UU(32),TB(32)
       COMMON
      1/GEOM/INDCOS,X(32),Y(32),DXEP(32),DXPW(32),DYNP(32),DYPS(32),
      1       SNS(32),SEW(32),XU(32),YV(32),R(32),RV(32),H1(32),Y1(32)
      1/FLUPR/URFVIS,VISCOS,DENSIT,PRANDT,DEN(30,30),VIS(30,30),
      2        VISD(30,30),TE1(32),ED1(32),U2(32)
      1/PROB1/UIN,TEIN,EDIN,FLOWIN,ALAMDA,
      2       RSMALL,RLARGE,AL1,AL2,JSTEP,ISTEP,JSTP1,JSTM1,ISTP1,ISTM1,
      3    NITER,US
      1/SUSP/SUKD(30,30),SPKD(30,30)
      1/COEF/AP(30,30),AN(30,30),AS(30,30),AE(30,30),AW(30,30),SU(30,30),
      1      SP(30,30)
       COMMON
      1/TURB/GEN(30,30),CD,CMU,C1,C2,CAPPA,ELOG,PRED,PRTE,CF(50),
      2      CK(50),C5,CE1(50)
      1/WALLF/YPLUSN(30,30),XPLUSW(30,30),TAUN(30,30),TAUW(30,30)
      1/TEMP/T(30,30),GAMH(30,30),RESORT,NSWPT,URFT,PRANDL,PFUN,
      2     TWALLN,TIN,GAMQ(30,30),TBOTOM
      1/MSTF/QE(30,30),PRQE,CQ1,CQ2,RESQE,URFQ,BETA,GRAVTY,C3,C4,NSWPQ,
      1       SUQE(30,30),GENQ(30,30),SPQE(30,30),RESORQ
C
CHAPTER  1  1  1  1  1  1  1  1  PROPERTIES  1  1  1  1  1  1  1  1  1
C
      ENTRY MODPRO
C-----NO MODIFICATIONS FOR THIS PROBLEM
      RETURN
C
CHAPTER  2  2  2  2  2  2  2  2  U MOMENTUM  2  2  2  2  2  2  2  2  2
C
      ENTRY MODU
      U(1,NJ)=.400
      CDTERM=CMU**0.25
      YP=Y(2)-YV(2)
      J=2
C     DO  210  I=3,NIM1
      SQRTK=SQRT(0.5*(TE(I,J)+TE(1,J)))
      DENU=0.5*(DEN(1,J)+DEN(1,J))
      YPLUSA=0.5*(YPLUSN(1,2)+YPLUSN(1,2))
      IF(YPLUSA.LE.11.63)       GO  TO  211
      TMULT=DENU*CDTERM*SQRTK*CAPPA/ALOG(ELOG*YPLUSA)
      GO  TO  212
  211 TMULT=VISCOS/YP
  212 TAUN(1,2)=-TMULT*U(1,J)
      SP(1,2)=-GREAT
  210 AS(1,2)=0.0
      SU(1,2)=0.17*GREAT
C     TAUN(2,NJM1)=TAUN(3,NJM1)
      TAUN(1,1)=TAUN(1,2)
      RETURN
C
CHAPTER 6 6 6 6 6 6 6 TURBULENT KINETIC ENERGY
C
      ENTRY MODTE
      CDTERM=CMU**0.25
```

```
      YP=Y(2)-YV(2)
      I=1
      J=2
      TE(1,NJ)=2.0E-3
C     DO  610  I=2,NIM1
      DENU=DEN(1,J)
      SQRTK=SQRT(TE(1,J))
      VOL=H1(J)*SNS(J)
      YPLUSN(1,2)=SQRTK*CDTERM*YP/VISCOS
C     TAUN(1,2)=DENSIT*CDTERM*SQRTK*CAPPA*U(1,J)/ALOG(ELOG*YPLUSN(1,2))
      GENCOU=0.5*(ABS(TAUN(1,2)*U(1,J))+ABS(TAUN(1,2)*U(1,J)))
     1/(YP*DENSIT)
C     YPLUSN(I,NJM1)=DENU*SQRTK*CDTERM*YP/VISCOS
      DUDY=((U(1,J)+U(1,J+1))/2.-(U(I,J)+
     1U(I,J-1))/2.)/SNS(J)
      GENRES=GEN(1,J)-VIS(1,J)*DUDY**2
      GEN(1,J)=GENRES+GENCOU
      IF(YPLUSN(I,NJM1).LE.11.63) GO TO 611
      DITERM=(CMU**.75)*SQRTK*ALOG(ELOG*YPLUSN(I,2
     1))/(CAPPA*YP)
      GO  TO  612
  611 CONTINUE
      DITERM=(CMU**.75)*SQRTK*YPLUSN(1,2)/YP
  612 CONTINUE
C     SU(I,J)=SUKD(I,J)+(CK(J)*(CF(J)**(3/2))*(U(I,J)**3)*SNS(J)/R(J))
C    1+GEN(I,J)*SNS(J)
C     SP(I,J)=-DITERM*SNS(J)+SPKD(I,J)
      SP(1,2)=-GREAT
      SU(1,2)=4.8E-4*GREAT
  610 AS(1,2)=0.0
C     GO TO 620
      RETURN
C
CHAPTER  7 7 7 7 7 7 7 7 DISSIPATION
C
      ENTRY MODED
C-----TOP WALL
      ED(1,NJ)=3.9E-3
      YP=Y(2)-YV(2)
      I=1
      J=2
      TERM=(CMU**.75)/(CAPPA*YP)
C     DO  710  I=2,NIM1
C     SU(I,J)=GREAT*TERM*TE(I,J)**1.5
      SU(I,J)=1.6E-4*GREAT
  710 SP(I,J)=-GREAT
      RETURN
```